Charles University, Faculty of Science
Department of Cell Biology

Doctoral study program: Immunology

M.Sc. Nataliia Pavliuchenko

Membrane Adaptor Proteins in Hematopoiesis and Immune Response

Membránové adaptorové proteiny v hematopoeze a imunitní odpovědi

Doctoral Dissertation Thesis

Supervisor: Mgr. Tomáš Brdička, Ph.D.

Prague, 2023

Declaration:

I declare that I prepared the final thesis independently and that I have listed all the information sources and literature used. This work, or a substantial part of it, has not been submitted for the award of another or the same academic degree.

Prague, 28.06.2023 …………………………… Nataliia Pavliuchenko

Acknowledgment

ABSTRACT

Membrane adaptor proteins are proteins associated with cellular membranes that do not themselves serve as receptors. Instead, they propagate or modify the signals of these receptors by recruiting other signaling and regulatory proteins and arranging them into supramolecular complexes. In this thesis, I sought to describe selected membrane adaptor proteins and their roles in inflammation and regulation of hematopoiesis in mouse models using a reverse genetics approach.

The main part of the work focused on the role of the membrane adaptor protein PSTPIP2 in suppressing inflammation. In mice, missense mutations in the *Pstpip2* gene causing loss of PSTPIP2 protein lead to the development of autoinflammatory disease chronic multifocal osteomyelitis (CMO) characterized by sterile inflammatory lesions in the bones and adjacent soft tissue. These mice represent a model of the human autoinflammatory disease, chronic recurrent multifocal osteomyelitis. At the molecular level, neutrophils in the absence of PSTPIP2 exhibit pathological hyperactivity of pathways regulating IL-1β and reactive oxygen species (ROS) production, which are both implicated in the etiology of the disease. PSTPIP2 interacts with several signaling regulators, including PEST family protein tyrosine phosphatases (PEST-PTPs) and inositol 5'-phosphatase SHIP1. We hypothesized that these binding partners play a key role in the suppression of inflammation by PSTPIP2. To test this hypothesis, we have generated mutant mouse strains, in which the PSTPIP2 binding sites for PEST-PTPs or SHIP1 were abolished. Analysis of these mouse mutants revealed that disruption of either of these two interactions results in increased production of IL-1β. However, only loss of the interaction between PSTPIP2 and PEST-PTP led to the production of harmful levels of ROS and subsequent bone damage. PEST-PTPs also appeared to be a major regulator of chemokine production by neutrophils, controlling neutrophil migration to the site of autoinflammation within a positive feedback loop.

To further characterize the pathways regulated by PSTPIP2-organized regulatory complex, we employed a mouse model of CMO deficient in receptor-type protein tyrosine phosphatase CD45, where the activity of Src-family kinases in leukocytes is substantially reduced. In these mice, we observed delayed disease onset and lower severity of sterile inflammation, as well as reduced IL-1β production. These findings, together with previously published data, suggested that the PSTPIP2-regulated pathway responsible for triggering autoinflammation is controlled by Src-family kinases, likely using ITAM motif-dependent signaling.

In this thesis I also present the results of functional analysis of two additional leukocyte membrane adaptor proteins LST1 and WBP1L and their functional roles in mice. They are both transmembrane proteins. LST1 was thought to be a negative regulator of signaling due to its interactions with the phosphatases SHP-1 and SHP-2, whereas virtually nothing was known about the physiological function of WBP1L. We found that LST1 deficiency *in vivo* leads to a protective effect against intestinal inflammation during acute colitis induced by sodium dextran sulfate, a model of human inflammatory bowel disease. Deficiency of WBP1L revealed its function as a negative regulator of CXCR4 signaling. The regulation is likely mediated by WBP1L binding to NEDD4 family ubiquitin ligases. We also observed an increased ability of WBP1L-deficient bone marrow cells to reconstitute the hematopoietic system after transplantation, demonstrating its role in the regulation of hematopoiesis.

ABSTRAKT

Membránové adaptorové proteiny jsou proteiny asociované s buněčnými membránami, které samy o sobě neslouží jako receptory. Místo toho šíří nebo modifikují signály těchto receptorů tím, že váží další signální a regulační proteiny a organizují je do supramolekulárních komplexů. V této práci jsem se snažila popsat vybrané membránové adaptorové proteiny a jejich roli v zánětu a regulaci krvetvorby na myších modelech pomocí přístupu reverzní genetiky.

Hlavní část práce byla zaměřena na roli membránového adaptorového proteinu PSTPIP2 v potlačování zánětu. Mutace v genu Pstpip2 způsobující ztrátu proteinu PSTPIP2 vedou u myší k rozvoji autoinflamatorního onemocnění chronické multifokální osteomyelitidy charakterizované sterilními zánětlivými lézemi v kostech a přilehlých měkkých tkáních. Tyto myši představují model lidského autoinflamatorního onemocnění chronické rekurentní multifokální osteomyelitidy. Na molekulární úrovni vykazují neutrofily při absenci PSTPIP2 patologickou hyperaktivitu drah regulujících produkci IL-1β a reaktivních kyslíkatých sloučenin (ROS), které se podílejí na etiologii onemocnění. PSTPIP2 interaguje s několika regulátory signalizace zahrnujícími protein tyrozin fosfatázy rodiny PEST (PEST-PTP) a inositol 5'-fosfatázu SHIP1. Předpokládali jsme, že tito vazební partneři hrají klíčovou roli v potlačování zánětu proteinem PSTPIP2. K ověření této hypotézy jsme vytvořili mutantní myší kmeny, u nichž byla odstraněna vazebná místa PSTPIP2 pro PEST-PTP nebo SHIP1. Analýza těchto myších mutantů odhalila, že narušení kterékoli z těchto dvou interakcí vede ke zvýšené produkci IL-1β. Avšak pouze ztráta interakce mezi PSTPIP2 a PEST-PTP vedla k produkci škodlivých hladin ROS a následnému poškození kostí. Ukázalo se, že PEST-PTP jsou také hlavním regulátorem produkce chemokinů neutrofily, které v rámci pozitivní zpětnovazebné smyčky řídí migraci neutrofilů do místa autoinflamace.

K charakterizaci drah regulovaných regulačním komplexem PSTPIP2 jsme použili též myší model CMO s deficitem proteinové tyrozinfosfatázy receptorového typu CD45, u kterého je výrazně snížena aktivita kináz rodiny Src v leukocytech. U těchto myší jsme pozorovali opožděný nástup onemocnění a nižší závažnost sterilního zánětu, jakož i sníženou produkci IL-1β. Tyto poznatky spolu s dříve publikovanými daty ukazují, že dráha regulovaná PSTPIP2, která je zodpovědná za spuštění autoinflamace, je řízena kinázami rodiny Src, pravděpodobně využívajícími signalizaci závislou na motivech ITAM.

V této práci představuji také výsledky funkční analýzy dalších dvou leukocytárních membránových adaptorových proteinů LST1 a WBP1L. Oba jsou transmembránovými proteiny. LST1 byl považován za negativní regulátor signalizace vzhledem ke svým interakcím s fosfatázami SHP1 a SHP2, zatímco o fyziologické funkci WBP1L nebylo téměř nic známo. Zjistili jsme, že inaktivace genu pro LST1 in vivo vede k ochrannému účinku proti střevnímu zánětu během akutní kolitidy vyvolané dextran sulfátem sodným, která je modelem nespecifického střevního zánětu u lidí. Deficit WBP1L pomohl identifikovat jeho funkci negativního regulátoru signalizace CXCR4. Regulace je pravděpodobně zprostředkována vazbou WBP1L na ubikvitin ligázy rodiny NEDD4. Pozorovali jsme také zvýšenou schopnost buněk kostní dřeně s deficitem WBP1L rekonstituovat hematopoetický systém po transplantaci, což ukazuje na jeho roli v regulaci krvetvorby.

TABLE OF CONTENTS

1. LIST OF ABBREVIATIONS

μCT - microcomputerized tomography

AIM2 - absent in melanoma 2

AKT - Protein kinase B

ALL - acute lymphoblastic leukemia

ATP - adenosine triphosphate

BMDC - bone marrow derived dendritic cells

BMDM - bone marrow derived macrophages

CAPS - cryopyrin-associated periodic syndrome

CARD9 - caspase recruitment domain–containing protein 9

Cas - Crk-associated substrate

CD - cluster of differentiation

CMO - Chronic Multifocal Osteomyelitis

CRMO - chronic recurrent multifocal osteomyelitis

CSK - C-terminal Src kinase

CTH - carboxyl-terminal homology

DAI - Disease Activity Index

DAMP - Damage-associated molecular pattern

DIRA - interleukin-1 receptor antagonist

DSS - dextran sodium sulphate

ELISA - enzyme-linked immunosorbent assay

ERK - Extracellular signal-regulated kinase

FAK - focal adhesion kinase

F-BAR - Fer kinase/CIP4 homology Bin-Amphiphysin-Rvs

FMF - familial Mediterranean fever

fMLF - N-Formylmethionyl-leucyl-phenylalanine

G-CSF - granulocyte colony-stimulating factor

GPCR - G-protein-coupled receptors

GSDMD - gasdermin D

HSPC - hematopoietic stem progenitor cells

IBD - inflammatory bowel disease

IFNγ - interferon gamma

IL - interleukin

ITAM - immunotyrosine activating motif

ITIM - immunoreceptor tyrosine-based inhibitory motifs

JAK - Janus kinase

L - ligand

LAT -Linker for Activation of T cells

Lck - lymphocyte-specific protein tyrosine kinase

LPS - lipopolysaccharide

LST1 - Leukocyte-specific transcript 1 protein

NADPH - Nicotinamide adenine dinucleotide phosphate

NET - neutrophil extracellular traps

NK - natural killer

NLRP - Nucleotide-binding oligomerization domain, Leucine rich Repeat and Pyrin domain containing

OCP - osteoclast precursor

OPAL1 - Outcome Predictor in Acute Leukemia 1

PAMP - Pathogen-associated molecular pattern

PAPA - pyogenic sterile arthritis, pyoderma gangrenosum, pyogenic arthritis, pyoderma gangrenosum, and acne syndrome

PH - pleckstrin homology

PI3K - phosphatidylinositol-3-kinase

PRR - Pattern recognition receptors

PSTPIP - Proline-serine-threonine-phosphatase-interacting protein

PTK - protein tyrosine kinase

PTP - protein tyrosine phosphatase

PTPRC - Protein tyrosine phosphatase receptor type C

Pyk2 - protein tyrosine kinase 2

RIPK3 - receptor-interacting serine/ threonine protein kinase 3

ROS - reactive oxygen species

SAPHO - synovitis, acne, pustulosis, hyperostosis, and osteitis

SFK - Src-family kinase

STAT - signal transducer and activator of transcription

SH - Src homology

SHIP1 - Src homology domain-containing inositol 5'-phosphatase 1

SHP - Src homology region 2 domain-containing phosphatase

SYK - Spleen tyrosine kinase

TLR – Toll-like receptor

TNF-α - tumor necrosis factor alpha

WASP - Wiskott Aldrich syndrome protein

WT - wild type

WBP1L - WW domain binding protein 1-like

2. INTRODUCTION

2.1. Receptor signaling in leukocytes

Functions of the immune system are highly dependent on leukocytes and their ability to detect pathogens and other environmental cues and to communicate with each other. Leukocytes are capable of sensing a wide array of molecules, including cytokines, growth factors, hormones, pathogen-associated molecular patterns (PAMPs), complement fragments and many other protein and non-protein molecules. Leukocytes can recognize and distinguish these molecules from each other and respond to their presence [1]. In the extracellular space, they are detected by receptors that bind these molecules extracellularly and transduce the signal intracellularly using various signaling motifs and/or enzymatic activities that further transmit the signal until the proper response is generated [2]. Intact signaling is absolutely crucial for proper leukocyte function. It is a complex process, which involves activation of multiple enzymes that at the end results in changes in cell behavior, proliferation, differentiation, metabolism and/or gene expression [3].

2.2. Regulation of leukocyte signaling

Receptor signaling must be closely regulated to ensure sufficient leukocyte sensitivity, but at the same time prevent excessive response, such as harmful inflammation or the development of autoimmunity. The outcome of the signaling is influenced by the availability of the receptor and the intensity and duration of the signaling. Receptor availability is governed by the receptor synthesis and delivery to the plasma membrane, as well as by its downregulation and degradation. Downregulation and degradation allow for rapid regulation, but also fine steady state tuning, of cell sensitivity to a particular ligand. Ubiquitination and endocytosis of surface receptors represent key mechanisms regulating their availability [4] [5]. Receptors that undergo ubiquitination can be removed from the cell surface by endocytosis, and then may be recycled back to the cell surface or targeted for lysosomal degradation [4, 6] [7]. Some ubiquitinated receptors can also be subjected to proteasomal degradation [8]. In addition to receptor availability, enzymatic activities employed in receptor signal transmission are also subject to tight regulation. Within this thesis, I will focus mainly on the regulation connected to protein and lipid phosphorylation.

Many receptors linked to cell activation are coupled to signaling pathways initiated by phosphorylation of tyrosine residues. Some of these receptors contain immunoreceptor tyrosine-based activation motifs (ITAMs) in their cytoplasmic domains [9]. These motifs containing two tyrosines usually spaced by 9-11 amino acids are typically phosphorylated by protein tyrosine kinases (PTK) from SRC-family [10]. This phosphorylation results in the recruitment of additional PTKs from Spleen tyrosine kinase (SYK) family and their activation [11]. Once activated, SRC and SYK kinases phosphorylate additional intracellular or transmembrane adaptors and enzymes that further propagate signaling resulting in cytoskeletal rearrangements, transcriptional activation, effector functions and, in the case of T cells and B cells, proliferation and differentiation [11] [12]. Another group of receptors crucial for leukocyte activation are cytokine receptors from hemopoietin family (Type I cytokine receptors). These receptors also mediate their functions by inducing the phosphorylation of tyrosine residues [13]. Although they do not have intrinsic PTK activity, they are coupled to the Janus kinase (Jak) family of cytoplasmic PTKs and their substrates, proteins of the STAT (signal transducer and activator of transcription) family, which are activated by

phosphorylation and then serve as transcription factors directly regulating gene expression in the nucleus [14].

Activity of PTKs is opposed by the activity of protein tyrosine phosphatases (PTPs). PTPs are divided into two categories: receptor-type PTPs that are transmembrane proteins containing extracellular, transmembrane and intracellular phosphatase domain, and non-receptor-type PTPs, located entirely inside the cell, mainly in the cytoplasm [15]. For the topics discussed in this thesis the most important representatives include receptor-type PTP CD45 and non-receptor-type PTPs, SH2 domain-containing protein tyrosine phosphatase-1 (SHP-1) and 2 (SHP-2), and PTPs from the PEST family (PEST-PTPs). Non-receptor-type Src homology domain-containing inositol 5'-phosphatase 1 (SHIP1) will also be discussed. Although phosphatases are perceived mostly as negative regulators, they can also have positive effects on cellular signaling [15].

CD45 (protein tyrosine phosphatase receptor type C, PTPRC) is an example of (predominantly) positive regulator. It is a transmembrane glycoprotein expressed by all nucleated cells of hematopoietic origin [16] [17]. It plays an essential role in antigen receptor signal transduction and lymphocyte development [18]. In addition, it modulates signals from integrin [19], Fc [20], cytokine [21], and other receptors in multiple hematopoietic lineages. Most of these various functions are accomplished by regulation of phosphorylation of Src family protein tyrosine kinases (SFKs). They are represented by 9 members SRC, LCK, LYN, BLK, HCK, FYN, YRK (not found in mammals), FGR, and YES [22]. SFKs are important for initiation of immune responses in T and B cells or innate responses of myeloid cells [23]. They also modulate signals from growth factor, cytokine, and integrin receptors [24] [25]. SFKs also function as negative regulators by phosphorylating ITIM motifs on inhibitory receptors, which then leads to the recruitment and activation of inhibitory molecules such as the phosphatases SHP-1 and SHP-2 and the SHIP-1 [26]. It was shown that CD45 positively regulates T cell activation and development through its ability to dephosphorylate the inhibitory tyrosine of SFKs in studies with CD45-deficient T cell lines and T cells from CD45-deficient mice [27]. In these cells high enhancement of phosphorylation at the inhibitory carboxy-terminal (C-terminal) tyrosine residues of the SFKs Lck and Fyn was observed, which prevented T cell activation [28].

Studies on the role of CD45 in myeloid lineage determined its unique function in integrin-mediated cell adhesion. Absence of CD45 resulted in deficiency to maintain long term adhesion to plastic by macrophages. CD45-deficient macrophages showed altered phosphorylation and activation of Src family kinases, Hck and Lyn, but not of Fgr. They also showed reduced FcR signaling and FcR-mediated phagocytosis, as well as decreased lipopolysaccharide (LPS)-triggered production of tumor necrosis factor (TNF) [29] [30]. In neutrophils, CD45 deficiency resulted in reduced adhesion, phagocytosis, oxidative burst and bacterial killing. They also showed reduced responses to G-protein-coupled receptor (GPCR) ligand N-Formylmethionyl-leucyl-phenylalanine (fMLF), including migration, calcium flux, extracellular signal-regulated kinase (ERK) and protein kinase B (AKT) phosphorylation [31].

SHP-1 (Ptpn6) is an intracellular PTP, acting as effector of inhibitory receptors in lymphocytes, including inhibitory natural killer (NK) receptors, CD22, PIR-B, and others. Mutant mouse strain deficient in SHP-1 known as "motheaten" shows severe defects in hematopoiesis, severe immune dysregulation and systemic autoimmunity [32]. In particular, these mice exhibit chronic inflammation of the skin (leading to fur loss, hence the name "motheaten"), splenomegaly, severe lung inflammation and die within 12 weeks of age [33].

To dissect the contribution of innate immune cells to the motheaten phenotype using floxed SHP-1 mice, it was shown that *Ptpn6* deletion in neutrophils resulted in enhanced neutrophil integrin signaling through SRC- and SYK-family kinases causing cutaneous inflammation but not autoimmunity. On the other hand, deficiency of SHP-1 in dendritic cells led to exaggerated MyD88-dependent signaling causing severe autoimmunity. These studies revealed contribution of SHP-1 to the regulation of multiple signaling cascades in different cell types that upon the loss of this phosphatase contribute to the development of motheaten disease [34]. In addition, disrupted SHP-1 signaling in mice (*Ptpn6*[spin] mice) due to Y208N amino acid substitution in the carboxy-terminus of SHP-1 leads to spontaneous development of severe inflammatory disease, characterized by persistent footpad swelling and inflammation [35] [36]. Interestingly, deletion of SHP-1 in BMDM also increases phagocytosis of tumor cells diminishing transduction of "don't eat me" signal derived from SIRPα [37].

All these data suggest SHP-1 function as negative regulator of signaling [38]. The predominant mechanism of activation of SHP-1 is through engagement of its SH2 domains by phosphorylated tyrosine residues, particularly those found within ITIM motifs. In this manner, SHP-1 can interact with a variety of tyrosine-phosphorylated molecules, especially receptors bearing ITIMs in their cytoplasmic domain. Recruitment of SHP-1 to ITIMs is initiated by tyrosine phosphorylation (by SFKs). During T cell activation, SHP-1 undergoes phosphorylation at a tyrosine in its C-terminal tail (Tyr564), which enables its binding to Lck and its future inactivation [39].

In contrast to SHP-1, the ubiquitously expressed SHP-2 is considered an overall positive regulator of cell signaling. Even though, the mechanism is poorly understood, it is known that SHP-2 promotes signaling through a variety of growth factor and cytokine receptors essential for lymphoid development [40] and myelopoiesis [41]. Interestingly, in leukocytes SHP-2 often binds the same ITIM motifs as SHP-1 [42] and it is possible that its negative regulatory functions are masked by partial redundancy with SHP-1.

Another group of phosphatases widely expressed in hematopoietic cells is SHIP family, represented by SHIP1 and SHIP2 [43]. SHIPs have the potential to regulate many effects induced by phosphatidylinositol-3-kinase (PI3K) pathway, including proliferation, differentiation, apoptosis, cell activation, cell movement and adhesion [42]. PI3Ks transmit signals from the cell surface to the cytoplasm by generating second messengers – phosphorylated phosphatidylinositols – which in turn activate multiple effector pathways, including AKT, nuclear factor-κB (NF-κB), and others [44]. SHIP1 and SHIP2 *in vivo* are responsible for breaking down the product of PI3K phosphatidylinositol-3,4,5-trisphosphate to phosphatidylinositol-3,4-bisphosphate [45], hence regulating PI3K pathway [46]. By dephosphorylating position 5 of the inositol ring, it is not exactly opposing PI3K activity, since PI3K phosphorylates position 3. However, studies using mice deficient in SHIP1 clearly show its inhibitory function. SHIP1-deficient mice develop splenomegaly and a shortened life span associated with massive myeloid cell infiltration to the lungs. Additionally, SHIP1$^{-/-}$ mice display M2-macrophage-mediated lung pathology [47]. Furthermore, SHIP1 activation may be pivotal in regulating neutrophil apoptosis in an inflammatory reaction and preventing tissue damage and subsequent fibrosis. Upon SHIP1 deletion, neutrophils show resistance to enhanced apoptosis as a result of maintained AKT activity [48]. SHIP2 deficiency in mice enhanced insulin receptor signaling and protected these animals from insulin resistance. However, its effects on the immune system function were relatively mild without major pathology [49] [50].

SHIP1 also has some positive effects on immune response through its negative regulation of myeloid-derived suppressor cells and Treg. Treatment with specific SHIP1 inhibitor, small molecule 3AC was shown to induce expansion of the myeloid-derived suppressor cells and impairment of the immune system's ability to prime allogeneic T cell responses [51] in mouse models. In collagen-induced inflammatory arthritis, inhibition of SHIP1 with 3AC expands myeloid-derived suppressor cells and Tregs and overproduction of these regulatory cells attenuates development of inflammatory arthritis in mice [52].

Another family of phosphatases the proline-, glutamic acid-, serine- and threonine-rich (PEST) family of PTPs contains 3 members: PTP-PEST (PTPN12), proline-enriched phosphatase (PEP, also known as lymphoid tyrosine phosphatase (LYP) or PTPN22), and PTP-hematopoietic stem cell fraction (PTP-HSCF, PTPN18) [53]. PEST family members are differently expressed in leukocytes. PTP-PEST is expressed in non-hematopoietic as well as hematopoietic cells with highest levels detected in neutrophils, mast cells and macrophages. PEP/LYP shows the highest expression in various lymphocyte subsets [53]. PTP-HSCF was identified mostly in primitive hematopoietic cells [54].

PTP-PEST is found mainly in the cytoplasm where it interacts with cellular proteins and performs various regulatory functions. PTP-PEST binds to the adaptor protein Crk-associated substrate (Cas), and its relatives Sin and CasL known to play important role in cell adhesion processes in neutrophils [55]. It also interacts with the LIM domains of paxillin, protein tyrosine kinase 2 (Pyk2) and focal adhesion kinase (FAK) involved in podosome formation in polymorphonuclear neutrophils during migration [56]. PTP-PEST also associates with SH3 domains of C-terminal Src kinase (CSK), involved in negative regulation of neutrophil migration, likely through its inhibitory effects on Src-family kinases [57] [58] [59].

Functions of PTP-PEST in non-hematopoietic cells were mostly identified from overexpression studies in fibroblasts and PTP-PEST-deficient mouse embryonic fibroblasts. They showed that PTP-PEST is a positive regulator of adhesion and migration and acts by dephosphorylating cytoskeletal proteins such as Cas, FAK, and Pyk2. PTP-PEST is also required for the dissociation of focal adhesions by activating integrins. These latter effects are correlated with dephosphorylation of the focal adhesion protein paxillin, Pyk2, Wiskott Aldrich syndrome protein (WASP)-binding protein, and Vav [60] [61]. Mice lacking PTP-PEST could not be properly analyzed due to early embryonic lethality (approximately at day 9.5). These animals, due to enhanced tyrosine phosphorylation of Cas and aberrant cytoskeletal organization, exhibited severe abnormalities in embryonic vascularization, mesenchyme formation, neurogenesis, and liver development [62]. However, mice with conditional deletion of PTP-PEST in several leukocyte subsets are viable and have been studied.

In T cells, PTP-PEST deficiency resulted in reduced secondary responses due to increased propensity of these cells to enter anergy-like states. It was at least in part a consequence of increased phosphorylation of PTP-PEST substrate PTK Pyk2, known to be important for adhesion and migration [63]. Macrophage-specific PTP-PEST-deficiency in mouse revealed the role of PTP-PEST in macrophage fusion. It resulted in specific hyperphosphorylation of the protein tyrosine kinase Pyk2 and the adaptor paxillin involved in critical events of macrophage fusion process, such as polarization, migration, and integrin-induced spreading [60]. Similar mechanism was shown in dendritic cells upon dendritic cell-specific loss of PTP-PEST. These cells exhibited hyperphosphorylation of Pyk2 and paxillin affecting their migration from peripheral sites to secondary lymphoid organs. Hence, *in vivo*

mice with dendritic cells deficient in PTP-PEST failed to fully induce T cell-dependent immune responses [64].

Moreover, PTP-PEST plays role in tumor suppression via suppression of cell survival, migration, and invasiveness. PTP-PEST controls glioblastoma cell invasion by guiding Cas to ATP-dependent protein segregase that selectively extracts ubiquitinated proteins from multiprotein complexes and targets them for degradation via the ubiquitin proteasome system [65].

Another member of this family, PEP, binds CSK, a PTK involved in inactivating Src-family kinases. Both proteins cooperate in inhibition of Src-family kinases in T cells by at the same time dephosphorylating the activation loop and phosphorylating C-terminal inhibitory tyrosine. PEP function in inhibition of T-cell activation was shown in overexpression studies with wild-type PEP in a mouse T-cell line (BI-141) [66]. Negative regulatory function of PEP was also supported by the data from PEP-deficient mice, which showed lymphadenopathy, splenomegaly, spontaneous germinal center formation, and increased effector memory T cell numbers, driven by enhanced SFK activity and TCR-mediated responses in effector memory T cells [67]. In humans a polymorphism in the non-catalytic domain of LYP (R620W) is associated with autoimmune diseases, including type 1 diabetes, rheumatoid arthritis, and systemic lupus erythematosus [68].

PTP-HSCF is the least studied member of the PEST family, identified mainly in primitive hematopoietic cells, brain and colon [53]. The role of PTP-HSCF was not elucidated to the full extent. PTP-HSCF transcript expression was found in very early hematopoietic progenitor cells and as cells differentiate it was downregulated suggesting role of this PTP in the regulation of some aspects of early hematopoietic progenitor cell biology [69]. Furthermore, PTP-HSCF was reported as tumor suppressor given important role in negative regulation of HER2 activation and following downstream events [70].

All three PEST-phosphatases bind adaptor proteins PSTPIP1 and PSTPIP2 through their conserved carboxyl-terminal homology (CTH) domains. Mutations in PSTPIP1 were identified in humans with pyogenic sterile arthritis, pyoderma gangrenosum, and acne (PAPA) syndrome and familial recurrent arthritis, two autoinflammatory diseases. The disease-causing mutations abrogate PSTPIP1 ability to bind PEST-PTPs, suggesting mutually redundant role of PEST-PTPs as negative regulators of inflammation [71].

The data discussed above provide evidence on the importance of PTPs and PTKs in leukocyte signaling, phosphorylating/dephosphorylating multiple substrates and either promoting the signaling or inhibiting it. Maintaining a healthy balance between PTK and PTP activities is important for adequate cell responses. Importantly, disruption of this equilibrium results in the conditions like immunodeficiency, autoimmunity [72] [73] or malignancy [74], which makes these molecules a perfect target for pharmacological interventions [75] [76] [77].

2.3. Membrane adaptor proteins in cell signaling

Another group of proteins important for cell signaling investigated in this work are membrane adaptor proteins. Some of them were already mentioned in the paragraphs above as binding partners of the reviewed enzymes. In contrast to these enzymes, membrane adaptor proteins are characterized by the lack of own enzymatic activity. However, this does not restrict their ability to alter key cellular decisions. They promote cell responses via different means,

employing their specific binding motifs/domains to organize signaling complexes at cellular membranes [78]. These specific motifs/domains define which components/proteins they can bind, bring together or recruit to a specific location and, consequently, which signaling pathways they regulate [79] [80]. Membrane adaptor proteins are involved in an array of biological and physiological processes. Via tyrosine or proline-containing motifs they bind enzymes essential for cell signaling and organize them into signaling complexes. Most studied examples of the domains that bind to transmembrane adaptor proteins are Src homology (SH) 2 and PTB domains binding to tyrosine phosphorylation sites and SH3 domains binding specific sequences containing proline residues [81] [82] [83]. These domains are found in many enzymes and additional cytoplasmic adapters involved in leukocyte receptor signaling and recruit these proteins to the complexes organized by membrane adaptors at plasma membrane or other membrane structures. Plasma membrane association of membrane adaptors is mediated by a transmembrane domain or one of the membrane lipid binding domains, such as pleckstrin homology (PH) or Fer kinase/CIP4 homology Bin-Amphiphysin-Rvs (F-BAR) domain [84].

The most important example from the first group is transmembrane adaptor protein Linker for activation of T cells (LAT) [85]. After TCR engagement LAT is rapidly phosphorylated by ZAP-70/SYK at its cytoplasmic tail and organizes a signaling complex critical for activation of downstream pathways [86]. It contains several key signaling molecules that bind to LAT either via SH2/SH3 domains (Grb2, Gads, PLCγ1, Cbl-b), or indirectly (SLP-76, Sos, Itk, Vav) via other adaptor molecules (i.e. Grb2, Gads) [87]. Mutant T cells lacking LAT fail to mobilize Ca^{2+} and are unable to upregulate downstream markers of activation, such as IL-2 or CD69, upon TCR stimulation. Mice deficient in this adaptor protein lack mature peripheral T cells, because their thymocytes fail to develop beyond the double-negative stage due to the early block in TCR signaling. On the other hand, they develop normal and functional population of B cells, NK cells, and platelets [88].

In myeloid cells LAT (36-kDa isoform) serves as an amplifier of FcγR-induced signal transduction. BMDM isolated from $Lat^{-/-}$ mice showed decreased phagocytosis in comparison to the wild type (WT) cells [89]. Also, essential role of LAT was demonstrated in FcεRI-mediated signaling in mast cells. LAT-deficient bone marrow–derived mast cells displayed reduced tyrosine phosphorylation of SLP-76, PLC-γ1, and PLC-γ2 and calcium mobilization following FcεRI engagement. In the absence of LAT these cells showed profound defects in activation of mitogen-activated protein kinase, degranulation, and cytokine production after FcεRI cross-linking [90].

Other transmembrane adaptors are less critical, but they still have important regulatory functions modulating signaling by membrane receptors. It is a group of more than ten proteins further extended by an array of membrane adaptors interacting with cellular membrane by means other than transmembrane domain as peripheral membrane proteins. For this thesis two proteins are particularly important, leukocyte-specific transcript 1 protein (LST1) from the transmembrane family and PSTPIP2 from the peripheral membrane group.

2.3.1. Leukocyte-specific transcript 1 protein (LST1)

LST1 protein has multiple splicing variants expressed at mRNA level, but only one isoform LST1/A, has been detected at protein level. It is also the only isoform detected across multiple mammalian species. It harbors key features of a transmembrane adaptor protein, a very short extracellular domain (including a possibly dimerizing cysteine), followed by a

transmembrane domain and a comparatively larger cytoplasmic tail. The protein lacks any domain with enzymatic activity. Moreover, LST1 is unlikely to act as a receptor per se due to its very short extracellular part. Previously, it was shown that *LST1* gene is located within MHCIII locus together with genes for TNF-α and Lymphotoxin-β [91]. Polymorphisms of human *LST1* gene that affect its gene expression and splicing, are associated with inflammatory conditions such as psoriasis, nephritis in systemic lupus erythematosus and rheumatoid arthritis, or graft versus host disease severity [92] [93] [94].

LST1/A intracellular part contains ITIM and ITIM-like motifs, making it a potential negative regulator of leukocyte receptor signaling. The ITIM and ITIM-like motifs in LST1/A are upon phosphorylation used as docking stations for SHP-1 and SHP-2 [95] [96]. As discussed above, both SHP-1 and SHP-2 were shown to be involved in the regulation of essential immune processes, controlling phagocytosis in macrophages [37] or cytokine signaling in myelopoiesis [97], respectively. These data suggest that LST1/A may play crucial role in myeloid cell signaling and hence control vital cell processes through the regulation of SHP-1 and SHP-2 phosphatases. Available data also pointed towards its role as a mediator of inflammation in gastrointestinal tract. First, a significant increase of LST1 expression was observed in intestinal epithelial and endothelial cells upon stimulation with common proinflammatory agents. Second, its expression was increased in inflamed colonic tissue from inflammatory bowel disease (IBD) patients [98].

2.3.2. Proline-serine-threonine-phosphatase-interacting protein 2 (PSTPIP2)

PSTPIP2 belongs to a superfamily of proteins harboring extended F-BAR domain [99]. F-BAR domains are characterized by compact banana-like shape and ability to bind phospholipids of cellular membranes. They are often involved in remodeling these membranes influencing membrane trafficking, cell morphology and migration [100]. They are also involved in the control of signal transduction. PSTPIP2 protein shows similarity to another F-BAR protein known as PSTPIP1. PSTPIP1 as many other members of F-BAR family proteins possesses N-terminal F-BAR domain and the C-terminal SH3 domain. The SH3 domain interacts with proline-rich motifs present in members of the WASP family and dynamin. WASP has many effects on the immune system and participates in actin remodeling, phagocytosis and cell migration [101] while dynamin-related proteins are important for endocytosis [102]. SH3 domain is absent in PSTPIP2, hence it does not interact with WASP. Instead, it possesses C-terminal tyrosine-phosphorylated sequence, which binds phosphoinositide phosphatase SHIP1 discussed above. It also binds CSK, but the binding site has not been identified yet [103]. Both PSTPIP1 and PSTPIP2 bind PEST-family phosphatases via a sequence containing conserved tryptophan residue (W232 in both cases) [104].

The mutations in both PSTPIP1 and PSTPIP2 are associated with autoinflammatory diseases in humans and/or mice. Previous reports have demonstrated that mutations in PSTPIP1 result in human PAPA syndrome (pyogenic sterile arthritis, pyoderma gangrenosum and acne) [105] and a spectrum of related autosomal dominant autoinflammatory diseases. In mice, PSTPIP2 gene is involved in murine autoinflammatory bone disorder CMO with symptoms similar to a sterile bone inflammation seen in the human SAPHO (synovitis, acne, pustulosis, hyperostosis, and osteitis) syndrome [106] and CRMO (chronic recurrent multifocal osteomyelitis) [107],.The PSTPIP2 mutations in *Pstpip2^cmo* (L98P) and *Pstpip2^Lupo* (I282N) mouse strains lead to autoinflammatory diseases with inflammatory bone resorption localized mainly to hind feet, tail, and in some reports also skin, claws and ears [108]. Bone lesions

in *Pstpip2^cmo* mice resemble those observed in SAPHO or CRMO, with both acute and chronic inflammatory bone resorption. The main difference with these diseases is the location of the lesions: long bones (limbs and clavicles) are often affected by the inflammatory process in SAPHO/CRMO patients but are spared in *Pstpip2^cmo* mice, where the inflammation is localized mainly to hind paws and tails. Interestingly, a study that involved 38 patients with SAPHO syndrome [109] did not reveal any specific *Pstpip2* variants in any of the patients studied. Frequency of an alternatively spliced form (ΔE11 isoform) of a *Pstpip2* haplotype was similar in affected patients and in healthy controls. Even though, till now this disease in human has not been associated with mutations in PSTPIP2 gene, it is believed that basic mechanisms underlying the disease development are similar in both humans and mice, therefore intensive studies are performed to investigate the mechanism behind the CMO development in the mouse model.

In *Pstpip2^cmo* mice, the point mutation in *Pstpip2* gene (L98P) results in a complete loss of detectable protein, while there are normal levels of *Pstpip2* mRNA. Absence of this protein in mice leads to elevated levels of pro-inflammatory cytokines: IL-1β, IL-6, MIP-1α, TNF-α and decreased levels of anti-inflammatory cytokines (IL-10) [110]. It was shown that neutrophils play a major role in CMO development and upon neutrophil depletion, mice remain healthy and with no bone inflammation [111].

PSTPIP2 controls autoinflammation via inhibition of two major pro-inflammatory pathways: oxidative burst that is enhanced in the *Pstpip2^cmo* neutrophils after various stimuli, and IL-1β production, shown to be increased in inflamed hind paw tissue. *In vitro* upon silica stimulation of the bone marrow cells isolated from *Pstpip2^cmo* mice, increased levels of active form of IL-1β p17 were also detected [111].

To test whether and how these pro-inflammatory pathways contribute to the disease development several studies were conducted. Firstly, mice with inactivated nicotinamide adenine dinucleotide phosphate (NADPH)-oxidase and hence absent oxidative burst in neutrophils and other phagocytes, still developed inflammation and had elevated levels of IL-1β in hind paws. On the other side, these animals showed almost no bone inflammation [111]. Secondly, IL-1β receptor deletion in *Pstpip2^cmo* mice completely prevented development of the disease. Similar results were also observed upon deletion of IL-1β [112]. Thus, while in the absence of neutrophils, IL-1β or its receptor, *Pstpip2^cmo* mice do not develop the disease, targeting NADPH-oxidase can prevent severe bone damage, but cannot resolve soft tissue inflammation [111].

PSTPIP2 interacts with several regulators of signaling. The most prominent include PEST-PTPs and SHIP1, binding of which is dependent on W232 and phosphorylated C-terminal tyrosines of PSTPIP2, respectively [103]. However, whether there is a link between these PSTPIP2 interactions and the pro-inflammatory pathways that drive disease symptoms development *in vivo* was unclear. A single study, where the interactions of PSTPIP2 were disturbed in osteoclast precursors showed how PSTPIP2 modulates osteoclast differentiation [113]. Authors cultured osteoclast precursors for 5 days with CSF-1 and RANKL, to develop multinucleated TRAP+ osteoclast-like cells. Mutant PSTPIP2 (W232A) unable to interact with PEST-type phosphatases suppressed TRAP+ osteoclast-like cell development, but was less effective at suppressing TRAP (marker of bone destruction) expression compared to osteoclast precursors expressing WT PSTPIP2. In contrast, the mutant (Y2F) with mutations in two out of the three C-terminal tyrosines forming the SHIP1 binding site lost the ability to suppress osteoclast development completely. W232A mutant was comparable with PSTPIP2 WT in its

ability to suppress osteoclast precursor (OCP) fusion, whereas the Y2F mutant, was less able to inhibit OCP fusion. Concluding that PSTPIP2 tyrosine phosphorylation is essential for its inhibition of TRAP expression and osteoclast precursor fusion, whereas interaction with PEST-type phosphatases is required for suppression of TRAP expression [113]. The effects of these mutations on the functions of neutrophils and on the disease development *in vivo* have not been studied.

2.4. Inflammation: signaling, mediators and regulation

Most signal transduction pathways amplify the incoming signal via signaling cascades [114] that transduce extracellular signals from a diverse range of stimuli and elicit the appropriate physiological response. One of the critical responses vital for an organism that is constantly exposed to invading pathogens is inflammation. It is indispensable for fighting the infections and for subsequent tissue repair [115]. PAMPs initiate a cascade of signals that alert neutrophils, macrophages and other innate immune cells to an ongoing infection [116]. As the first line of defense, these cells phagocytose the pathogen and produce additional cytokines, chemokines and pro-inflammatory mediators to recruit and activate more innate immune cells and cells of adaptive immunity.

Neutrophils are among the first cells that enter the infected tissue. They develop in the bone marrow from granulocyte–monocyte progenitors under the control of granulocyte colony-stimulating factor (G-CSF). Once fully mature, neutrophils enter the circulation from where they can migrate to the inflammation sites [117]. Neutrophil extravasation, migration towards the site of infection and neutralization of invading microorganisms requires multiple receptors, including various chemokine and chemoattractant receptors, adhesion receptors (such as selectins/selectin ligands and integrins), Fc-receptors, Toll-like receptors (TLRs) and C-type lectins. These receptors allow neutrophils to sense and locate the pathogen and/or inflammatory environment and mount an appropriate response [118] [119]. They are equipped with several potent antimicrobial mechanisms, including phagocytosis, neutrophil extracellular traps (NET) generation, release of toxic granules, ROS, and pro-inflammatory cytokines (IL-1β, TNF-α) [120] [121] [122]. These cytokines mediate further development of inflammation, activating cells by binding cognate receptors and further amplifying a wide variety of effects associated with innate immunity to help the organism to fight the infection [123, 124] [125].

Neutrophils also contribute to the resolution of inflammation by phagocytosing debris, limiting NETosis, and helping repair damaged tissues. Phagocytosis of apoptotic neutrophils also exerts anti-inflammatory effects on macrophages. However, these processes are disturbed during chronic inflammation that keeps neutrophils activated, releasing NETs, and exacerbating the tissue damage [126]. Emerging evidence suggests that unresolved neutrophil-mediated inflammation plays an important role in several chronic diseases, such as atherosclerosis, diabetes mellitus, nonalcoholic fatty liver disease and autoimmune disorders [127] [128]. Although properly controlled and time-limited inflammation is a vital process for the host, unresolved, chronic inflammation towards persistent agent can be harmful [129]. Severe or repetitive tissue injury that accompany chronic inflammation and failure to adequately contain or eliminate the inciting factors can lead to a chronic wound-healing response, with continued tissue damage, repair and regeneration, excessive accumulation of fibrous connective tissue components of the extracellular matrix and, ultimately, fibrosis [130] [131].

Inflammation can also develop in the absence of microorganisms, as the result of injury or exposure to toxic agents. Such an inflammation, which develops in the absence of invading microorganisms, is termed "sterile inflammation". It helps the body prevent infection of injured tissue and start the healing processes. Similar to the inflammation triggered by infection, sterile inflammation also involves recruitment of innate immune cells, particularly, neutrophils and macrophages and production of pro-inflammatory cytokines like TNF and IL-1. It has also similar negative side effects [129].

Sterile inflammation was shown to develop and persist in multiple diseases. Constant activation of alveolar macrophages by repeated inhalation of irritants may result in interstitial lung fibrosis [132]. Myocardial infraction followed by restoration of blood flow leads to granulocyte infiltration, enhanced production of ROS and inflammatory responses to necrotic cells [133]. Sterile inflammation is also implicated in gout, where acute neutrophilic infiltration in the joints caused by deposits of monosodium urate crystals results in chronic inflammation, fibrosis and cartilage destruction [134]. Understanding the molecular mechanisms of sterile inflammation is important for the development of treatment strategies and identification of disease markers.

The development of inflammation caused either by a pathogen or sterile agent is similar, and may involve a similar network of receptors. The mechanism of the inflammatory response to a pathogen involves sensing of the PAMPs carried or produced by microbes via pattern recognition receptors (PRRs) [135]. Engagement of these receptors activates NF-κB, MAPK and/or type I interferon pathways that trigger the production of pro-inflammatory cytokines, chemokines and other mediators of inflammation. Upon severe tissue damage cells often die by necrotic cell death allowing escape of intracellular material from the cell, such as chromatin-associated protein high-mobility group box 1, heat shock proteins, and purine metabolites such as adenosine triphosphate (ATP) and uric acid [136]. These cellular endogenous factors, which under healthy physiological conditions are hidden intracellularly from recognition by the immune system, have functions similar to PAMPs in activating pro-inflammatory pathways upon their release and are referred to as damage-associated molecular patterns (DAMPs). Hence, the presence of DAMPs in the extracellular space indicates tissue injury.

One of the mediators of sterile inflammation is IL-1β. Release of this cytokine by macrophages results in upregulation of adhesion molecules on endothelial cells, important for the recruitment of neutrophils and monocytes and for the induction of additional pro--inflammatory mediators [137]. In gout, elevated IL-1β production leads to joint inflammation and destruction of the bones [138].

IL-1β secretion involves several steps. The first step includes production of its inactive precursor pro-IL-1β and upregulation of inflammasome components typically triggered by PRR. The second step involves activation of inflammasomes containing caspase-1, which cleave pro-IL-1β, generating its biologically active form. Caspase-1 also cleaves gasdermin D (GSDMD) triggering its translocation to the plasma membrane to form round, pore-like structures that are used to release IL-1β [139]. When these pores are present in large numbers they also cause inflammatory cell death known as pyroptosis [140]. It is important to mention that IL-1β precursor can also be processed by other proteases, such as Caspase-8 or those present in neutrophil granules, including elastase, cathepsins, and proteinase-3 [141] however with less efficiency [142].

Activation of inflammasomes is triggered by sensor proteins, majority of which are from NOD-like receptor family. They can directly sense microbial products, or indirectly microbial activities or cellular stress. The most studied of these is nucleotide-binding oligomerization domain, leucine rich repeat and pyrin domain containing 3 (NLRP3). Its activation is triggered by various forms of cellular stress via unclear molecular mechanism. NLRP3 activators include ATP, potassium efflux, lysosomal damage or ROS production. ATP binds to purinergic receptor P2X7, which leads to the opening of an ATP-gated cation channel that induces K^+ efflux that is further sensed by NLRP3. ATP and lysosomal damage may occur during necrosis and activate inflammasome. ROS production by neutrophils important for pathogen destruction in high levels can lead to oxidative stress, cell death and necrosis, also resulting in NLRP3 stimulation [143] [144]. NLRP3 inflammasome is associated with various sterile inflammatory diseases as it is able to respond to sterile stimuli. Deletion or inhibition of NLRP3 reduced levels of tissue infiltration by neutrophils or macrophages due to decreased levels of IL-1β [145] [146]. Conversely, genetic defects leading to constitutive NLRP3 inflammasome activation are the cause of autoinflammatory diseases [147].

2.4.1. Autoinflammatory diseases driven by IL-1β

Autoinflammatory disorders are characterized by sterile tissue inflammation and inflammatory tissue damage mediated solely by cells of innate immune system, in particular monocytes, macrophages, and/or neutrophils. Pathways related to PRR signaling, including NF-κB and inflammasome activation, type I interferon signaling and immuno-proteasome are involved in the pathology of autoinflammatory diseases causing the respective pathologies [139]. This group of diseases is characterized by inflammatory flares involving combined variations of manifestations mainly in the skin, musculoskeletal and gastrointestinal systems that develop in the absence of autoantibodies or autoreactive T lymphocytes [148]. Autoinflammation is a systemic disease affecting multiple organs, where tissues are infiltrated with innate cells that produce and release excessive amounts of pro-inflammatory cytokines, including TNF-α and IL-1β, in response to innocuous signals causing collateral damage to the surrounding tissues. The treatment strategies include various non-specific anti-inflammatory treatments or biological treatments targeting dysregulated molecular mechanism(s) [149].

Among the best studied are autoinflammatory diseases driven by dysregulated IL-1β production. IL-1β is pro-inflammatory cytokine that plays key roles in acute and chronic inflammatory and autoimmune disorders [150]. Indeed a number of inflammatory disorders can be treated by targeted anti-IL-1 therapy [151]. The dysregulation in IL-1β production can be caused by enhanced activity of IL-1β (and IL-18) processing platforms inflammasomes (inflammasomopathies) or dysregulation of other mechanisms regulating production of IL-1β. Inflammasome-triggered diseases include cryopyrin-associated autoinflammatory syndromes (CAPS) caused by gain-of-function mutations in NLRP3 leading to constitutive activation of the NLRP3 inflammasome (i.e. extremely low threshold for activation) and excessive secretion of active IL-1β [152]. Another pathology within this group called Familial Mediterranean fever (FMF) is caused by a mutation in another inflammasome protein pyrin, a part of so-called pyrin inflammasome. Gain-of-function mutations in pyrin result in constitutive activation pyrin inflammasome and IL-1β secretion [153]. PAPA syndrome in humans is rare genetic disorder caused by mutation in the gene of adaptor protein *PSTPIP1*. It was discovered that the PAPA-inducing mutation in *PSTPIP1* results in aberrant pyrin inflammasome activation, overproduction of IL-1β, driving development of pyogenic inflammation of the skin and joints in patients [71].

Another type of autoinflammatory disease includes the disorder caused by mutations of IL1RN (interleukin-1 receptor antagonist) with prominent involvement of skin and bone, resulting in a condition called deficiency of IL-1 receptor antagonist (DIRA). IL-1RA deficiency results in uncontrolled IL-1α, IL-1β and NF-κB signaling [154]. Pro-inflammatory cytokine IL-1 drives another inflammatory bone disease Majeed syndrome. This extremely rare multi-system inflammatory disorder is caused by mutation in the gene encoding the phosphatidic acid phosphatase LIPIN2. Disruption of the activity of Lipin2 results in enhanced activation of the NLRP3 inflammasome leading to increased production of IL-1β and autoinflammation [155].

Some of the IL-β mediated diseases, including DIRA, Majeed and PAPA syndromes are accompanied by sterile bone inflammation and autoinflammatory bone damage. Sterile bone inflammation is also characteristic of another autoinflammatory disease CRMO. This disease is sporadic, characterized by inflammatory bone lesions affecting almost any site of skeleton. It seems to be driven by an imbalance between pro- and anti-inflammatory cytokine expressions in monocytes [156], however the exact molecular pathophysiology of CRMO remains elusive. To better understand the mechanisms driving this disease, several mouse models were developed. Of these the best studied is the already mentioned *Pstpip2^cmo* mouse strain. These mice develop disease described as CMO, showing a phenotype similar to the symptoms of CRMO, mainly a sterile inflammation of the bones and surrounding soft tissue. It is predominantly localized to the hind feet and tail. As mentioned above, IL-1β and ROS production by neutrophils are the crucial steps in disease development [111].

Extensive research was performed to identify additional factors and mechanisms contributing to the CMO development [108] employing *Pstpip2^cmo* mice deficient in various additional molecules potentially involved in the disease pathophysiology in these mice. It demonstrated that inflammasome associated molecule absent in melanoma 2 (AIM2), receptor-interacting serine/ threonine protein kinase 3 (RIPK3), and caspase recruitment domain–containing protein 9 (CARD9) are each non-essential for osteomyelitis initiation in *Pstpip2^cmo* mice, whereas genetic deletion of SYK completely abrogated the disease phenotype [157]. As noted above, SYK is an essential component of ITAM-dependent signaling. In neutrophils, this type of signaling is employed by several receptors, including Fc receptors, integrins, selectin ligands (PSGL-1), paired immunoglobulin-like receptors /leukocyte immunoglobin-like receptors, TARM1, TREM-1/2, dectins and other C-type lectins [158] [159] [160] [161] [162]. Neutrophils deficient in SYK kinase fail to initiate respiratory burst, degranulation, or spreading in response to proinflammatory stimuli [163].

Additional critical proteins, deficiencies of which ameliorate the disease include caspase-1 and caspase-8. In their case, only combined deficiency of both proteins attenuates CMO, suggesting that they have redundant roles in cleaving IL-1β and promoting this disease [164]. Genetic data also suggest additional involvement of neutrophil proteases known to process pro-IL-1β to active IL-1β. This redundancy in pro-IL-1β processing pathways raises the possibility that some upstream mechanism, such as enhanced activity of NF-κB leading to increased levels of pro-IL1β could be a key element in the CMO development. Increased amounts of pro-IL-1β could then be processed by any of these redundant pathways.

2.4.2. WBP1L (WW domain binding protein 1-like)

The last adaptor protein discussed in this thesis is WW domain binding protein 1-like (WBP1L, also known as Outcome Predictor in Acute Leukemia 1 (OPAL1)) of the

transmembrane group of membrane adaptor family. Published data brought attention to this adaptor protein as a potential novel prognostic marker. *WBP1L* was identified among the top discriminating genes highly predictive of outcome in 254 patients with childhood acute lymphoblastic leukemia (ALL). Interestingly, WBP1L was overexpressed mainly in ALL cells positive for the ETV6-RUNX1 gene fusion that correlates with favorable prognosis in the total ALL group. [165] [166]

Further prognostic importance of WBP1L expression was investigated in 2 independent cohorts of children with ALL treated on Cooperative Study Group for Childhood Acute Lymphoblastic Leukemia (n = 180) and St Jude Total Therapy (n = 257), i.e. two independent protocols with similar chemotherapeutic agents. WBP1L expression was found to be 2.8-fold higher in ETV6-RUNX1–positive ALL compared with ETV6-RUNX1–negative ALL in both cohorts. However, it was not consistently associated with other favorable prognostic indicators, supporting the interpretation that this marker may not be an independent prognostic feature in childhood ALL [167]. Interestingly, another study consistently discovered an association between WBP1L expression and ETV6-RUNX1 chromosomal translocation [168]. ETV6-RUNX1 is a fusion gene, which despite having oncogenic properties, it has also been correlating with favorable prognosis of B-cell precursor ALL [169]. This fact could probably explain the initial observation of the correlation of WBP1L expression and similar outcome. These data also raised the possibility that WBP1L may is some way functionally contribute to the good prognosis of ETV6-RUNX1^{+} leukemia. However, despite the promising value, almost nothing was known about the function of WBP1L.

3. AIMS OF THE WORK

Aim 1: Available data on PSTPIP2 adaptor protein highlight the importance of neutrophils in the development of CMO. They also describe the main binding partners (PEST-PTPs, SHIP1) and crucial pathways for the disease development. However, no research has been done to determine whether these negative regulators of signaling contribute to the disease prevention and what signaling pathways they control within CMO. The major goal of my doctoral research was to determine the role of PSTPIP2 interactions with PEST-PTPs and SHIP1 via the analysis of mutant mouse strains, where these interactions were abrogated. This included three specific tasks:

- Monitoring of the generated mouse strains for the symptoms of autoinflammation to find out whether abrogation of PSTPIP2 interactions with PEST-PTPs or SHIP1 are sufficient to initiate the disease development.
- Analysis of ROS and IL-1β production to verify how PSTPIP2 interactions with PEST-PTPs and SHIP1 control these crucial inflammatory processes.
- Investigation of neutrophil infiltration and levels of chemokines involved in neutrophil recruitment at the site of inflammation in the mutant mice and if possible, identification of their source.

Aim 2: To investigate the involvement of Src-family kinases in the development of the CMO disease via analysis of *Pstpip2^{cmo}* mice deficient in their major positive regulator protein tyrosine phosphatase CD45.

Aim 3: To contribute to the studies of *in vivo* functions of transmembrane adaptor proteins LST1 and WBP1L in the regulation of leukocyte development and functions.

4. RESULTS AND DISCUSSION

4.1. Molecular interactions of adaptor protein PSTPIP2 control neutrophil-mediated responses leading to autoinflammation

4.1.1. Generation of PSTPIP2 mutant mouse strains

We sought to describe the role of PSTPIP2 interactions with its most prominent binding partners, PEST family phosphatases (PEST-PTPs) and phosphoinositide phosphatase SHIP1, in the molecular pathways leading to CMO [103]. Using CRISPR/Cas9 technology [170], we generated mutant mouse strains harboring mutations in PSTPIP2 that abrogate these interactions. To prevent interaction with PEST phosphatases, we mutated their binding site W232 and replaced it with alanine, resulting in the mouse strain $Pstpip2^{W232A}$. To abrogate SHIP1 binding we had to introduce mutations in the C-terminal tyrosines (Y323, Y329, Y333), that provide binding sites for SHIP1 upon phosphorylation. We used several approaches to generate these mutant mice, however, only two were successful and provided mutants that were used for the future analysis. These were, a strain where a 17 bp deletion resulted in a stop codon immediately after Y323 ($Pstpip2^{\Delta C\text{-}term}$) and strain where Y323 is replaced with phenylalanine ($Pstpip2^{Y323F}$). In addition, we generated mouse strain with complete loss of PSTPIP2 expression ($Pstpip2^{-/-}$).

Interestingly, W232A mutation resulted in lower expression of PSTPIP2 protein in neutrophils to the levels observed in $Pstpip2^{+/-}$ heterozygotes. This observation was noted previously using a cell line harboring equal mutation [113]. Hence, we included $Pstpip2^{+/-}$ mice in subsequent analysis to monitor for the effects of reduced PSTPIP2 expression on the phenotype of $Pstpip2^{W232A}$ mice. Other two mouse strains harboring mutations introduced in the C-terminus of the protein had PSTPIP2 expression level comparable to neutrophils isolated from wild-type mice. Predictably, no PSTPIP2 protein was detected in $Pstpip2^{cmo}$ and $Pstpip2^{-/-}$ neutrophils.

4.1.2. PSTPIP2 mutations prevent binding of PTP-PEST and SHIP1

The effect of the introduced mutations on PSTPIP2 interactome was tested by immunoprecipitation of PSTPIP2 from bone marrow cells isolated from the aforementioned mouse strains. PTP-PEST, SHIP1, and (phospho-)PSTPIP2 were detected in the immunoprecipitates by immunoblotting.

Deletion of the PSTPIP2 C-terminus after Y323 resulted in the loss of phosphorylation of PSTPIP2 protein and consequent loss of SHIP1 binding without affecting PTP-PEST interaction, while single Y323 mutation did not perturb SHIP1-PSTPIP2 interaction. Furthermore, binding of PTP-PEST was abrogated with W232A mutation while no effect on phosphorylation status was noted, suggesting that PEST-PTPs do not regulate PSTPIP2 phosphorylation.

4.1.3. Disruption of PSTPIP2-PTP-PEST interaction in vivo leads to the development of the osteomyelitis symptoms

To evaluate the function of PSTPIP2 interactions in the development of osteomyelitis, we monitored mutant mice for the occurrence of visible symptoms of the disease [110]. Mice deficient in PSTPIP2 protein, $Pstpip2^{-/-}$ and $Pstpip2^{cmo}$ were the first to develop symptoms within 8 weeks after birth. Among all the other mutants, only

Pstpip2^{W232A} strain developed visible symptoms. However, disease seemed to appear later (14-16 weeks of age), was not 100% penetrant, and showed milder symptoms than in *Pstpip2^{cmo}*. In addition, part of the animals remained asymptomatic throughout the entire 42 weeks of observation. Importantly, this phenotype did not result from lower expression of the PSTPIP2 protein, as *Pstpip2^{+/-}* mice did not develop any visible symptoms of osteomyelitis.

These observations were in line with microcomputerized tomography (μCT) data of the hind paws of these mice. Only *Pstpip2^{cmo}*, *Pstpip2^{-/-}*, and *Pstpip2^{W232A}* mice showed significantly elevated bone fragmentation, which in *Pstpip2^{W232A}* was milder than in the other two strains. On the contrary, animals carrying mutations in the C-terminus (*Pstpip2^{ΔC-term}*, *Pstpip2^{Y323F}*) had no signs of bone damage. Typical osteomyelitis symptoms also include soft tissue swelling. Soft tissue volume was significantly elevated only in *Pstpip2^{cmo}* and *Pstpip2^{-/-}* mice, but not in the other mutants, including *Pstpip2^{W232A}*. The reason why we failed to detect increase in the soft tissue volume in *Pstpip2^{W232A}* mice, despite clearly visible enlargement of inflamed toes is not entirely clear. It is possible that the affected area was too small (mostly a single inflamed toe or no visual symptoms at all at the time of measurement) or that the inflammation was limited only to the bones. Taken together, inflammation that involves visible symptoms or symptoms detected by μCT is controlled via interaction of PSTPIP2 and PTP-PEST, while, binding of SHIP1 is not critical and even in the absence of SHIP1 binding, PSTPIP2 is still able to prevent detectable inflammatory tissue damage.

4.1.4. Differential control of ROS and IL-1β production by PSTPIP2 binding partners

Next, we focused on the mechanisms responsible for the development of the symptoms in *Pstpip2^{W232A}* mice. These include IL-1β and ROS production pathways known to be altered in neutrophils of *Pstpip2^{cmo}* mice. IL-1β is known to trigger inflammation, while ROS contribute to the bone damage [111].

Following this notion, we aimed to evaluate whether and how PSTPIP2 binding partners control these pathways to provide an explanation for the differences in the disease severity among our mutants. As expected, bone marrow cells isolated from PSTPIP2 deficient strains *Pstpip2^{cmo}* and *Pstpip2^{-/-}* showed substantially deregulated ROS production upon silica stimulation. Very interestingly, equally deregulated ROS levels were observed also in the bone marrow cells from *Pstpip2^{W232A}* mutants. In contrast, cells with mutations in PSTPIP2 C-terminus, *Pstpip2^{ΔC-term}*, *Pstpip2^{Y323F}* as well as *Pstpip2^{+/-}* showed only minor elevation of ROS production compared to WT bone marrow cells.

Next, we analyzed the levels of IL-1β in the inflamed tissues of hind paws, the sites of disease manifestation [171], by enzyme-linked immunosorbent assay (ELISA). In contrast to ROS production, we detected significantly increased levels of IL-1β in the lysates prepared from hind paws of all mutant strains (*Pstpip2^{cmo}*, *Pstpip2^{-/-}*, *Pstpip2^{W232A}*, and *Pstpip2^{ΔC-term}*). Although in the strains, where the interaction of PSTPIP2 with PTP-PEST or SHIP1 was abolished (*Pstpip2^{W232A}* and *Pstpip2^{ΔC-term}*, respectively) this elevation was significantly lower than the one observed in PSTPIP2 fully deficient strains *Pstpip2^{cmo}* and *Pstpip2^{-/-}*. The same pattern was also observed when the active form of IL-1β p17 was detected in these lysates by Western blot and when production of IL-1β precursor, pro-IL-1β was induced *in vitro* by LPS stimulation of bone marrow cells or purified neutrophils.

These affirming observations show comparable control of IL-1β production by both PEST-PTPs and SHIP1, while the control of the oxidative burst is dominantly regulated by PEST-PTPs.

These data suggest that both binding partners contribute to the suppression of crucial signaling pathways during autoinflammation. However, only the loss of PSTPIP2-PEST-PTP binding in $Pstpip2^{W232A}$ mice results in the development of visual disease symptoms. It is likely due to the dominant role of PEST-PTPs in the control of oxidative burst, previously shown to be crucial for inducing inflammatory bone damage in $Pstpip2^{cmo}$ mice [111]. However due to the substantially milder dysregulation of IL-1β production in $Pstpip2^{W232A}$ mice, the overall symptoms are also milder. Generation of the mouse model with simultaneous loss of both binding sites (W232 and C-terminal tyrosines) in PSTPIP2 may result in similar deregulation of IL-1β production as under the full PSTPIP2 deficiency with the development of the same visual symptoms. However, currently, such a model is not available. It is also possible that some other binding partners or features of PSTPIP2 are contributing to the control of inflammation in addition to PEST-PTPs and SHIP1 that we are not aware of at the moment.

In conclusion, we can hypothesize that abrogation of PSTPIP2-PEST-PTP or PSTPIP2-SHIP1 interactions results in relatively mild dysregulation of IL-1β production by neutrophils, which in itself is asymptomatic. This phenotype is transformed to a symptomatic disease by increased levels of ROS observed only in mice lacking PSTPIP2-PEST-PTP interaction. In line with this statement, previously published data showed that ROS production is critical for the bone damage in mice lacking PSTPIP2 but is not required for enhanced IL-1β production and soft tissue inflammation. In agreement with this notion, we have not detected soft tissue swelling in hind paws of $Pstpip2^{W232A}$ mice, suggesting that dominant role of increased ROS production is in triggering inflammation of the bone, but not of the surrounding soft tissue. These data also support the idea of exploiting NADPH oxidase as a potential pharmacological target in treatment strategies for inflammatory bone diseases in humans.

4.1.5. Neutrophil recruitment to the site of inflammation under control of PTP-PEST-PSTPIP2 interaction

It was previously published that neutrophils accumulate at the site of inflammation in $Pstpip2^{cmo}$ mice [172]. Therefore, to see whether milder symptoms of the disease in $Pstpip2^{W232A}$ mice are still accompanied by neutrophil infiltration and to compare it to the mutant without the visible symptoms of the disease, $Pstpip2^{\Delta C-term}$, we assessed the neutrophil infiltration via detection of neutrophil markers elastase and Ly6G in the hind paw lysates by Western blot. We included both symptomatic and asymptomatic $Pstpip2^{W232A}$ mice in this analysis. We have detected increased presence of neutrophil markers in hind paws from $Pstpip2^{cmo}$ and $Pstpip2^{-/-}$ mice. Strikingly, we detected increase in neutrophil markers also in the hind paws of $Pstpip2^{W232A}$ mice, regardless of the symptom presence (although in asymptomatic mice the increase was less strong). However, no increase in these markers was present in $Pstpip2^{\Delta C-term}$ mice. This observation suggests that PEST-PTPs regulate neutrophil accumulation in the inflamed tissues and also that neutrophil infiltration likely precedes the symptom appearance.

Next, we sought to find out how are the neutrophils attracted to the sites of sterile inflammation in our mouse strains. We first focused on chemokines as neutrophil

chemoattractants and IL-17 which controls their expression at the site of inflammation [173] [174] [175]. Increased IL-17A/F levels were detected in the hind paw lysates from $Pstpip2^{cmo}$ mice, but no alternations were detected in $Pstpip2^{W232A}$ nor in $Pstpip2^{\Delta C\text{-}term}$ mice, suggesting that IL-17A/F may mediate the neutrophil recruitment in CMO mice but not in $Pstpip2^{W232A}$ mice. Next, hind paw lysates were tested for the presence of the most prominent chemokines involved in neutrophils recruitment to the site of inflammation, CCL3 (MIP-1α), CXCL1 (KC), and CXCL2 (MIP-2) [176] via ELISA. While we noted increased concentrations of all aforementioned chemokines in $Pstpip2^{cmo}$ mice, only CXCL2 was significantly upregulated in $Pstpip2^{W232A}$ mice and none in $Pstpip2^{\Delta C\text{-}term}$. This data suggest that initial recruitment of neutrophils could be under the (sole) control of CXCL2. As the disease progresses, the ongoing inflammation may promote secondary expression of IL-17 and additional chemokines. Next, we asked what could be the source of CXCL2 in the inflamed tissue. Data from ImGen Consortium show high expression of CXCL2 in thioglycolate induced neutrophils. Hence, we hypothesized that neutrophils could be the source of this chemokine in $Pstpip2^{cmo}$ and $Pstpip2^{W232A}$ mice. We isolated neutrophils from the hind paws and measured their $Cxcl2$ mRNA levels. Remarkably, only neutrophils isolated from the hind feet of the mutant mice that develop autoinflammatory disease $Pstpip2^{cmo}$ and $Pstpip2^{W232A}$ had similar substantially increased levels of $Cxcl2$ mRNA. No difference from WT mice was noted for $Pstpip2^{\Delta C\text{-}term}$ neutrophils. Collectively, these data indicate that during the development of the disease, neutrophils are fueling their initial own recruitment via a positive feedback loop driven by production of CXCL2, ongoing inflammation than triggers expression of additional chemokines that further support neutrophil infiltration of inflamed tissues. This may be also assisted by IL-17 and chemokine expression triggered by this chemokine. However, in $Pstpip2^{W232A}$ mice, none of these secondary events is required for the symptom development.

Our data also raised an interesting question of what makes the regulation of CXCL2 expression different from the other chemokines (CXCL1, CCL3) in $Pstpip2^{W232A}$ mice. All are known to be involved in neutrophil recruitment. Similar to pro-IL-1β, expression of all three chemokines is controlled by transcription factor NF-κB [177] [178] [179] [157]. However only the expression of CXCL1 and CCL3 are negatively regulated by activating transcription factor 3 (ATF3), itself a target of NF-κB. Hence, it is possible that under the low level of NF-κB activity, ATF3 keeps CXCL1 and CCL3 loci silent and only CXCL2, which is not regulated by ATF3 [180] [181] [182], can be expressed and drive neutrophil recruitment. As the inflammation progresses, signaling by pro-inflammatory cytokines and mediators overcomes inhibition by ATF3 and CXCL1 and CCL3 can join the response. Similar observation was described in [180].

Thus, obtained data suggested that production of neutrophil-attracting chemokines is the third critical pathway (in addition to the production of IL-β and ROS) that drives CMO disease development. It allows neutrophils to create a positive feedback loop propagated further via CXCL2, amplifying neutrophil response and recruitment, exacerbating (in collaboration with IL-1β) production of additional CXCL2 and other chemokines and propelling the disease to its symptomatic stage.

Above, I hypothesized that at mild level of IL-1β dysregulation in $Pstpip2^{W232A}$ and $Pstpip2^{\Delta C\text{-}term}$ mice, increased ROS production determines the outcome. However, it is very likely, that chemokine production, also under the control of PSTPIP2-bound PEST-PTPs, makes additional key contribution. The network of chemokines together with IL-17 may be

important as potential pharmacological targets/biomarkers in similar diseases in humans. However, to properly address their role, it is necessary to generate mice double deficient in PSTPIP2 and chemokines/chemokine receptors or other critical components of these pathways.

4.2. The receptor-type protein tyrosine phosphatase CD45 promotes onset and severity of IL-1β-mediated autoinflammatory osteomyelitis

Previous publications revealed two potentially important mechanisms in the development of sterile osteomyelitis. Firstly, it was shown that the composition of microbiota affects the disease development. These data suggested potential involvement of TLR signaling in CMO [183]. Secondly, SYK was shown to be required for the initiation of sterile osteomyelitis in *Pstpip2^cmo^* mice [157]. This finding rather suggested that receptors signaling through ITAMs (immunoreceptor tyrosine-based activating motifs) could be part of the disease triggering mechanism.

ITAMs are typically phosphorylated by SFKs. Their phosphorylation leads to the recruitment of SYK, which further propagates the signal. Due to their involvement in ITAM phosphorylation, we hypothesized that SFKs could be involved in the CMO development in our mouse model. SFKs can be found in two main conformations. The closed inactive conformation is maintained via intramolecular interaction of their own SH2 domain with their C-terminal negative regulatory phosphotyrosine, inducing changes to the kinase domain resulting in the suppression of catalytic activity. De-phosphorylation of the C-terminal tyrosine allows the kinase to assume an active conformation. It is mainly performed by CD45 protein tyrosine phosphatase, which is the major positive regulator of SFKs in leukocytes [184]. To investigate the role of SFKs in CMO disease development we could not use the typical approach of inactivating SFK genes in *Pstpip2^cmo^* mice, since too many largely redundant members of Src family are expressed in neutrophils. Instead, we decided to inactivate *Ptprc* gene coding for their major positive regulator CD45. This was expected to lead to the suppression of majority of SFK activity in leukocytes.

4.2.1. Essential role of CD45 in CMO development, while MyD88- and TRIF-mediated signaling are dispensable

To investigate the effect of TLRs and SFKs on the development of CMO we crossbred *Pstpip2^cmo^* mouse strain with mice where genes coding for MyD88 or TRIF, a key signal transducers downstream of TLRs were inactivated or with *Ptprc^−/−^* mice to abolish CD45 expression. This way we could compare the effects of TLR-dependent and SFK-dependent pathways on CMO development. In case of MyD88, we could not use whole body MyD88 knock out because of its involvement in IL-1 receptor signaling. Therefore, we employed transplantation of *Pstpip2^cmo^*/MyD88 deficient bone marrow cells into WT recipients, since the CMO disease development does not require of IL-1R signaling in leukocytes (only IL-1R on radioresistant cells is required [185]).

Monitoring of the generated *Pstpip2^cmo^* mice deficient in MyD88 or TRIF adaptor proteins revealed that they had no influence on the course of autoinflammatory osteomyelitis symptom development. Both strains had symptoms identical to *Pstpip2^cmo^* mice, leading to a conclusion that MyD88/TRIF-mediated signaling does not contribute to CMO development. On the other hand, visual monitoring of *Pstpip2^cmo^*/*Ptprc^−/−^* mice showed significantly delayed development of symptoms. Moreover, part of the mice remained healthy throughout the whole period of monitoring. Further analysis of *Pstpip2^cmo^*/*Ptprc^−/−^* mice using μCT scans of hind paws demonstrated that bone damage was significantly lower than in *Pstpip2^cmo^* mice, though still present. Collectively these data suggested that tyrosine phosphorylation mediated

signaling regulated by CD45 rather than MyD88/TRIF dependent signaling is responsible for CMO development.

4.2.2. SFK phosphorylation in *Pstpip2^{cmo}* and *Pstpip2^{cmo}/Ptprc$^{-/-}$* mice

As mentioned above, tyrosine phosphatase CD45 is a major SFK regulator. Of the SFKs expressed in neutrophils, three are considered the most important, including LYN, HCK, and FGR [186]. Next, we assessed the phosphorylation of their inhibitory tyrosines in bone marrow cells and neutrophils from WT and mutant mice. As expected, lysates of bone marrow cells and neutrophils displayed increased phosphorylation of inhibitory tyrosine of HCK and LYN upon CD45 deletion, while FGR was not affected by CD45 deficiency. PSTPIP2 was shown to interact with CSK, a kinase responsible for phosphorylating C-terminal SFK tyrosine. Surprisingly, the absence of PSTPIP2 did not alter phosphorylation of any of the SFKs investigated. These data demonstrated that on the global scale, PSTPIP2 does not regulate SFK activity despite the interaction with CSK.

4.2.3. CD45 deficiency attenuates IL-1β production by neutrophils, but has no effect on oxidative burst

Next, we investigated how CD45 deficiency affects major pathways involved in CMO development in *Pstpip2^{cmo}* mice, including ROS and IL-1β production. Cells isolated from *Pstpip2^{cmo}* and *Pstpip2^{cmo}/Ptprc$^{-/-}$* mice both showed substantially increased superoxide levels upon silica or fMLP challenge. Since ROS were increased to a similar extent, and no significant difference between *Pstpip2^{cmo}* and *Pstpip2^{cmo}/Ptprc$^{-/-}$* was detected, we concluded that CD45 does not regulate to the production of superoxide during sterile inflammation.

Strikingly, *Pstpip2^{cmo}/Ptprc$^{-/-}$* bone marrow cells showed significantly reduced levels of active IL-1β p17, a main driver of the disease upon activation of inflammasome by silica particles. Moreover, we observed substantially reduced IL-1β levels *in vivo* in the footpads of *Pstpip2^{cmo}/Ptprc$^{-/-}$* mice when compared with *Pstpip2^{cmo}*. On the other hand, in LPS and silica-stimulated purified neutrophils, we failed to detect any IL-1β p17. We could only detect an alternative form of active IL-1β p21 known to be generated via cleavage of pro-IL-1β by neutrophil proteases. The levels of IL-1β p21 in *Pstpip2^{cmo}/Ptprc$^{-/-}$* neutrophils were reduced compared to *Pstpip2^{cmo}* neutrophils.

Even though silica is a commonly used activator of inflammasome *in vitro*, it is very likely not involved in the CMO disease development in vivo. The agent activating inflammasome during sterile inflammation in *Pstpip2^{cmo}* mice is not known. Moreover, NLRP3 inflammasome containing Caspase-1 plays a redundant role with Caspase-8-dependent mechanism in the development of CMO and partially also with neutrophil proteases [185] [171]. This led us to hypothesize that dysregulation may happen at the level of pro-IL-1β precursor synthesis rather than its processing. Indeed, upon stimulation with relatively low concentration of 10 ng/ml LPS, we detected a significantly higher pro-IL-1β production in *Pstpip2^{cmo}* bone marrow cells and neutrophils when compared to WT cells. This altered production of pro-IL-1β was attenuated by CD45 deficiency. The same results were obtained upon crosslinking of Fc receptors on both bone marrow cells and neutrophils [187]. These observations changed our understanding of which step in the proinflammatory pathway leading to IL-1β production is altered in *Pstpip2^{cmo}* mice and shifted our attention from possible dysregulation of Caspase-1 and Caspase-8 containing inflammasomes to an upstream step of pro-IL-1β precursor generation as a major control point, dysregulation of which drives the

disease in *Pstpip2^cmo* mice. The reason why this was missed in previously published work is probably in the higher LPS concentrations used in the earlier studies to induce pro-IL-1β production, under which the differences are not observed. However, the low-level activation might better reflect the situation in vivo, where pro-IL-1β production may be driven by less powerful signals than high concentrations of LPS.

Taken together our data and previously published work show the involvement of protein tyrosine phosphorylation-dependent pathway in the development of CMO in our mouse model. Involvement of both SFKs and SYK suggests that receptors containing ITAMs can potentially play a crucial role within the development of CMO. There are multiple such receptors present in neutrophils (see chapter 3.4.1. above). Engagement of one or more of these receptors may lead to pro-IL-1β synthesis. In the absence of PSTPIP2, this signaling is enhanced, resulting in hyperproduction of pro-IL1β and disease initiation. Interestingly, despite being involved in disease initiation/progression, SFKs do not appear to be regulated by PSTPIP2, since no changes in their phosphorylation were detected in the absence of PSTPIP2. This suggests that PSTPIP2 regulates a segment of the signaling cascade that is further downstream from SFKs. Thus, I hypothesize that activation of so far unknown, receptor/receptors (ligand-triggered or not) that contain ITAM motifs initiates normal early phosphorylation events by SFKs. However, at some point downstream of these kinases the lack PSTPIP2-mediated inhibition results in increased phosphorylation of one or more components of the pathway and enhanced signaling leading to enhanced production of IL-1β with all the deleterious consequences.

4.3. Regulation of inflammatory response by transmembrane adaptor protein LST1

As stated above, LST1 is a member of transmembrane adaptor protein family. It contains a short extracellular peptide and a transmembrane domain followed by cytoplasmic tail with two ITIMs that can bind SHP-1 and SHP-2 phosphatases suggesting the role of LST1 as a negative regulator of signaling. It was published previously that expression of LST1 is upregulated during inflammation and can be enhanced by LPS or TNF-α. Accordingly, upregulated LST1 expression was detected in samples derived from patients suffering from IBD and rheumatoid arthritis. However, the function of LST1 in the immune system was unknown.

To analyze LST1 role *in vivo*, we have obtained *Lst1*$^{-/-}$ mice. We found that expression of murine LST1 is restricted to the cells of myeloid lineage (macrophages, monocytes and neutrophils) and is elevated in BMDM and bone marrow derived dendritic cells (BMDC) *in vitro* upon overnight stimulation with pro-inflammatory agents (interferon gamma (IFNγ), LPS, TNF-α and PolyI:C).

Male LST1-deficient mice showed reduced numbers of less segmented trabeculae in the trabecular bone tissue (determined as reduced ratio of trabecular bone surface and bone volume).

Analysis of multiple organs did not show any significant differences in total leukocyte numbers between the WT and *Lst1*$^{-/-}$ animals. However, percentages of myeloid splenocytes (neutrophils, macrophages) and lymphoid cell subsets (NK and NKT cells) were reduced in mutant mice. We observed decrease in percentages of macrophages and dendritic cells in the colon and dendritic cells in the bone marrow that potentially can be related to altered migration of these cells. Hence, we next aimed to investigate the expression levels of the chemokine receptors and migration ability of these cells. BMDM from *Lst1*$^{-/-}$ mice showed higher migration efficacy towards CXCL12, ligand of chemokine receptor CXCR4, than WT cells in a transwell assay. At the same time CXCR4 expression was not affected by LST1 deficiency, suggesting that LST1 negatively regulates CXCR4-mediated signaling or migration.

Interestingly, NK and NKT cells, which showed reduced numbers in *Lst1*$^{-/-}$ mice, do not express LST1. Therefore, it is possible that the effect of LST1 deficiency on these cells might be indirect, mediated by myeloid cell-derived factors. Hence, we tested mRNA expression of several cytokines that could affect NK cell numbers, including IL-15, IL-18, and IL-12 in BMDCs and BMDMs. However, the mRNA levels of these cytokines were not altered in *Lst1*$^{-/-}$ cells. Since equal numbers of WT and *Lst1*$^{-/-}$ cells were used in this experiment, it is still possible, that reduced numbers of myeloid cells producing these cytokines *in vivo* can be responsible for the reduction of NK cell numbers.

To investigate the role of LST1 in systemic inflammation we challenged *Lst1*$^{-/-}$ and WT mice with LPS. During LPS-induced systemic inflammation we observed differences in the cell numbers similar to those seen during the steady state. TNF-α and IL-6 cytokine levels in the blood at 4 hours after LPS challenge were also not affected by LST1 deficiency. Moreover, no alterations were detected *in vitro* in LPS-induced cytokine mRNA expression, including *IL-1β, IL-6, IL-12, TNF-α, IL-15, IL-18, IL-10*, and *TGFβ* in LST1 deficient BMDC. Additionally, expression levels of LST1 binding partners SHP-1 and SHP-2 or activation of NF-kB pathway also were not influenced by LST1 deficiency in LPS-treated BMDM. These data suggest that LST1 in not involved in the regulation of inflammatory pathways induced by LPS.

4.3.1. Mice show increased resistance to DSS-induced colitis upon LST1 deletion

Connections of LST1 expression to IBD and various other inflammatory conditions, lead us to investigate the effects of LST1 deficiency on inflammatory response during dextran sodium sulphate (DSS)-induced colitis, as a mouse model of IBD. Male mice were given DSS in drinking water over the 6-day-long-period, followed by plain water for additional 2 days. Disease activity was scored using Disease Activity Index – DAI (an integrated value encompassing weight loss, rectal bleeding and stool consistency). In addition, we monitored *Lst1* mRNA expression, count and area of the inflammatory lesions, length of the colon in these mice.

During this experiment we did not detect any significant changes in mRNA levels of *Lst1* in the colon tissue. Importantly, the course of the disease was milder and delayed in *Lst1$^{-/-}$* mice. While *Lst1$^{-/-}$* and WT mice showed similar disease activity on day 4 of DSS treatment, starting from day 6, DAI in the *Lst1$^{-/-}$* mice was significantly lower than in the WT mice, which was manifested by less severe rectal bleeding, better stool consistency, and milder colon shortening compared to WT animals, with no impact on the body weight. Histology analysis also confirmed that *Lst1$^{-/-}$* mice had significantly smaller areas of damaged epithelium at day 6 and 8, and reduced levels of pro-inflammatory cytokines detected in colonic lysates at day 5.

Surprisingly, WT mice recovered faster after the switch from DSS to plane water, and by the end of the experiment both strains had similar DAI with no detectable differences in cytokine production at the day 8. However, colonic lesions still remained larger in *Lst1$^{-/-}$* mice on day 8. Interestingly, myeloid lineage cell percentages showed similar changes in *Lst1$^{-/-}$* and WT mice during DSS treatment.

During IBD in humans and DSS-induced colitis in mice, it was shown that the first wave of immune response is initiated by resident and newly infiltrating myeloid immune cells. Hence, the reduced percentages of myeloid cells in *Lst1$^{-/-}$* colon and lymphatic tissue prior to the start of the experiment could be potentially responsible for the slower kinetics of disease development.

In conclusion, we determined protein expression profile of LST1 adaptor protein in mice and alternations in leukocyte subset composition upon its deletion at steady state and under inflammatory conditions. We demonstrated the impact of LST1 deficiency on DSS-induced colitis progression. These data suggest important regulatory functions. However, precise mechanisms of these functions still remain unknown.

4.4. Transmembrane adaptor protein WBP1L regulates CXCR4 signaling and murine hematopoiesis

WBP1L became a potentially interesting target when its expression was noticed to correlate with good prognosis in childhood ALL. Apart from that, the protein remained completely uncharacterized. Our goal was to determine its physiological function, which would allow us to better understand the regulation of hematopoiesis, but also potentially give us some clues about its role in leukemia response to treatment.

Since adaptor proteins mainly function by recruiting other effector molecules, we first set out to map the interactions of WBP1L with other proteins to identify the singling pathways it may be potentially involved in. We expressed FLAG-STREP-tagged WBP1L construct in immortalized monocyte/macrophage progenitors, followed by tandem purification of WBP1L and its interactome for mass spectrometry analysis. We detected that WBP1L interacts with several members of NEDD4-family ubiquitin ligases: WWP2, ITCH, WWP1, and NEDD4L. Intracellular part of WBP1L contains multiple [L/P]PXY motifs, which are known to interact with WW domains of NEDD4-family ubiquitin ligases and we experimentally confirmed their involvement in this interaction. We could also show that binding to WBP1L activates multiple members of this ubiquitin ligase family, suggesting WBP1L acts as general regulator of these enzymes.

One of the best-studied targets of NEDD4-family ubiquitin ligases is the chemokine receptor CXCR4, involved in maintaining hematopoietic stem and progenitor cells (HSPC) in the bone marrow by interacting with CXCL12 produced by stromal cells of the hematopoietic niches. Interestingly, co-expression of WBP1L with CXCR4 in HEK293 cells resulted in increased ubiquitination of CXCR4 and reduction in its protein levels. Moreover, WBP1L downregulation in ETV6/RUNX1$^+$ cell line REH and in immortalized murine monocyte/macrophage progenitors resulted in enhanced CXCR4 signaling.

To further analyze the function of WBP1L *in vivo*, we obtained *Wbp1l*$^{-/-}$ mice. Basic phenotyping of leukocyte subsets showed that *Wbp1l*$^{-/-}$ adult mice had significant increase of marginal zone B cells and dendritic cells in the spleen. Percentages of B1 cells were reduced in peritoneal cavity with no alternations in percentages of other leukocyte subsets. In the bone marrow we observed reduced percentages of B cell progenitors and increased percentages of LSK cells (Lin$^-$ Sca1$^+$ c-kit$^+$), which encompass stem and very early progenitor cell subsets.

The last observation prompted us to analyze the function of *Wbp1l*$^{-/-}$ hematopoietic stem and progenitor cells in a competitive transplantation assay. *Wbp1l*$^{-/-}$ Ly5.2 bone marrow cells were mixed 1:1 with WT Ly5.1/Ly5.2 and transplanted into lethally irradiated recipient mice (Ly5.1). The results showed significantly better engraftment of *Wbp1l*$^{-/-}$ bone marrow cells. Moreover, this difference was not the result of increased homing to the bone marrow or increased proliferation, as no alternations to these processes were observed.

Our data show WBP1L as a negative regulator of hematopoietic stem and progenitor cell function. Whether it is connected to its role in the regulation of CXCR4 is unclear, since only acute deletion or downregulation of WBP1L resulted in increased function of CXCR4. In the case of germline deletion in mice, leukocytes and their progenitors were largely able to compensate for WBP1L loss. The underlying mechanism of this compensation remains unknown. It is still unclear whether our data could explain correlation of WBP1L expression with positive outcome in leukemia or if WBP1L has any role in better treatment response of

ETV6-RUNX1$^+$ BCP-ALL. ETV6 is known to repress WBP1L gene expression. In ETV6-RUNX1$^+$ BCP-ALL, ETV6 is typically inactivated by fusion of one allele with RUNX1 and mutation in the other allele, which leads to increased WBP1L expression. It can be speculated that the increase of WBP1L expression would attenuate CXCR4 signaling and disrupt interaction of leukemic (stem) cells with the protective bone marrow niches, making them more vulnerable to the drugs used during the treatment. In any case our data made WBP1L a relevant target for future investigation.

5. CONCLUSIONS

The research presented in this thesis was aimed at describing the role of selected membrane adaptor proteins in cell signaling and impact of these proteins on immune processes.

My first author publication focused on the role of PSTPIP2 binding partners PEST-PTPs and SHIP1 in the development of sterile osteomyelitis. We have found that PEST-PTPs and SHIP1 bound to PSTPIP2, differentially regulate pathways crucial for the development of CMO disease and production of IL-β, ROS, and neutrophil-attracting chemokines. We have shown that recruitment of PEST-PTPs by PSTPIP2 is crucial for the regulation of neutrophil migration to the site of inflammation. This is mediated, at least in part, by a positive feedback loop where enhanced CXCL2 production by neutrophils attracts additional neutrophils that produce more CXCL2 potentially spiraling neutrophil recruitment out of control. The recruitment of PEST-PTPs to PSTPIP2 is also crucial for the control of ROS. On the other hand, control of IL-1β pathway was similarly regulated by PSTPIP2 interaction with PEST-PTPs and SHIP1.

In the publication where I shared the first authorship, we described how CD45 contributes to CMO disease progression via positive regulation of SFKs. We showed that CD45 is involved in the regulation of the critical pathway controlling production of IL-1β the main driver of CMO.

In a publication related to LST1 we determined the protein expression profile of LST1 in mice and described alterations in leukocyte subset composition upon its deletion at steady state and under inflammatory conditions. We also demonstrated LST1 involvement in controlling the progression of DSS-induced colitis.

Finally, we investigated of the role of WBP1L in hematopoiesis. We were able to show that WBP1L can interact with NEDD4-family ubiquitin ligases and act as a negative regulator of CXCR4. Moreover, we found that WBP1L is a negative regulator of hematopoiesis affecting the ability of hematopoietic stem and progenitor cells to reconstitute hematopoiesis after bone marrow transplantation.

6. CONTRIBUTION

With the great support of my supervisor and close collaboration with my colleagues we were able to bring most of my work to a publication stage as listed below:

1. **Pavliuchenko**, N., Duric, I., Kralova, J., Fabisik, M., Spoutil, F., Prochazka, J., Kasparek, P., Pokorna, J., Skopcova, T., Sedlacek, R., & Brdicka, T. (2022). Molecular interactions of adaptor protein PSTPIP2 control neutrophil-mediated responses leading to autoinflammation. *Frontiers in Immunology*, *13*, 1035226.

For the main project and the related publication, I was responsible for the design and execution of the majority of the experiments as well as writing the first draft of the manuscript.

2. **Kralova**, J.*, **Pavliuchenko, N.***, Fabisik, M., Ilievova, K., Spoutil, F., Prochazka, J., Pokorna, J., Sedlacek, R., & Brdicka, T. (2021). The receptor-type protein tyrosine phosphatase CD45 promotes onset and severity of IL-1β-mediated autoinflammatory osteomyelitis. *The Journal of Biological Chemistry*, *297*(4), 101131.
   *- authors contributed equally

In this publication, I have performed most of the experiments during the revisions, that included various immunoprecipitations, animal work and *in vitro* experiments. I also performed optimization and testing of pro-IL-1β production in bone marrow cells and neutrophils.

3. Fabisik, M., Tureckova, J., **Pavliuchenko, N.**, Kralova, J., Balounova, J., Vicikova, K., Skopcova, T., Spoutil, F., Pokorna, J., Angelisova, P., Malissen, B., Prochazka, J., Sedlacek, R., & Brdicka, T. (2021). Regulation of Inflammatory Response by Transmembrane Adaptor Protein LST1. *Frontiers in Immunology*, *12*, 618332.

During the work related to this manuscript I performed analysis of protein expression in various cell types, and in dendritic cells and macrophages upon stimulations. I also performed various ELISAs where we measured IL-6 and TNF-α. Moreover, I tested SHP-1 and SHP-2 expression by Western blot.

4. Borna, S., Drobek, A., Kralova, J., Glatzova, D., Splichalova, I., Fabisik, M., Pokorna, J., Skopcova, T., Angelisova, P., Kanderova, V., Starkova, J., Stanek, P., Matveichuk, O. V., **Pavliuchenko, N.**, Kwiatkowska, K., Protty, M. B., Tomlinson, M. G., Alberich-Jorda, M., Korinek, V., & Brdicka, T. (2020). Transmembrane adaptor protein WBP1L regulates CXCR4 signalling and murine haematopoiesis. *Journal of Cellular and Molecular Medicine*, *24*(2), 1980–1992.

I contributed to the paper during the revisions and performed several Western blot analyses.

I hereby confirm that the author of the thesis, Nataliia Pavliuchenko, has substantially contributed to the publications listed above. For her first-author publications, she performed the major part of experimental work and contributed to the first draft of the manuscript.

……………………………………… Mgr. Tomáš Brdička, Ph.D.

7. REFERENCES

1. Stenken, J.A. and A.J. Poschenrieder, *Bioanalytical chemistry of cytokines--a review.* Anal Chim Acta, 2015. **853**: p. 95-115.
2. Nair, A., et al., *Conceptual Evolution of Cell Signaling.* Int J Mol Sci, 2019. **20**(13).
3. Seth, A., et al., *Signal transduction within the nucleus by mitogen-activated protein kinase.* J Biol Chem, 1992. **267**(34): p. 24796-804.
4. Huangfu, W.C. and S.Y. Fuchs, *Ubiquitination-dependent regulation of signaling receptors in cancer.* Genes Cancer, 2010. **1**(7): p. 725-34.
5. Burton, J.C. and N.J. Grimsey, *Ubiquitination as a Key Regulator of Endosomal Signaling by GPCRs.* Frontiers in Cell and Developmental Biology, 2019. **7**.
6. Skieterska, K., P. Rondou, and K. Van Craenenbroeck, *Regulation of G Protein-Coupled Receptors by Ubiquitination.* Int J Mol Sci, 2017. **18**(5).
7. Acconcia, F., S. Sigismund, and S. Polo, *Ubiquitin in trafficking: the network at work.* Exp Cell Res, 2009. **315**(9): p. 1610-8.
8. Bhattacharya, A. and L. Qi, *ER-associated degradation in health and disease - from substrate to organism.* J Cell Sci, 2019. **132**(23).
9. Isakov, N., *Immunoreceptor tyrosine-based activation motif (ITAM), a unique module linking antigen and Fc receptors to their signaling cascades.* J Leukoc Biol, 1997. **61**(1): p. 6-16.
10. Ivashkiv, L.B., *Cross-regulation of signaling by ITAM-associated receptors.* Nat Immunol, 2009. **10**(4): p. 340-7.
11. Lowell, C.A., *Src-family and Syk kinases in activating and inhibitory pathways in innate immune cells: signaling cross talk.* Cold Spring Harb Perspect Biol, 2011. **3**(3).
12. Ackermann, J.A., et al., *Syk tyrosine kinase is critical for B cell antibody responses and memory B cell survival.* J Immunol, 2015. **194**(10): p. 4650-6.
13. Bagley, C.J., et al., *The structural and functional basis of cytokine receptor activation: lessons from the common beta subunit of the granulocyte-macrophage colony-stimulating factor, interleukin-3 (IL-3), and IL-5 receptors.* Blood, 1997. **89**(5): p. 1471-82.
14. Hu, X., et al., *The JAK/STAT signaling pathway: from bench to clinic.* Signal Transduct Target Ther, 2021. **6**(1): p. 402.
15. Tonks, N.K., *Protein tyrosine phosphatases: from genes, to function, to disease.* Nat Rev Mol Cell Biol, 2006. **7**(11): p. 833-46.
16. Donovan, J.A. and G.A. Koretzky, *CD45 and the immune response.* J Am Soc Nephrol, 1993. **4**(4): p. 976-85.
17. Al Barashdi, M.A., et al., *Protein tyrosine phosphatase receptor type C (PTPRC or CD45).* J Clin Pathol, 2021. **74**(9): p. 548-552.
18. Ledbetter, J.A., et al., *CD45 regulates signal transduction and lymphocyte activation by specific association with receptor molecules on T or B cells.* Proc Natl Acad Sci U S A, 1988. **85**(22): p. 8628-32.
19. Geng, X., et al., *Integrin CD11a cytoplasmic tail interacts with the CD45 membrane-proximal protein tyrosine phosphatase domain 1.* Immunology, 2005. **115**(3): p. 347-57.
20. Gao, H., et al., *Effects of the protein tyrosine phosphatase CD45 on FcgammaRIIa signaling and neutrophil function.* Exp Hematol, 2000. **28**(9): p. 1062-70.
21. Irie-Sasaki, J., et al., *CD45 is a JAK phosphatase and negatively regulates cytokine receptor signalling.* Nature, 2001. **409**(6818): p. 349-54.

22. Amata, I., M. Maffei, and M. Pons, *Phosphorylation of unique domains of Src family kinases.* Front Genet, 2014. **5**: p. 181.

23. Mócsai, A., et al., *Kinase pathways in chemoattractant-induced degranulation of neutrophils: the role of p38 mitogen-activated protein kinase activated by Src family kinases.* J Immunol, 2000. **164**(8): p. 4321-31.

24. Abram, C.L. and C.A. Lowell, *The diverse functions of Src family kinases in macrophages.* Front Biosci, 2008. **13**: p. 4426-50.

25. Eliceiri, B.P., *Integrin and growth factor receptor crosstalk.* Circ Res, 2001. **89**(12): p. 1104-10.

26. Hermiston, M.L., Z. Xu, and A. Weiss, *CD45: a critical regulator of signaling thresholds in immune cells.* Annu Rev Immunol, 2003. **21**: p. 107-37.

27. Byth, K.F., et al., *CD45-null transgenic mice reveal a positive regulatory role for CD45 in early thymocyte development, in the selection of CD4+CD8+ thymocytes, and B cell maturation.* J Exp Med, 1996. **183**(4): p. 1707-18.

28. Courtney, A.H., et al., *CD45 functions as a signaling gatekeeper in T cells.* Sci Signal, 2019. **12**(604).

29. Roach, T., et al., *CD45 regulates Src family member kinase activity associated with macrophage integrin-mediated adhesion.* Curr Biol, 1997. **7**(6): p. 408-17.

30. Zhu, J.W., et al., *Structurally distinct phosphatases CD45 and CD148 both regulate B cell and macrophage immunoreceptor signaling.* Immunity, 2008. **28**(2): p. 183-96.

31. Zhu, J.W., et al., *Receptor-like tyrosine phosphatases CD45 and CD148 have distinct functions in chemoattractant-mediated neutrophil migration and response to S. aureus.* Immunity, 2011. **35**(5): p. 757-69.

32. Tsui, H.W., et al., *Motheaten and viable motheaten mice have mutations in the haematopoietic cell phosphatase gene.* Nat Genet, 1993. **4**(2): p. 124-9.

33. Zhang, J., A.K. Somani, and K.A. Siminovitch, *Roles of the SHP-1 tyrosine phosphatase in the negative regulation of cell signalling.* Semin Immunol, 2000. **12**(4): p. 361-78.

34. Abram, C.L., et al., *Distinct roles for neutrophils and dendritic cells in inflammation and autoimmunity in motheaten mice.* Immunity, 2013. **38**(3): p. 489-501.

35. Abram, C.L. and C.A. Lowell, *Shp1 function in myeloid cells.* J Leukoc Biol, 2017. **102**(3): p. 657-675.

36. Tartey, S., et al., *Cutting Edge: Dysregulated CARD9 Signaling in Neutrophils Drives Inflammation in a Mouse Model of Neutrophilic Dermatoses.* J Immunol, 2018. **201**(6): p. 1639-1644.

37. Myers, D.R., et al., *Shp1 Loss Enhances Macrophage Effector Function and Promotes Anti-Tumor Immunity.* Front Immunol, 2020. **11**: p. 576310.

38. Gross, A.J., et al., *Developmental acquisition of the Lyn-CD22-SHP-1 inhibitory pathway promotes B cell tolerance.* J Immunol, 2009. **182**(9): p. 5382-92.

39. Chiang, G.G. and B.M. Sefton, *Specific dephosphorylation of the Lck tyrosine protein kinase at Tyr-394 by the SHP-1 protein-tyrosine phosphatase.* J Biol Chem, 2001. **276**(25): p. 23173-8.

40. Qu, C.K., et al., *A deletion mutation in the SH2-N domain of Shp-2 severely suppresses hematopoietic cell development.* Mol Cell Biol, 1997. **17**(9): p. 5499-507.

41. Christofides, A., et al., *SHP-2 and PD-1-SHP-2 signaling regulate myeloid cell differentiation and antitumor responses.* Nat Immunol, 2023. **24**(1): p. 55-68.

42. Lorenz, U., *SHP-1 and SHP-2 in T cells: two phosphatases functioning at many levels.* Immunol Rev, 2009. **228**(1): p. 342-59.

43. Helgason, C.D., et al., *Targeted disruption of SHIP leads to hemopoietic perturbations, lung pathology, and a shortened life span.* Genes Dev, 1998. **12**(11): p. 1610-20.

44.   Bai, D., L. Ueno, and P.K. Vogt, *Akt-mediated regulation of NFkappaB and the essentialness of NFkappaB for the oncogenicity of PI3K and Akt.* Int J Cancer, 2009. **125**(12): p. 2863-70.

45.   Krystal, G., et al., *SHIPs ahoy.* Int J Biochem Cell Biol, 1999. **31**(10): p. 1007-10.

46.   Akinleye, A., et al., *Phosphatidylinositol 3-kinase (PI3K) inhibitors as cancer therapeutics.* J Hematol Oncol, 2013. **6**(1): p. 88.

47.   Rauh, M.J., et al., *SHIP represses the generation of alternatively activated macrophages.* Immunity, 2005. **23**(4): p. 361-74.

48.   Gardai, S., et al., *Activation of SHIP by NADPH oxidase-stimulated Lyn leads to enhanced apoptosis in neutrophils.* J Biol Chem, 2002. **277**(7): p. 5236-46.

49.   Michael, M., et al., *The 5-Phosphatase SHIP2 Promotes Neutrophil Chemotaxis and Recruitment.* Front Immunol, 2021. **12**: p. 671756.

50.   Sleeman, M.W., et al., *Absence of the lipid phosphatase SHIP2 confers resistance to dietary obesity.* Nat Med, 2005. **11**(2): p. 199-205.

51.   Brooks, R., et al., *SHIP1 inhibition increases immunoregulatory capacity and triggers apoptosis of hematopoietic cancer cells.* J Immunol, 2010. **184**(7): p. 3582-9.

52.   So, E.Y., et al., *Inhibition of lipid phosphatase SHIP1 expands myeloid-derived suppressor cells and attenuates rheumatoid arthritis in mice.* Am J Physiol Cell Physiol, 2021. **321**(3): p. C569-c584.

53.   Veillette, A., et al., *PEST family phosphatases in immunity, autoimmunity, and autoinflammatory disorders.* Immunol Rev, 2009. **228**(1): p. 312-24.

54.   Yang, Q., et al., *Cloning and expression of PTP-PEST. A novel, human, nontransmembrane protein tyrosine phosphatase.* J Biol Chem, 1993. **268**(9): p. 6622-8.

55.   Nakamoto, T., et al., *Expression and tyrosine phosphorylation of Crk-associated substrate lymphocyte type (Cas-L) protein in human neutrophils.* J Cell Biochem, 2008. **105**(1): p. 121-8.

56.   Fuortes, M., et al., *Role of the tyrosine kinase pyk2 in the integrin-dependent activation of human neutrophils by TNF.* J Clin Invest, 1999. **104**(3): p. 327-35.

57.   Thomas, R.M., et al., *C-terminal SRC kinase controls acute inflammation and granulocyte adhesion.* Immunity, 2004. **20**(2): p. 181-91.

58.   Aomatsu, K., et al., *Toll-like receptor agonists stimulate human neutrophil migration via activation of mitogen-activated protein kinases.* Immunology, 2008. **123**(2): p. 171-80.

59.   Davidson, D. and A. Veillette, *PTP-PEST, a scaffold protein tyrosine phosphatase, negatively regulates lymphocyte activation by targeting a unique set of substrates.* Embo j, 2001. **20**(13): p. 3414-26.

60.   Rhee, I., et al., *Macrophage fusion is controlled by the cytoplasmic protein tyrosine phosphatase PTP-PEST/PTPN12.* Mol Cell Biol, 2013. **33**(12): p. 2458-69.

61.   Souza, C.M., et al., *The phosphatase PTP-PEST/PTPN12 regulates endothelial cell migration and adhesion, but not permeability, and controls vascular development and embryonic viability.* J Biol Chem, 2012. **287**(51): p. 43180-90.

62.   Sirois, J., et al., *Essential function of PTP-PEST during mouse embryonic vascularization, mesenchyme formation, neurogenesis and early liver development.* Mech Dev, 2006. **123**(12): p. 869-80.

63.   Stanford, S.M., N. Rapini, and N. Bottini, *Regulation of TCR signalling by tyrosine phosphatases: from immune homeostasis to autoimmunity.* Immunology, 2012. **137**(1): p. 1-19.

64. Rhee, I., et al., *Control of dendritic cell migration, T cell-dependent immunity, and autoimmunity by protein tyrosine phosphatase PTPN12 expressed in dendritic cells.* Mol Cell Biol, 2014. **34**(5): p. 888-99.

65. Chen, Z., et al., *PTPN12/PTP-PEST Regulates Phosphorylation-Dependent Ubiquitination and Stability of Focal Adhesion Substrates in Invasive Glioblastoma Cells.* Cancer Res, 2018. **78**(14): p. 3809-3822.

66. Cloutier, J.F. and A. Veillette, *Cooperative inhibition of T-cell antigen receptor signaling by a complex between a kinase and a phosphatase.* J Exp Med, 1999. **189**(1): p. 111-21.

67. Hasegawa, K., et al., *PEST domain-enriched tyrosine phosphatase (PEP) regulation of effector/memory T cells.* Science, 2004. **303**(5658): p. 685-9.

68. Fiorillo, E., et al., *Autoimmune-associated PTPN22 R620W variation reduces phosphorylation of lymphoid phosphatase on an inhibitory tyrosine residue.* J Biol Chem, 2010. **285**(34): p. 26506-18.

69. Cheng, J., et al., *A novel protein tyrosine phosphatase expressed in lin(lo)CD34(hi)Sca(hi) hematopoietic progenitor cells.* Blood, 1996. **88**(4): p. 1156-67.

70. Gensler, M., M. Buschbeck, and A. Ullrich, *Negative regulation of HER2 signaling by the PEST-type protein-tyrosine phosphatase BDP1.* J Biol Chem, 2004. **279**(13): p. 12110-6.

71. Smith, E.J., et al., *Clinical, Molecular, and Genetic Characteristics of PAPA Syndrome: A Review.* Curr Genomics, 2010. **11**(7): p. 519-27.

72. Yang, L. and Y. Yan, *Protein kinases are potential targets to treat inflammatory bowel disease.* World J Gastrointest Pharmacol Ther, 2014. **5**(4): p. 209-17.

73. Szilveszter, K.P., T. Németh, and A. Mócsai, *Tyrosine Kinases in Autoimmune and Inflammatory Skin Diseases.* Front Immunol, 2019. **10**: p. 1862.

74. Qi, X.M., et al., *Targeting an oncogenic kinase/phosphatase signaling network for cancer therapy.* Acta Pharm Sin B, 2018. **8**(4): p. 511-517.

75. Turdo, A., et al., *Targeting Phosphatases and Kinases: How to Checkmate Cancer.* Front Cell Dev Biol, 2021. **9**: p. 690306.

76. Pan, J., et al., *Targeting protein phosphatases for the treatment of inflammation-related diseases: From signaling to therapy.* Signal Transduct Target Ther, 2022. **7**(1): p. 177.

77. Martellucci, S., et al., *Src Family Kinases as Therapeutic Targets in Advanced Solid Tumors: What We Have Learned so Far.* Cancers (Basel), 2020. **12**(6).

78. Alberts, B., *Molecular biology of the cell.* 2017.

79. Do, J., et al., *Glucocerebrosidase and its relevance to Parkinson disease.* Mol Neurodegener, 2019. **14**(1): p. 36.

80. Lahiry, P., et al., *Kinase mutations in human disease: interpreting genotype-phenotype relationships.* Nat Rev Genet, 2010. **11**(1): p. 60-74.

81. Jadwin, J.A., et al., *Src homology 2 domains enhance tyrosine phosphorylation in vivo by protecting binding sites in their target proteins from dephosphorylation.* J Biol Chem, 2018. **293**(2): p. 623-637.

82. Borowicz, P., et al., *Adaptor proteins: Flexible and dynamic modulators of immune cell signalling.* Scand J Immunol, 2020. **92**(5): p. e12951.

83. Wagner, M.J., et al., *Molecular mechanisms of SH2- and PTB-domain-containing proteins in receptor tyrosine kinase signaling.* Cold Spring Harb Perspect Biol, 2013. **5**(12): p. a008987.

84. Salzer, U., J. Kostan, and K. Djinović-Carugo, *Deciphering the BAR code of membrane modulators.* Cell Mol Life Sci, 2017. **74**(13): p. 2413-2438.

85. Horejsí, V., *Transmembrane adaptor proteins in membrane microdomains: important regulators of immunoreceptor signaling.* Immunol Lett, 2004. **92**(1-2): p. 43-9.

86.   Zhang, W., et al., *Functional analysis of LAT in TCR-mediated signaling pathways using a LAT-deficient Jurkat cell line.* Int Immunol, 1999. **11**(6): p. 943-50.

87.   Yamasaki, S., et al., *Gads/Grb2-mediated association with LAT is critical for the inhibitory function of Gab2 in T cells.* Mol Cell Biol, 2003. **23**(7): p. 2515-29.

88.   Zhang, W., et al., *Essential role of LAT in T cell development.* Immunity, 1999. **10**(3): p. 323-32.

89.   Tridandapani, S., et al., *The adapter protein LAT enhances fcgamma receptor-mediated signal transduction in myeloid cells.* J Biol Chem, 2000. **275**(27): p. 20480-7.

90.   Saitoh, S., et al., *LAT is essential for Fc(epsilon)RI-mediated mast cell activation.* Immunity, 2000. **12**(5): p. 525-35.

91.   de Baey, A., et al., *Complex expression pattern of the TNF region gene LST1 through differential regulation, initiation, and alternative splicing.* Genomics, 1997. **45**(3): p. 591-600.

92.   Mewar, D., et al., *Haplotype-specific gene expression profiles in a telomeric major histocompatibility complex gene cluster and susceptibility to autoimmune diseases.* Genes Immun, 2006. **7**(8): p. 625-31.

93.   Kilding, R., et al., *Additional genetic susceptibility for rheumatoid arthritis telomeric of the DRB1 locus.* Arthritis Rheum, 2004. **50**(3): p. 763-9.

94.   Bettens, F., et al., *Association of TNFd and IL-10 polymorphisms with mortality in unrelated hematopoietic stem cell transplantation.* Transplantation, 2006. **81**(9): p. 1261-7.

95.   Draber, P., et al., *LST1/A is a myeloid leukocyte-specific transmembrane adaptor protein recruiting protein tyrosine phosphatases SHP-1 and SHP-2 to the plasma membrane.* J Biol Chem, 2012. **287**(27): p. 22812-21.

96.   Stepanek, O., P. Draber, and V. Horejsi, *Palmitoylated transmembrane adaptor proteins in leukocyte signaling.* Cell Signal, 2014. **26**(5): p. 895-902.

97.   Niogret, C., W. Birchmeier, and G. Guarda, *SHP-2 in Lymphocytes' Cytokine and Inhibitory Receptor Signaling.* Front Immunol, 2019. **10**: p. 2468.

98.   Heidemann, J., et al., *Regulated expression of leukocyte-specific transcript (LST) 1 in human intestinal inflammation.* Inflamm Res, 2014. **63**(7): p. 513-7.

99.   Roberts-Galbraith, R.H. and K.L. Gould, *Setting the F-BAR: functions and regulation of the F-BAR protein family.* Cell Cycle, 2010. **9**(20): p. 4091-7.

100.   Frost, A., V.M. Unger, and P. De Camilli, *The BAR domain superfamily: membrane-molding macromolecules.* Cell, 2009. **137**(2): p. 191-6.

101.   Thrasher, A.J., *WASp in immune-system organization and function.* Nat Rev Immunol, 2002. **2**(9): p. 635-46.

102.   Leibman-Markus, M., et al., *Dynamin-Related Proteins Enhance Tomato Immunity by Mediating Pattern Recognition Receptor Trafficking.* Membranes (Basel), 2022. **12**(8).

103.   Drobek, A., et al., *PSTPIP2, a Protein Associated with Autoinflammatory Disease, Interacts with Inhibitory Enzymes SHIP1 and Csk.* J Immunol, 2015. **195**(7): p. 3416-26.

104.   Wu, Y., S.D. Spencer, and L.A. Lasky, *Tyrosine phosphorylation regulates the SH3-mediated binding of the Wiskott-Aldrich syndrome protein to PSTPIP, a cytoskeletal-associated protein.* J Biol Chem, 1998. **273**(10): p. 5765-70.

105.   Lindwall, E., et al., *Novel PSTPIP1 gene mutation in a patient with pyogenic arthritis, pyoderma gangrenosum and acne (PAPA) syndrome.* Semin Arthritis Rheum, 2015. **45**(1): p. 91-3.

106.   Hussain, A., et al., *Synovitis, Acne, Pustulosis, Hyperostosis, Osteitis (SAPHO): An Interesting Clinical Syndrome.* Cureus, 2020. **12**(9): p. e10184.

107. Sergi, C.M., et al., *Chronic recurrent multifocal osteomyelitis. A narrative and pictorial review.* Front Immunol, 2022. **13**: p. 959575.

108. Chitu, V., et al., *Primed innate immunity leads to autoinflammatory disease in PSTPIP2-deficient cmo mice.* Blood, 2009. **114**(12): p. 2497-505.

109. Hurtado-Nedelec, M., et al., *Genetic susceptibility factors in a cohort of 38 patients with SAPHO syndrome: a study of PSTPIP2, NOD2, and LPIN2 genes.* J Rheumatol, 2010. **37**(2): p. 401-9.

110. Ferguson, P.J., et al., *A missense mutation in pstpip2 is associated with the murine autoinflammatory disorder chronic multifocal osteomyelitis.* Bone, 2006. **38**(1): p. 41-7.

111. Kralova, J., et al., *Dysregulated NADPH Oxidase Promotes Bone Damage in Murine Model of Autoinflammatory Osteomyelitis.* J Immunol, 2020. **204**(6): p. 1607-1620.

112. Lukens, J.R., et al., *Critical role for inflammasome-independent IL-1β production in osteomyelitis.* Proc Natl Acad Sci U S A, 2014. **111**(3): p. 1066-71.

113. Chitu, V., et al., *PSTPIP2 deficiency in mice causes osteopenia and increased differentiation of multipotent myeloid precursors into osteoclasts.* Blood, 2012. **120**(15): p. 3126-35.

114. Zhang, W. and H.T. Liu, *MAPK signal pathways in the regulation of cell proliferation in mammalian cells.* Cell Res, 2002. **12**(1): p. 9-18.

115. Abdulkhaleq, L.A., et al., *The crucial roles of inflammatory mediators in inflammation: A review.* Vet World, 2018. **11**(5): p. 627-635.

116. Tang, D., et al., *PAMPs and DAMPs: signal 0s that spur autophagy and immunity.* Immunol Rev, 2012. **249**(1): p. 158-75.

117. Roberts, A.W., *G-CSF: a key regulator of neutrophil production, but that's not all!* Growth Factors, 2005. **23**(1): p. 33-41.

118. Borroni, E.M., et al., *Chemoattractant Receptors and Leukocyte Recruitment: More Than Cell Migration.* Science Signaling, 2009. **2**(59): p. pe10-pe10.

119. Futosi, K., S. Fodor, and A. Mócsai, *Neutrophil cell surface receptors and their intracellular signal transduction pathways.* Int Immunopharmacol, 2013. **17**(3): p. 638-50.

120. Rosales, C., *Neutrophil: A Cell with Many Roles in Inflammation or Several Cell Types?* Front Physiol, 2018. **9**: p. 113.

121. Dunne, A. and L.A. O'Neill, *The interleukin-1 receptor/Toll-like receptor superfamily: signal transduction during inflammation and host defense.* Sci STKE, 2003. **2003**(171): p. re3.

122. Tecchio, C., A. Micheletti, and M.A. Cassatella, *Neutrophil-derived cytokines: facts beyond expression.* Front Immunol, 2014. **5**: p. 508.

123. Eder, C., *Mechanisms of interleukin-1beta release.* Immunobiology, 2009. **214**(7): p. 543-53.

124. Delgado-Rizo, V., et al., *Neutrophil Extracellular Traps and Its Implications in Inflammation: An Overview.* Front Immunol, 2017. **8**: p. 81.

125. Mortaz, E., et al., *Update on Neutrophil Function in Severe Inflammation.* Front Immunol, 2018. **9**: p. 2171.

126. Castanheira, F.V.S. and P. Kubes, *Neutrophils and NETs in modulating acute and chronic inflammation.* Blood, 2019. **133**(20): p. 2178-2185.

127. Herrero-Cervera, A., O. Soehnlein, and E. Kenne, *Neutrophils in chronic inflammatory diseases.* Cell Mol Immunol, 2022. **19**(2): p. 177-191.

128. Wright, H.L., et al., *Neutrophil function in inflammation and inflammatory diseases.* Rheumatology (Oxford), 2010. **49**(9): p. 1618-31.

129. Chen, G.Y. and G. Nuñez, *Sterile inflammation: sensing and reacting to damage.* Nat Rev Immunol, 2010. **10**(12): p. 826-37.

130. Wynn, T.A., *Cellular and molecular mechanisms of fibrosis.* J Pathol, 2008. **214**(2): p. 199-210.

131. Wynn, T.A. and T.R. Ramalingam, *Mechanisms of fibrosis: therapeutic translation for fibrotic disease.* Nat Med, 2012. **18**(7): p. 1028-40.

132. Gu, Y., et al., *The emerging roles of interstitial macrophages in pulmonary fibrosis: A perspective from scRNA-seq analyses.* Front Immunol, 2022. **13**: p. 923235.

133. Xu, T., et al., *Oxidative Stress in Cell Death and Cardiovascular Diseases.* Oxid Med Cell Longev, 2019. **2019**: p. 9030563.

134. Shi, Y., A.D. Mucsi, and G. Ng, *Monosodium urate crystals in inflammation and immunity.* Immunol Rev, 2010. **233**(1): p. 203-17.

135. Li, D. and M. Wu, *Pattern recognition receptors in health and diseases.* Signal Transduct Target Ther, 2021. **6**(1): p. 291.

136. Gamrekelashvili, J., T.F. Greten, and F. Korangy, *Immunogenicity of necrotic cell death.* Cell Mol Life Sci, 2015. **72**(2): p. 273-83.

137. Lopez-Castejon, G. and D. Brough, *Understanding the mechanism of IL-1β secretion.* Cytokine Growth Factor Rev, 2011. **22**(4): p. 189-95.

138. Busso, N. and A. So, *Mechanisms of inflammation in gout.* Arthritis Res Ther, 2010. **12**(2): p. 206.

139. Masumoto, J., et al., *Molecular biology of autoinflammatory diseases.* Inflamm Regen, 2021. **41**(1): p. 33.

140. Bergsbaken, T., S.L. Fink, and B.T. Cookson, *Pyroptosis: host cell death and inflammation.* Nat Rev Microbiol, 2009. **7**(2): p. 99-109.

141. Clancy, D.M., et al., *Extracellular Neutrophil Proteases Are Efficient Regulators of IL-1, IL-33, and IL-36 Cytokine Activity but Poor Effectors of Microbial Killing.* Cell Rep, 2018. **22**(11): p. 2937-2950.

142. Afonina, I.S., et al., *Proteolytic Processing of Interleukin-1 Family Cytokines: Variations on a Common Theme.* Immunity, 2015. **42**(6): p. 991-1004.

143. Abais, J.M., et al., *Redox regulation of NLRP3 inflammasomes: ROS as trigger or effector?* Antioxid Redox Signal, 2015. **22**(13): p. 1111-29.

144. Gombault, A., L. Baron, and I. Couillin, *ATP release and purinergic signaling in NLRP3 inflammasome activation.* Front Immunol, 2012. **3**: p. 414.

145. Huang, N., et al., *Deletion of Nlrp3 protects from inflammation-induced skeletal muscle atrophy.* Intensive Care Med Exp, 2017. **5**(1): p. 3.

146. Zhu, F., et al., *NLRP3 Inhibition Ameliorates Severe Cutaneous Autoimmune Manifestations in a Mouse Model of Autoimmune Polyendocrinopathy-Candidiasis-Ectodermal Dystrophy-Like Disease.* J Invest Dermatol, 2021. **141**(6): p. 1404-1415.

147. Fernandes, F.P., et al., *Inflammasome genetics and complex diseases: a comprehensive review.* Eur J Hum Genet, 2020. **28**(10): p. 1307-1321.

148. Doria, A., et al., *Autoinflammation and autoimmunity: bridging the divide.* Autoimmun Rev, 2012. **12**(1): p. 22-30.

149. Doherty, T.A., S.D. Brydges, and H.M. Hoffman, *Autoinflammation: translating mechanism to therapy.* J Leukoc Biol, 2011. **90**(1): p. 37-47.

150. Ren, K. and R. Torres, *Role of interleukin-1beta during pain and inflammation.* Brain Res Rev, 2009. **60**(1): p. 57-64.

151. Mai, W. and Y. Liao, *Targeting IL-1β in the Treatment of Atherosclerosis.* Front Immunol, 2020. **11**: p. 589654.

152. Yu, J.R. and K.S. Leslie, *Cryopyrin-associated periodic syndrome: an update on diagnosis and treatment response.* Curr Allergy Asthma Rep, 2011. **11**(1): p. 12-20.

153. Loeven, N.A., N.P. Medici, and J.B. Bliska, *The pyrin inflammasome in host-microbe interactions.* Curr Opin Microbiol, 2020. **54**: p. 77-86.

154. Aksentijevich, I., et al., *An autoinflammatory disease with deficiency of the interleukin-1-receptor antagonist.* N Engl J Med, 2009. **360**(23): p. 2426-37.

155. Ferguson, P.J. and H. El-Shanti, *Majeed Syndrome: A Review of the Clinical, Genetic and Immunologic Features.* Biomolecules, 2021. **11**(3).

156. Hofmann, S.R., et al., *Chronic Recurrent Multifocal Osteomyelitis (CRMO): Presentation, Pathogenesis, and Treatment.* Curr Osteoporos Rep, 2017. **15**(6): p. 542-554.

157. Dasari, T.K., et al., *The nonreceptor tyrosine kinase SYK drives caspase-8/NLRP3 inflammasome-mediated autoinflammatory osteomyelitis.* J Biol Chem, 2020. **295**(11): p. 3394-3400.

158. Futosi, K. and A. Mócsai, *Tyrosine kinase signaling pathways in neutrophils.* Immunol Rev, 2016. **273**(1): p. 121-39.

159. Zarbock, A. and K. Ley, *Mechanisms and consequences of neutrophil interaction with the endothelium.* Am J Pathol, 2008. **172**(1): p. 1-7.

160. Lewis Marffy, A.L. and A.J. McCarthy, *Leukocyte Immunoglobulin-Like Receptors (LILRs) on Human Neutrophils: Modulators of Infection and Immunity.* Front Immunol, 2020. **11**: p. 857.

161. Radjabova, V., et al., *TARM1 Is a Novel Leukocyte Receptor Complex-Encoded ITAM Receptor That Costimulates Proinflammatory Cytokine Secretion by Macrophages and Neutrophils.* J Immunol, 2015. **195**(7): p. 3149-59.

162. Wu, M., et al., *TREM-1 amplifies corneal inflammation after Pseudomonas aeruginosa infection by modulating Toll-like receptor signaling and Th1/Th2-type immune responses.* Infect Immun, 2011. **79**(7): p. 2709-16.

163. Mócsai, A., et al., *Syk is required for integrin signaling in neutrophils.* Immunity, 2002. **16**(4): p. 547-58.

164. Phillips, F.C., P. Gurung, and T.D. Kanneganti, *Microbiota and caspase-1/caspase-8 regulate IL-1β-mediated bone disease.* Gut Microbes, 2016. 7(4): p. 334-341.

165. Yeoh, E.J., et al., *Classification, subtype discovery, and prediction of outcome in pediatric acute lymphoblastic leukemia by gene expression profiling.* Cancer Cell, 2002. **1**(2): p. 133-43.

166. Sawyers, C.L., *Resistance to imatinib: more and more mutations.* Blood, 2003. **102**(1): p. 4-5.

167. Holleman, A., et al., *Expression of the outcome predictor in acute leukemia 1 (OPAL1) gene is not an independent prognostic factor in patients treated according to COALL or St Jude protocols.* Blood, 2006. **108**(6): p. 1984-90.

168. Kanderova, V., et al., *High-resolution Antibody Array Analysis of Childhood Acute Leukemia Cells.* Mol Cell Proteomics, 2016. **15**(4): p. 1246-61.

169. Zaliova, M., et al., *ETV6/RUNX1-like acute lymphoblastic leukemia: A novel B-cell precursor leukemia subtype associated with the CD27/CD44 immunophenotype.* Genes Chromosomes Cancer, 2017. **56**(8): p. 608-616.

170. Jenickova, I., et al., *Efficient allele conversion in mouse zygotes and primary cells based on electroporation of Cre protein.* Methods, 2021. **191**: p. 87-94.

171. Cassel, S.L., et al., *Inflammasome-independent IL-1β mediates autoinflammatory disease in Pstpip2-deficient mice.* Proc Natl Acad Sci U S A, 2014. **111**(3): p. 1072-7.

172. Liao, H.J., et al., *Increased neutrophil infiltration, IL-1 production and a SAPHO syndrome-like phenotype in PSTPIP2-deficient mice.* Rheumatology (Oxford), 2015. **54**(7): p. 1317-26.

173. Zenobia, C. and G. Hajishengallis, *Basic biology and role of interleukin-17 in immunity and inflammation.* Periodontol 2000, 2015. **69**(1): p. 142-59.

174. Flannigan, K.L., et al., *IL-17A-mediated neutrophil recruitment limits expansion of segmented filamentous bacteria.* Mucosal Immunol, 2017. **10**(3): p. 673-684.

175. Jin, W. and C. Dong, *IL-17 cytokines in immunity and inflammation.* Emerg Microbes Infect, 2013. **2**(9): p. e60.

176. Capucetti, A., F. Albano, and R. Bonecchi, *Multiple Roles for Chemokines in Neutrophil Biology.* Front Immunol, 2020. **11**: p. 1259.

177. Burke, S.J., et al., *NF-κB and STAT1 control CXCL1 and CXCL2 gene transcription.* Am J Physiol Endocrinol Metab, 2014. **306**(2): p. E131-49.

178. Widmer, U., et al., *Genomic cloning and promoter analysis of macrophage inflammatory protein (MIP)-2, MIP-1 alpha, and MIP-1 beta, members of the chemokine superfamily of proinflammatory cytokines.* J Immunol, 1993. **150**(11): p. 4996-5012.

179. Takahashi, T., et al., *Induction of chemokine CCL3 by NF-κB reduces methylmercury toxicity in C17.2 mouse neural stem cells.* Environ Toxicol Pharmacol, 2019. **71**: p. 103216.

180. Boespflug, N.D., et al., *ATF3 is a novel regulator of mouse neutrophil migration.* Blood, 2014. **123**(13): p. 2084-93.

181. Chandrasekar, B., et al., *Regulation of chemokines, CCL3 and CCL4, by interferon γ and nitric oxide synthase 2 in mouse macrophages and during Salmonella enterica serovar typhimurium infection.* J Infect Dis, 2013. **207**(10): p. 1556-68.

182. Förstner, P., et al., *Neuroinflammation after Traumatic Brain Injury Is Enhanced in Activating Transcription Factor 3 Mutant Mice.* J Neurotrauma, 2018. **35**(19): p. 2317-2329.

183. Ferguson, P.J. and R.M. Laxer, *New discoveries in CRMO: IL-1β, the neutrophil, and the microbiome implicated in disease pathogenesis in Pstpip2-deficient mice.* Semin Immunopathol, 2015. **37**(4): p. 407-12.

184. Hermiston, M.L., J. Zikherman, and J.W. Zhu, *CD45, CD148, and Lyp/Pep: critical phosphatases regulating Src family kinase signaling networks in immune cells.* Immunol Rev, 2009. **228**(1): p. 288-311.

185. Gurung, P., A. Burton, and T.D. Kanneganti, *NLRP3 inflammasome plays a redundant role with caspase 8 to promote IL-1β-mediated osteomyelitis.* Proc Natl Acad Sci U S A, 2016. **113**(16): p. 4452-7.

186. Kovács, M., et al., *The Src family kinases Hck, Fgr, and Lyn are critical for the generation of the in vivo inflammatory environment without a direct role in leukocyte recruitment.* J Exp Med, 2014. **211**(10): p. 1993-2011.

187. Wang, Y. and F. Jönsson, *Expression, Role, and Regulation of Neutrophil Fcγ Receptors.* Front Immunol, 2019. **10**: p. 1958.

8. REPRINT OF PUBLICATIONS

1. Pavliuchenko N, Duric I, Kralova J, et al. Molecular interactions of adaptor protein PSTPIP2 control neutrophil-mediated responses leading to autoinflammation. *Front Immunol*. 2022;13:1035226. Published 2022 Dec 20. doi:10.3389/fimmu.2022.1035226

2. Kralova J, Pavliuchenko N, Fabisik M, et al. The receptor-type protein tyrosine phosphatase CD45 promotes onset and severity of IL-1β-mediated autoinflammatory osteomyelitis. *J Biol Chem*. 2021;297(4):101131. doi:10.1016/j.jbc.2021.101131

3. Fabisik M, Tureckova J, Pavliuchenko N, et al. Regulation of Inflammatory Response by Transmembrane Adaptor Protein LST1. *Front Immunol*. 2021;12:618332. Published 2021 Apr 27. doi:10.3389/fimmu.2021.618332

4. Borna S, Drobek A, Kralova J, et al. Transmembrane adaptor protein WBP1L regulates CXCR4 signalling and murine haematopoiesis. *J Cell Mol Med*. 2020;24(2):1980-1992. doi:10.1111/jcmm.14895

Molecular interactions of adaptor protein PSTPIP2 control neutrophil-mediated responses leading to autoinflammation

Nataliia Pavliuchenko[1,2], Iris Duric[1,2], Jarmila Kralova[1], Matej Fabisik[1], Frantisek Spoutil[3], Jan Prochazka[3,4], Petr Kasparek[3], Jana Pokorna[1], Tereza Skopcova[1], Radislav Sedlacek[3,4] and Tomas Brdicka[1]*

[1]Laboratory of Leukocyte Signalling, Institute of Molecular Genetics of the Czech Academy of Sciences, Prague, Czechia, [2]Department of Cell Biology, Charles University, Faculty of Science, Prague, Czechia, [3]Czech Centre for Phenogenomics, Institute of Molecular Genetics of the Czech Academy of Sciences, Vestec, Czechia, [4]Laboratory of Transgenic Models of Diseases, Institute of Molecular Genetics of the Czech Academy of Sciences, Vestec, Czechia

Introduction: Autoinflammatory diseases are characterized by dysregulation of innate immune system leading to spontaneous sterile inflammation. One of the well-established animal models of this group of disorders is the mouse strain *Pstpip2^{cmo}*. In this strain, the loss of adaptor protein PSTPIP2 leads to the autoinflammatory disease chronic multifocal osteomyelitis. It is manifested by sterile inflammation of the bones and surrounding soft tissues of the hind limbs and tail. The disease development is propelled by elevated production of IL-1β and reactive oxygen species by neutrophil granulocytes. However, the molecular mechanisms linking PSTPIP2 and these pathways have not been established. Candidate proteins potentially involved in these mechanisms include PSTPIP2 binding partners, PEST family phosphatases (PEST-PTPs) and phosphoinositide phosphatase SHIP1.

Methods: To address the role of these proteins in PSTPIP2-mediated control of inflammation, we have generated mouse strains in which PEST-PTP or SHIP1 binding sites in PSTPIP2 have been disrupted. In these mouse strains, we followed disease symptoms and various inflammation markers.

Results: Our data show that mutation of the PEST-PTP binding site causes symptomatic disease, whereas mice lacking the SHIP1 interaction site remain asymptomatic. Importantly, both binding partners of PSTPIP2 contribute equally to the control of IL-1β production, while PEST-PTPs have a dominant role in the regulation of reactive oxygen species. In addition, the interaction of PEST-PTPs with PSTPIP2 regulates the production of the chemokine CXCL2 by

neutrophils. Its secretion likely creates a positive feedback loop that drives neutrophil recruitment to the affected tissues.

Conclusions: We demonstrate that PSTPIP2-bound PEST-PTPs and SHIP1 together control the IL-1β pathway. In addition, PEST-PTPs have unique roles in the control of reactive oxygen species and chemokine production, which in the absence of PEST-PTP binding to PSTPIP2 shift the balance towards symptomatic disease.

1 Introduction

Chronic recurrent multifocal osteomyelitis (CRMO) is an autoinflammatory disease characterized by the development of sterile inflammatory lesions in the bones. Treatment strategies include various ways to suppress inflammation. However, they often fail to induce long-term remission and in many patients the disease relapses (1–3). In part, this is the consequence of the fact that the molecular mechanisms and genetic causes of this disease are poorly understood. To gain better insight into the mechanisms driving CRMO development, several mouse models have been generated. One of the best studied is chronic multifocal osteomyelitis (CMO) mouse model *Pstpip2^{cmo}*, which develops sterile bone inflammation in the hind feet and tail (4). The disease is caused by a point mutation in the *Pstpip2* gene, which results in a complete loss of detectable expression of the adaptor protein PSTPIP2 (proline-serine-threonine phosphatase-interacting protein 2) (5, 6). The development of osteomyelitis in the *Pstpip2^{cmo}* mice is hematopoietically driven and occurs in the absence of lymphocytes, consistent with an autoinflammatory mechanism of the disease (6). However, similar to human CRMO, the signaling and inflammatory pathways critical for CMO in mice are incompletely understood. Previous studies identified neutrophil granulocytes as a crucial cell type critical for the disease development in *Pstpip2^{cmo}* mice (7, 8). They display pathological hyperactivity of the pathways regulating production of active IL-1β and reactive oxygen species (ROS). While IL-1β triggers autoinflammation, ROS production is critical for the bone damage (7–11). Little is known about the molecular mechanisms connecting PSTPIP2 to these pathways.

PSTPIP2 interacts with several regulators of signaling. The most prominent include PEST-family protein tyrosine phosphatases (PEST-PTPs) and Src homology 2-domain–containing inositol 5-phosphatase 1 (SHIP1), binding of which is dependent on W232 and phosphorylated C-terminal tyrosines of PSTPIP2, respectively (12–14). These proteins are the best candidates, through which PSTPIP2 could negatively regulate pro-inflammatory signaling. The family of PEST-PTPs has three members, PTPN12 (PTP-PEST), PTPN22 (LYP/PEP), and PTPN18 (BDP1/PTP-HSCF), which all interact with PSTPIP2 (14, 15). While little is known about the roles of PTPN12 and PTPN18 in neutrophils, deficiency in PTPN22 was shown to impair neutrophil functions triggered by Fc receptor stimulation, including adhesion, ROS production, degranulation, and development of K/B×N arthritis (16). These results suggested that PTPN22 promotes, rather than inhibits, neutrophil-driven inflammation. On the other hand, the *in vitro* data from overexpression studies in cell lines suggested that PSTPIP2-bound PEST-PTPs suppress pro-inflammatory signaling (14). While the data from *in vivo* models are generally more reliable than cell line overexpression studies, in this case the single deficiency in the mouse model could have revealed only the unique role of PTPN22, while the functions, where it is redundant with other PEST-PTPs, could have remained hidden, leaving the overall role of PEST-PTPs in neutrophil-mediated inflammatory response unclear.

Another known binding partner of PSTPIP2, SHIP1 (14) is a multifunctional protein expressed predominantly by hematopoietic cells and osteoblasts. SHIP1 removes the 5' phosphate from the product of PI3-kinase, PtdIns(3,4,5)P3, to generate PtdIns(3,4)P2 and this way partially antagonizes PI3-kinase pathway (17). SHIP1 deficiency results in enhanced ROS production and in reduced migration of neutrophils as a consequence of increased cell adhesion (18). *In vivo*, SHIP1-deficiency in mice causes inflammatory disease with myeloid infiltrates to the lungs and other organs (19). These data are generally consistent with anti-inflammatory function of SHIP1 and with connection to PSTPIP2. However, despite some

common features, there are also many differences between the consequences of SHIP1 and PSTPIP2 deficiency and it has been unclear which functions of SHIP1 depend on their interaction.

To understand the *in vivo* function of PSTPIP2 interactions with PEST-PTPs or SHIP1, we have investigated the effects of mutations in PSTPIP2 that prevent binding of PEST-PTPs or SHIP1 *in vivo*. We have established the links between PSTPIP2 interactions, dysregulations of the pro-inflammatory pathways and disease symptoms and identified the functions of PEST-PTPs and SHIP1 in the context of their interactions with PSTPIP2 and autoinflammation.

2 Materials and methods

2.1 Mice

Pstpip2cmo mice on C57Bl/6NCrl genetic background carrying the c.293T→C mutation in the *Pstpip2* gene, were generated from C.Cg-*Pstpip2cmo*/J mouse strain on Balb/C genetic background (4, 5) obtained from The Jackson Laboratory (Bar Harbor, ME), by backcrossing for more than 10 generations to C57Bl/6J (7) and then for more than 5 generations to C57Bl/6NCrl. C57BL/6NCrl and C57BL/6J inbred strains were obtained from the animal facility of Institute of Molecular Genetics, Czech Academy of Sciences (Prague, Czech Republic). To generate mouse strains carrying mutations in the C-terminal part of the *Pstpip2* gene (*Pstpip2Y323F*, *Pstpip2ΔC-term*, and *Pstpip2Y323**), specific guide RNA recognizing exon 14 of *Pstpip2* gene (5′-AGATG ATCCTGATTACTCTG-3′) was designed and off-target analysis was performed using the online software CRISPOR Design Tool (http://crispor.tefor.net/). Cas9 protein and gRNAs with corresponding ssDNA template (5′-CCAGGCAG GTTAATGACTCTTACCACCTCTGACGTCACTGgaA GAGCAAACTGaAATCTTCAACCACActaaaATCcGGAT CATCTGCAAAGGGAAGGGCACAGGACAGAACTCAGC-3′) were used for a zygote electroporation as described elsewhere (20). Similarly, mouse strains *Pstpip2W232A* and *Pstpip2-/-* were prepared by electroporation of gRNA recognizing exon 10 of *Pstpip2* (5′-ACTTCTTCCGGAATGCACTG-3′) together with a corresponding ssDNA template (5′-CATTTGCGA CACATTGTTGTGACAGCTGATTCAGATGCAAtgcCAaTG CATTCCGGAAGAAGTTGATTCGTTCACATTCCTGAGC C-3′) (Figure 1A). Each strain was then backcrossed to C57BL/6NCrl background for more than 5 generations. Unless indicated otherwise, age of animals ranged from 8 to 12 weeks. Experiments in this work conducted on animals were approved by the Expert Committee on the Welfare of Experimental Animals of the Institute of Molecular Genetics and by the Czech Academy of Sciences and were in accordance with local legal requirements and ethical guidelines.

2.2 Micro computed tomography

Hind paws of 3-5 mice per strain (16-25 weeks old) were used for the micro-CT analysis. They were scanned *in vivo* in X-ray micro-CT Skyscan 1176 (Bruker, Belgium) using the following parameters: voltage: 50 kV, current: 250 µA, filter: 0.5 mm aluminium, voxel size: 8.67 µm, exposure time: 2 s, rotation step: 0.3° for 180° total, object to source distance: 119.271 mm, and camera to source distance: 171.987 mm, time of scanning: 26 min. Virtual sections were reconstructed in NRecon software 1.7.1.0 (Bruker, Belgium) with following parameters: smoothing = 3, ring artifact correction = 4, and beam hardening correction = 36%. Intensities of interest for reconstruction were in the range from 0.0045 to 0.0900 Attenuation units. Same orientation of virtual sections was achieved with the use of the DataViewer 1.5.4 software (Bruker, Belgium). Micro-CT data analysis was performed using CT Analyser 1.18.4.0 (Bruker, Beelgium). Scans affected by technical artifacts resulting from spontaneous movements of animals were excluded from the analysis. Only distal half of the paws (from the half of the length of the longest metatarsal bone to fingertips) were analyzed. Bone damage (Figure 2D) is represented by bone fragmentation, which is calculated as the average number of bony objects (i.e. the bone with high density) per one virtual section. Without bone damage, 4-5 bone fragments (i.e. objects) per section are typically observed. With bone damage, this number increases. To calculate the volume of the soft tissue (Figure 2E), volumes of both high density and low density (newly formed) bone were subtracted from the volume of the entire paw (without background and noise).

2.3 Superoxide detection

Superoxide production *in vitro* was assessed by luminol-based chemiluminescence assay (21, 22). BM cells in IMDM supplemented with 0.2% FCS were plated at a density of 10^6 cells per well into a black 96-well plate in duplicates (SPL Life Sciences, Naechon-Myeon, Korea). Cells were rested for 10 min at 37°C and 5% CO_2. Then, luminol (123072, Sigma-Aldrich) at final concentration 100 mM and silica (S5631, Sigma-Aldrich) 50 mg/cm^2 were added. Luminescence was measured immediately on an EnVision plate reader (Perkin Elmer, Waltham, MA); each well was scanned every minute for 60 min.

2.4 Real-time quantitative PCR

RNA from neutrophils purified by negative selection was isolated with Zymo Research Quick-RNA Miniprep Plus Kit. The reverse transcription was performed with RevertAid First

Strand cDNA Synthesis Kit (ThermoFisher Scientific). Real-time quantitative PCR was carried out using LightCycler 480 SYBR Green I Master mix (Roche) on Roche LightCycler 480 II instrument. The following primers were used (5'-3'):

Cxcl2 AGTTTGCCTTGACCCTGAAGCC, CCAGGTCAGTTAGCCTTGCCTTTG;

Actb (β-actin) GATCTGGCACCACACCTTCT, GGGGTGTTGAAGGTCTCAAA;

Pstpip2 CGGACTTGCTCATACATCTC, CTGGCAGAGTGAACACATTA.

2.5 Antibodies

Rabbit monoclonal antibodies to murine IL-1β (clone D3H1Z), neutrophil elastase (clone E8U3X), PTP-PEST (clone D4W7W), and rabbit polyclonal antibody to SHIP1 (D1163) were from Cell Signaling Technology, rabbit polyclonal antibody to GAPDH (#G9545) from Sigma-Aldrich. The monoclonal antibodies to phosphotyrosine (clone 4G10) and PSTPIP2 (clones PSTPIP2-01 and PSTPIP2-03 (14)) were produced in-house with the use of respective hybridomas. Flow cytometry antibodies Ly6G-FITC (catalog # 127606, also used for Western blot), Ly6C-PE-Cy7 (# 128018), CD11b-PE (# 101208) were from Biolegend and CD62L-APC (# 177-0621-81) was from eBioscience (ThermoFisher).

2.6 Cell isolation and activation

Hind paw leukocytes were isolated by crushing the tissue using mortar and pestle in PBS with 2% FCS. The resulting suspension was filtered over the cell strainer, followed by centrifugation (500 x g, 5 min, 2°C) and erythrocyte lysis in ACK buffer (150 mM NH$_4$Cl, 0.1 mM EDTA (disodium salt), 1 mM KHCO$_3$). Bone marrow cells were isolated by flushing femurs (cut at extremities) with PBS supplemented with 2% FCS, followed by red blood cell lysis with ACK buffer. Neutrophils were isolated from bone marrow cells by negative selection using mouse Neutrophil Isolation Kit (Miltenyi Biotec, catalog # 130-097-658) and autoMACS Pro magnetic cell separator (Miltenyi Biotec) according to manufacturer's instructions. For LPS activation, 2×10^6 cells in 700 μL IMDM with 0.1% FCS were placed in low protein-binding microcentrifuge tubes (Thermo Fisher Scientific). Subsequently, the cells were activated with 10 ng/ml LPS (L4516, Sigma-Aldrich) for 3 hours at 37°C, 5% CO$_2$. For pervanadate activation, pervanadate was prepared by mixing 10 mM sodium orthovanadate with 0.3% hydrogen peroxide followed by 20 min incubation at room temperature. 100 μl of the resulting mixture was used for activation of 1.2×10^7 cells in 1 ml media (20 min at 37°C).

2.7 Cell lysis, and immunoprecipitation

For immunoblotting cell suspensions described above were lysed by addition of an equal volume of a 2× concentrated SDS-PAGE sample buffer (128 mM Tris [pH 6.8], 10% glycerol, 4% SDS, 2% DTT), followed by the sonication and heating (99°C for 2 min). For immunoprecipitation cells were lysed in lysis buffer (50 mM TRIS-HCl pH 7.5; 150 mM NaCl; 1% *n*-dodecyl β-d-maltoside; 1000× diluted Diisopropyl-fluorophosphate [Sigma, Merck]; cOmplete EDTA-free protease inhibitor cocktail (Roche), PhosStop phosphatase inhibitor cocktail (Roche) at 1.2×10^8 cells in 1.2 ml, for 30 min on ice. Post-nuclear supernatants were then incubated for 1 h with PSTPIP2-03 antibody (4.5 μg), followed by 1.5 h of incubation with 40 μl Protein A/G Plus agarose bead suspension (Santa Cruz Biotechnology) at 4°C. After washing on spin columns (Micro Bio-Spin columns, Bio-Rad Laboratories), immunoprecipitates were eluted with 30 μl SDS-PAGE sample buffer.

2.8 Tissue homogenates

Hind paw tissue was cut into small pieces and homogenized with Avans AHM1 Homogenizer (30 s, speed 25) in 1 ml RIPA buffer (TRIS-HCl pH7.5, 150 mM NaCl, 1% NP-40, 1% Deoxycholate, and 0.1% SDS, 5 mM iodoacetamide, 100× diluted Protease Inhibitor Cocktail set III [Calbiochem]). After two rounds of centrifugation (each 20,000 x g, 5 min, 2°C) the lysates were snap-frozen in liquid nitrogen and stored in -80°C.

2.9 ELISA

Frozen tissue homogenates (from 12-25 weeks old mice) described above were thawed, total protein concentration was measured using Pierce BCA Protein Assay Kit (Thermo Scientific #23227) and the samples were adjusted to equal protein concentration. ELISA was performed according to manufacturer's instructions using IL-1 beta Mouse Uncoated ELISA Kit, MIP-2/CXCL2 Mouse ELISA Kit, MIP-1a (CCL3) Mouse Uncoated ELISA Kit (Invitrogen, ThermoFisher Scientific, catalog numbers 88-7013-88, EMCXCL2, and 88-56013-88), Mouse IL-17A/F Heterodimer DuoSet ELISA, and Mouse CXCL1/KC DuoSet ELISA DY5390-05, and DuoSet ELISA Ancillary Reagent Kit 2 (R&D Systems, catalog numbers DY5390-05, DY453-05, DY008).

2.10 Flow cytometry

Single-cell suspensions were labeled with 100× - 200× diluted antibodies and Hoechst 33342 dye (to detect dead

cells) in PBS/2%FCS for 40 min on ice. Cells were then washed in PBS/2% FCS and analyzed on a BD Symphony flow cytometer. The data were analyzed with FlowJo software (BD Biosciences, Franklin Lakes, NJ).

2.11 Statistical analysis

The p values were calculated in GraphPad Prism software (GraphPad Software, La Jolla, CA) using one-way ANOVA with *post-hoc* t-test for data in Figures 3B, E, F, 4B-G (with Welch's correction where variances were unequal) or Kruskal-Wallis test with *post-hoc* Mann-Whitney test for data with non-normal distribution (Figures 2D, E, 3C-D). For multiple comparisons, significance threshold was adjusted with Holm-Bonferroni method. The p values for disease-free curves (Figure 2A) were calculated using the long-rank (Mantel-Cox) test.

3 Results

3.1 Generation of mouse strains with mutations in *Pstpip2*

To investigate the role of the interactions between PSTPIP2 and PEST-PTPs or SHIP1, we employed CRISPR/Cas9 technology to generate mutant mouse strains harboring mutations in PSTPIP2 that abrogate these interactions. Binding to PEST-family phosphatases is known to require W232, while binding to SHIP1 is dependent on C-terminal tyrosines (Y323, Y329, Y333) (Figure 1A). First, we generated mouse strain where W232 was replaced with alanine to prevent interaction with PEST phosphatases ($Pstpip2^{W232A}$)(Figure 1A and Supplementary Figure 1A). In addition we attempted to generate a strain where all three C-terminal tyrosines were replaced with phenylalanines. Our targeting strategy was expected to also result in various truncations in the PSTPIP2 C-terminus. While the attempt to generate triple tyrosine mutant was unsuccessful, we obtained a strain, where a single nucleotide insertion into the codon of the first C-terminal tyrosine (Y323) created a stop codon resulting in the loss of the last twelve amino-acids (323–334), including all three targeted tyrosines ($Pstpip2^{Y323*}$) (Supplementary Figure 1B). In addition we also obtained a strain where a 17 bp deletion resulted in a stop codon immediately after the first of the three tyrosines, Y323 ($Pstpip2^{\Delta C\text{-}term}$) (Figure 1A and Supplementary Figure 1C). In this strain, while Y323 is preserved, the absence of the amino acids immediately following it was expected to result in a loss of SHIP1 SH2 domain binding, because the amino acids downstream of the phosphorylated tyrosine are critical for this interaction (23–25). Thus, we expected that in this strain

PSTPIP2 C-terminus including all the C-terminal tyrosines was effectively non-functional. Finally, within this attempt we obtained an additional strain where Y323 is replaced with phenylalanine ($Pstpip2^{Y323F}$) (Figure 1A and Supplementary Figure 1C). In addition we generated mouse strain with 116 bp deletion encompassing part of the exon coding W232 together with a part of the preceding intron, resulting in the complete loss of PSTPIP2 expression ($Pstpip2^{-/-}$) (Supplementary Figure 1D). Alignments of mutant and wild-type sequences are shown in Supplementary Figures 1A–D.

While PSTPIP2 protein levels were normal in $Pstpip2^{Y323F}$ mouse strain (Figure 1B), other mutations we introduced influenced its protein expression levels in neutrophil granulocytes. This was most evident in $Pstpip2^{Y323*}$ mice where we detected only very low amounts of PSTPIP2 protein, ca 20 - 25% of wild-type levels (Supplementary Figure 1E). Interestingly, in $Pstpip2^{\Delta C\text{-}term}$ mice, where the stop codon was only one position downstream, PSTPIP2 expression was comparable to wild-type (WT) mice. Since it was not possible to distinguish the effects of reduced PSTPIP2 expression on disease development from the effects of the mutation, we excluded $Pstpip2^{Y323*}$ from subsequent analysis. Expression levels of *W232A* mutant were also somewhat reduced. However, they were comparable to PSTPIP2 expression in $Pstpip2^{+/-}$ heterozygotes (Figure 1B). Hence, we included $Pstpip2^{+/-}$ mice in subsequent analysis to control for the effects of reduced PSTPIP2 expression on the phenotype of $Pstpip2^{W232A}$ mice. PSTPIP2 protein was not detected in $Pstpip2^{cmo}$ and $Pstpip2^{-/-}$ neutrophils (Figure 1B). Interestingly, $Pstpip2$ mRNA levels were normal in $Pstpip2^{cmo}$ neutrophils, while only traces of $Pstpip2$ mRNA could be detected in $Pstpip2^{-/-}$ cells (Supplementary Figure 1F).

3.2 *Pstpip2* mutations abolish binding to PTP-PEST and SHIP1

To verify that the mutations had the intended effect and abolished interactions with major PSTPIP2 binding partners, we immunoprecipitated PSTPIP2 from bone marrow cells isolated from the individual mouse strains, followed by detection of PTP-PEST, SHIP1 and (phospho-)PSTPIP2 by immunoblotting. W232A mutation resulted in the loss of PTP-PEST binding without affecting PSTPIP2 phosphorylation, suggesting that PEST-PTPs bound to PSTPIP2 do not control its phosphorylation (Figure 1C). Conversely, the deletion of PSTPIP2 C-terminus resulted in the loss of PSTPIP2 phosphorylation, but it did not affect binding to PTP-PEST (Figure 1C). As expected, deletion of PSTPIP2 C-terminus also resulted in the loss of SHIP1 binding. Interestingly, mutation of a single C-terminal tyrosine Y323 did not have any effect on SHIP1 binding (Figure 1D).
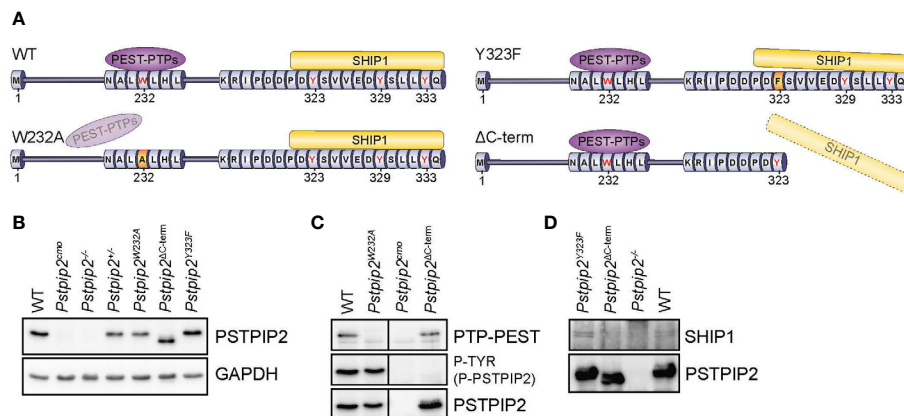
FIGURE 1

PSTPIP2 mutations in mice and verification of their effects on the interactions with binding partners. **(A)** Schematic representation of mutant PSTPIP2 proteins and their interactions in the individual mouse strains. **(B)** Lysates of purified neutrophils from WT and PSTPIP2 mutant mice were subjected to immunoblotting with the indicated antibodies to detect PSTPIP2 protein levels in the individual mouse strains. **(C)** PSTPIP2 was immunoprecipitated from the lysates of bone marrow cells from the indicated mouse strains. Co-immunoprecipitated PTP-PEST and PSTPIP2 tyrosine phosphorylation were detected by immunoblotting with PTP-PEST and phosphotyrosine antibodies, respectively. **(D)** Similar experiment as in **(C)** to detect interaction of PSTPIP2 with SHIP1. To maximize PSTPIP2 phosphorylation, cells in **(D)** were treated with pervanadate.

3.3 Mutation of W232 results in symptomatic disease, while mutations of the PSTPIP2 C-terminus do not cause disease symptoms

Each mutant mouse strain was monitored for the development of chronic multifocal osteomyelitis symptoms (Figure 2A). $Pstpip2^{-/-}$ and $Pstpip2^{cmo}$ mice developed the first visually observable symptoms within 8 weeks after birth. In $Pstpip2^{W232A}$ strain the first symptom occurrence was delayed till 14-16 weeks of age. Only hind paws were affected in this strain. Visible kinks or swelling in the tails were not detected. In addition, the disease was much milder and not 100% penetrant since part of the animals remained asymptomatic throughout the entire 42 weeks of observation. The mutations of the PSTPIP2 C-terminus did not result in any visually detectable symptoms. The same was true for heterozygous $Pstpip2^{+/-}$ mice (Figures 2A, B).

In agreement with these results, micro-CT data (Figure 2C) showed significantly elevated bone damage in $Pstpip2^{cmo}$, $Pstpip2^{-/-}$, and $Pstpip2^{W232A}$ mice, while in the animals carrying mutations in the C-terminus ($Pstpip2^{\Delta C-term}$, $Pstpip2^{Y323F}$), no bone damage was detected (Figure 2D). Compared to $Pstpip2^{cmo}$ and $Pstpip2^{-/-}$, the bone damage in $Pstpip2^{W232A}$ animals was very mild, though still significantly increased. Soft tissue volume, a measure of swelling, was significantly higher only in $Pstpip2^{cmo}$ and $Pstpip2^{-/-}$ mice (Figure 2E). No significant increase of soft tissue swelling was detected in $Pstpip2^{W232A}$ animals. Taken together, the interaction with PEST-PTPs abrogated by W232A mutation

plays more important role in the control of inflammation than binding of SHIP1, the loss of which does not contribute to the development of visible symptoms.

3.4 Differential control of ROS and IL-1β production by PSTPIP2 binding partners

Two key pro-inflammatory pathways are known to be dysregulated in $Pstpip2^{cmo}$ neutrophils, pathway leading to the activation of NADPH oxidase and pathway stimulating production of IL-1β. While IL-1β overproduction triggers spontaneous inflammation, superoxide production by NADPH oxidase is critical for the bone damage (8). Therefore, we aimed to evaluate whether the interactions of PSTPIP2 with PEST-PTPs and SHIP1 control these pathways and, consequently a pathogenesis of CMO. Consistent with previously published data, we observed substantially increased ROS production by $Pstpip2^{cmo}$ and $Pstpip2^{-/-}$ cells upon silica stimulation. Strikingly, in $Pstpip2^{W232A}$ cells ROS production was deregulated to a similar extent as in $Pstpip2^{cmo}$ and $Pstpip2^{-/-}$ cells. On the other hand, cells from mice that do not develop any visible disease symptoms, including $Pstpip2^{\Delta C-term}$, $Pstpip2^{Y323F}$ and $Pstpip2^{+/-}$ showed only minor elevation of ROS production (Figures 3A, B). To test the activity of IL-1β pathway, we measured the concentration of IL-1β in the lysates from hind paws of WT and mutant mice. IL-1β levels measured by ELISA were significantly increased in $Pstpip2^{cmo}$, $Pstpip2^{-/-}$, $Pstpip2^{W232A}$, and $Pstpip2^{\Delta C-term}$ mice. However, in contrast to the ROS production, IL-1β pathway dysregulation was milder in
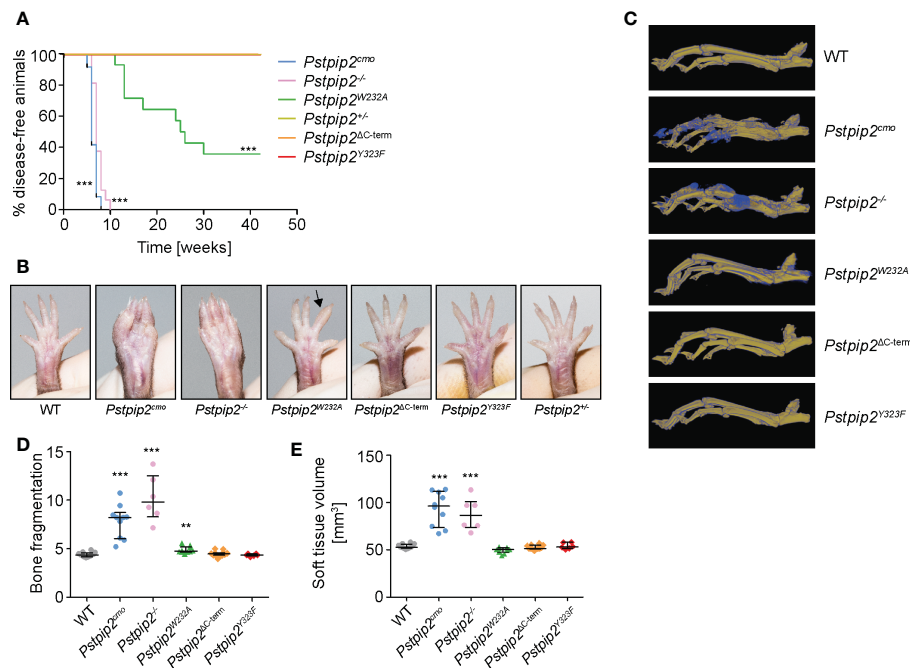
FIGURE 2

Symptoms of osteomyelitis in mutant mouse strains. **(A)** Mice of the indicated mouse strains were monitored for the onset of disease symptoms. The graph shows percentages of animals that were free of visible symptoms at the given time-point. Animal numbers and sexes in this experiment were as follows: *Pstpip2⁺/⁻* [6 males (m), 6 females (f)], *Pstpip2⁻/⁻* [7 m, 9 f], *Pstpip2^cmo* [3 m, 11 f], *Pstpip2^W232A* [4 m, 10 f], *Pstpip2^ΔC-term* [5 m, 9 f], *Pstpip2^Y323F* [2 m, 12 f]. **(B)** Photographs of hind paws of WT and mutant mice. 18-27 weeks old WT, *Pstpip2^cmo*, *Pstpip2⁻/⁻*, and *Pstpip2^W232A*, are compared to more than 50 weeks old *Pstpip2^ΔC-term*, *Pstpip2^Y323F*, and *Pstpip2⁺/⁻* mice. **(C)** Micro-CT reconstructions of hind paw bones of WT and mutant mice. Pseudocolors mark old (in yellow) and newly formed (in blue) bone mass. **(D)** Quantification of bone damage measured as bone fragmentation in paw bones of multiple mice detected in micro-CT scans. **(E)** Calculation of soft tissue volume from micro-CT scans as a measure of soft tissue swelling. Error bars represent median with interquartile range. Asterisks describe p values for comparisons with *Pstpip2⁺/⁻* **(A)** or WT **(D, E)**; **p ≤ 0.01, ***p ≤ 0.001. See *Materials and Methods* for further details on statistical analysis.

Pstpip2^W232A and *Pstpip2^ΔC-term* mice, when compared to the strains completely lacking PSTPIP2 protein (Figure 3C). We have also performed an analysis of active form IL-1β p17 in the strains that had abrogated binding between PSTPIP2 and its interacting partners. It showed similar results with the highest increase in *Pstpip2^cmo* mice and a small increase in *Pstpip2^W232A* and *Pstpip2^ΔC-term* mice (Figure 3D). Next, we sought to evaluate the *in vitro* ability of isolated bone marrow cells from these mutants to produce pro-IL-1β upon LPS stimulation. Consistent with the *in vivo* results, the highest pro-IL-1β production was observed in *Pstpip2^cmo* and *Pstpip2⁻/⁻* cells while *Pstpip2^W232A* and *Pstpip2^ΔC-term* displayed only moderate increase (Figure 3E). Similar results were also obtained with purified bone marrow neutrophils, although in *Pstpip2^ΔC-term* mice the increase in pro-IL-1β production was not statistically significant (Figure 3F). These observations suggest that PSTPIP2-bound PEST-PTPs play dominant role in the control of the oxidative burst, while the regulation of IL-1β production is more equally divided between the both PSTPIP2 binding partners.

3.5 PEST-PTPs regulate neutrophil recruitment to the site of inflammation

Neutrophils, a critical cell type in osteomyelitis development in *Pstpip2^cmo* mice, were found to infiltrate the sites of inflammation in these animals. To assess the extent of neutrophil infiltration, we detected neutrophil markers neutrophil elastase and Ly6G in the lysates prepared from hind paws of WT and mutant animals. Increased presence of these markers was detected in *Pstpip2^cmo*, *Pstpip2⁻/⁻*, and *Pstpip2^W232A* tissues even in the absence of visible symptoms, but not in *Pstpip2^ΔC-term* (Figure 4A). These data confirm the involvement of neutrophils in the development of sterile inflammation. They also document the importance of PSTPIP2 binding to PEST-PTPs, which prevents neutrophil accumulation in the affected tissues. To further assess the activation status of these neutrophils, we measured the levels of CD62L on neutrophils isolated from hind paws of these animals. CD62L is shed as a result of neutrophil activation
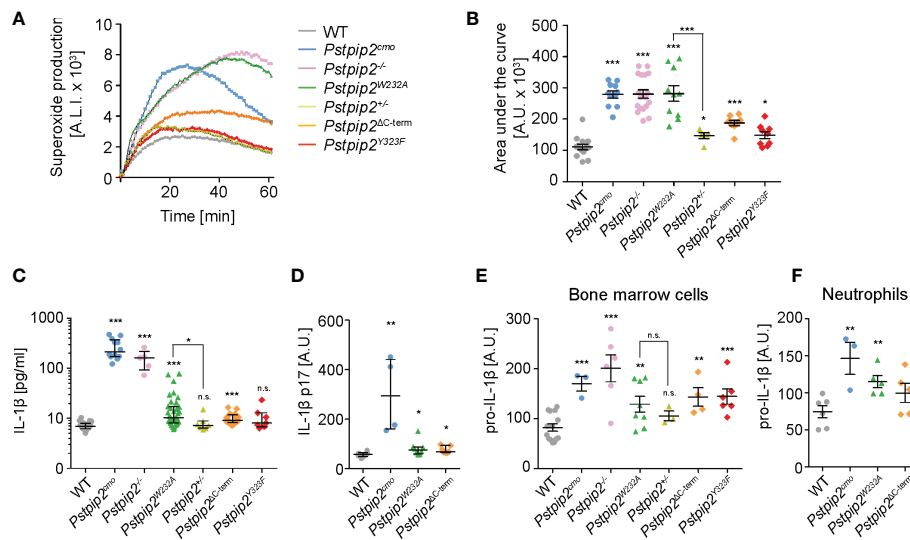
FIGURE 3
Production of superoxide and pro-IL-1β by neutrophils from WT and mutant mouse strains. **(A)** Superoxide production by silica-stimulated bone marrow cells measured in 1-min intervals by luminol-based chemiluminescence assay. **(B)** Quantification of the area under the curve for superoxide production measurements performed as in **(A)** on bone marrow cells from multiple mice. **(C)** IL-1β concentration in hind paw lysates detected by ELISA. **(D)** Quantification of active IL-1β p17 in hind paw lysates detected by Western blot. **(E, F)** Pro-IL-1β production by bone marrow cells **(E)** or purified neutrophils **(F)** activated with 10 ng/ml LPS detected by immunoblotting. Error bars represent mean $\pm$ SEM in **(B, E, F)** and median with interquartile range in **(C, D)**. Asterisks above individual columns describe p values for comparisons with WT, asterisks above connecting lines describe p values for comparisons of the columns connected by these lines; *p $\leq$ 0.05, **p $\leq$ 0.01, ***p $\leq$ 0.001, n.s. not significant. See *Materials and Methods* for further details on statistical analysis.

and lost from neutrophil surface (26). In *Pstpip2^cmo* mice, the proportion of activated (CD62L⁻) neutrophils was significantly increased, when compared to the WT animals. Strikingly, group that contained both symptomatic and asymptomatic *Pstpip2^W232A* mice also showed significantly increased levels of neutrophil activation. No such increase was observed in *Pstpip2^ΔC-term* mice (Figure 4B). Thus, PEST-PTP binding to PSTPIP2 is an important component of the mechanism controlling neutrophil activation and infiltration to the site of inflammation.

Chemokines play a key role in the neutrophil recruitment to the inflamed tissues (27). One of the factors able to control chemokine production in these tissues is IL-17 (28). Indeed, IL-17A/F levels were increased in the lysates prepared from footpads of *Pstpip2^cmo* mice (Figure 4C). However, *Pstpip2^W232A* and *Pstpip2^ΔC-term* mice did not show any alterations. Thus, while in *Pstpip2^cmo* mice IL17A/F could be contributing to the neutrophil recruitment to the inflammatory lesions, in *Pstpip2^W232A* mice this recruitment appears to be IL17A/F independent. Next, we focused on the most prominent chemokines known to attract neutrophils to the sites of inflammation, including CCL3 (MIP-1α), CXCL1 (KC), and CXCL2 (MIP-2). Concentration of all three chemokines measured by ELISA in hind paw lysates was increased in *Pstpip2^cmo* mice (Figures 4D–F). Importantly, only the concentration of CXCL2 was elevated in *Pstpip2^W232A* mice

and none in *Pstpip2^ΔC-term* animals, suggesting that dysregulation of CXCL2 is responsible for the early neutrophil recruitment initiating the disease development. Production of the other chemokines, as well as IL-17A/F, may be triggered later on as a secondary effect of progressing inflammation. CXCL2 is known to be secreted by tissue resident cells, such as epithelial cells, fibroblasts, mast cells or macrophages (29–34). However, the data of Immunological Genome Project Consortium (35) showed a very high expression of CXCL2 in thioglycolate induced peritoneal neutrophils, raising the possibility that in the context of CMO, neutrophils could be a major source of this chemokine. Strikingly, neutrophils purified from footpads of *Pstpip2^cmo* and *Pstpip2^W232A* mice both showed similar substantially increased levels of *Cxcl2* mRNA. On the other hand, *Pstpip2^Δ-term* neutrophils displayed levels comparable to their WT counterparts (Figure 4G). These results support the hypothesis that during CMO disease development, neutrophils are fueling their own recruitment via a positive feedback loop driven by production of CXCL2, which is further assisted by other chemokines in the later stages of the disease.

4 Discussion

During inflammatory response, neutrophils are capable of producing substantial collateral damage. It is exemplified by the
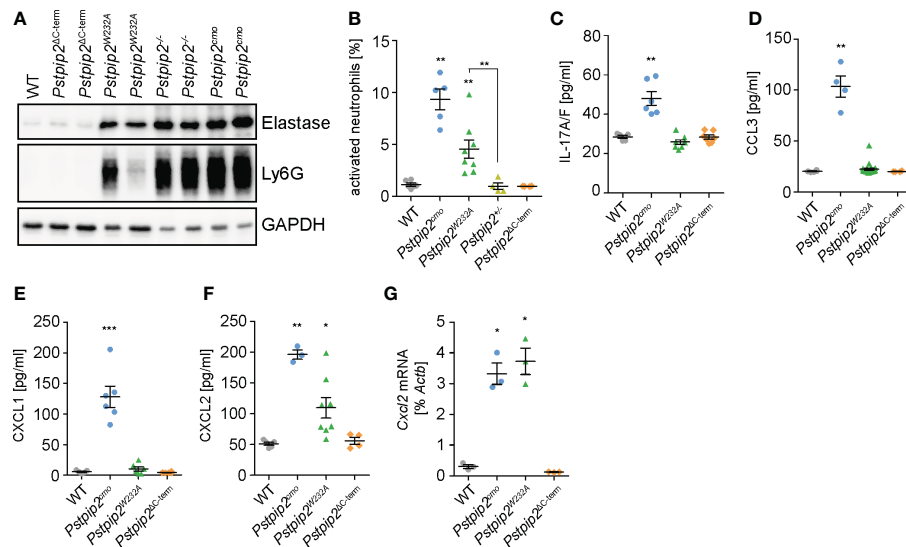
FIGURE 4

Neutrophil recruitment to the sites of inflammation. **(A)** Detection of neutrophil elastase and Ly6G in the hind paw lysates as a hallmark of neutrophil presence. **(B)** Percentages of activated (CD62L⁻) neutrophils within total neutrophils isolated from hind paws of the mice of indicated mouse strains measured by flow cytometry. **(C-F)** Concentrations of IL-17A/F **(C)**, CCL3 **(D)**, CXCL1 **(E)**, and CXCL2 **(F)** in hind paw lysates detected by ELISA. **(G)** *Cxcl2* mRNA levels in neutrophils purified from hind paws of the mice of indicated mouse strains determined by quantitative RT-PCR. Error bars represent mean ± SEM. Asterisks above individual columns describe p values for comparisons with WT, asterisks above connecting lines describe p values for comparisons of the columns connected by these lines; *$p \leq 0.05$, **$p \leq 0.01$, ***$p \leq 0.001$. See *Materials and Methods* for further details on statistical analysis.

development of autoinflammatory disease caused by the loss of PSTPIP2 adaptor protein, where hyper-activated neutrophils are the critical cell type required for inducing harm to the tissues (7, 8). Similar to other adaptor proteins, function of PSTPIP2 is mediated by its interactions with other signaling molecules. The most prominent include PEST-family PTPs and SHIP1 (12–14). However, their particular roles in the suppression of inflammation by PSTPIP2 have been unknown. Our data demonstrate the importance of the interactions of PEST-PTPs with PSTPIP2. The loss of their binding leads to the development of autoinflammatory disease, which is milder but otherwise similar to the disease that develops as a consequence of the inactivation of PSTPIP2 gene. The loss of interaction with SHIP1 does not result in visible disease symptoms. Nevertheless, certain level of immune system dysregulation can still be observed. These data suggest that both binding partners contribute to the suppression of pro-inflammatory signaling and autoinflammation. However, only the loss of PEST-PTP binding results in the dysregulation strong enough to cause visually observable disease symptoms.

Interestingly, PEST-PTPs play an important role in another autoinflammatory disorder named PAPA syndrome (pyogenic sterile arthritis, pyoderma gangrenosum, and acne) which is caused by the loss of their binding to PSTPIP1, a homologue of PSTPIP2. However the mechanism triggering the disease is very likely different. In PSTPIP1, the loss of PEST-PTP binding

results in PSTPIP1 hyperphoshorylation and consequent hyperactivation of pyrin inflammasome (36). Here, we did not observe any changes in PSTPIP2 phosphorylation after the loss of PEST-PTP binding. Moreover, when we abrogated this phosphorylation by the deletion of PSTPIP2 C-terminus, we observed increase of pro-inflammatory markers, while if the analogy with PSTPIP1 were valid, we would rather expect the opposite.

Interestingly, the mouse strains, where interactions with PEST-PTPs or SHIP1 were abolished, both displayed similar level of dysregulation of IL-1β pathway. Thus, the observed differences in disease manifestation cannot be explained by differential IL-1β production. On the other hand, ROS production in *Pstpip2^{W232A}* mice lacking PSTPIP2 - PEST-PTP interaction was deregulated to a similar extent as in mice entirely lacking PSTPIP2 protein, while the loss of SHIP1 binding in *Pstpip2^{ΔC-term}* animals had only mild effect on ROS. These data suggested that deregulated ROS production determines whether the mice develop bone damage and visible disease symptoms. We have shown before that ROS production is critical for damage to the bones in mice lacking PSTPIP2 but it is not required for enhanced IL-1β production and soft tissue inflammation (8). In line with this finding, our microCT analysis did not detect any evidence of soft tissue swelling in *Pstpip2^{W232A}* mice. Our data suggest that in mild variants of CMO disease, ROS production may decide between

symptomatic and asymptomatic outcome and could be considered as a potential pharmacological target in treatment strategies for similar diseases in humans.

The milder dysregulation of IL-1β production in $Pstpip2^{W232A}$ than in $Pstpip2^{-/-}$ and $Pstpip2^{cmo}$ mice can potentially explain the milder phenotype observed in these mice. These data show that PEST-PTPs are not sufficient for PSTPIP2-mediated control of inflammation and other factors must play a role. Similar level of IL-1β dysregulation in $Pstpip2^{\Delta C-term}$ mice suggests that SHIP1 can to some extent control IL-1β pathway and attenuate inflammatory response in $Pstpip2^{W232A}$ mice. Analysis of a mouse model with simultaneous loss of both binding sites in PSTPIP2 could help clarify the role of SHIP1, since IL-1β deregulation there may reach higher levels sufficient for the development of fully expressed symptoms. However, at present, such a model is not available. It is also possible that some other binding partners or features of PSTPIP2 are contributing to the control of inflammation in addition to PEST-PTPs and SHIP1.

The increased neutrophil infiltration in hind paws of $Pstpip2^{W232A}$ and PSTPIP2-fully deficient mouse strains but not in $Pstpip2^{\Delta C-term}$ animals suggested that chemokine production regulating neutrophil recruitment could also be dysregulated and help explain differences in disease manifestation between $Pstpip2^{W232A}$ and $Pstpip2^{\Delta C-term}$ animals. Indeed, we have observed increased amounts of CXCL1, CXCL2, and CCL3 in the hind paws of PSTPIP2 fully deficient mice. However only CXCL2 showed increased levels in $Pstpip2^{W232A}$ mice. Moreover, we detected high increase of $Cxcl2$ mRNA expression in $Pstpip2^{cmo}$ and $Pstpip2^{W232A}$ neutrophils purified from the site of inflammation. This increase appeared higher (more than ten-fold) than overall increase in the inflamed tissues (less than four-fold). These data suggested that neutrophils are a major source of CXCL2 during CMO development. Increased activation of transcription factor NF-κB was demonstrated in $Pstpip2^{cmo}$ mice (37). Production of pro-IL-1β, which is elevated in these mice, as well as production of CXCL1, CXCL2 and CCL3 are driven by this transcription factor (37–45). This suggests that there could be a common pathway, which is dysregulated in $Pstpip2^{cmo}$ mice, leading to enhanced NF-κB activity followed by increased production of pro-IL-1β and the chemokines. In contrast to $Cxcl1$ and $Ccl3$, $Cxcl2$ gene expression is not negatively regulated by a transcription factor ATF3, which may explain increased sensitivity of $Cxcl2$ gene expression to pro-inflammatory signaling and selective upregulation in $Pstpip2^{W232A}$ mice (46–48). CXCL2 production by neutrophils may represent an additional critical step in disease progression. It is very likely that activation of the positive feedback loops driven by neutrophil-produced IL-1β and CXCL2 result in substantial amplification of neutrophil response via further neutrophil recruitment and secondary production of additional IL-1β, CXCL2 and other chemokines, propelling the disease to its symptomatic stage. Our results also suggest that chemokine networks together with IL-17 may represent potential pharmacological targets/biomarkers in similar diseases in humans. However, proper analysis of their role would require further testing using mice double deficient in $Pstpip2$ and receptors or other critical components of these pathways.

In summary, together with earlier published results, our data demonstrate dysregulation of three major pathways, including production of IL-β, reactive oxygen species, and neutrophil-attracting chemokines, which jointly contribute to the development of CMO disease in $Pstpip2^{cmo}$ mouse model. Recruitment of PEST-PTPs and SHIP1 by PSTPIP2 have differential regulatory effects on these pathways. PEST-PTPs have a dominant role in the control of reactive oxygen species and to some extent also in the control of chemokine production, while they appear similarly important as SHIP1 in the control of IL-1β pathway. Direct targets of these phosphatases that regulate these pathways still remain unknown. However, the new mouse models generated within this work will be instrumental for their future identification.

Data availability statement

The original contributions presented in the study are included in the article Supplementary Material. Further inquiries can be directed to the corresponding author.

Ethics statement

The animal study was reviewed and approved by Expert Committee on the Welfare of Experimental Animals of the Institute of Molecular Genetics and the Czech Academy of Sciences.

Author contributions

TB and RS conceived, designed and supervised the study. NP, ID, JK, MF, FS, JPr, PK, JPo, and TS performed experiments. NP, JK, FS, JPr, PK and TB analyzed and interpreted the data. NP and TB wrote the first draft of the manuscript. All authors contributed to the article and approved the submitted version.

Funding

Acknowledgments

Conflict of interest

The authors declare that the research was conducted in the absence of any commercial or financial relationships that could be construed as a potential conflict of interest.

Publisher's note

All claims expressed in this article are solely those of the authors and do not necessarily represent those of their affiliated organizations, or those of the publisher, the editors and the reviewers. Any product that may be evaluated in this article, or claim that may be made by its manufacturer, is not guaranteed or endorsed by the publisher.

Supplementary material

The Supplementary Material for this article can be found online at: https://www.frontiersin.org/articles/10.3389/fimmu.2022.1035226/full#supplementary-material

References

1. Zhao Y, Ferguson PJ. Chronic non-bacterial osteomyelitis and autoinflammatory bone diseases. *Clin Immunol* (2020) 216:108458. doi: 10.1016/j.clim.2020.108458

2. Hofmann SR, Kapplusch F, Girschick HJ, Morbach H, Pablik J, Ferguson PJ, et al. Chronic recurrent multifocal osteomyelitis (CRMO): Presentation, pathogenesis, and treatment. *Curr Osteoporos Rep* (2017) 15(6):542–54. doi: 10.1007/s11914-017-0405-9

3. Zhao DY, McCann L, Hahn G, Hedrich CM. Chronic nonbacterial osteomyelitis (CNO) and chronic recurrent multifocal osteomyelitis (CRMO). *J Transl Autoimmun* (2021) 4:100095. doi: 10.1016/j.jtauto.2021.100095

4. Byrd L, Grossmann M, Potter M, Shen-Ong GL. Chronic multifocal osteomyelitis, a new recessive mutation on chromosome 18 of the mouse. *Genomics* (1991) 11(4):794–8. doi: 10.1016/0888-7543(91)90002-V

5. Ferguson PJ, Bing X, Vasef MA, Ochoa LA, Mahgoub A, Waldschmidt TJ, et al. A missense mutation in pstpip2 is associated with the murine autoinflammatory disorder chronic multifocal osteomyelitis. *Bone* (2006) 38 (1):41–7. doi: 10.1016/j.bone.2005.07.009

6. Chitu V, Ferguson PJ, de Bruijn R, Schlueter AJ, Ochoa LA, Waldschmidt TJ, et al. Primed innate immunity leads to autoinflammatory disease in PSTPIP2-deficient cmo mice. *Blood* (2009) 114(12):2497–505. doi: 10.1182/blood-2009-02-204925

7. Lukens JR, Gurung P, Vogel P, Johnson GR, Carter RA, McGoldrick DJ, et al. Dietary modulation of the microbiome affects autoinflammatory disease. *Nature* (2014) 516(7530):246–9. doi: 10.1038/nature13788

8. Kralova J, Drobek A, Prochazka J, Spoutil F, Fabisik M, Glatzova D, et al. Dysregulated NADPH oxidase promotes bone damage in murine model of autoinflammatory osteomyelitis. *J Immunol* (2020) 204(6):1607–20. doi: 10.4049/jimmunol.1900953

9. Cassel SL, Janczy JR, Bing X, Wilson SP, Olivier AK, Otero JE, et al. Inflammasome-independent IL-1β mediates autoinflammatory disease in Pstpip2-deficient mice. *Proc Natl Acad Sci* (2014) 111(3):1072–7. doi: 10.1073/pnas.1318685111

10. Gurung P, Burton A, Kanneganti TD. NLRP3 inflammasome plays a redundant role with caspase 8 to promote IL-1β-mediated osteomyelitis. *Proc Natl Acad Sci U.S.A.* (2016) 113(16):4452–7. doi: 10.1073/pnas.1601636113

11. Lukens JR, Gross JM, Calabrese C, Iwakura Y, Lamkanfi M, Vogel P, et al. Critical role for inflammasome-independent IL-1β production in osteomyelitis. *Proc Natl Acad Sci U.S.A.* (2014) 111(3):1066–71. doi: 10.1073/pnas.1318688111

12. Wu Y, Dowbenko D, Lasky LA. PSTPIP 2, a second tyrosine phosphorylated, cytoskeletal-associated protein that binds a PEST-type protein-tyrosine phosphatase. *J Biol Chem* (1998) 273(46):30487–96. doi: 10.1074/jbc.273.46.30487

13. Chitu V, Nacu V, Charles JF, Henne WM, McMahon HT, Nandi S, et al. PSTPIP2 deficiency in mice causes osteopenia and increased differentiation of multipotent myeloid precursors into osteoclasts. *Blood* (2012) 120(15):3126–35. doi: 10.1182/blood-2012-04-425595

14. Drobek A, Kralova J, Skopcova T, Kucova M, Novák P, Angelisová P, et al. PSTPIP2, a protein associated with autoinflammatory disease, interacts with inhibitory enzymes SHIP1 and csk. *J Immunol* (2015) 195(7):3416–26. doi: 10.4049/jimmunol.1401494

15. Veillette A, Rhee I, Souza CM, Davidson D. PEST family phosphatases in immunity, autoimmunity, and autoinflammatory disorders. *Immunol Rev* (2009) 228(1):312–24. doi: 10.1111/j.1600-065X.2008.00747.x

16. Vermeren S, Miles K, Chu JY, Salter D, Zamoyska R, Gray M. PTPN22 is a critical regulator of Fcγ receptor-mediated neutrophil activation. *J Immunol* (2016) 197(12):4771–9. doi: 10.4049/jimmunol.1600604

17. Fernandes S, Iyer S, Kerr WG. Role of SHIP1 in cancer and mucosal inflammation. *Ann N Y Acad Sci* (2013) 1280(1):6–10. doi: 10.1111/nyas.12038

18. Mondal S, Subramanian KK, Sakai J, Bajrami B, Luo HR. Phosphoinositide lipid phosphatase SHIP1 and PTEN coordinate to regulate cell migration and adhesion. *Mol Biol Cell* (2012) 23(7):1219–30. doi: 10.1091/mbc.e11-10-0889

19. Pauls SD, Marshall AJ. Regulation of immune cell signaling by SHIP1: A phosphatase, scaffold protein, and potential therapeutic target. *Eur J Immunol* (2017) 47(6):932–45. doi: 10.1002/eji.201646795

20. Jenickova I, Kasparek P, Petrezselyova S, Elias J, Prochazka J, Kopkanova J, et al. Efficient allele conversion in mouse zygotes and primary cells based on electroporation of cre protein. *Methods* (2021) 191:87–94. doi: 10.1016/j.ymeth.2020.07.005

21. Nauseef WM. Detection of superoxide anion and hydrogen peroxide production by cellular NADPH oxidases. *Biochim Biophys Acta* (2014) 1840 (2):757–67. doi: 10.1016/j.bbagen.2013.04.040

22. Bedouhène S, Moulti-Mati F, Hurtado-Nedelec M, Dang PM, El-Benna J. Luminol-amplified chemiluminescence detects mainly superoxide anion produced by human neutrophils. *Am J Blood Res* (2017) 7(4):41–8.

23. Wagner MJ, Stacey MM, Liu BA, Pawson T. Molecular mechanisms of SH2- and PTB-domain-containing proteins in receptor tyrosine kinase signaling. *Cold Spring Harb Perspect Biol* (2013) 5(12):a008987. doi: 10.1101/cshperspect.a008987

24. Sweeney MC, Wavreille AS, Park J, Butchar JP, Tridandapani S, Pei D. Decoding protein-protein interactions through combinatorial chemistry: sequence specificity of SHP-1, SHP-2, and SHIP SH2 domains. *Biochemistry* (2005) 44 (45):14932–47. doi: 10.1021/bi051408h

25. Zhang Y, Wavreille AS, Kunys AR, Pei D. The SH2 domains of inositol polyphosphate 5-phosphatases SHIP1 and SHIP2 have similar ligand specificity but different binding kinetics. *Biochemistry* (2009) 48(46):11075–83. doi: 10.1021/bi9012462

26. Ivetic A, Hoskins Green HL, Hart SJ. L-selectin: A major regulator of leukocyte adhesion, migration and signaling. *Front Immunol* (2019) 10:1068. doi: 10.3389/fimmu.2019.01068

27. Capucetti A, Albano F, Bonecchi R. Multiple roles for chemokines in neutrophil biology. *Front Immunol* (2020) 11:1259. doi: 10.3389/fimmu.2020.01259

28. Mills KHG. IL-17 and IL-17-producing cells in protection versus pathology. *Nat Rev Immunol* (2022), 1–17. doi: 10.1038/s41577-022-00746-9

29. De Filippo K, Dudeck A, Hasenberg M, Nye E, van Rooijen N, Hartmann K, et al. Mast cell and macrophage chemokines CXCL1/CXCL2 control the early stage of neutrophil recruitment during tissue inflammation. *Blood* (2013) 121(24):4930–7. doi: 10.1182/blood-2013-02-486217

30. Iida N, Grotendorst GR. Cloning and sequencing of a new gro transcript from activated human monocytes: expression in leukocytes and wound tissue. *Mol Cell Biol* (1990) 10(10):5596–9. doi: 10.1128/mcb.10.10.5596-5599.1990

31. Lehmann R, Müller MM, Klassert TE, Driesch D, Stock M, Heinrich A, et al. Differential regulation of the transcriptomic and secretomic landscape of sensor and effector functions of human airway epithelial cells. *Mucosal Immunol* (2018) 11 (3):627–42. doi: 10.1038/mi.2017.100

32. Liu S, Liu J, Yang X, Jiang M, Wang Q, Zhang L, et al. Cis-acting lnc-Cxcl2 restrains neutrophil-mediated lung inflammation by inhibiting epithelial cell CXCL2 expression in virus infection. *Proc Natl Acad Sci U.S.A.* (2021) 118(41): e2108276118. doi: 10.1073/pnas.2108276118

33. Angiolilli C, Leijten EFA, Bekker CPJ, Eeftink E, Giovannone B, Nordkamp MO, et al. ZFP36 family members regulate the proinflammatory features of psoriatic dermal fibroblasts. *J Invest Dermatol* (2022) 142(2):402–13. doi: 10.1016/j.jid.2021.06.030

34. Meddeb M, Carpentier W, Cagnard N, Nadaud S, Grillon A, Barthel C, et al. Homogeneous inflammatory gene profiles induced in human dermal fibroblasts in response to the three main species of borrelia burgdorferi sensu lato. *PloS One* (2016) 11(10):e0164117. doi: 10.1371/journal.pone.0164117

35. Heng TS, Painter MW. The immunological genome project: networks of gene expression in immune cells. *Nat Immunol* (2008) 9(10):1091–4. doi: 10.1038/ni1008-1091

36. Broderick L, Hoffman HM. IL-1 and autoinflammatory disease: Biology, pathogenesis and therapeutic targeting. *Nat Rev Rheumatol* (2022) 18(8):448–63. doi: 10.1038/s41584-022-00797-1

37. Dasari TK, Geiger R, Karki R, Banoth B, Sharma BR, Gurung P, et al. The nonreceptor tyrosine kinase SYK drives caspase-8/NLRP3 inflammasome-mediated autoinflammatory osteomyelitis. *J Biol Chem* (2020) 295(11):3394–400. doi: 10.1074/jbc.RA119.010623

38. Kralova J, Pavliuchenko N, Fabisik M, Ilievova K, Spoutil F, Prochazka J, et al. The receptor-type protein tyrosine phosphatase CD45 promotes onset and severity of IL-1β-mediated autoinflammatory osteomyelitis. *J Biol Chem* (2021) 297 (4):101131. doi: 10.1016/j.jbc.2021.101131

39. Grove M, Plumb M. C/EBP And c-ets family members and transcriptional regulation of the cell-specific and inducible macrophage inflammatory protein 1 alpha immediate-early gene. *Mol Cell Biol* (1993) 13(9):5276–89. doi: 10.1128/mcb.13.9.5276-5289.1993

40. Widmer U, Manogue KR, Cerami A, Sherry B. Genomic cloning and promoter analysis of macrophage inflammatory protein (MIP)-2, MIP-1 alpha, and MIP-1 beta, members of the chemokine superfamily of proinflammatory cytokines. *J Immunol* (1993) 150(11):4996–5012. doi: 10.4049/jimmunol.150.11.4996

41. Takahashi T, Kim MS, Iwai-Shimada M, Hoshi T, Fujimura M, Toyama T, et al. Induction of chemokine CCL3 by NF-κB reduces methylmercury toxicity in C17.2 mouse neural stem cells. *Environ Toxicol Pharmacol* (2019) 71:103216. doi: 10.1016/j.etap.2019.103216

42. Kim DS, Han JH, Kwon HJ. NF-kappaB and c-jun-dependent regulation of macrophage inflammatory protein-2 gene expression in response to lipopolysaccharide in RAW 264.7 cells. *Mol Immunol* (2003) 40(9):633–43. doi: 10.1016/j.molimm.2003.07.001

43. Lu Y, Li B, Xu A, Liang X, Xu T , Jin H, et al. NF-κB and AP-1 are required for the lipopolysaccharide-induced expression of MCP-1, CXCL1, and Cx43 in cultured rat dorsal spinal cord astrocytes. *Front Mol Neurosci* (2022) 15:859558. doi: 10.3389/fnmol.2022.859558

44. Burke SJ, Lu D, Sparer TE, Masi T, Goff MR, Karlstad MD, et al. NF-κB and STAT1 control CXCL1 and CXCL2 gene transcription. *Am J Physiol Endocrinol Metab* (2014) 306(2):E131–49. doi: 10.1152/ajpendo.00347.2013

45. Cogswell JP, Godlevski MM, Wisely GB, Clay WC, Leesnitzer LM, Ways JP, et al. NF-kappa b regulates IL-1 beta transcription through a consensus NF-kappa b binding site and a nonconsensus CRE-like site. *J Immunol* (1994) 153(2):712–23. doi: 10.4049/jimmunol.153.2.712

46. Boespflug ND, Kumar S, McAlees JW, Phelan JD, Grimes HL, Hoebe K, et al. ATF3 is a novel regulator of mouse neutrophil migration. *Blood* (2014) 123 (13):2084–93. doi: 10.1182/blood-2013-06-510909

47. Chandrasekar B, Deobagkar-Lele M, Victor ES, Nandi D. Regulation of chemokines, CCL3 and CCL4, by interferon γ and nitric oxide synthase 2 in mouse macrophages and during salmonella enterica serovar typhimurium infection. *J Infect Dis* (2013) 207(10):1556–68. doi: 10.1093/infdis/jit067

48. Förstner P, Rehman R, Anastasiadou S, Haffner-Luntzer M, Sinske D, Ignatius A, et al. Neuroinflammation after traumatic brain injury is enhanced in activating transcription factor 3 mutant mice. *J Neurotrauma* (2018) 35(19):2317–29. doi: 10.1089/neu.2017.5593
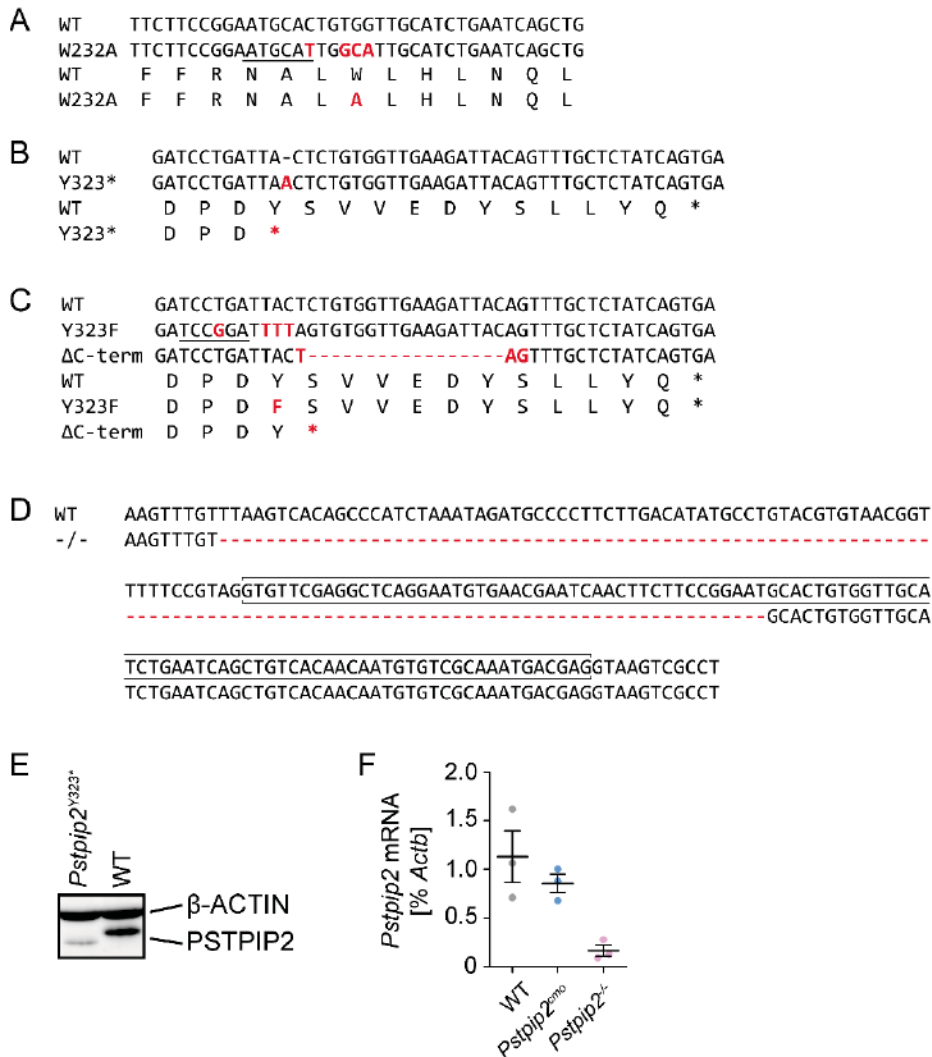
Supplementary Material

Molecular interactions of adaptor protein PSTPIP2 control neutrophil-mediated responses leading to autoinflammation

Nataliia Pavliuchenko, Iris Duric, Jarmila Kralova, Matej Fabisik, Frantisek Spoutil, Jan Prochazka, Petr Kasparek, Jana Pokorna, Tereza Skopcova, Radislav Sedlacek, Tomas Brdicka*

* Correspondence: Tomas Brdicka: tomas.brdicka@img.cas.cz

Supplementary Figure

A
```
WT      TTCTTCCGGAATGCACTGTGGTTGCATCTGAATCAGCTG
W232A   TTCTTCCGGAATGCATTGGCATTGCATCTGAATCAGCTG
WT       F  F  R  N  A  L  W  L  H  L  N  Q  L
W232A    F  F  R  N  A  L  A  L  H  L  N  Q  L
```

B
```
WT      GATCCTGATTA-CTCTGTGGTTGAAGATTACAGTTTGCTCTATCAGTGA
Y323*   GATCCTGATTAACTCTGTGGTTGAAGATTACAGTTTGCTCTATCAGTGA
WT        D  P  D  Y  S  V  V  E  D  Y  S  L  L  Y  Q  *
Y323*     D  P  D  *
```

C
```
WT      GATCCTGATTACTCTGTGGTTGAAGATTACAGTTTGCTCTATCAGTGA
Y323F   GATCCGGATTTTAGTGTGGTTGAAGATTACAGTTTGCTCTATCAGTGA
ΔC-term GATCCTGATTACT------------------AGTTTGCTCTATCAGTGA
WT        D  P  D  Y  S  V  V  E  D  Y  S  L  L  Y  Q  *
Y323F     D  P  D  F  S  V  V  E  D  Y  S  L  L  Y  Q  *
ΔC-term   D  P  D  Y  *
```

D
```
WT      AAGTTTGTTTAAGTCACAGCCCATCTAAATAGATGCCCCTTCTTGACATATGCCTGTACGTGTAACGGT
-/-     AAGTTTGT---------------------------------------------------------------

        TTTTCCGTAGGTGTTCGAGGCTCAGGAATGTGAACGAATCAACTTCTTCCGGAATGCACTGTGGTTGCA
        ------------------------------------------------------GCACTGTGGTTGCA

        TCTGAATCAGCTGTCACAACAATGTGTCGCAAATGACGAGGTAAGTCGCCT
        TCTGAATCAGCTGTCACAACAATGTGTCGCAAATGACGAGGTAAGTCGCCT
```

E

F

Supplementary Figure 1. (A-D). Alignments of WT and mutant nucleotide and amino acid sequences. The sequences were determined by Sanger sequencing of PCR products generated by amplification of the targeted regions from the genomic DNA. **(A)** *Pstpip2*^{W232A}; mutated nucleotides and corresponding amino acid are labelled in red, sequence of NsiI restriction cleavage site introduced for genotyping purposes is underlined. **(B)** *Pstpip2*^{Y323*}; inserted nucleotide is labelled in red, the resulting stop codon is at the amino acid level represented by red asterisk. **(C)** *Pstpip2*^{Y323F}, *Pstpip2*$^{ΔC-term}$; mutated nucleotides and corresponding amino acid are labelled in red, sequence of BspEI restriction cleavage site introduced for genotyping purposes is underlined. Deletion is depicted as dashed red line, the resulting stop codon is labelled in red and at the amino acid level represented by red asterisk. **(D)** *Pstpip2*$^{-/-}$; deletion is depicted as dashed red line, affected exon is boxed. **(E)** PSTPIP2 protein expression in neutrophils from *Pstpip2*^{Y323*} mouse strain detected by immunoblotting. As a loading control β-ACTIN was stained on the same membrane. **(F)** *Pstpip2* mRNA level in WT, *Pstpip2*^{cmo}, and *Pstpip2*$^{-/-}$ neutrophils was determined by quantitative real-time PCR.

The receptor-type protein tyrosine phosphatase CD45 promotes onset and severity of IL-1β–mediated autoinflammatory osteomyelitis

Jarmila Kralova[1,‡], Nataliia Pavliuchenko[1,2,‡], Matej Fabisik[1,2], Kristyna Ilievova[1], Frantisek Spoutil[3], Jan Prochazka[3,4], Jana Pokorna[1], Radislav Sedlacek[3,4], and Tomas Brdicka[1,*]

From the [1]Laboratory of Leukocyte Signaling, Institute of Molecular Genetics of the Czech Academy of Sciences, Prague, Czech Republic; [2]Charles University, Faculty of Science, Prague, Czech Republic; and [3]Czech Centre for Phenogenomics and [4]Laboratory of Transgenic Models of Diseases, Institute of Molecular Genetics of the Czech Academy of Sciences, Vestec, Czech Republic

Edited by Dennis Voelker

A number of human autoinflammatory diseases manifest with severe inflammatory bone destruction. Mouse models of these diseases represent valuable tools that help us to understand molecular mechanisms triggering this bone autoinflammation. The *Pstpip2^cmo* mouse strain is among the best characterized of these; it harbors a mutation resulting in the loss of adaptor protein PSTPIP2 and development of autoinflammatory osteomyelitis. In *Pstpip2^cmo* mice, overproduction of interleukin-1β (IL-1β) and reactive oxygen species by neutrophil granulocytes leads to spontaneous inflammation of the bones and surrounding soft tissues. However, the upstream signaling events leading to this overproduction are poorly characterized. Here, we show that *Pstpip2^cmo* mice deficient in major regulator of Src-family kinases (SFKs) receptor-type protein tyrosine phosphatase CD45 display delayed onset and lower severity of the disease, while the development of autoinflammation is not affected by deficiencies in Toll-like receptor signaling. Our data also show deregulation of pro-IL-1β production by *Pstpip2^cmo* neutrophils that are attenuated by CD45 deficiency. These data suggest a role for SFKs in autoinflammation. Together with previously published work on the involvement of protein tyrosine kinase spleen tyrosine kinase, they point to the role of receptors containing immunoreceptor tyrosine-based activation motifs, which after phosphorylation by SFKs recruit spleen tyrosine kinase for further signal propagation. We propose that this class of receptors triggers the events resulting in increased pro-IL-1β synthesis and disease initiation and/or progression.

Cytokine-driven inflammation is a critical component of the immune system's defense mechanisms. However, its dysregulation can cause a severe harm to the host. To date, a number of mutations compromising the regulation of proinflammatory cytokine production have been identified. In extreme cases, deregulated cytokine secretion caused by these mutations can result in spontaneous inflammation and severe disease. One of the frequently affected cytokines capable of driving pathological inflammation is interleukin-1β (IL-1β). Mutations to the genes controlling the level of its secretion often lead to autoinflammatory disorders characterized by seemingly unprovoked fever attacks and sterile inflammatory damage to various organs and tissues (1). While it is clear that deregulated production of IL-1β is key part of this pathological response, the initiating events that trigger harmful inflammation remain unknown in many cases. They may include excessive response to innocuous endogenous ligands or microbiota or receptor-independent activity of proinflammatory signaling pathways.

In order to understand the mechanisms of autoinflammatory diseases, mouse models proved highly valuable. One of the best studied is the mouse strain known as *Pstpip2^cmo* (2). This strain harbors a point mutation in *Pstpip2* gene resulting in complete absence of corresponding PSTPIP2 protein (3, 4). Its deficiency leads to chronic multifocal osteomyelitis (CMO), an autoinflammatory disease characterized by inflammatory bone damage and soft tissue swelling localized mainly to hind paws and tail area. The disease resembles several human autoinflammatory disorders, including chronic recurrent multifocal osteomyelitis and synovitis–acne–pustulosis–hyperostosis–osteitis syndrome (2, 5). CMO development in *Pstpip2^cmo* mouse strain can be prevented by inactivation of the genes coding for IL-1β or its receptor (6–8), demonstrating that IL-1β is critical for disease initiation. The disease can also be prevented by inactivation of *Myd88* gene essential for signal transduction by IL-1 receptor (9). In addition, increased production of active IL-1β was observed in affected tissues and in *Pstpip2^cmo* neutrophils (6–8, 10), a cell type critical for triggering this disease (7, 9). These results clearly demonstrated that IL-1β is a crucial element of the mechanism driving spontaneous inflammation and bone damage in *Pstpip2^cmo* mouse strain. However, similar to a number of other autoinflammatory diseases, the initial triggering event remains unclear. Gut microbiota may play a role, since it has been shown that their altered composition is important for the disease development in *Pstpip2^cmo* mice (7). In addition, excessive reactive oxygen species (ROS) production by *Pstpip2^cmo* neutrophils has been observed *in vivo* in tissues typically affected by the disease weeks before the first

visible symptoms, suggesting that *Pstpip2^{cmo}* neutrophils are responding to a so far unknown stimulus in the affected tissues early on during the disease development (9).

Since PSTPIP2 is an adaptor protein, its function is likely dependent on its interaction partners. These include all members of the PEST family of protein tyrosine phosphatases, phosphoinositide phosphatase SHIP1, and inhibitory kinase Csk, key negative regulator of Src-family kinases (SFKs) (10, 11). To what extent each partner contributes to IL-1β regulation and CMO development has not been studied so far. However, these interactions suggest that PSTPIP2 regulates signaling pathways dependent on protein tyrosine (and phosphoinositide) phosphorylation. Csk and PEST-family PTPs were shown to bind each other and cooperate in the negative regulation of SFK (12–15). SFKs are critical for initiation of signaling by a number of key leukocyte receptors, including those expressed by neutrophils (16). Moreover, there is a growing evidence about regulation of a major activator of IL-1β processing, NLRP3 inflammasome, by SFKs and downstream protein tyrosine kinases (17–23).

Crossbreeding of *Pstpip2^{cmo}* mice with strains lacking components of IL-1β pathway proved a useful strategy in determining the roles of these molecules in disease development (6–8, 24, 25). However, it is not possible to use this strategy for SFK. Neutrophils express almost all Src family members, which are to a significant extent redundant with each other (26). It is not technically feasible to genetically inactivate all these kinases simultaneously. Therefore, to analyze the role of SFKs in CMO disease outcome, we decided to crossbreed *Pstpip2^{cmo}* mice with mice lacking receptor-like protein tyrosine phosphatase CD45 encoded by *Ptprc* gene. CD45 is an abundantly expressed surface glycoprotein in the cells of hematopoietic origin. One of the major roles of CD45 phosphatase is in allowing the activation of SFK by dephosphorylation of their C-terminal inhibitory tyrosine (27). It counterbalances the effect of Csk kinase, which is the main negative regulator of SFKs and binding partner of PSTPIP2 (10, 28). By inactivating *Ptprc* gene in *Pstpip2^{cmo}* mice, we aimed at reducing SFK activity in leukocytes of these mice by increasing the phosphorylation of their inhibitory tyrosines to obtain evidence supporting the involvement of SFK-dependent signaling in CMO development. We show that while deficiencies in components of Toll-like receptor signaling pathways do not affect CMO development, deficiency in CD45 phosphatase lowers IL-1β levels in *Pstpip2^{cmo}* mice leading to mitigation of osteomyelitis and tissue inflammation. These data suggest an important role of CD45 phosphatase in the regulation of the signaling pathways leading to enhanced IL-1β production and imply SFK-dependent receptors in the development of autoinflammatory osteomyelitis. At the same time, they bring evidence against the major role of TLRs.

Results

MYD88- and TRIF-mediated signaling are dispensable for CMO development while CD45 plays an important role

First, we compared the effects of MyD88-/TRIF-dependent Toll-like receptor signaling and signaling dependent mainly on protein tyrosine phosphorylation in the development of autoinflammatory osteomyelitis. To do this, we crossbred *Pstpip2^{cmo}* mouse strain with strains deficient in key components of these pathways, including adaptor proteins MyD88 (29) and TRIF (30) and receptor protein tyrosine phosphatase CD45 (encoded by *Ptprc* gene) (31). As a result, we obtained three double-mutant strains *Pstpip2^{cmo}/Myd88$^{-/-}$*, *Pstpip2^{cmo}/Trif$^{Lps2/Lps2}$*, and *Pstpip2^{cmo}/Ptprc$^{-/-}$*. We have shown previously that *Pstpip2^{cmo}/Myd88$^{-/-}$* mice do not develop any symptoms of the disease, demonstrating the key role of this adapter in CMO development (9). It can be likely explained by its involvement in IL-1 receptor signaling, which is required for the disease development in *Pstpip2^{cmo}* mice. Importantly, expression of IL-1 receptor on nonhematopoietic (radioresistant) cells is required while its expression on radiosensitive hematopoietic cells does not appear to play a role in CMO (24). This allowed us to analyze the contribution of leukocyte-expressed TLR/MyD88 to the disease development using bone marrow chimeras. We performed bone marrow transplantation from young asymptomatic *Pstpip2^{cmo}* or *Pstpip2^{cmo}/Myd88$^{-/-}$* donors into lethally irradiated WT recipients. Unexpectedly, we observed complete disease development without any delay in disease progression, regardless of the donor cell origin (Fig. 1*A*). Since TRIF is not critical for IL-1 receptor signaling, we could analyze the role of TRIF directly in *Pstpip2^{cmo}/Trif$^{Lps2/Lps2}$* mice without the transplantation. *Pstpip2^{cmo}/Trif$^{Lps2/Lps2}$* mice developed the CMO disease with identical kinetics as *Pstpip2^{cmo}* mice (Fig. 1*B*). These data suggest that priming of leukocytes through TLR/MyD88 or TLR/TRIF signaling does not play any major role in CMO development since *Pstpip2^{cmo}* hematopoietic cells without functional MyD88 or TRIF adaptors were fully capable of driving the autoinflammation. This result also confirmed the earlier finding that IL-1 receptor on hematopoietic cells is dispensable for CMO development (24). In contrast, monitoring of *Pstpip2^{cmo}/Ptprc$^{-/-}$* mice revealed that the disease development in these mice was significantly delayed with part of the mice remaining healthy throughout the experiment (Fig. 1*C*). These results suggested that protein tyrosine phosphorylation regulated by CD45 contributes to CMO development.

Symptoms of autoinflammation in Pstpip2^{cmo} *mice are milder in the absence of CD45*

To better understand the effects of CD45, we performed more careful analysis of *Pstpip2^{cmo}/Ptprc$^{-/-}$* mice. Symptom evaluation revealed that the severity of the disease was substantially milder than in *Pstpip2^{cmo}* strain (Fig. 2*A*). Microcomputerized tomography (μCT) scans of hind paws demonstrated that bone damage was significantly lower than in *Pstpip2^{cmo}* mice, though still present (Fig. 2, *B* and *C*). Soft tissue swelling was also detected by μCT in some animals, although for the entire group as the whole it did not reach the level of statistical significance because of the presence of a number of animals where
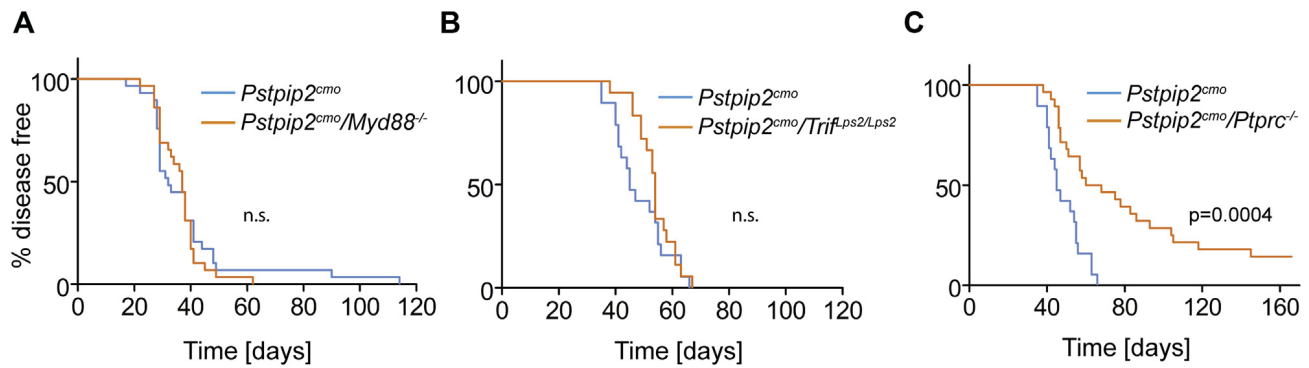
Figure 1. CD45 deficiency but not deficiencies in Toll-like receptor signaling adaptors attenuate autoinflammatory osteomyelitis progression in ***Pstpip2^cmo*** **mice.** *A*, WT mice were lethally irradiated and transplanted with bone marrow from *Pstpip2^cmo* or *Pstpip2^cmo/Myd88^−/−* mice. Appearance of diseases symptoms was followed for 120 days (n = 29). *B* and *C*, time of disease symptom appearance in *Pstpip2^cmo*, *Pstpip2^cmo/Trif^-Lps2/Lps2*, and *Pstpip2^cmo/Ptprc^−/−* mice (n > 18). In (*B*) *Pstpip2^cmo* and *Pstpip2^cmo/Trif^-Lps2/Lps2* mice are compared, whereas in (*C*), the same *Pstpip2^cmo* mice are compared with *Pstpip2^cmo/Ptprc^−/−*.

the swelling was only mild or not observed at all (Fig. 2*D*). These data demonstrate that CMO disease is clearly present in CD45-deficient *Pstpip2^cmo* mice. However, its severity is significantly lower than in *Pstpip2^cmo* mice expressing CD45.

Phosphorylation of SFK inhibitory tyrosine is increased in the absence of CD45, while the loss of PSTPIP2 does not have any effect

CD45 is a major activator of SFKs, since it dephosphorylates their C-terminal inhibitory tyrosine (27). In addition, PSTPIP2
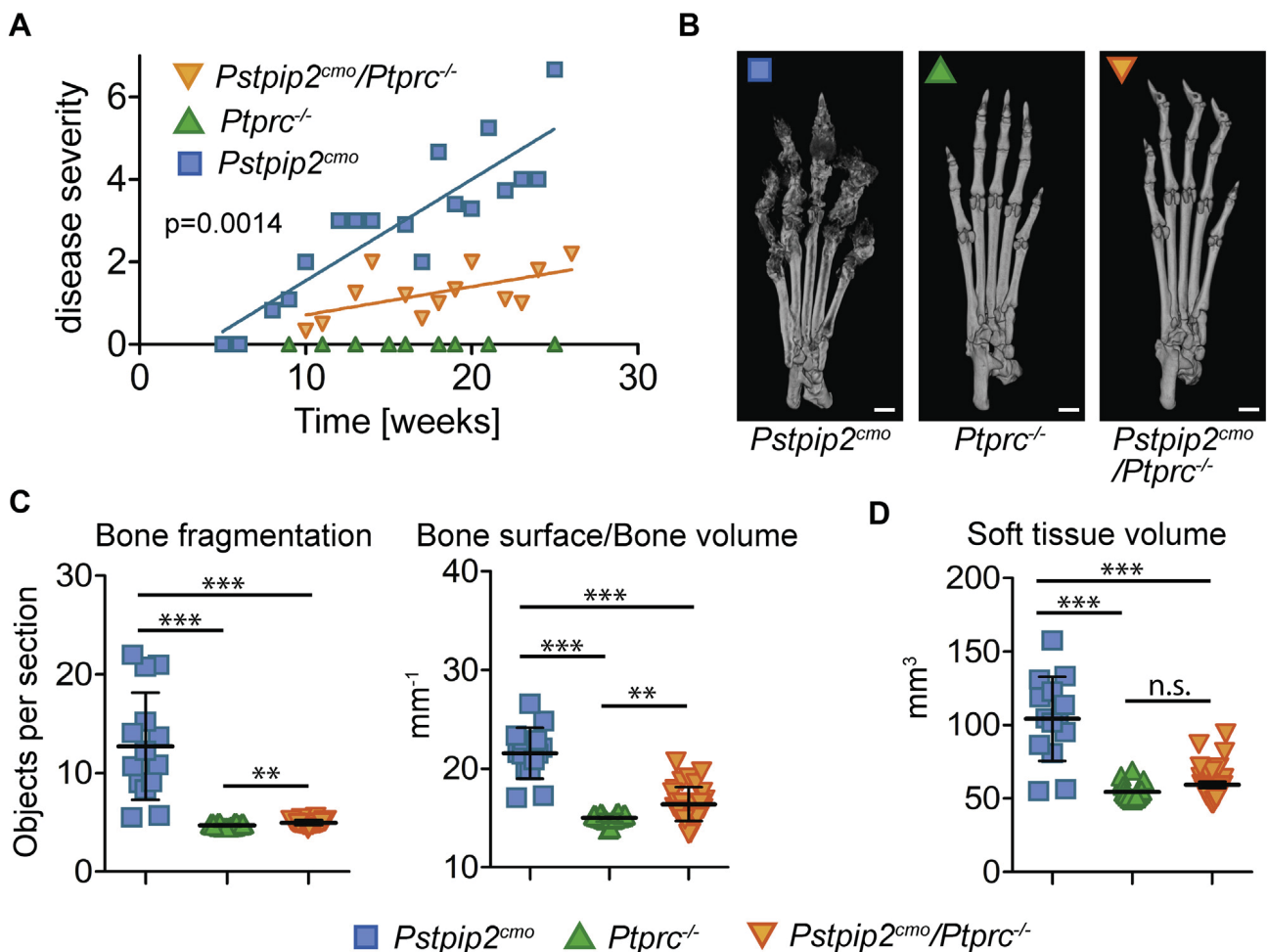
Figure 2. Milder disease symptoms in CD45-deficient ***Pstpip2^cmo*** **mice.** *A*, disease severity scored by visual inspection of the hind paw photographs collected over the course of this study (scale from 0 to 8). Each point is a mean value representing the mice of the same age and genotype. Lines were generated using linear regression. *B*, representative X-ray μCT scans of hind paw bones from 20-week-old mice. The scale bar represents 1 mm. *C*, quantification of bone damage from X-ray μCT scans obtained from multiple mice. Two different parameters were calculated, bone fragmentation and the ratio of bone surface and volume. *D*, volume of soft tissue in hind paws calculated from X-ray μCT data. Values were obtained by subtracting bone volume from a total paw volume (total paw volume is the volume of the paw reconstructed from μCT scans, including all soft tissues and the bone).

via binding to Csk, a kinase phosphorylating this tyrosine, is expected to inhibit SFK activity (10, 32, 33). To assess the effects of the loss of CD45 and PSTPIP2 on SFK phosphorylation at their inhibitory tyrosines, we prepared lysates from bone marrow cells and purified neutrophils of mice carrying these mutations and probed for phosphorylation of these sites. We focused on the three most important myeloid cell SFKs LYN, HCK, and FGR. As expected, in both, bone marrow cells and purified neutrophils, CD45 deficiency resulted in a substantial increase in phosphorylation detected by antibody to inhibitory tyrosine of SFK LYN (Fig. 3, *A* and *B*). For HCK inhibitory tyrosine, we only obtained reliable signal from purified neutrophils. There, the pattern of phosphorylation was similar to Lyn (Fig. 3*C*). To further verify these results, we immunoprecipitated LYN from bone marrow cell lysates followed by staining with antibody to LYN inhibitory tyrosine. Similar to the whole cell lysates, LYN was hyperphosphorylated on inhibitory tyrosine in both samples lacking CD45 (Fig. 3*D*). Unfortunately, three different antibodies to HCK we tested did not immunoprecipitate murine HCK, and so for HCK, we could not perform this experiment. To our knowledge, there are no reliable phosphospecific antibodies to Fgr inhibitory tyrosine. However, we found that after immunoprecipitation with FGR-specific antibody, it is recognized by antibody to inhibitory tyrosine of SFK LCK, C terminus of which shows sequence homology to FGR. Surprisingly, CD45 deficiency did not have any effect on FGR phosphorylation detected by this antibody (Fig. 3*E*). The absence of CD45 only mildly affected phosphorylation of the SFK activating tyrosine (Fig. 3, *D–G*). Interestingly, the presence or the absence of PSTPIP2 did not alter phosphorylation of any of these SFK (Fig. 3, *A–G*).

CD45 deficiency does not affect generation of ROS

So far, two important processes dysregulated in *Pstpip2^cmo* mice have been shown to contribute to CMO disease severity. These are generation of ROS by phagocyte NADPH oxidase and production of IL-1β mediated by NLRP3 inflammasome, caspase-8, and neutrophil proteases (6–9, 24, 25). Our measurements of ROS production in bone marrow cells after silica or fMLP exposure confirmed previous observations of substantially increased superoxide levels generated by *Pstpip2^cmo* cells. Surprisingly, superoxide production by *Pstpip2^cmo*/*Ptprc^−/−* cells was increased to a similar extent, and no significant difference between *Pstpip2^cmo* and *Pstpip2^cmo*/*Ptprc^−/−* was detected (Fig. 4, *A* and *B*).

Reduced IL-1β production in CD45-deficient mice

In contrast to the ROS production, exacerbated production of processed IL-1β p17 observed after activation of inflammasome by silica particles in *Pstpip2^cmo* bone marrow cells was significantly reduced in *Pstpip2^cmo*/*Ptprc^−/−* cells (Fig. 5, *A* and *B*). In addition, we also observed substantially reduced IL-1β levels *in vivo* in the footpads of *Pstpip2^cmo*/*Ptprc^−/−* mice when compared with *Pstpip2^cmo* (Fig. 5*C*). Neutrophils are the most critical cell type indispensable for disease development in

Pstpip2^cmo mice (7, 9). However, we did not observe any p17 in neutrophil lysates after induction of pro-IL-1β production by lipopolysaccharide (LPS) followed by inflammasome activation by silica (Fig. 5*D*). Nor could we detect any inflammasome-generated caspase-1 p20 or any significant differences in gasdermin D cleavage between *Pstpip2^cmo* and *Pstpip2^cmo*/*Ptprc^−/−* cells that could help explain differences in disease severity between these two strains (Fig. S1). On the other hand, we could observe IL-1β p21 thought to be generated *via* cleavage of pro-IL-1β by neutrophil proteases (34) with the highest levels in *Pstpip2^cmo* neutrophils that were significantly reduced in *Pstpip2^cmo*/*Ptprc^−/−* cells (Fig. 5, *D* and *E*).

Published observations demonstrating the roles of multiple caspases and neutrophil proteases in CMO disease development (7, 24) suggested that there might be a step upstream of all these factors that is dysregulated in *Pstpip2^cmo* mice. This notion prompted us to investigate the production of IL-1β precursor—pro-IL-1β. Our previous observations suggested that LPS-induced pro-IL-1β production is not altered in *Pstpip2^cmo* bone marrow cells and neutrophils (10). However, relatively high LPS doses were used in those experiments. When we used lower dose of 10 ng/ml LPS, we detected a significantly higher pro-IL-1β production in *Pstpip2^cmo* bone marrow cells when compared with WT cells (Fig. 6*A*). In addition, we also detected deregulated LPS-induced production of pro-IL-1β in purified *Pstpip2^cmo* neutrophils (Fig. 6*B*). Importantly, CD45 deficiency significantly attenuated this production. Given the dependence of LPS-triggered signaling on MYD88, our data in Figure 1*A* make LPS an unlikely candidate for CMO triggering factor in *Pstpip2^cmo* mice *in vivo*. On the other hand, published data on the critical importance of spleen tyrosine kinase (SYK) (35), as well as the data presented in this article, suggest an involvement of an immunoreceptor tyrosine-based activation motif (ITAM)-containing receptor. As a model of these receptors we selected Fc receptors, where the signaling is dependent on the ITAM motif in the receptor gamma chain. First, we tested if Fc receptor crosslinking results in any production of pro-IL-1β in bone marrow cells. This experiment demonstrated that Fc receptor activation is capable of triggering pro-IL-1β synthesis in these cells. Importantly, its production was significantly higher in bone marrow cells from *Pstpip2^cmo* mice (Fig. 6*C*). Next, we performed a similar experiment on purified neutrophils from mice of all four genotypes. This experiment again showed enhanced production of pro-IL-1β by *Pstpip2^cmo* neutrophils, which was significantly attenuated in CD45-deficient *Pstpip2^cmo*/*Ptprc^−/−* cells (Fig. 6*D*). This experiment suggested an involvement of ITAM-containing receptors in disease initiation in *Pstpip2^cmo* mice and a role of pro-IL-1β generation in this process.

Discussion

In mice, PSTPIP2 deficiency results in CMO, an autoinflammatory disease driven by deregulated IL-1β and ROS production by neutrophils (6–9, 24, 25). The signaling event that triggers the disease onset *in vivo* is currently unknown.
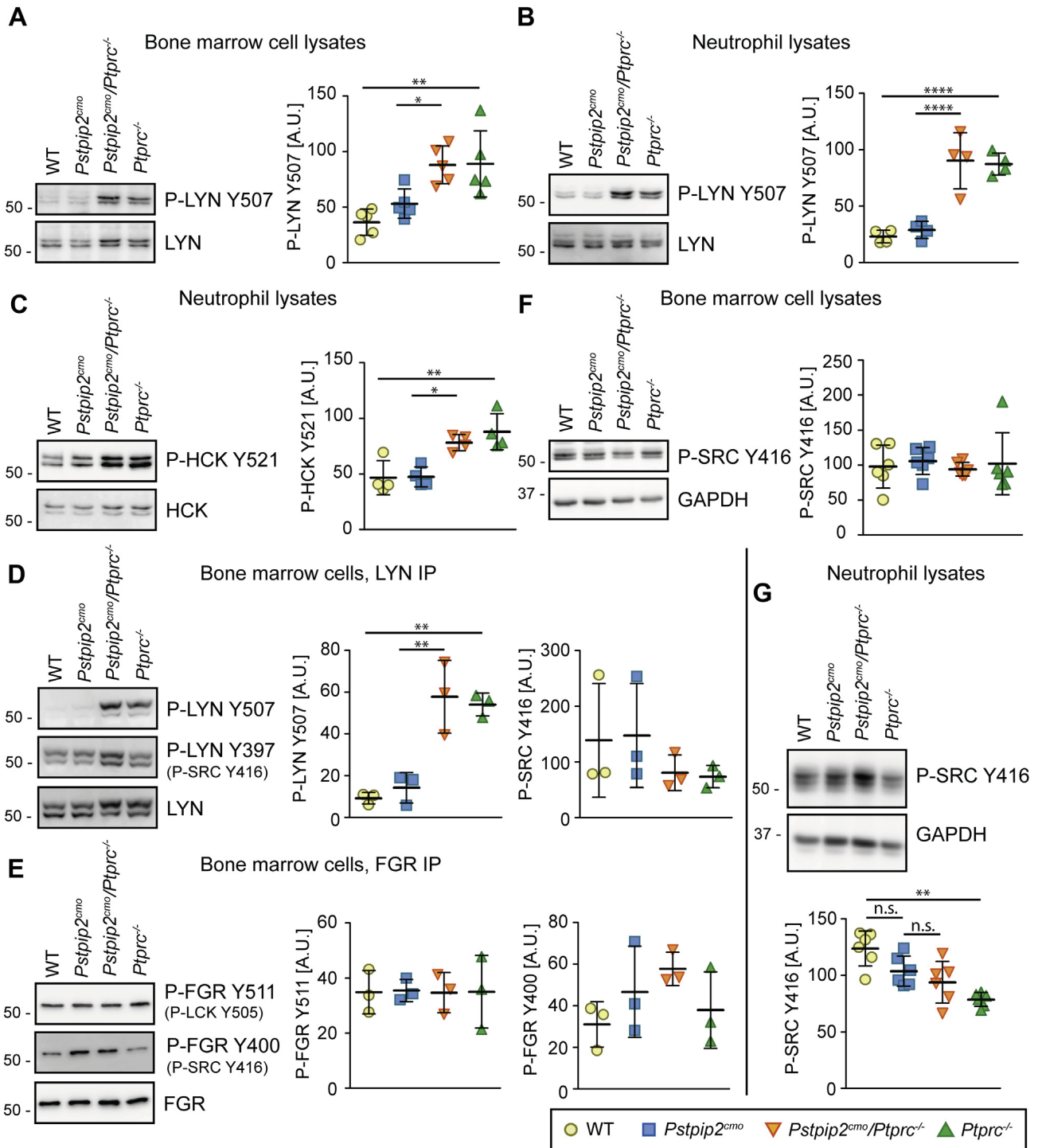
Figure 3. Inhibitory tyrosine of Src-family kinases LYN and HCK is hyperphosphorylated in *Ptprc*⁻/⁻ and *Pstpip2^cmo^/Ptprc*⁻/⁻ cells. *A*, lysates of bone marrow cells from mice of indicated genotypes were subjected to immunoblotting with antibody to inhibitory phosphotyrosine of LYN (P-LYN Y507). *B*, similar experiment as in (*A*) on purified neutrophils. *C*, lysates of purified neutrophils from mice of indicated genotypes were subjected to immunoblotting with antibody to inhibitory phosphotyrosine of HCK (P-HCK Y521). *D* and *E*, LYN (*D*) or FGR (*E*) was immunoprecipitated from the lysates of bone marrow cells obtained from mice of indicated genotypes, followed by immunoblotting with antibodies to their inhibitory and activating phosphotyrosines. In case of FGR, inhibitory phosphorylation was detected with antibody to similar phosphotyrosine of LCK (P-LCK Y505). For detection of activating phosphorylation, antibody to P-SRC Y416 crossreacting with multiple Src-family members was used in both (*D*) and (*E*). *F*, lysates of bone marrow cells from mice of indicated genotypes were subjected to immunoblotting with antibody to activating phosphotyrosine of multiple SFK (P-SRC Y416). *G*, similar experiment as in (*F*) on purified neutrophils. For each experiment, representative immunoblot and quantification of multiple experiments is shown. *A–E*, phospho-SFK signals were normalized to total SFK. *F* and *G*, because of the crossreactivity of P-SRC Y416 antibody with multiple Src family members, the signal was normalized to GAPDH. To allow better comparison of multiple experiments in (*F*) the obtained values were further normalized to experiment average. A.U., arbitrary units; IP, immunoprecipitation.
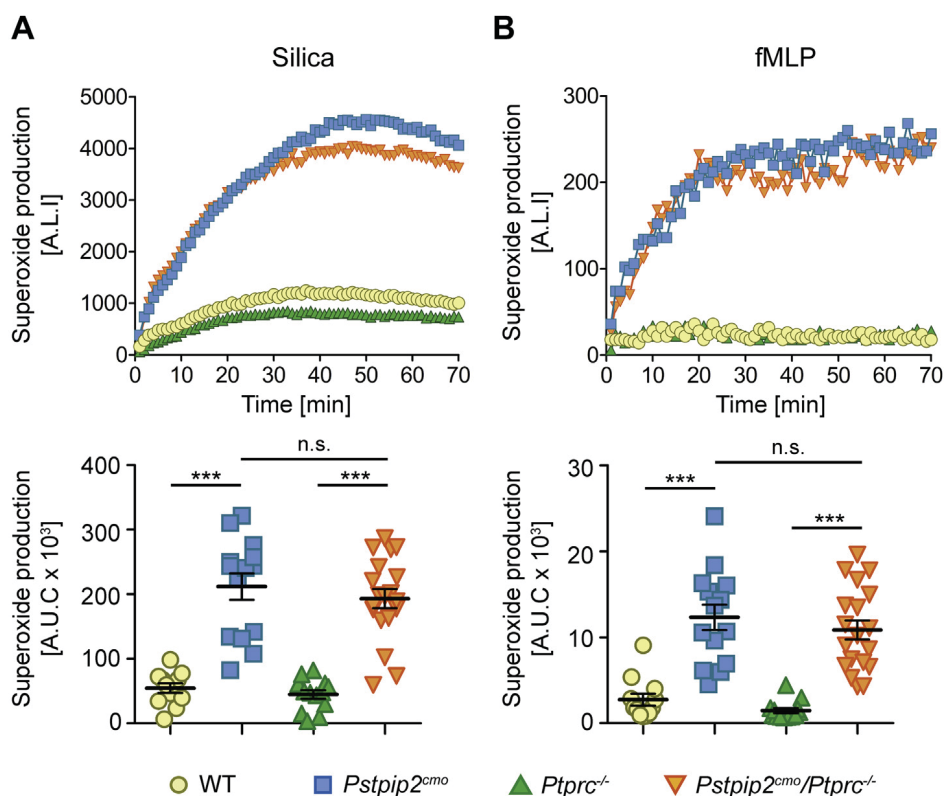
Figure 4. Similar dysregulation of ROS production in *Pstpip2^cmo^* and *Pstpip2^cmo^/Ptprc^−/−^* mice. *A* and *B*, representative time course and area under the curve quantification of multiple time-course measurements of superoxide production by bone marrow cells from mice of indicated genotypes. The cells were activated by silica particles in (*A*) and by fMLP in (*B*). A.L.I., arbitrary luminescence intensity; A.U.C., area under the curve.

Because of the strong effect of microbiota on the disease course (7), we have suspected that one or more TLRs might be involved in its initiation. However, our analysis of *Pstpip2^cmo^* mice with deficiencies in essential TLR signaling adaptors MYD88 in hematopoietic cells or TRIF in the whole body demonstrated that the disease development is triggered with unchanged kinetics even when they are inactivated. It should be noted that there may be a certain level of redundancy between MYD88 and TRIF, and so their role still cannot be completely excluded. On the other hand, the loss of CD45, which results in downregulation of the activity of SFK-dependent pathways, resulted in delayed kinetics and alleviation of the disease symptoms. Apart from SFK, CD45 has been reported to dephosphorylate other substrates, including TCRζ, SKAP55, DAP12, JAK kinases, and PAG/Cbp (36–39). However, to our knowledge, SFKs are the only enzymes where CD45 has positive regulatory function (either direct or *via* some of the aforementioned substrates). Reduced disease severity observed in *Pstpip2^cmo^/Ptprc^−/−^* mice is consistent with the loss of activating effect of CD45, rather than lack of inhibitory function associated with substrates other than SFK. These observations strongly support the hypothesis that symptom alleviation is caused by reduced activity of SFK. Importantly, Dasari *et al.* (35) recently demonstrated that another protein tyrosine kinase, SYK, is also essential for triggering the disease in *Pstpip2^cmo^* mice. Both SFK and SYK are key components of ITAM signaling pathways (40). Hence, these results suggest that the exaggerated signaling leading to

CMO disease may be initiated by an ITAM-containing receptor. There are number of these receptors in neutrophils, including Fc receptors, dectins, integrins, paired immunoglobulin-like receptors/leukocyte immunoglobin-like receptors, TARM1, TREM-1/2, and other FcRγ chain or DAP12-associated receptors, number of which have endogenous ligands (16, 41–44). We have shown previously that Fc receptor signaling is deregulated in *Pstpip2^cmo^* mice. However, it is possible that other ITAM-dependent receptors could be similarly affected by PSTPIP2 deficiency, since they share the same basic signaling mechanisms.

Interestingly, we have not observed any changes in SFK phosphorylation in *Pstpip2^cmo^* mice. These results favor the interpretation that the dysregulation of signaling caused by the absence of PSTPIP2 is not at the level of SFK activity or ITAM phosphorylation by SFK but rather further downstream in this pathway. In such case, ITAM-containing receptors themselves still could be essential for disease development, yet not directly deregulated in the absence of PSTPIP2. This interpretation would also be consistent with a rather generalized hypersensitivity of *Pstpip2^cmo^* neutrophils to a broad range of different stimuli observed previously (9, 10). However, precisely which part of the ITAM-dependent signaling cascade is affected by PSTPIP2 deficiency remains still unclear.

We have observed increased production of active IL-1β p17, typically generated by inflammasome, in nonseparated *Pstpip2^cmo^* bone marrow cells. On the other hand, in purified neutrophils, we were unable to detect this protein.
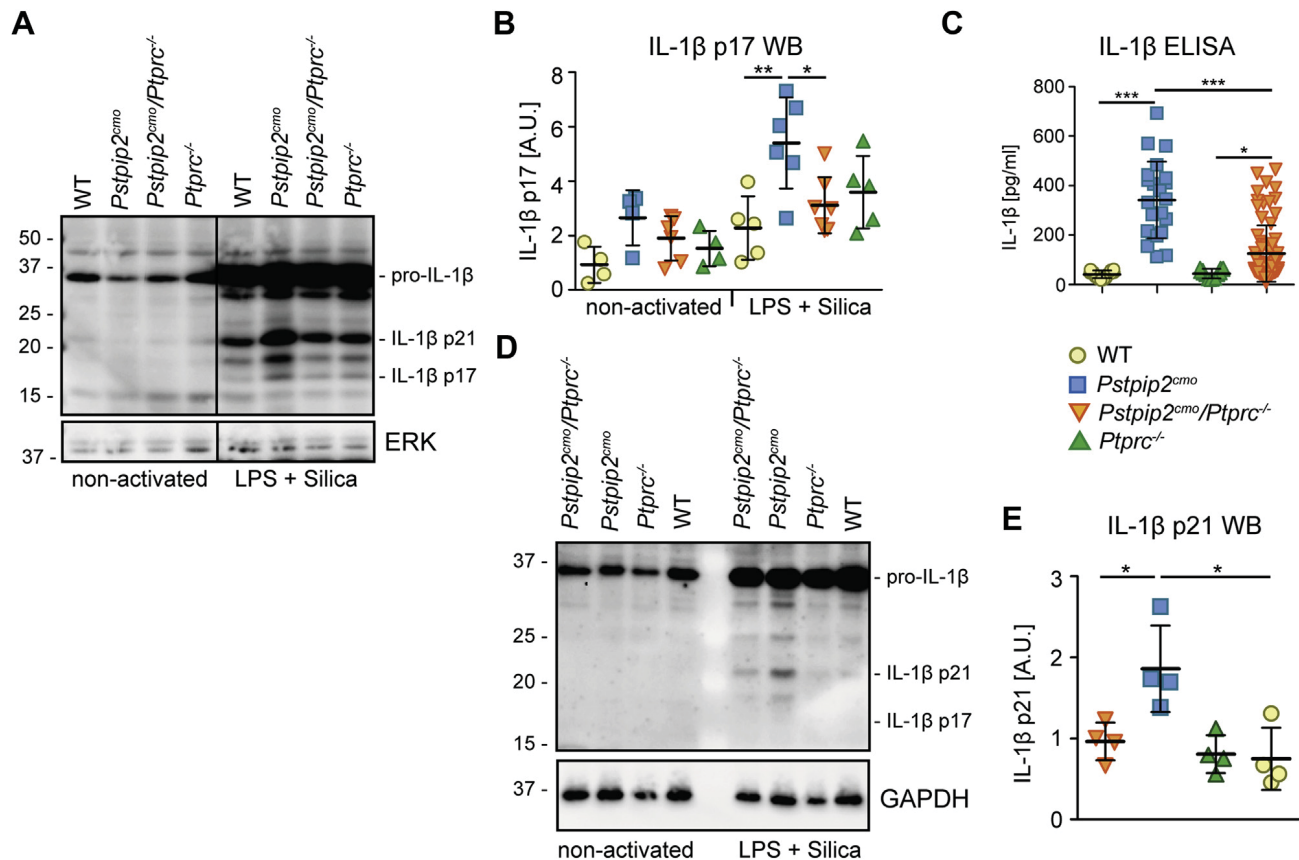
Figure 5. CD45 deficiency results in a significant reduction of active IL-1β production in *Pstpip2^cmo* mice. *A* and *B*, IL-1β processing to active IL-1β p17 was analyzed by immunoblotting of bone marrow cells activated by LPS and silica. Representative Western blot (*A*) and quantification of multiple experiments (normalized to ERK and reference sample loaded on each gel) (*B*) are shown. *C*, IL-1β in the footpad homogenates from 20-week-old mice of indicated genotypes was quantified by ELISA. *D* and *E*, IL-1β processing in purified neutrophils activated by LPS and silica was analyzed by immunoblotting of the whole cell lysates. Representative Western blot (*D*) and quantification of p21 signal from multiple experiments normalized to GAPDH signal (*E*) are shown. Vertical line in (*A*) separates samples that were at different positions on the same immunoblot membrane. A.U., arbitrary units.

Nevertheless, neutrophils were shown to be absolutely required for CMO disease development in *Pstpip2^cmo* mice (7, 9). It is possible that deregulated activity of *Pstpip2^cmo* neutrophils promotes production of active IL-1β by monocytes present in the same bone marrow cell samples or that neutrophil's own production is below Western blot detection limit but still present and compensated for by large neutrophil numbers *in vivo*. There are multiple pathways of pro-IL-1β processing and production of active protein involved in CMO development in mice, including NLRP3 inflammasome/ caspase-1, additional mechanism involving caspase-8, and neutrophil proteases (multiple have been tested in *Pstpip2^cmo* mice, including elastase, proteinase 3, cathepsins B, C, G) (7, 24). Genes for all these proteins have been individually inactivated in *Pstpip2^cmo* mice without any effect on disease development (with the exception of limited but significant disease alleviation in case of cathepsin C, which is known to be an essential upstream activator of the other neutrophil proteases) (7, 8, 24, 45). Importantly, combined deficiency of the individual inflammasome components and caspase-8 almost completely prevented disease development (7, 24). These data suggested that any of the two pathways, (*i.e.*, NLRP3 inflammasome or caspase-8) can drive the disease on its own with some contribution from neutrophil proteases, whereas none of

these pathways alone is critical because of their mutual redundancy. There may be more efficient activators of these pathways in neutrophils than silica. Silica has been frequently used as a model inflammasome activator in studies of *Pstpip2^cmo* mice (7–10), but it is unlikely to be responsible for the CMO disease initiation *in vivo*. There are many other inflammasome activators of both endogenous and exogenous origin (46), some of which may be more potent activators in neutrophils and also more important *in vivo*. Inflammasome activation triggered by these activators does not have to be dysregulated in *Pstpip2^cmo* neutrophils for the disease to develop. The dysregulation at the level of synthesis of pro-IL-1β, a precursor of active IL-1β, would likely be sufficient to drive the disease development in *Pstpip2^cmo* mice. Dysregulation at this upstream step could explain the redundancy of multiple downstream pathways of pro-IL-1β processing into active protein.

Increased pro-IL-1β production by *Pstpip2^cmo* neutrophils can be triggered not only by LPS exposure but also by Fc receptor stimulation. Consistent with ITAM/SFK role in the disease development discussed previously, it is likely that Fc or other ITAM-dependent receptor is involved in disease initiation *in vivo*. Fc receptor signaling pathway is well defined, and CD45 and SFK are both important players in Fc receptor
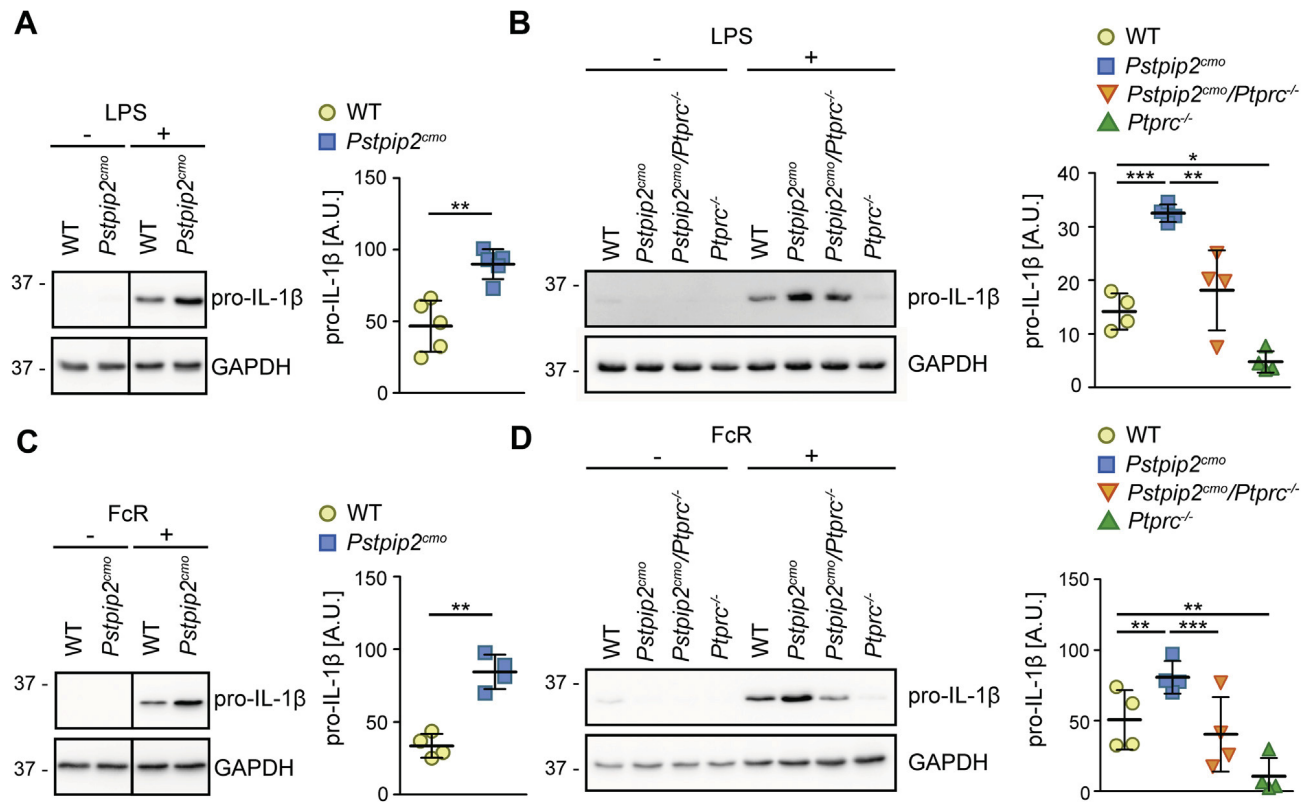
Figure 6. Enhanced production of pro-IL-1β in *Pstpip2^cmo* mice and its attenuation by CD45 deficiency. *A*, lysates of bone marrow cells from WT and *Pstpip2^cmo* mice activated with a low dose of LPS (10 ng/ml) were subjected to immunoblotting with antibody to pro-IL-1β. *B*, similar experiment as in (*A*) on lysates of purified neutrophils from mice of indicated genotypes. *C*, lysates of Fc receptor–activated bone marrow cells from WT and *Pstpip2^cmo* mice were subjected to immunoblotting with antibody to pro-IL-1β. *D*, similar experiment as in (*C*) on lysates of purified neutrophils from mice of indicated genotypes. For each experiment, representative immunoblot and quantification of multiple experiments after normalization to GAPDH signal are shown. *Vertical line* in (*A*) and (*C*) separates samples that were at different positions on the same immunoblot membrane. A.U., arbitrary units.

signaling in myeloid cells (28, 40, 47). Thus, our current knowledge leads to a conclusion that the reduced SFK activity in CD45-deficient *Pstpip2^cmo* cells results in attenuated Fc receptor signaling and diminished Fc receptor-dependent pro-IL-1β production. Given the universality of the basic principles of ITAM-mediated signaling, similar mechanism, potentially involving other ITAM-bearing receptors, is also likely at play *in vivo*.

In summary, based on our findings and previously published data, we propose a hypothesis where PSTPIP2 negatively regulates a step common to multiple signaling pathways in neutrophils, among which ITAM-dependent signaling plays a key role. A so far unknown endogenous ligand/ligands or, perhaps, even tonic signals in the absence of any ligand trigger ITAM-dependent signaling, which after reaching the step regulated by PSTPIP2, becomes exacerbated and drives increased pro-IL-1β production making more of this precursor available for inflammasome, caspase-8, and neutrophil protease cleavage. Increased IL-1β generation then leads to disease development. In the absence of CD45, SFKs become hyperphosphorylated on their inhibitory tyrosines, which results in their reduced activity, reduced ITAM signaling, and pro-IL-1β production, ultimately resulting in disease alleviation. The identity of the pathway step directly regulated by PSTPIP2 still remains unclear. Available data nevertheless suggest that inhibition of ITAM-mediated signaling by pharmacological

inhibitors should be considered as therapeutic approach in similar diseases in humans.

Experimental procedures

Antibodies

Rabbit polyclonal antibodies to phospho-LYN Y507 (#2731), phospho-LCK Y505 (#2751), and phospho-Src Family Y416 (#2101), and rabbit monoclonal antibodies to IL-1β (clone D3H1Z; #12507) and gasdermin D (clone E9S1X; #39754) were from Cell Signaling Technology; rabbit polyclonal antibody to phospho-HCK Y521 (PA5-37592) was from Invitrogen, Thermo Fisher Scientific; rabbit polyclonal antibody to GAPDH (G9545) and mouse monoclonal antibody to β-actin (clone AC-74) were from Sigma–Aldrich; rabbit polyclonal antibody to ERK (C-14, sc-154), and mouse monoclonal antibodies to HCK (clone 3D12E10) and FGR (D-6) were from Santa Cruz Biotechnology; mouse monoclonal antibody to caspase-1 (p20, Casper-1) was from AdipoGen Life Sciences. Mouse monoclonal antibody to LYN was a kind gift of Petr Draber, Institute of Molecular Genetics of the Czech Academy of Sciences.

Mice

Pstpip2^cmo mice on C57Bl/6J genetic background carrying the c.293T→C mutation in the *Pstpip2* gene, which results in a

loss of PSTPIP2 protein, were described earlier ([9](#)). They were generated from C.Cg-*Pstpip2^cmo*/J mouse strain on Balb/C genetic background ([2](#), [3](#)) obtained from The Jackson Laboratory, by backcrossing for more than ten generations to C57Bl/6J. All *Pstpip2^cmo^* mice and their derivatives used in this study were on C57Bl/6J background. *Ptprc^−/−^* mouse strain backcrossed to C57Bl/6J (B6;129–*Ptprc^tm1Holm^*/H), lacking the expression of CD45 because of exon 9 deletion ([31](#)) was obtained from European Mouse Mutant Archive ([48](#)). *Pstpip2^cmo^/MyD88^−/−^* mouse strain was described earlier ([9](#)) and was generated with the use of B6.129P2(SJL)-*Myd88^tm1.1Defr^*/J mouse strain ([29](#)) obtained from The Jackson Laboratory. TRIF-deficient mouse strain *Trif^Lps2/Lps2^* ([30](#)) was a kind gift from B. Beutler. C57Bl/6J inbred strain was obtained from the animal facility of Institute of Molecular Genetics, Academy of Sciences of the Czech Republic. Experiments in this work that were conducted on animals were approved by the Expert Committee on the Welfare of Experimental Animals of the Institute of Molecular Genetics and by the Academy of Sciences of the Czech Republic and were in agreement with local legal requirements and ethical guidelines.

Cell activation, ROS, and IL-1β detection

Bone marrow cells were isolated from mice (sacrificed by cervical dislocation) by flushing femurs and tibias, cut at the extremities, with PBS containing 2% fetal bovine serum (FBS). Erythrocytes were removed by lysis in ACK buffer (150 mM NH_4Cl, 0.1 mM EDTA [disodium salt], 1 mM $KHCO_3$). Neutrophils were isolated from bone marrow cells using Neutrophil Isolation Kit (Miltenyi Biotec; #130-097-658) according to the manufacturer's instructions followed by separation on Miltenyi AutoMACS magnetic cell sorter (negative selection). Purity of isolated neutrophils was verified by flow cytometry using CD11b, Ly6C, and Ly6G markers. For measurement of ROS (superoxide) production by luminol-based assay ([49](#), [50](#)), bone marrow cells were plated in a black 96-well plate (SPL Life Sciences) at 10^6 cells per well in IMDM supplemented with 0.2% FBS and rested for 30 min at 37 °C and 5% CO_2. Then 100 μM luminol and 50 μg/cm^2 silica or 100 μM luminol and 1 μg/ml fMLP (all from Sigma–Aldrich) were added, and the luminescence was immediately measured on EnVison plate reader (PerkinElmer) every minute for 70 min. For detection of IL-1β p17 and p21 by immunoblotting, cells were plated in 96-well tissue culture plate at 2×10^6 per well in IMDM containing 0.1% FBS and 100 ng/ml LPS. After 3 h at 37 °C and 5% CO_2, silica at 50 μg/cm^2 was added for additional 30 min. Then the cells were lysed by adding equal volume of 2× concentrated SDS-PAGE sample buffer followed by 15-s sonication and subjected to immunoblotting with IL-1β antibodies. For detection of pro-IL-1β, 2×10^6 cells in 700 μl IMDM containing 0.1% FBS and 10 ng/ml LPS were placed in low protein-binding microcentrifuge tubes (Thermo Fisher Scientific) and incubated 3 h at 37 °C and 5% CO_2. Next, the cells were centrifuged, resuspended in 100 μl IMDM containing 0.1% FBS, and lysed by adding equal volume of 2× concentrated SDS-PAGE sample buffer followed by 15-s

sonication and immunoblotting with IL-1β antibodies. For Fc receptor activation, the cells were incubated with 50× diluted culture supernatant from 2.4G2 rat hybridoma ([51](#)) (American Type Culture Collection) producing antimouse Fc receptor (CD16/CD32) antibodies (30 min on ice, low protein-binding microcentrifuge tubes). Then, the cells were centrifuged, resuspended in 700 μl IMDM containing 0.1% FBS and 5 μg/ml F(ab')$_2$ Mouse Anti-Rat antibody (Jackson ImmunoResearch), and incubated for 3 h at 37 °C and 5% CO_2. The lysis and immunoblotting procedures were the same as for the aforementioned LPS activation. For measurement of IL-1β concentrations *in vivo*, footpads from mice sacrificed by cervical dislocation were homogenized using Avans AHM1 Homogenizer (30 s, speed 25) in 1 ml radioimmunoprecipitation lysis buffer (20 mM Tris, pH 7.5, 150 mM NaCl, 1% NP-40, 1% sodium deoxycholate, and 0.1% SDS) supplemented with 5 mM iodoacetamide (Sigma) and 100× diluted Protease Inhibitor Cocktail Set III (Calbiochem, Merck). Insoluble material was removed by centrifugation (20,000g, 5 min, 2 °C). Protein concentration in the supernatants was determined using Bradford solution (AppliChem) and adjusted to equal level. Concentrations of IL-1β were then determined by Ready-SET-Go! ELISA kit from eBioscience (Thermo Fisher Scientific) according to the manufacturer's instructions.

Immunoprecipitation of SFKs

About 8×10^7 bone marrow cells were resuspended in 1 ml lysis buffer (50 mM Tris–HCl, pH 7.5, 150 mM NaCl, 1% *n*-dodecyl β-D-maltoside, 100× diluted Protease Inhibitor Cocktail Set III [Calbiochem, Merck], 1000× diluted Diisopropylfluorophosphate [Sigma, Merck] and 50× diluted PhosStop solution made by dissolving 1 PhosStop pellet [Roche] in 200 μl water) and incubated for 30 min on ice. Next the lysates were centrifuged at 25,000g for 10 min. About 2 μg antibody per sample were added followed by 1-h incubation on ice. Next, 30 μl of protein A/G agarose resin (Santa Cruz Biotechnology) was added followed by incubation at 4 to 8 °C with rotation for 90 min (in case of LYN, the antibody was first incubated with protein A/G agarose and then added to the lysates). The resin was washed two times (50 mM Tris–HCl, pH 7.5, 150 mM NaCl, 0.1% *n*-dodecyl β-D-maltoside, 100× diluted Protease Inhibitor Cocktail Set III, and 200× diluted PhosStop), and the proteins were eluted using 2× concentrated SDS-PAGE sample buffer.

Bone marrow transplantations

In bone marrow transplantation experiments, recipient mice were lethally irradiated with a single dose of 7 Gy. After 6 h, mice were injected with 2×10^6 bone marrow cells from *Pstpip2^cmo^* or *Pstpip2^cmo^/MyD88^−/−^* mice into tail vein. Mice were monitored for the presence of paw swelling and inflammation twice a week.

X-ray μCT

Hind paws were scanned *in vivo* in X-ray μCT Skyscan 1176 (Bruker) using the following parameters: voltage: 50 kV,

current: 250 μA, filter: 0.5 mm aluminium, voxel size: 8.67 μm, exposure time: 2 s, rotation step: 0.3° for 180° total, object to source distance: 119.271 mm, camera to source distance: 171.987 mm, and time of scanning: 30 min. Virtual sections were reconstructed in NRecon software 1.7.1.0 (Bruker) with the following parameters: smoothing = 3, ring artifact correction = 4, and beam hardening correction = 36%. Intensities of interest for reconstruction were in the range from 0.0045 to 0.0900 attenuation units. Same orientation of virtual sections was achieved with the use of the DataViewer 1.5.4 software (Bruker). μCT data analysis was performed using CT Analyser 1.18.4.0 (Bruker). Scans affected by technical artifacts caused by spontaneous movements of animals were excluded from the analysis. Only distal half of the paws (from the half of the length of the longest metatarsal bone to fingertips) were analyzed. Bone fragmentation (Fig. 2C) is represented by the average number of bony objects per section. Total object (*i.e.*, distal paw) volume, total bone volume, and total bone surface were computed to compute bone surface/bone volume ratio (Fig. 2C) as the second parameter corresponding to bone fragmentation, and volume of the soft tissue (as total volume minus total bone volume—Fig. 2D).

Statistical analysis

The *p* values were calculated with GraphPad Prism software, version 5.04 (Graphpad Software, Inc), using Gehan–Breslow–Wilcoxon test for Figure 1; Kruskal–Wallis test with Dunn's multiple comparison test for Figures 2, C and D, 4, A and B, and 5C; repeated-measures ANOVA and Bonferroni's multiple comparison post-test for Figures 3, 5E, and 6, B and D; one-way ANOVA and Bonferroni's multiple comparison post-test for Figure 5B; paired *t* test, two-tailed, for Figure 6, A and C. The asterisks represent *p* values as follows: *$p \leq 0.05$, **$p \leq 0.01$, ***$p \leq 0.001$, ****$p \leq 0.0001$, n.s.—not significant. Error bars in the figures represent mean ± standard deviation.

Data availability

Representative experiments are shown in the figures. For any additional information, please contact the corresponding author.

Abbreviations—The abbreviations used are: CMO, chronic multifocal osteomyelitis; FBS, fetal bovine serum; IL-1β, interleukin-1β; ITAM, immunoreceptor tyrosine-based activation motif; LPS, lipopolysaccharide; μCT, microcomputerized tomography; ROS, reactive oxygen species; SFK, Src-family kinase; SYK, spleen tyrosine kinase.

References

1. Martinez-Quiles, N., and Goldbach-Mansky, R. (2018) Updates on autoinflammatory diseases. *Curr. Opin. Immunol.* **55**, 97–105
2. Byrd, L., Grossmann, M., Potter, M., and Shen-Ong, G. L. (1991) Chronic multifocal osteomyelitis, a new recessive mutation on chromosome 18 of the mouse. *Genomics* **11**, 794–798
3. Ferguson, P. J., Bing, X., Vasef, M. A., Ochoa, L. A., Mahgoub, A., Waldschmidt, T. J., Tygrett, L. T., Schlueter, A. J., and El-Shanti, H. (2006) A missense mutation in pstpip2 is associated with the murine autoinflammatory disorder chronic multifocal osteomyelitis. *Bone* **38**, 41–47
4. Chitu, V., Ferguson, P. J., de Bruijn, R., Schlueter, A. J., Ochoa, L. A., Waldschmidt, T. J., Yeung, Y. G., and Stanley, E. R. (2009) Primed innate immunity leads to autoinflammatory disease in PSTPIP2-deficient cmo mice. *Blood* **114**, 2497–2505
5. Hurtado-Nedelec, M., Chollet-Martin, S., Chapeton, D., Hugot, J. P., Hayem, G., and Gerard, B. (2010) Genetic susceptibility factors in a cohort of 38 patients with SAPHO syndrome: A study of PSTPIP2, NOD2, and LPIN2 genes. *J. Rheumatol.* **37**, 401–409
6. Lukens, J. R., Gross, J. M., Calabrese, C., Iwakura, Y., Lamkanfi, M., Vogel, P., and Kanneganti, T. D. (2014) Critical role for inflammasome-independent IL-1beta production in osteomyelitis. *Proc. Natl. Acad. Sci. U. S. A.* **111**, 1066–1071
7. Lukens, J. R., Gurung, P., Vogel, P., Johnson, G. R., Carter, R. A., McGoldrick, D. J., Bandi, S. R., Calabrese, C. R., Walle, L. V., Lamkanfi, M., and Kanneganti, T.-D. (2014) Dietary modulation of the microbiome affects autoinflammatory disease. *Nature* **516**, 246–249
8. Cassel, S. L., Janczy, J. R., Bing, X., Wilson, S. P., Olivier, A. K., Otero, J. E., Iwakura, Y., Shayakhmetov, D. M., Bassuk, A. G., Abu-Amer, Y., Brogden, K. A., Burns, T. L., Sutterwala, F. S., and Ferguson, P. J. (2014) Inflammasome-independent IL-1beta mediates autoinflammatory disease in Pstpip2-deficient mice. *Proc. Natl. Acad. Sci. U. S. A.* **111**, 1072–1077
9. Kralova, J., Drobek, A., Prochazka, J., Spoutil, F., Fabisik, M., Glatzova, D., Borna, S., Pokorna, J., Skopcova, T., Angelisova, P., Gregor, M., Kovarik, P., Sedlacek, R., and Brdicka, T. (2020) Dysregulated NADPH oxidase promotes bone damage in murine model of autoinflammatory osteomyelitis. *J. Immunol.* **204**, 1607–1620
10. Drobek, A., Kralova, J., Skopcova, T., Kucova, M., Novak, P., Angelisova, P., Otahal, P., Alberich-Jorda, M., and Brdicka, T. (2015) PSTPIP2, a protein associated with autoinflammatory disease,

interacts with inhibitory enzymes SHIP1 and Csk. *J. Immunol.* **195**, 3416–3426

11. Wu, Y., Dowbenko, D., and Lasky, L. A. (1998) PSTPIP 2, a second tyrosine phosphorylated, cytoskeletal-associated protein that binds a PEST-type protein-tyrosine phosphatase. *J. Biol. Chem.* **273**, 30487–30496

12. Cloutier, J. F., and Veillette, A. (1996) Association of inhibitory tyrosine protein kinase p50csk with protein tyrosine phosphatase PEP in T cells and other hemopoietic cells. *EMBO J.* **15**, 4909–4918

13. Cloutier, J. F., and Veillette, A. (1999) Cooperative inhibition of T-cell antigen receptor signaling by a complex between a kinase and a phosphatase. *J. Exp. Med.* **189**, 111–121

14. Davidson, D., Cloutier, J. F., Gregorieff, A., and Veillette, A. (1997) Inhibitory tyrosine protein kinase p50csk is associated with protein-tyrosine phosphatase PTP-PEST in hemopoietic and non-hemopoietic cells. *J. Biol. Chem.* **272**, 23455–23462

15. Wang, B., Lemay, S., Tsai, S., and Veillette, A. (2001) SH2 domain-mediated interaction of inhibitory protein tyrosine kinase Csk with protein tyrosine phosphatase-HSCF. *Mol. Cell Biol.* **21**, 1077–1088

16. Futosi, K., and Mócsai, A. (2016) Tyrosine kinase signaling pathways in neutrophils. *Immunol. Rev.* **273**, 121–139

17. Chung, I. C., Yuan, S. N., OuYang, C. N., Lin, H. C., Huang, K. Y., Chen, Y. J., Chung, A. K., Chu, C. L., Ojcius, D. M., Chang, Y. S., and Chen, L. C. (2018) Src-family kinase-Cbl axis negatively regulates NLRP3 inflammasome activation. *Cell Death Dis.* **9**, 1109

18. Shio, M. T., Eisenbarth, S. C., Savaria, M., Vinet, A. F., Bellemare, M. J., Harder, K. W., Sutterwala, F. S., Bohle, D. S., Descoteaux, A., Flavell, R. A., and Olivier, M. (2009) Malarial hemozoin activates the NLRP3 inflammasome through Lyn and Syk kinases. *PLoS Pathog.* **5**, e1000559

19. Kankkunen, P., Valimaki, E., Rintahaka, J., Palomaki, J., Nyman, T., Alenius, H., Wolff, H., and Matikainen, S. (2014) Trichothecene mycotoxins activate NLRP3 inflammasome through a P2X7 receptor and Src tyrosine kinase dependent pathway. *Hum. Immunol.* **75**, 134–140

20. Lin, G., Tang, J., Guo, H., Xiao, Y., Gupta, N., Tang, N., and Zhang, J. (2017) Tyrosine phosphorylation of NLRP3 by Lyn suppresses NLRP3 inflammasome activation. *J. Immunol.* **198**, 136.2

21. Spalinger, M. R., Lang, S., Gottier, C., Dai, X., Rawlings, D. J., Chan, A. C., Rogler, G., and Scharl, M. (2017) PTPN22 regulates NLRP3-mediated IL1B secretion in an autophagy-dependent manner. *Autophagy* **13**, 1590–1601

22. Mambwe, B., Neo, K., Javanmard Khameneh, H., Leong, K. W. K., Colantuoni, M., Vacca, M., Muimo, R., and Mortellaro, A. (2019) Tyrosine dephosphorylation of ASC modulates the activation of the NLRP3 and AIM2 inflammasomes. *Front. Immunol.* **10**, 1556

23. Spalinger, M. R., Schwarzfischer, M., and Scharl, M. (2020) The role of protein tyrosine phosphatases in inflammasome activation. *Int. J. Mol. Sci.* **21**, 5481

24. Gurung, P., Burton, A., and Kanneganti, T. D. (2016) NLRP3 inflammasome plays a redundant role with caspase 8 to promote IL-1beta-mediated osteomyelitis. *Proc. Natl. Acad. Sci. U. S. A.* **113**, 4452–4457

25. Phillips, F. C., Gurung, P., and Kanneganti, T. D. (2016) Microbiota and caspase-1/caspase-8 regulate IL-1beta-mediated bone disease. *Gut Microbes* **7**, 334–341

26. Ear, T., Tatsiy, O., Allard, F. L., and McDonald, P. P. (2017) Regulation of discrete functional responses by Syk and src family tyrosine kinases in human neutrophils. *J. Immunol. Res.* **2017**, 4347121

27. Hermiston, M. L., Xu, Z., and Weiss, A. (2003) CD45: A critical regulator of signaling thresholds in immune cells. *Annu. Rev. Immunol.* **21**, 107–137

28. Zhu, J. W., Brdicka, T., Katsumoto, T. R., Lin, J., and Weiss, A. (2008) Structurally distinct phosphatases CD45 and CD148 both regulate B cell and macrophage immunoreceptor signaling. *Immunity* **28**, 183–196

29. Hou, B., Reizis, B., and DeFranco, A. L. (2008) Toll-like receptors activate innate and adaptive immunity by using dendritic cell-intrinsic and -extrinsic mechanisms. *Immunity* **29**, 272–282

30. Hoebe, K., Du, X., Georgel, P., Janssen, E., Tabeta, K., Kim, S. O., Goode, J., Lin, P., Mann, N., Mudd, S., Crozat, K., Sovath, S., Han, J., and Beutler, B. (2003) Identification of Lps2 as a key transducer of MyD88-independent TIR signalling. *Nature* **424**, 743–748

31. Byth, K. F., Conroy, L. A., Howlett, S., Smith, A. J., May, J., Alexander, D. R., and Holmes, N. (1996) CD45-null transgenic mice reveal a positive regulatory role for CD45 in early thymocyte development, in the selection of CD4+CD8+ thymocytes, and B cell maturation. *J. Exp. Med.* **183**, 1707–1718

32. Nada, S., Okada, M., MacAuley, A., Cooper, J. A., and Nakagawa, H. (1991) Cloning of a complementary DNA for a protein-tyrosine kinase that specifically phosphorylates a negative regulatory site of p60c-src. *Nature* **351**, 69–72

33. Sicheri, F., and Kuriyan, J. (1997) Structures of Src-family tyrosine kinases. *Curr. Opin. Struct. Biol.* **7**, 777–785

34. Netea, M. G., Simon, A., van de Veerdonk, F., Kullberg, B. J., Van der Meer, J. W., and Joosten, L. A. (2010) IL-1beta processing in host defense: Beyond the inflammasomes. *PLoS Pathog.* **6**, e1000661

35. Dasari, T. K., Geiger, R., Karki, R., Banoth, B., Sharma, B. R., Gurung, P., Burton, A., and Kanneganti, T. D. (2020) The nonreceptor tyrosine kinase SYK drives caspase-8/NLRP3 inflammasome-mediated autoinflammatory osteomyelitis. *J. Biol. Chem.* **295**, 3394–3400

36. Furukawa, T., Itoh, M., Krueger, N. X., Streuli, M., and Saito, H. (1994) Specific interaction of the CD45 protein-tyrosine phosphatase with tyrosine-phosphorylated CD3 zeta chain. *Proc. Natl. Acad. Sci. U. S. A.* **91**, 10928–10932

37. Wu, L., Fu, J., and Shen, S. H. (2002) SKAP55 coupled with CD45 positively regulates T-cell receptor-mediated gene transcription. *Mol. Cell Biol.* **22**, 2673–2686

38. Irie-Sasaki, J., Sasaki, T., Matsumoto, W., Opavsky, A., Cheng, M., Welstead, G., Griffiths, E., Krawczyk, C., Richardson, C. D., Aitken, K., Iscove, N., Koretzky, G., Johnson, P., Liu, P., Rothstein, D. M., *et al.* (2001) CD45 is a JAK phosphatase and negatively regulates cytokine receptor signalling. *Nature* **409**, 349–354

39. Davidson, D., Bakinowski, M., Thomas, M. L., Horejsi, V., and Veillette, A. (2003) Phosphorylation-dependent regulation of T-cell activation by PAG/Cbp, a lipid raft-associated transmembrane adaptor. *Mol. Cell Biol.* **23**, 2017–2028

40. Latour, S., and Veillette, A. (2001) Proximal protein tyrosine kinases in immunoreceptor signaling. *Curr. Opin. Immunol.* **13**, 299–306

41. Jakus, Z., Fodor, S., Abram, C. L., Lowell, C. A., and Mócsai, A. (2007) Immunoreceptor-like signaling by beta 2 and beta 3 integrins. *Trends Cell Biol.* **17**, 493–501

42. Lewis Marffy, A. L., and McCarthy, A. J. (2020) Leukocyte immunoglobulin-like receptors (LILRs) on human neutrophils: Modulators of infection and immunity. *Front. Immunol.* **11**, 857

43. Radjabova, V., Mastroeni, P., Skjødt, K., Zaccone, P., de Bono, B., Goodall, J. C., Chilvers, E. R., Juss, J. K., Jones, D. C., Trowsdale, J., and Barrow, A. D. (2015) TARM1 is a novel leukocyte receptor complex-encoded ITAM receptor that costimulates proinflammatory cytokine secretion by macrophages and neutrophils. *J. Immunol.* **195**, 3149–3159

44. Arts, R. J., Joosten, L. A., van der Meer, J. W., and Netea, M. G. (2013) TREM-1: Intracellular signaling pathways and interaction with pattern recognition receptors. *J. Leukoc. Biol.* **93**, 209–215

45. Korkmaz, B., Caughey, G. H., Chapple, I., Gauthier, F., Hirschfeld, J., Jenne, D. E., Kettritz, R., Lalmanach, G., Lamort, A. S., Lauritzen, C., Łęgowska, M., Lesner, A., Marchand-Adam, S., McKaig, S. J., Moss, C., *et al.* (2018) Therapeutic targeting of cathepsin C: From pathophysiology to treatment. *Pharmacol. Ther.* **190**, 202–236

46. Swanson, K. V., Deng, M., and Ting, J. P. (2019) The NLRP3 inflammasome: Molecular activation and regulation to therapeutics. *Nat. Rev. Immunol.* **19**, 477–489

47. Fitzer-Attas, C. J., Lowry, M., Crowley, M. T., Finn, A. J., Meng, F., DeFranco, A. L., and Lowell, C. A. (2000) Fcgamma receptor-mediated phagocytosis in macrophages lacking the Src family tyrosine kinases Hck, Fgr, and Lyn. *J. Exp. Med.* **191**, 669–682

48. Hagn, M., Marschall, S., and Hrabè de Angelis, M. (2007) EMMA– the European mouse mutant archive. *Brief Funct. Genomic Proteomic* **6**, 186–192

49. Goodridge, H. S., Reyes, C. N., Becker, C. A., Katsumoto, T. R., Ma, J., Wolf, A. J., Bose, N., Chan, A. S., Magee, A. S., Danielson, M. E., Weiss, A., Vasilakos, J. P., and Underhill, D. M. (2011) Activation of the innate immune receptor Dectin-1 upon formation of a 'phagocytic synapse. *Nature* **472**, 471–475

50. Bedouhene, S., Moulti-Mati, F., Hurtado-Nedelec, M., Dang, P. M., and El-Benna, J. (2017) Luminol-amplified chemiluminescence detects mainly superoxide anion produced by human neutrophils. *Am. J. Blood Res.* **7**, 41–48

51. Unkeless, J. C. (1979) Characterization of a monoclonal antibody directed against mouse macrophage and lymphocyte Fc receptors. *J. Exp. Med.* **150**, 580–596

The receptor-type protein tyrosine phosphatase CD45 promotes onset and severity of IL-1β-mediated autoinflammatory osteomyelitis
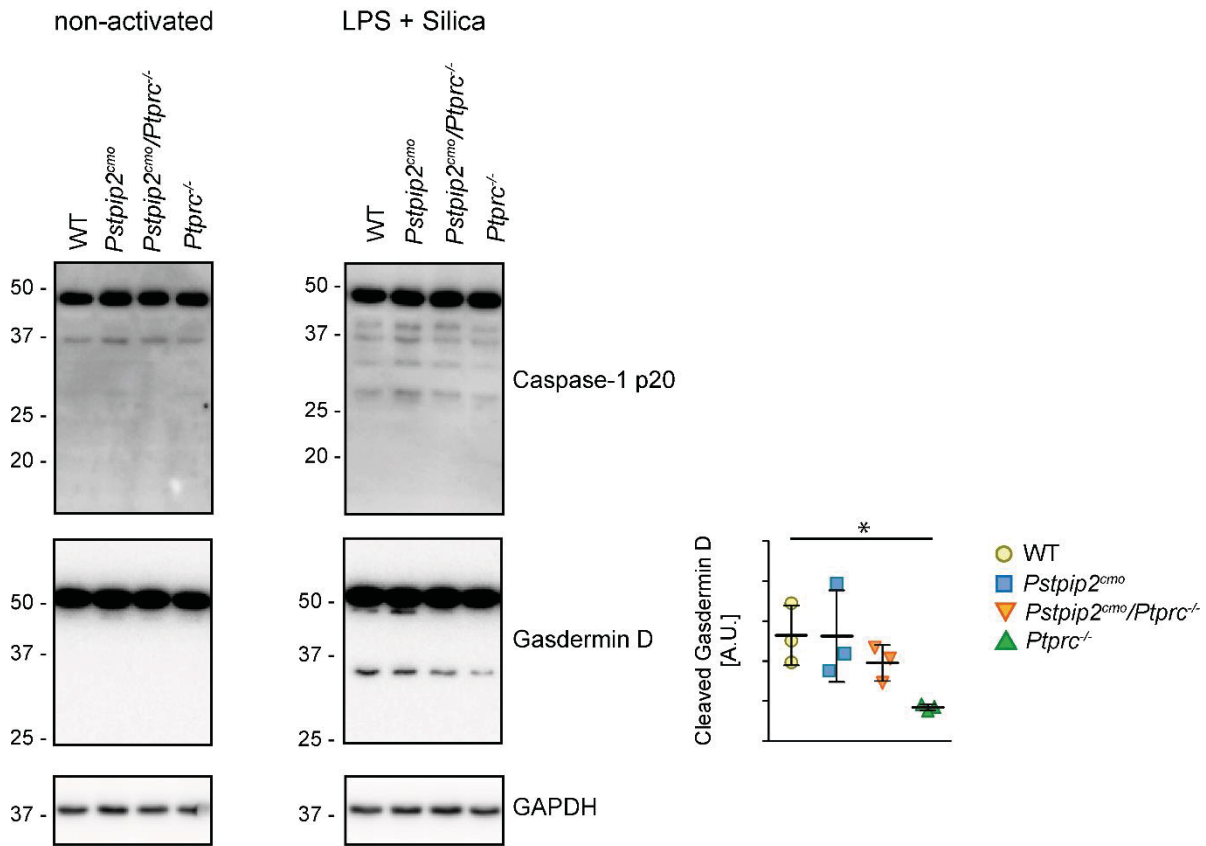
Supporting information

Figure S1. Inflammasome activity in neutrophils. Lysates of non-stimulated and LPS/silica stimulated neutrophils isolated from mice of indicated genotypes were analyzed by immunoblotting with antibodies to Caspase-1 p20 and Gasdermin D. GAPDH staining served as a loading control. Quantification of cleaved gasdermin D (p30) after normalization to GAPDH signal in activated samples from multiple experiments is shown on the right.

Regulation of Inflammatory Response by Transmembrane Adaptor Protein LST1

Matej Fabisik[1,2], Jolana Tureckova[3,4], Nataliia Pavliuchenko[1,2], Jarmila Kralova[1], Jana Balounova[4], Kristina Vicikova[4], Tereza Skopcova[1], Frantisek Spoutil[4], Jana Pokorna[1], Pavla Angelisova[1], Bernard Malissen[5], Jan Prochazka[3,4], Radislav Sedlacek[3,4] and Tomas Brdicka[1]*

[1] Laboratory of Leukocyte Signalling, Institute of Molecular Genetics of the Czech Academy of Sciences, Prague, Czechia, [2] Faculty of Science, Charles University, Prague, Czechia, [3] Laboratory of Transgenic Models of Diseases, Institute of Molecular Genetics of the Czech Academy of Sciences, Vestec, Czechia, [4] Czech Centre for Phenogenomics, Institute of Molecular Genetics of the Czech Academy of Sciences, Vestec, Czechia, [5] Centre d'Immunophénomique, Aix Marseille Université, INSERM, CNRS, Marseille, France

LST1 is a small adaptor protein expressed in leukocytes of myeloid lineage. Due to the binding to protein tyrosine phosphatases SHP1 and SHP2 it was thought to have negative regulatory function in leukocyte signaling. It was also shown to be involved in cytoskeleton regulation and generation of tunneling nanotubes. *LST1* gene is located in MHCIII locus close to many immunologically relevant genes. In addition, its expression increases under inflammatory conditions such as viral infection, rheumatoid arthritis and inflammatory bowel disease and its deficiency was shown to result in slightly increased sensitivity to influenza infection in mice. However, little else is known about its role in the immune system homeostasis and immune response. Here we show that similar to humans, LST1 is expressed in mice in the cells of the myeloid lineage. *In vivo*, its deficiency results in alterations in multiple leukocyte subset abundance in steady state and under inflammatory conditions. Moreover, LST1-deficient mice show significant level of resistance to dextran sodium sulphate (DSS) induced acute colitis, a model of inflammatory bowel disease. These data demonstrate that LST1 regulates leukocyte abundance in lymphoid organs and inflammatory response in the gut.

Keywords: LST1, inflammation, colitis, inflammatory bowel disease, myeloid cells

INTRODUCTION

Leukocyte-specific transcript 1 protein (LST1) is a small, 97 amino acid long, transmembrane adaptor protein. It is composed of a very short extracellular segment with a dimerization cysteine, a single transmembrane domain, immediately followed by a palmitoylation site, and a larger cytoplasmic tail with two immunoreceptor tyrosine-based inhibitory motifs (ITIM). Despite of its small size, at least 16 *LST1* splice variants of various length (transmembrane and soluble isoforms) were described in human mRNA. However, only one of these variants LST1/A has been detected at the protein level (1–4). The role of this extensive splicing is not known. It has been

speculated that it might function as a transcription and translation regulation tool (5). Interestingly, only two RNA splice forms have been detected in mouse (2). In this report, we will refer to the protein expressed from human and murine *LST1* genes only as LST1.

Our previous analysis of LST1 expression pattern by in-house generated monoclonal antibody LST1/02 recognizing human but not murine LST1 revealed its expression exclusively in leukocytes of the myeloid lineage (macrophages, dendritic cells, monocytes, granulocytes) and in related cell lines (U-937, THP-1) (1). However, there is a discrepancy between these results and results obtained with another monoclonal antibody 7E2, which showed expression of LST1 also in lymphoid (Jurkat, B cells) and non-hematopoietic cells (HeLa, Capan-1, HepG2) (3). LST1 expression appears to be regulated during inflammation. Increased expression of LST1 mRNA isoforms was detected in cell lines after treatment with pro-inflammatory compounds (LPS, TNFα). Its expression was also elevated in histological colon samples from patients with inflammatory bowel disease (IBD) (6) and in the synovial fluid of patients with rheumatoid arthritis (7).

LST1 is coded by *LST1* gene (also known as *B144*) localized in *MHCIII* locus. This genomic site harbors many immunologically important genes, such as genes coding for Lymphotoxin-β, Tumor Necrosis Factor α, several complement proteins and others. High LST1 expression in leukocytes together with localization of its gene in one of the immunologically most important loci, raises a question about the function of LST1 in the immune system (8, 9). Previous work from our laboratory demonstrated that ITIM motifs in LST1 bind phosphatases SHP1 and SHP2 and suggested that it is a negative regulator of signaling in myeloid cells, although the processes that LST1 regulates *in vivo* were not defined (1).

In HeLa cells, overexpression of LST1 induced formation of tunneling nanotubes *via* interaction with RalA–M-Sec–exocyst complex, and transfer of MHC class I molecules through these nanotubes between the cells (10–12). In a genomic study, *Lst1* was identified as a gene connected to host response to influenza virus (13). This was further corroborated by a subsequent study showing that LST1-deficient mice display higher susceptibility to influenza infection when compared to the wild type mice (14). Increased expression of *LST1* in tissues affected by IBD or rheumatoid arthritis suggests that it may also be involved in other inflammatory conditions. In this work we describe basic features of LST1 deficient mice and analyze the role of LST1 in the dextran sodium sulphate (DSS)-induced colitis, a mouse model of IBD. We show that the LST1 deficiency results in alterations in innate leukocyte subset composition and in milder progress of DSS-induced colitis, demonstrating LST1 involvement in the regulation of leukocyte homeostasis and inflammation.

MATERIALS AND METHODS

Mice
LST1-deficient mouse strain LST1[tm1(KOMP)Vlcg] on C57Bl/6J genetic background (abbreviated as *Lst1^{-/-}*) was obtained from International Knockout Mouse Consortium. These animals were crossed to C57Bl/6J mice from Animal facility of the Institute of Molecular Genetics to obtain heterozygotes *Lst1^{-/-}* x C57Bl/6J. Their homozygote offspring were used as littermates for comparative experiments at the age of 6 - 10 weeks. Animal experiments were approved by the Animal Care and Use Committee of the Institute of Molecular Genetics and were in agreement with local legal requirements and ethical guidelines.

Primary Cell Isolation and Activation
Animals were sacrificed by cervical dislocation and single cell suspensions were prepared. Lymph node and splenic cell suspensions were prepared by pressing the lymph node or spleen tissue through 42 µm cell strainer. Bone marrow cells were isolated by flushing femurs cut at the extremities with cold PBS/2% FCS using syringe and 30 Gauge needle. Erythrocytes were removed by lysis in ACK buffer (150 mM NH_4Cl, 0.1 mM EDTA (disodium salt), 1 mM $KHCO_3$). Colon lamina propria cells were isolated from entire colon. The colon was opened longitudinally, washed with cold PBS and then rocked for 1 hour in 10 ml solution of 5mM EDTA/2% FCS/HBSS without Ca^{2+} and Mg^{2+} at 4°C followed by washing with 10 ml HBSS/2% FCS. Colon was then cut to 3 mm pieces and digested with the solution containing collagenase II (2 mg/ml, Gibco #17101-015, CAS No. 9001-12-1) and DNase I (0.5mg/ml, Sigma powder DN25-100MG; CAS No. 9003-98-9) in DMEM/2% FCS with shaking (37°C, 2 × 30 min). After each digestion round, tissues were poured onto petri dish and triturated gently with plastic Pasteur pipette in order to obtain the lamina propria cells. Cell suspension was filtered through 100 µm Sysmex filters, centrifuged, resuspended in 5 ml of PBS/2% FCS and kept on ice. After the second round of digestion, cells were pooled together, centrifuged, resuspended in PBS/2% FCS and filtered again through 50 µm Sysmex filters to obtain single cell suspension of colon lamina propria cells. For murine colonic epithelial cell isolation, colon was opened longitudinally and washed vigorously in PBS on ice. Then it was cut to shorter fragments and incubated in 20 ml pre-heated HBSS, 3% FBS, 2 mM EDTA twice at 37°C. The suspension with released cells was then collected and filtered through 100 µm filter. Filtered cells were resuspended in 1 ml (1 min, 37°C) TrypLE[TM] Express Enzyme (Thermo Fischer Scientific, 12605010), resuspended by pipetting and filtered again through 40 µm filter into 15 ml tubes. TrypLE[TM] enzymes were neutralized by washing filter with 3 ml of HBSS (without Ca^{2+} and Mg^{2+}), 3% FBS, 2 mM EDTA (pH 8.0, ice cold). Cells were centrifuged for 10 min (4°C, 300 × g), stained with CD45 and EpCAM fluorescent antibodies and sorted on BD FACSAria[TM] cell sorter as CD45^{-} EpCAM^{++}. Bone marrow derived dendritic cells (BMDC) and bone marrow derived macrophages (BMDM) were generated from isolated mouse bone marrow cells by culturing in IMDM culture media supplemented with 10% FCS and 3% supernatant from J558 cells containing GM-CSF for 10 days (BMDC) or 5% supernatant from CMG 14-12 cells containing M-CSF for 7 days (BMDM) as described in detail here (15).

Glycosylation Assay
BMDM were plated in a 6-well plate at 2×10^6 cells per well and treated with Tunicamycin (Sigma) - 0.5 µg/ml and 1 µg/ml for

24 hours followed by lysis (300 μl 2× concentrated SDS-PAGE sample buffer). Lysed samples were sonicated, heated to 95°C for 10 minutes and analyzed by immunoblotting under non-reducing conditions.

Cell Activation

BMDM and BMDC were cultured overnight in DMEM without M-CSF/GM-CSF in a 12-well tissue culture plate (10^6 cells per well) and then incubated for indicated time-points with IFNγ (Peprotech) – 50 ng/ml, TNFα (Peprotech) – 20 ng/ml, LPS (Sigma) – 100 ng/ml and PolyI:C (Invivogen, low molecular weight) – 20 μg/ml, GM-CSF – 3% supernatant from J558 cells. Subsequently, cells were lysed in 2 × concentrated SDS-PAGE sample buffer (128 mM Tris pH 6.8, 10% glycerol, 4% SDS, 1% DTT) and subjected to immunoblotting with indicated antibodies.

Antibodies

Flow cytometry antibodies are listed in **Supplementary Table S1**. LST1/06 mouse mAb recognizing murine LST1 on Western blots and in immunoprecipitation was generated by immunization of $Lst1^{-/-}$ mice with recombinant intracellular domain of murine LST1 (starting at Cys40) produced in *Escherichia coli*. After immunization, splenocytes were fused with Sp2/0 myeloma cells and antibody producing hybridomas were cloned by limiting dilution. Antibodies used for Western blot detection: SHP-1 (SH-PTP1 Antibody, C-19, Santa Cruz Biotechnology), SHP-2 (SH-PTP2 N-16, Santa Cruz Biotechnology), GAPDH (Anti-GAPDH antibody produced in rabbit, Sigma-Aldrich), IκBα (Cell Signaling Technology, #9242). Western blot ECL signals were detected with Azure c300 imaging system (Azure Biosystems) and quantified using AIDA image analyzer software (Elysia-raytest, Straubenhardt, Germany).

Flow Cytometry

Cells of bone marrow, spleen and lymph nodes were incubated with fluorescently labeled antibodies and Fc-receptor blocking antibody (2.4G2) and analyzed on BD^{TM} LSRII flow cytometer (Becton Dickinson). Staining was divided into two sets – A (CD3, CD4, CD8, CD19, NK1.1), B (CD11b, CD11c, F4/80, Ly6C, Ly6G). Cell populations were gated as: CD4 T cells – $CD3^+$ $CD4^+$; CD8 T cells – $CD3^+$ $CD8^+$; B cells – $CD19^+$ $CD3^-$; NK cells – $NK1.1^+$ $CD3^-$; $NK1.1^+CD3^+$; Macrophages – $CD11b^{low}$ $F4/80^+$; Monocytes – $CD11b^+$ $Ly6C^{hi}$ $Ly6G^-$; Neutrophils – $CD11b^+$ $Ly6C^{med}$ $Ly6G^+$; Dendritic cells – $CD11b^+$ $CD11c^+$. Colon leukocytes were measured on BD^{TM} FACSymphony flow cytometer (Becton Dickinson) according to International Mouse Phenotyping Consortium standards[1] and gated as CD45+ cells. Staining was divided into two sets – A (CD49d, CD4, Klrg1, CD44, CD8a, γδTCR, NK1.1, GITR, CD25, CD62L), B (Ly6G, CD19, Ly6C, CD11b, CD21/CD35, F4/80, Bst2, NK1.1, CD23, CD11c, MHCII). Populations were gated as: CD4 T cells – $CD5^+$ $CD4^+$; CD8 T cells – $CD5^+$ $CD8^+$; B cells – $CD19^+$ $MHCII^+$; NK cells – $CD5^-$ $CD161^+$; NKT cells – $CD5^+$ $CD161^+$; Monocytes – $CD11b^+$ $Ly6C^+$ $Ly6G^-$; Neutrophils –

CD11b$^+$ Ly6C^{med} Ly6G$^+$; Macrophages – CD11b$^+$ F4/80$^+$; Dendritic cells – CD11b$^{+/-}$ MHCII$^+$ CD11c$^+$. Data were analyzed in FlowJo^{TM} software.

Cytokine Detection by ELISA

Blood from tail vein was collected into EDTA tubes (EDTA 1000A, ref. 078035, KABE LABORTECHNIK, GmbH) and centrifuged (16 000 × g, 10 min, 4°C). Supernatant (plasma) was then transfered to fresh tubes and frozen in -80°C. Colons were homogenized in 400 μl RIPA lysis buffer (20 mM TRIS pH 7.5, 150 mM NaCl, 1% Nonidet P-40, 1% sodium deoxycholate, 0.1% SDS) containing 5 mM iodoacetamide (Sigma-Aldrich) and diluted Protease Inhibitor Cocktail Set III (Calbiochem, Merck) using AvansAHM1 Homogenizer on ice (10 s, maximum speed). The homogenates were cleared by centrifugation and frozen in -80°C. Concentrations of cytokines in blood plasma or colonic lysates were determined using IL-6 and TNF alpha Mouse Uncoated ELISA Kit with Plates (88-7324-22, 88-7064-22, Thermo Fischer Scientific) according to the manufacturer´s protocols.

Bone MicroCT Analysis

Femurs of 28 mice were scanned in-vivo under 20% zoletile anesthesia in SkyScan 1176 (Bruker, Belgium) at the resolution of 8.67 μm with 0.5 mm aluminum filter (voltage = 50 kV, current = 250 μA, step rotation = 0.3°) with 180° rotation, and reconstructed in NRecon 1.6.10.4 (Bruker, Belgium) with parameters of smoothing = 4, ring artifact correction = 7, beam hardening correction = 23%, and spread of intensities from 0.007 to 0.11 AU. Only reconstructions without artifacts underwent analysis resulting in 42 femurs analyzed. The femurs were segmented in CT Analyzer 1.16.4.1 (Bruker, Belgium) and reoriented in DataViewer 1.5.2 (Bruker, Belgium). CT Analyzer was also used for semiautomatic selection of regions of interest (central diaphysis for cortical bone, and distal metaphysis for trabecular bone) and subsequent 2D and 3D analysis. Parameters describing bone volume, porosity, and structural complexity were recorded. Bone mineral density (BMD) and tissue mineral density (TMD) were recorded for trabeculae and corticals, respectively, based on the correlation with calibrated hydroxyapatite phantoms.

Induction of Inflammatory Response
In Vivo

For LPS challenge, mice were intraperitoneally injected with LPS (50 μg per animal). After 4 and 16 hours blood samples were collected and then mice were sacrificed by cervical dislocation and splenocyte subsets analyzed. To induce colitis with dextran sodium sulphate (DSS), littermates of $Lst1^{-/-}$ and WT mice (males, 8 weeks old) were fed with 2,5% DSS dissolved in drinking water for 6 days to induce acute colitis. Starting on day 7, DSS solution was changed for plain water. Parameters defining disease activity index, i.e. stool consistency, occult bleeding (Hemoccult Fecal Occult Blood Test, Beckman Coulter) and body weight on days 0, 2, 4, 5, 6, 8 were measured during the experiment. Mice in control group were administered only plain water. On day 8, mice were anesthetized with isoflurane (0.3L/min) for collection of blood sample from the

---

[1] https://www.mousephenotype.org/impress/ProcedureInfo?action=list&procID= 1225&pipeID=7

eye vein and sacrificed. Colon length was recorded, organs were collected (spleen, mesenteric lymph nodes, blood sample and colon), processed into single cell suspensions and measured with BD™ FACSymphony flow cytometer. Disease Activity Index was evaluated as average of the three measured parameters (weight loss, stool consistency and occult bleeding index) on a particular day. Scoring values were normalized to day 0, which has an arbitrary value 0. Scoring system for body weight: 1, loss of 1% – 5% weight; 2, loss of 5% –10% weight; 3, loss of 10% –20% weight; 4, 20% and higher body weight loss. Stool consistency: 0, well-formed stool pellets; 1, loose stool pellets; 2, pasty and semi-formed stools that did not adhere to the anus (mild diarrhea); 3, slimy stool (moderate diarrhea); 4, severe watery diarrhea that adhered to the anus and contained with blood. Occult bleeding: 0, no blood; 2, positive Hemoccult test, and 4, gross rectal bleeding.

Histology
The entire colon was opened longitudinally, flushed with PBS and fixed in 4% neutral buffered formaldehyde for 48 hours as swiss roll. Samples were dehydrated, embedded in paraffin and sectioned at 5 μm and stained with hematoxylin-eosin. For histological evaluation, areas of inflammatory lesions were microscopically evaluated and quantified as described (16). Area of damaged colon epithelium was assessed in FIJI editor after recalculating pixel area to the real area in mm^2 (4-5 animals per group).

Migration Assay
Corning 6.5 mm diameter Transwell Permeable Supports with 8.0 μm pores were used. Inserts (upper well) with pores were coated with 100 μl fibronectin (50 μg/ml) for 2 hours at room temperature and washed two times with migration media (IMDM without antibiotics, 0.5% BSA). 10^5 macrophages were added into the insert with migration media and 600 μl of migration media with CXCL12 (100 ng/ml) into the bottom well. After 2 hours at 37°C, 5% CO_2 migrated cells were collected (attached cells were released with 0.2% EDTA in PBS). The collected cells were mixed with 10 μl of Flow Cytometry Absolute Count Standard™ (Bangs Laboratories) and counted in BD™ FACSymphony flow cytometer (Becton Dickinson).

Quantitative Real-Time PCR
The total cellular RNA was isolated using Quick-RNA Miniprep Plus kit and transcribed into cDNA by RevertAid RT Reverse Transcription Kit, both used according to manufacturer's instructions. The cDNA was then used as a template for real-time quantitative PCR performed on LightCycler 480 using SYBR Green I Master mix (Roche). Primers used in cytokine mRNA detection are listed in **Supplementary Table S2**.

Statistics
Student´s t-test (two-tailed, unpaired) and One-way ANOVA with Tukey posttest for P-values and two-sided Grubb´s test for outlier recognition was performed in Graphpad Prism Software. Bars in figures represent mean ± SD, if not stated otherwise. P values lower than 0.05 are marked with asterisks as follows: * $p \leq 0.05$, ** $p \leq 0.01$, *** $p \leq 0.005$, **** $p \leq 0.0001$.

RESULTS

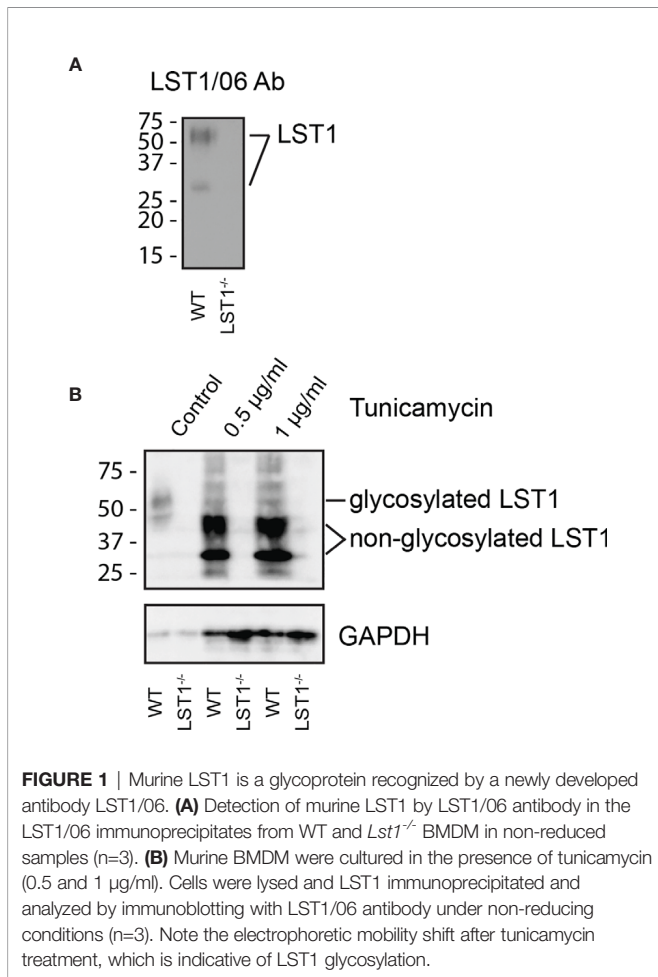## Murine LST1 Is Glycosylated Transmembrane Adaptor Protein
LST1 is a small transmembrane adaptor protein, which makes homo-dimers *via* cysteine bridges (1). Our previously generated monoclonal antibody LST1/02 to human LST1 (1) did not recognize murine protein. For detection of murine LST1, we have generated a novel monoclonal antibody LST1/06, against recombinant intracellular segment of murine LST1 and verified its specificity (**Figure 1A**). It preferentially binds LST1 under non-reducing conditions, i.e. in its dimeric form, which can be detected on Western blot as a broad double-band of ca 27-37 and 42-71 kDa, depending on the cell type (**Figures 1A, B, 2**). Lower than expected electrophoretic mobility and presence of N-glycosylation motif (NxS) in the short extracellular sequence suggested that murine LST1 could be glycosylated. Indeed, after addition of glycosylation inhibitor tunicamycin to the BMDM, its apparent molecular mass decreased to ca 29-48 kDa (**Figure 1B**).

LST1 Protein Levels Are Increased by Pro-Inflammatory Stimuli
The LST1 protein expression analysis using LST1/06 antibody, revealed that LST1 expression in cells that were not activated by proinflammatory stimuli is relatively low. As a result, multiple background bands cross-reacting with LST1/06 antibody, including a band of a similar molecular weight as LST1, became apparent during prolonged Western blot exposures. However, the use of the $Lst1^{-/-}$ cells as controls allowed us to distinguish the specific signal. Under these conditions, LST1 could be detected in the cells of myeloid lineage, including macrophages (MF), neutrophils (Neu), monocytes (Mon), but not in lymphoid lineage cells (T, B cells and NK cells) (**Figure 2A**). Since it has been observed previously that LST1 expression is elevated by inflammatory stimuli in human cell lines and in inflamed colon tissue (6), we decided to test if LST1 expression is upregulated under inflammatory conditions in leukocytes of myeloid lineage. Indeed, we observed elevated expression of LST1 *in vitro* in murine BMDM and BMDC after overnight (16 hours) stimulation with IFNγ, LPS, TNFα and PolyI:C (**Figures 2B, C**).

LST1 Deficiency Results in Sex-Dependent Alterations of Trabecular Bone Structure in Mice
$Lst1^{-/-}$ mice were born at standard Mendelian ratios without any manifestation of disease during their aging. The phenotypical analysis of this mouse strain presented on the website of International mouse phenotyping consortium[2] (17), showed slight increase in the bone mineral density in $Lst1^{-/-}$ animals, suggesting potential effect on the function of osteoclasts or overall bone homeostasis, which are known to be affected by immune system activity. Though the finding was not considered significant, low p-value associated with the data prompted us to re-evaluate these results. Our analysis by microcomputerized

FIGURE 1 | Murine LST1 is a glycoprotein recognized by a newly developed antibody LST1/06. **(A)** Detection of murine LST1 by LST1/06 antibody in the LST1/06 immunoprecipitates from WT and *Lst1⁻/⁻* BMDM in non-reduced samples (n=3). **(B)** Murine BMDM were cultured in the presence of tunicamycin (0.5 and 1 µg/ml). Cells were lysed and LST1 immunoprecipitated and analyzed by immunoblotting with LST1/06 antibody under non-reducing conditions (n=3). Note the electrophoretic mobility shift after tunicamycin treatment, which is indicative of LST1 glycosylation.

FIGURE 2 | Murine LST1 is expressed in the cells of myeloid lineage and its expression increases after pro-inflammatory stimuli. **(A)** Murine LST1 was detected in total cell lysates by immunoblotting (n=3). MF – bone marrow derived macrophages, DC – bone marrow derived dendritic cells, Neu – Neutrophils, B – B cells, T – T cells, Mono – monocytes, NK – NK cells. Its molecular weight varies between 42 to 71 kDa, likely due to the glycosylation. **(B, C)** Expression of LST1 in bone marrow derived macrophages **(B)** and dendritic cells **(C)** after treatment with various pro-inflammatory stimuli (n=3, see *Materials and Methods* for concentrations).

tomography (µCT) did not confirm any differences in the bone mineral density (not shown). On the other hand, it revealed reduced numbers of trabeculae in the trabecular bone tissue of *Lst1⁻/⁻* mice (**Figures 3A, B**). The trabeculae were also less segmented as demonstrated by the reduced ratio of trabecular bone surface and bone volume (**Figure 3B**). Interestingly, these differences were restricted only to male animals (**Figures 3A,B**; **Supplementary Figure S1**).
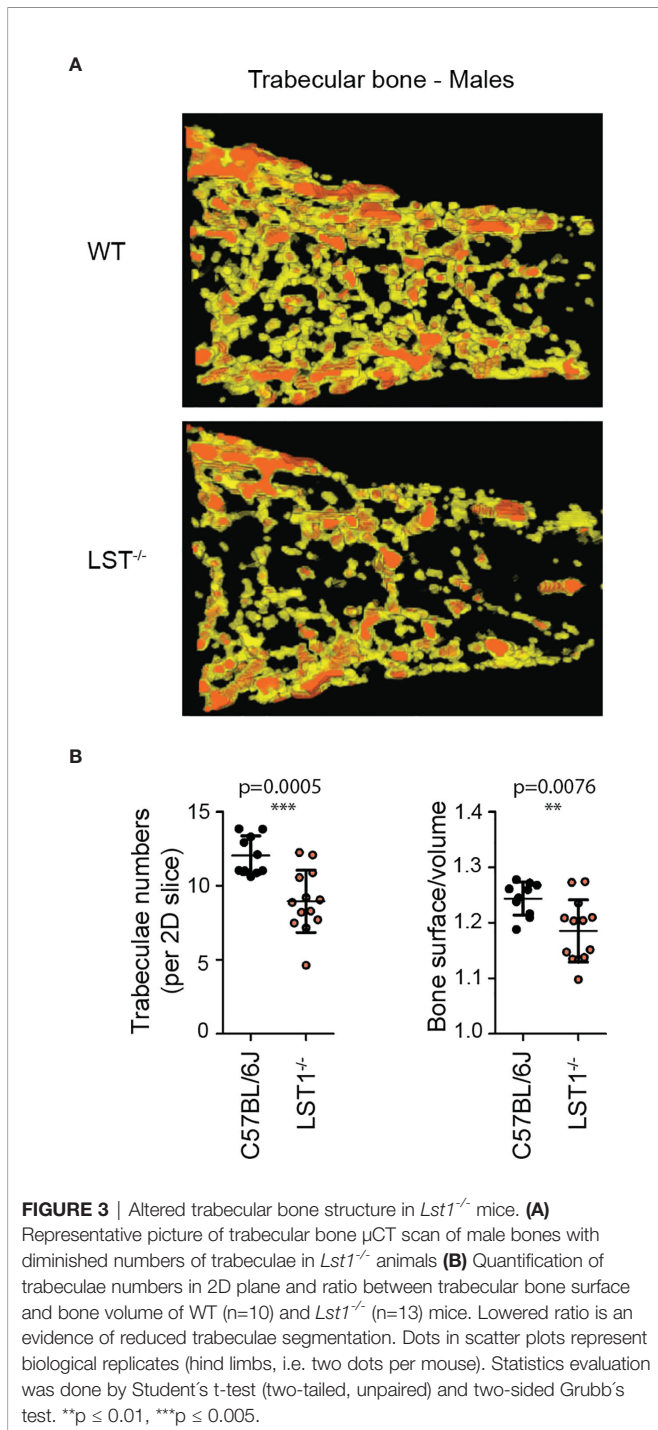
LST1 Deficient Mice Show Alterations in Leukocyte Subset Composition

Analysis of steady state lymphocyte populations in *Lst1⁻/⁻* mice revealed that while B cell and T cell subsets are without change and their percentages are comparable to the wild type mice (WT), other populations show reduced numbers. These include mainly bone marrow and splenic NK cells and splenic NKT cells (**Figures 4A-C**). Among the splenocytes of myeloid lineage, reduced percentages were observed for neutrophils, F4/80⁺ macrophages and to some extent also dendritic cells (**Figure 4C**). Reduced percentages were also observed for dendritic cells in the bone marrow (**Figure 4A**). Importantly, we also observed
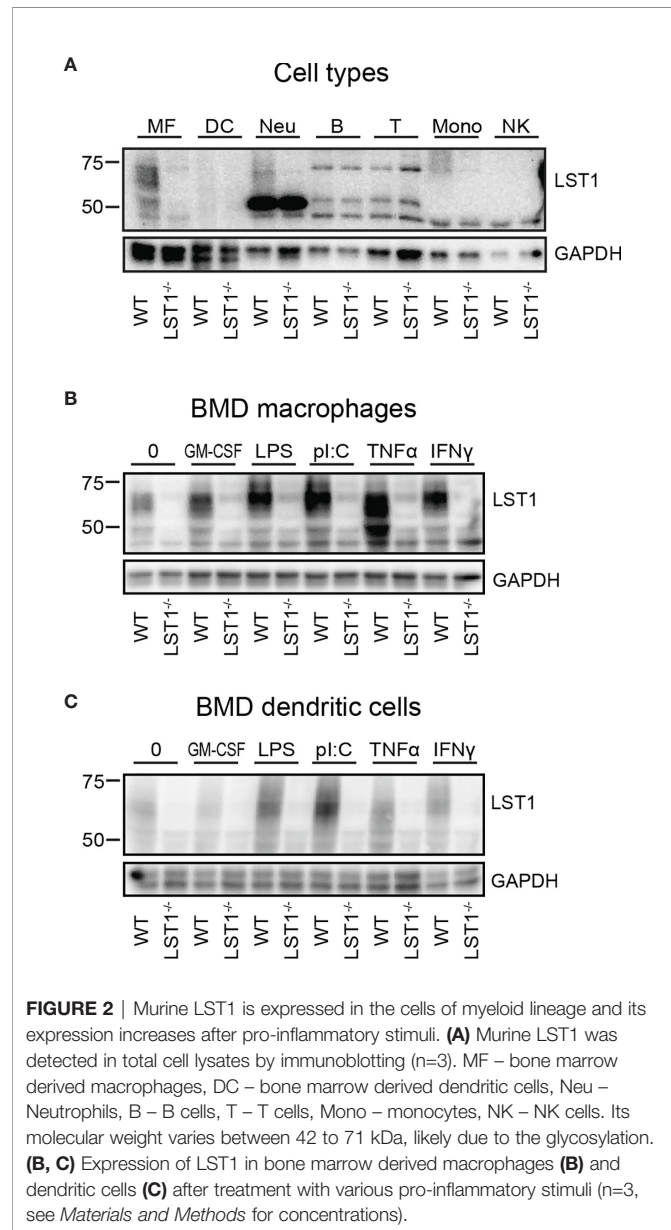
decrease in macrophage and dendritic cell percentages in the colon (**Figure 4D**). Total cell numbers were not significantly changed between the WT and *Lst1⁻/⁻* animals in any of the organs analyzed (**Figure 4E**). Reduced percentages of multiple leukocyte subsets could result from defect in cellular migration. To test the migratory capacity of LST1-deficient cells we analyzed chemokine-mediated migration of *Lst1⁻/⁻* bone marrow-derived macrophages in a transwell assay. Surprisingly, *Lst1⁻/⁻* cells migrated more efficiently towards CXCL12, ligand of chemokine receptor CXCR4, than WT cells (**Figure 4F**). At the same time CXCR4 expression was not affected by LST1 deficiency (**Figure 4G**). This finding suggests that LST1 negatively regulates CXCR4-mediated migration. It also shows that the migratory capacity of *Lst1⁻/⁻* cells is not compromised and that there is no general defect in cellular migration that could

FIGURE 3 | Altered trabecular bone structure in *Lst1⁻/⁻* mice. **(A)** Representative picture of trabecular bone µCT scan of male bones with diminished numbers of trabeculae in *Lst1⁻/⁻* animals **(B)** Quantification of trabeculae numbers in 2D plane and ratio between trabecular bone surface and bone volume of WT (n=10) and *Lst1⁻/⁻* (n=13) mice. Lowered ratio is an evidence of reduced trabeculae segmentation. Dots in scatter plots represent biological replicates (hind limbs, i.e. two dots per mouse). Statistics evaluation was done by Student´s t-test (two-tailed, unpaired) and two-sided Grubb´s test. **p ≤ 0.01, ***p ≤ 0.005.

be responsible for reduced percentages of leukocyte subsets described above.

Normal Response of *Lst1⁻/⁻* Mice to LPS Challenge

Data showing increase in LST1 expression level after exposure to pro-inflammatory stimuli indicated that LST1 could be involved in the control of inflammation. In addition, we expected that the differences between WT and *Lst1⁻/⁻* mice will be more apparent under the conditions where LST1 expression is high in WT

animals. Therefore, we decided to induce systemic inflammation in WT and *Lst1⁻/⁻* mice by intraperitoneal injection of LPS. In the spleens of both strains, this resulted in increased percentages of B cells and neutrophils and decreased percentages of other cell populations. When comparing WT and *Lst1⁻/⁻* mice, majority of the differences and trends observed in the steady state remained preserved or even enhanced. These included mainly reduced percentages of NK and NKT cells, monocytes, dendritic cells and similar (but outside the borderline of statistical significance) reduction in neutrophils (**Figure 5A**). Total numbers of splenocytes remained comparable (**Figure 5B**). In the bone marrow and blood, no additional alterations in *Lst1⁻/⁻* mice were observed (not shown). TNFα and IL-6 levels in the blood at 4 hours after LPS challenge were also not affected by LST1 deficiency (**Supplementary Figure S2A**). In BMDCs LST1 deficiency did not result in any alteration in LPS-induced cytokine mRNA expression, including IL-1β, IL-6, IL-12, TNFα, IL-15, IL-18, IL-10, and TGFβ (**Supplementary Figure S2B**). Similar results were also obtained in a more limited analysis of BMDM (not shown). In line with these observations, LPS-induced NF-κB activation pathway in BMDM was not affected by LST1 deficiency (**Supplementary Figure S2C**). Moreover, expression of LST1 binding partners SHP1 and SHP2 also was not influenced by LST1 deficiency in LPS-treated BMDM (**Supplementary Figure S2D**) Thus, we concluded that LPS challenge did not reveal any new major differences between leukocyte subset composition and behavior in WT and *Lst1⁻/⁻* mice.

Lst1⁻/⁻ Mice Show Increased Resistance to Acute Colitis Induced by DSS

Previously published article (6) showed elevated expression of LST1 in inflamed colon tissue from a patient with inflammatory bowel disease (IBD). This disease is characterized by an exaggerated immune response to commensal microbiota and breach of intestinal barrier. However, its etiology is still not completely understood. DSS-induced acute colitis is a widely used mouse model of IBD, where myeloid cells play a major role (18, 19). Due to LST1 expression in the target tissues and our data showing effects of LST1 deficiency on several myeloid populations, we decided to induce DSS colitis in *Lst1⁻/⁻* male mice to test the effects of LST1 deficiency on the severity of this disease. We used only males for this experiment, since they are more sensitive to DSS treatment (20). This way we reduced variability and a number of animals needed for this experiment and increased probability of detecting differences between WT and *Lst1⁻/⁻* mice. DSS at concentration 2.5% dissolved in drinking water was administered to the mice for 6 days. Then, DSS solution was changed for plain water for the remaining two days of the experiment (day 7 and 8). Mice were monitored for *Lst1* mRNA expression and for number and area of inflammatory lesions, length of the colon and overall disease activity defined by Disease Activity Index – DAI (an integrated value encompassing weight loss, rectal bleeding and stool consistency). *Lst1* mRNA expression in the colon tissue did not significantly change during the course of the experiment
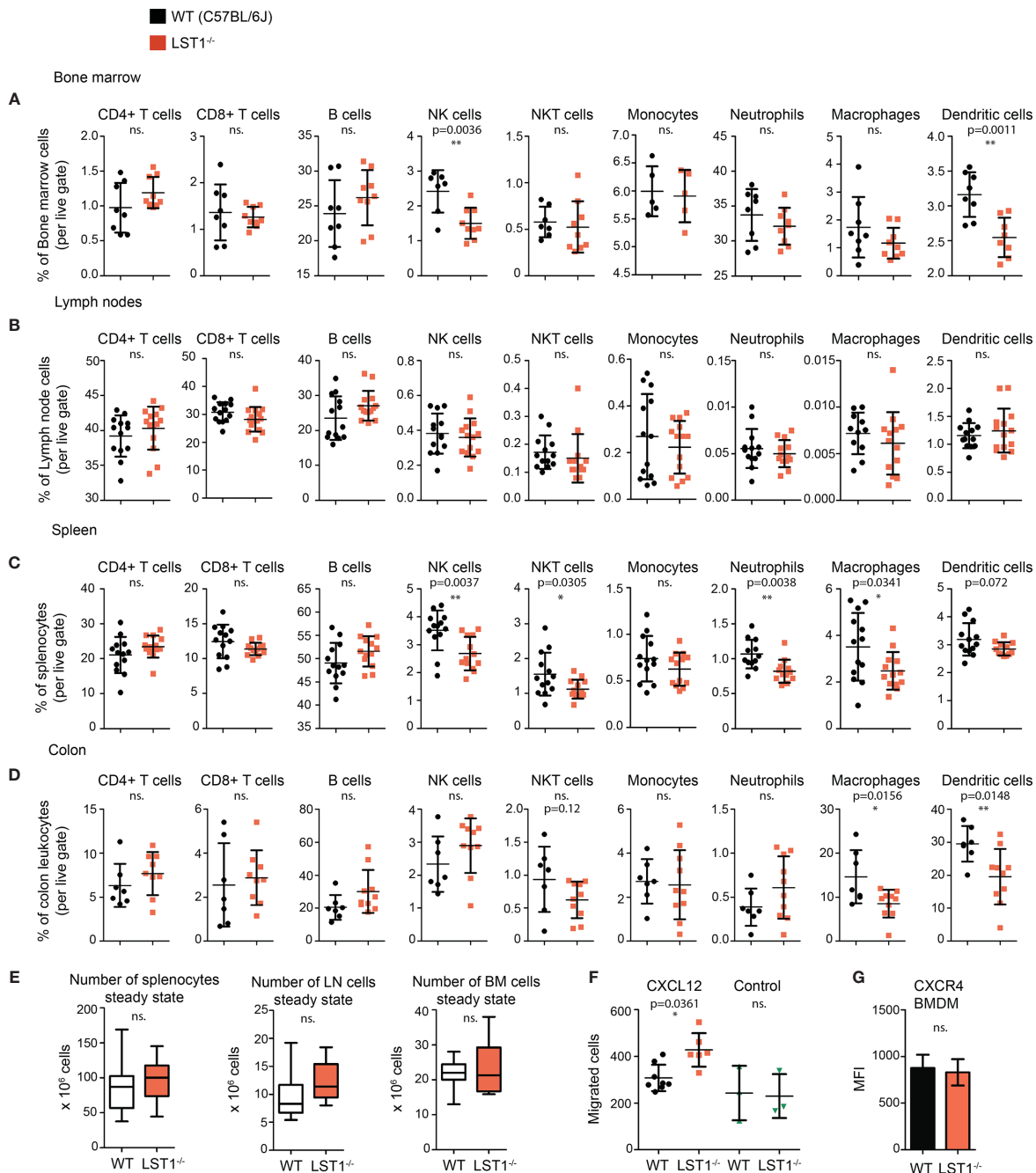
FIGURE 4 | Alterations of leukocyte subset percentages in *Lst1*⁻/⁻ mice. **(A–D)** Steady state percentages of main leukocyte subsets (n=5-15) in the bone marrow **(A)**, lymph nodes **(B)**, spleen **(C)**, and colon **(D)**. Dots in scatter plots represent biological replicates. **(E)** Absolute numbers of cells in steady state spleen, bone marrow and lymph nodes (n=14-25). **(F)** Number of bone marrow derived macrophages (BMDM) that after 2 hours migrated towards CXCL12 (100 ng/ml) (n=6-8). Control samples were without CXCL12 chemo-attractant (n=3). **(G)** Quantification of CXCR4 expression on BMDM surface (n=6). Dots in scatter plots represent biological replicates. Statistics evaluation was done by Student´s t-test (two-tailed, unpaired) and two-sided Grubb´s test. *p ≤ 0.05, **p ≤ 0.01, ns, not significant.

and it was absent from isolated colonic epithelial cells. (**Supplementary Figure S3A**). Disease activity was similar in both WT and *Lst1*⁻/⁻ mice until the day 4 of DSS treatment. However, from the sixth day on, the colitis DAI of *Lst1*⁻/⁻ mice appeared significantly lower than that of WT animals (**Figure 5C**). *Lst1*⁻/⁻ mice displayed less severe rectal bleeding, better stool

consistency, and milder colon shortening than WT animals (**Supplementary Figure S3B**). Moreover, areas of damaged colonic epithelium were significantly smaller at days 6 and 8 in the *Lst1*⁻/⁻ mice (**Figures 5D, E**). Expression of pro-inflammatory cytokines detected in colonic lysates was also reduced at day 5 of the experiment (**Figure 5F**). Surprisingly, these differences in
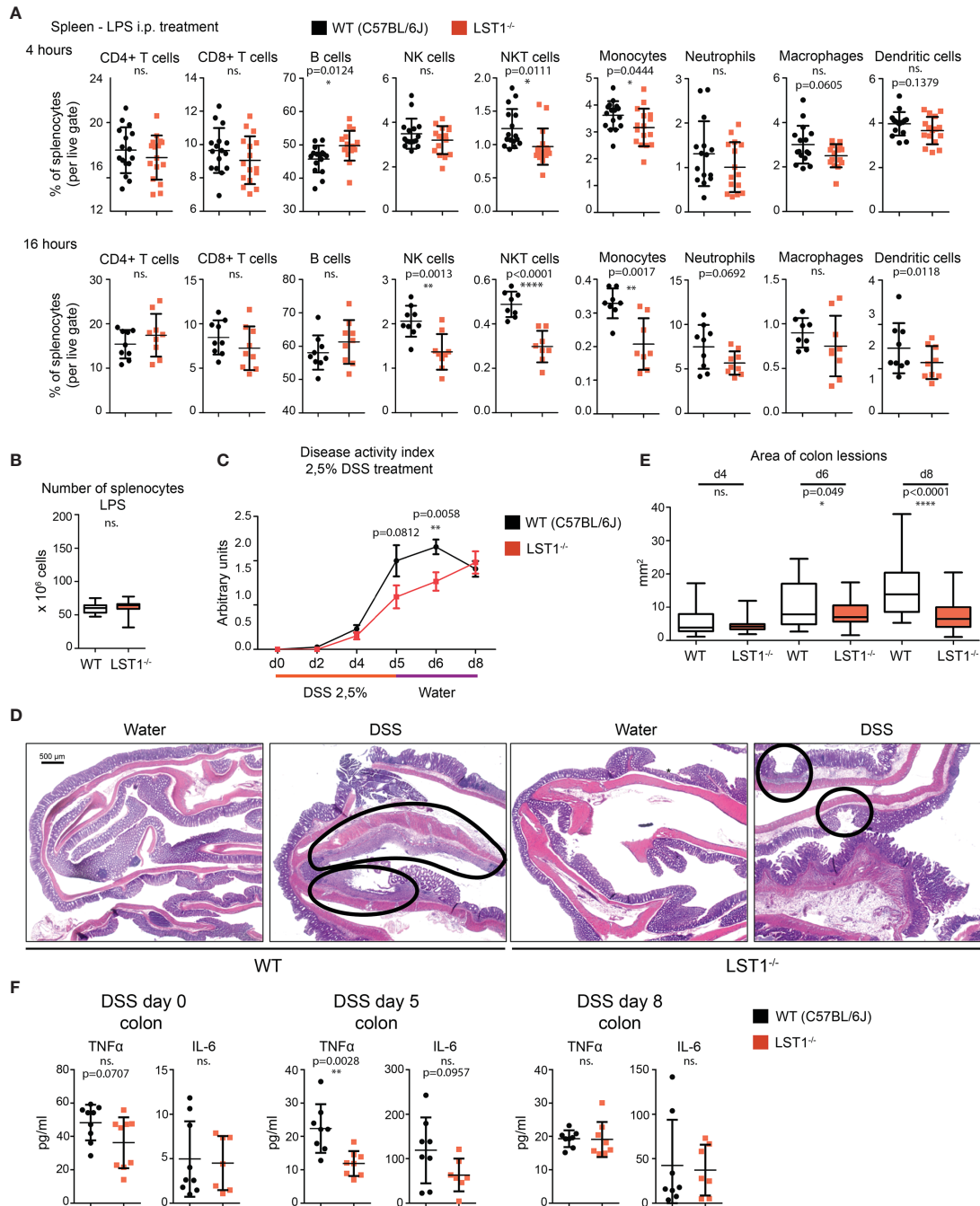
FIGURE 5 | Inflammatory response in *Lst1*⁻/⁻ mice. **(A)** Percentages of major splenocytes subsets 4 and 16 hours after IP injection of LPS (n=8-9). Dots in scatter plots represent biological replicates. **(B)** Spleen cellularity 16 hours after LPS IP injection. (n=10) **(C)** DSS-induced colitis disease activity index (n=6-19 per time point) determined as described in Materials and Methods (higher numbers correspond to more severe symptoms) **(D)** Representative picture of colon sections stained with hematoxylin and eosin from control and DSS challenged WT and *Lst1*⁻/⁻ mice. Lesions are highlighted with black line (100x magnification) **(E)** Quantitative evaluation of the size of colonic lesions induced by DSS treatment during multiple experiments (n=3-5 animals [26-56 lesions] per time point). **(F)** Concentrations of TNFα and IL-6 in colon homogenates from DSS-treated mice. Statistics evaluation was done by Student´s t-test (two-tailed, unpaired) and two-sided Grubb´s test. **p ≤ 0.01, ****p ≤ 0.0001, ns, not significant.

colon inflammation did not have an impact on body weight loss, which was similar for both genotypes (**Supplementary Figure S3B**). After changing DSS solution for plain water, WT mice began to recover more rapidly and the DAI reached the same

values for both strains at the end of the experiment (**Figure 5C**). The differences in cytokine expression were also no longer detectable at day 8 (**Figure 5F**). On the other hand, colonic lesions in *Lst1*⁻/⁻ animals were still significantly smaller at that

time point (**Figure 5E**). Surprisingly, flow cytometry analysis of leukocyte subsets in the colon did not show any striking differences between WT and *Lst1*$^{-/-}$ mice. DSS treatment resulted in multiple changes in myeloid immune cells percentages (**Figure 4D**, **Supplementary Figure S3C**). However, they were similar in both genotypes. In the lymphoid compartment, we observed slightly reduced *Lst1*$^{-/-}$ T cell percentages on day 5 which then recovered, and increased *Lst1*$^{-/-}$ CD4 T cell percentages could be observed on days 6 and 8 (**Supplementary Figure S3C**). Together, these data suggest that LST1 is not just an expression marker in colon samples of IBD patients but likely also an immune system regulator with moderate effects on leukocyte functions, homeostasis and development of colitis.

DISCUSSION

During the past two decades multiple observations have been made of elevated LST1 mRNA and protein levels under inflammatory conditions and during disease, including IBD, rheumatoid arthritis, and influenza (2, 6–8, 14, 21). Location of LST1 gene in MHCIII locus also suggests function in the regulation of immune response or inflammation. In spite of this, its role in these processes or in leukocyte homeostasis remained largely unknown. In this article, we provide data on LST1 protein expression in mice and show alterations in leukocyte subset composition caused by LST1 deficiency at steady state and under inflammatory conditions. In addition we bring evidence of LST1 effects on the severity of experimentally induced acute colitis.

Expression of LST1 protein has previously been analyzed in human cells and tissues with conflicting results. Monoclonal antibody LST1/02 recognizing human but not murine LST1, which was developed in our laboratory, revealed expression pattern largely restricted to the leukocytes of myeloid linage (1), while antibody developed by Schiller et al. showed broad expression pattern including expression outside hematopoietic system (3, 6). Here we describe another monoclonal antibody LST1/06, which recognizes murine LST1. It was generated separately from LST1/02 after immunization with recombinant protein comprising the entire cytoplasmic part of the murine LST1 and its specificity was validated on HEK293 transfectants expressing the murine LST1 (data not shown) and on LST1-deficient mice. The intensity of signals we obtain with LST1/06 antibody on Western blots is generally lower than the intensities we typically observe when using LST1/02 antibody on human samples. However, the reactivities of both antibodies are very similar, showing expression pattern restricted to myeloid cells and an absence in lymphocytes [**Figure 2A** and (1)]. Publically available data on human LST1 mRNA expression from Human Protein Atlas (22) and on mouse LST1 mRNA from ImmGen consortium (23) both support conclusions reached with our antibodies showing myeloid cell-restricted expression pattern, though low level of expression in other tissues cannot be completely excluded. Consistently with already published data (2, 6), pro-inflammatory stimuli enhanced expression of LST1 in myeloid cells.

LST1 deficiency in the mouse influences leukocyte homeostasis. We observed decreased percentages of myeloid cells in *Lst1*$^{-/-}$ mice. Significant reduction or at least a similar tendency were almost universally observed for majority of analyzed myeloid cell subsets in the bone marrow, spleen and colon, though the changes were usually relatively modest (**Figures 4A–D**). Some of the possible explanations of this phenotype include differences in chemokine receptor expression and differences in migration ability. We have analyzed expression of chemokine receptors CCR5, CCR6 and CXCR4 on leukocyte subsets in the spleen, bone marrow and colon at steady state and after DSS treatment, but we did not observe any significant differences between WT and *Lst1*$^{-/-}$ animals that could explain alterations in frequencies of these subsets (not shown). Intriguingly, *Lst1*$^{-/-}$ BMDM showed enhanced migration towards CXCL12. While this observation is interesting, it does not show any attenuation of migratory capacity and, as a result, cannot explain the reduced percentages of macrophages and other cell types in the lymphoid organs analyzed in this study. Reduced percentages were frequently observed also for LST1 non-expressing NK and NKT cells (**Figures 4A, C**). Since NK and NKT cells do not express LST1 the effect on these cells must be indirect, possibly mediated by myeloid cell-derived cytokines or other factors. We have tested mRNA expression of several cytokines that could affect NK cell numbers, including IL-15, IL-18, and IL-12 in *Lst1*$^{-/-}$ BMDCs and BMDMs. However, their levels were not altered in these cells (**Supplementary Figure S2B** and not shown). It is also possible that other cytokines were involved or that the NK cell supporting cytokine production *in vivo* was attenuated due to the diminished numbers of myeloid cells producing these cytokines rather than due to the reduction in cytokine expression levels.

Immune system of the gut and gut microbiota are known to have effects on bone homeostasis (24, 25). Germ-free mice were shown to have increased trabecular bone volume while gut dysbiosis after antibiotic treatment results in reduction in trabecular bone volume (26, 27). One could speculate that effects of LST1 on the activity of the immune system of the gut are linked to the alterations in trabecular bone structure observed in the present study. The experiments with the mouse model of DSS induced colitis suggested altered response to intestinal microbiota in *Lst1*$^{-/-}$ mice. On the other hand, we have not detected any changes in pro-inflammatory cytokine production in the steady state gut in *Lst1*$^{-/-}$ mice that could be a sign of altered activity of the gut immune system. In addition, during DSS-induced colitis, LST1 deficiency had mitigating effects on gut inflammation further arguing against the possibility that the lack of LST1 in the gut promoted inflammation-driven changes in trabecular bone structure. Chronic inflammation in other parts of the body could potentially also affect various parameters of the bone. However, so far we have not found any evidence of chronic inflammation in *Lst1*$^{-/-}$ mice. Finally, it is also possible that LST1 deficiency in the osteoclasts leads to alterations in their function and defects in trabecular bone formation. Currently available data do not provide sufficient support for any of these explanations and further research is needed to clarify this issue.

A number of polymorphisms have been detected in human *LST1* gene (5). Some of these polymorphisms, thought to affect mainly *LST1* gene expression and splicing, are associated with inflammatory conditions such as psoriasis, nephritis in systemic lupus erythromatosus and rheumatoid arthritis, or graft versus host disease severity (5). Moreover, expression of LST1 is increased in rheumatoid arthritis patients (7) and in colon samples from patients with inflammatory bowel disease (IBD) (6). These connections to IBD and various other inflammatory conditions, prompted us to test the effects of LST1 deficiency on inflammatory response and, in particular, on DSS-induced colitis in mice. DSS-induced collitis is one of the most widely used models of human IBD (28). Its overall symptoms and course are similar to this disease (19). DSS ingested by experimental animals with drinking water is cleaved into smaller fragments, penetrates colon barrier and dissolves the mucus layer. This leads to infiltration, colonization and damaging of colon epithelium by bacteria and viruses. Colonization of colon epithelia by bacteria is followed by infiltration of myeloid immune cells (neutrophils, dendritic cells, monocytes), causing acute colon inflammation and its symptoms (blood in the stool, colon shortage, diarrhea). Lymphoid cells (T, B, NK cells) and their interplay with myeloid immune cells also showed important impact on the severity of acute colitis (29–35).

Strikingly, *Lst1*$^{-/-}$ mice showed milder and delayed course of the disease. Disease Activity Index was significantly lower on the 6th day of DSS treatment. These results were also confirmed by histology, which showed less severe destruction of colon epithelium (**Figures 5D, E**). In the final part of the experiment, after changing DSS solution for plain water on day 6, DAI of WT animals improved while in the *Lst1*$^{-/-}$ mice DAI kept rising even after DSS solution was changed for plain water. On day 8, DAI reached the same severity as already improving WT mice. Data from mouse and patient samples show that resident and newly infiltrating myeloid immune cells are responsible for the first wave of immune response during DSS induced colitis (36). Reduced myeloid cell percentages in *Lst1*$^{-/-}$ colon and lymphatic tissue might explain the slower kinetics of disease development. On the other hand, LST1 may also be contributing to the resolution of inflammation. This could explain why the DAI in *Lst1*$^{-/-}$ mice was still raising after day 6, when the WT mice were already in the process of healing. However, there are currently no data addressing the role of LST1 in the resolution of inflammation. Additional possibilities include direct effects of LST1 expressed by epithelial cells on their barrier function or compensatory changes in SHP1 and SHP2 expression in myeloid cells. However, we could not detect any *Lst1* mRNA in colonic epithelial cells nor any compensatory changes in SHP1/2 expression in LPS-treated BMDM. On the other hand, we observed significant reduction in TNFα expression in the gut on day 5 of DSS colitis and a similar trend for IL-6. TNFα is known to be involved in the pathogenesis of IBD and can be upstream of IL-6 expression (37). It is produced not only by myeloid cells, but also by Th1 cells. Myeloid cell numbers in the gut and their ability to produce TNFα *in vitro* were not affected by LST1 deficiency. On the other hand, overall T cell numbers were reduced in the gut on day 5 of DSS colitis. Since T cells do not express LST1, their reduced numbers could be the result of altered chemokine expression by myeloid cells or altered kinetics of dendritic cell-mediated antigen presentation, T cell activation or differentiation in *Lst1*$^{-/-}$ mice. Any of these changes could lead to transient reduction in Th1 cell numbers in the gut and reduced TNFα production. However, these hypotheses have to be further elucidated in future studies. Molecules and molecular mechanisms affecting the course and outcome of DSS-induced collitis often play a role in human IBD (19). Our results suggest that defects in LST1 expression and LST1 polymorphisms should be considered in future studies of this and related diseases in humans.

DATA AVAILABILITY STATEMENT

The raw data supporting the conclusions of this article will be made available by the authors, without undue reservation.

ETHICS STATEMENT

The animal study was reviewed and approved by Animal Care and Use Committee of the Institute of Molecular Genetics.

AUTHOR CONTRIBUTIONS

MF and JT with contribution from NP, JK, JB and TS performed majority of experiments and data analysis. JT, JB, KV and MF performed analysis of mouse colitis model. NP carried out analysis of LST1 and SHP1/2 expression analysis and ELISA assays. MF, JK, TS and NP performed flow cytometry analysis of healthy mice. FS and JPr carried out µCT analysis. JPo and PA generated LST1/06 hybridoma and corresponding monoclonal antibody. TB, JPr and RS contributed to experimental design and data analysis. BM assisted with *Lst1*$^{-/-}$ mice rederivation and preliminary phenotype analysis. TB, BM and RS secured funding and supervised the study. TB and MF wrote the paper. All authors contributed to the article and approved the submitted version.

FUNDING

d'Avenir program PHENOMIN (French National Infrastructure for mouse Phenogenomics; ANR-10-INBS-07).

ACKNOWLEDGMENTS

We want to acknowledge staff of the Institute of Molecular Genetics flow cytometry core facility for excellent support and help. We also thank Tomas Brabec from the Laboratory of Immunobiology, Institute of Molecular Genetics CAS, Prague, for help with colonic epithelium isolation. Finally, we thank

nonparticipant members of Laboratory of Leukocyte Signalling and Laboratory of Hematooncology for fruitful discussion, ideas and friendly working environment.

SUPPLEMENTARY MATERIAL

The Supplementary Material for this article can be found online at: https://www.frontiersin.org/articles/10.3389/fimmu.2021.618332/full#supplementary-material

REFERENCES

1. Draber P, Stepanek O, Hrdinka M, Drobek A, Chmatal L, Mala L, et al. LST1/A is a Myeloid Leukocyte-Specific Transmembrane Adaptor Protein Recruiting Protein Tyrosine Phosphatases SHP-1 and SHP-2 to the Plasma Membrane. *J Biol Chem* (2012) 287(27):22812–21. doi: 10.1074/jbc.M112.339143

2. de Baey A, Fellerhoff B, Maier S, Martinozzi S, Weidle U, Weiss EH. Complex Expression Pattern of the TNF Region Gene LST1 Through Differential Regulation, Initiation, and Alternative Splicing. *Genomics* (1997) 45(3):591–600. doi: 10.1006/geno.1997.4963

3. Schiller C, Nitschke MJ, Seidl A, Kremmer E, Weiss EH. Rat Monoclonal Antibodies Specific for LST1 Proteins. *Hybridoma (Larchmt)* (2009) 28(4):281–6. doi: 10.1089/hyb.2009.0021

4. Rollinger-Holzinger I, Eibl B, Pauly M, Griesser U, Hentges F, Auer B, et al. LST1: A Gene With Extensive Alternative Splicing and Immunomodulatory Function. *J Immunol* (2000) 164(6):3169–76. doi: 10.4049/jimmunol.164.6.3169

5. Weidle UH, Rohwedder I, Birzele F, Weiss EH, Schiller C. LST1: A Multifunctional Gene Encoded in the MHC Class III Region. *Immunobiology* (2018) 223(11):699–708. doi: 10.1016/j.imbio.2018.07.018

6. Heidemann J, Kebschull M, Tepasse PR, Bettenworth D. Regulated Expression of Leukocyte-Specific Transcript (LST) 1 in Human Intestinal Inflammation. *Inflamm Res* (2014) 63(7):513–7. doi: 10.1007/s00011-014-0732-6

7. Fritsch-Stork RD, Silva-Cardoso SC, Groot Koerkamp MJ, Broen JC, Lafeber FF, Bijlsma JW. Expression of ERAP2 and LST1 is Increased Before Start of Therapy in Rheumatoid Arthritis Patients With Good Clinical Response to Glucocorticoids. *Clin Exp Rheumatol* (2016) 34(4):685–9.

8. Yau AC, Tuncel J, Haag S, Norin U, Houtman M, Padyukov L, et al. Conserved 33-kb Haplotype in the MHC Class III Region Regulates Chronic Arthritis. *Proc Natl Acad Sci USA* (2016) 113(26):E3716–24. doi: 10.1073/pnas.1600567113

9. Nalabolu SR, Shukla H, Nallur G, Parimoo S, Weissman SM. Genes in a 220-kb Region Spanning the TNF Cluster in Human MHC. *Genomics* (1996) 31(2):215–22. doi: 10.1006/geno.1996.0034

10. D'Aloia A, Berruti G, Costa B, Schiller C, Ambrosini R, Pastori V, et al. RalGPS2 is Involved in Tunneling Nanotubes Formation in 5637 Bladder Cancer Cells. *Exp Cell Res* (2018) 362(2):349–61. doi: 10.1016/j.yexcr.2017.11.036

11. Schiller C, Huber JE, Diakopoulos KN, Weiss EH. Tunneling Nanotubes Enable Intercellular Transfer of MHC Class I Molecules. *Hum Immunol* (2013) 74(4):412–6. doi: 10.1016/j.humimm.2012.11.026

12. Schiller C, Diakopoulos KN, Rohwedder I, Kremmer E, von Toerne C, Ueffing M, et al. LST1 Promotes the Assembly of a Molecular Machinery Responsible for Tunneling Nanotube Formation. *J Cell Sci* (2013) 126(Pt 3):767–77. doi: 10.1242/jcs.114033

13. Nedelko T, Kollmus H, Klawonn F, Spijker S, Lu L, Hessman M, et al. Distinct Gene Loci Control the Host Response to Influenza H1N1 Virus Infection in a Time-Dependent Manner. *BMC Genomics* (2012) 13:411. doi: 10.1186/1471-2164-13-411

14. Leist SR, Kollmus H, Hatesuer B, Lambertz RL, Schughart K. Lst1 Deficiency has a Minor Impact on Course and Outcome of the Host Response to Influenza A H1N1 Infections in Mice. *Virol J* (2016) 13:17. doi: 10.1186/s12985-016-0471-0

15. Kralova J, Glatzova D, Borna S, Brdicka T. Expression of Fluorescent Fusion Proteins in Murine Bone Marrow-Derived Dendritic Cells and Macrophages. *J Vis Exp* (2018) 140:e58081. doi: 10.3791/58081

16. Brauer R, Tureckova J, Kanchev I, Khoylou M, Skarda J, Prochazka J, et al. MMP-19 Deficiency Causes Aggravation of Colitis Due to Defects in Innate Immune Cell Function. *Mucosal Immunol* (2016) 9(4):974–85. doi: 10.1038/mi.2015.117

17. Dickinson ME, Flenniken AM, Ji X, Teboul L, Wong MD, White JK, et al. High-Throughput Discovery of Novel Developmental Phenotypes. *Nature* (2016) 537(7621):508–14. doi: 10.1038/nature19356

18. Dieleman LA, Ridwan BU, Tennyson GS, Beagley KW, Bucy RP, Elson CO. Dextran Sulfate Sodium-Induced Colitis Occurs in Severe Combined Immunodeficient Mice. *Gastroenterology* (1994) 107(6):1643–52. doi: 10.1016/0016-5085(94)90803-6

19. Eichele DD, Kharbanda KK. Dextran Sodium Sulfate Colitis Murine Model: An Indispensable Tool for Advancing Our Understanding of Inflammatory Bowel Diseases Pathogenesis. *World J Gastroenterol* (2017) 23(33):6016–29. doi: 10.3748/wjg.v23.i33.6016

20. Mahler M, Bristol IJ, Leiter EH, Workman AE, Birkenmeier EH, Elson CO, et al. Differential Susceptibility of Inbred Mouse Strains to Dextran Sulfate Sodium-Induced Colitis. *Am J Physiol* (1998) 274(3):G544–51. doi: 10.1152/ajpgi.1998.274.3.G544

21. Pommerenke C, Wilk E, Srivastava B, Schulze A, Novoselova N, Geffers R, et al. Global Transcriptome Analysis in Influenza-Infected Mouse Lungs Reveals the Kinetics of Innate and Adaptive Host Immune Responses. *PloS One* (2012) 7(7):e41169. doi: 10.1371/journal.pone.0041169

22. Uhlén M, Fagerberg L, Hallström BM, Lindskog C, Oksvold P, Mardinoglu A, et al. Proteomics. Tissue-based Map of the Human Proteome. *Science* (2015) 347(6220):1260419. doi: 10.1126/science.1260419

23. Heng TS, Painter MW. The Immunological Genome Project: Networks of Gene Expression in Immune Cells. *Nat Immunol* (2008) 9(10):1091–4. doi: 10.1038/ni1008-1091

24. Cooney OD, Nagareddy PR, Murphy AJ, Lee MKS. Healthy Gut, Healthy Bones: Targeting the Gut Microbiome to Promote Bone Health. *Front Endocrinol (Lausanne)* (2021) 11:620466. doi: 10.3389/fendo.2020.620466

25. Castaneda M, Strong JM, Alabi DA, Hernandez CJ. The Gut Microbiome and Bone Strength. *Curr Osteoporos Rep* (2020) 18(6):677–83. doi: 10.1007/s11914-020-00627-x

26. Sjögren K, Engdahl C, Henning P, Lerner UH, Tremaroli V, Lagerquist MK, et al. The Gut Microbiota Regulates Bone Mass in Mice. *J Bone Miner Res* (2012) 27(6):1357–67. doi: 10.1002/jbmr.1588

27. Schepper JD, Collins FL, Rios-Arce ND, Raehtz S, Schaefer L, Gardinier JD, et al. Probiotic Lactobacillus Reuteri Prevents Postantibiotic Bone Loss by Reducing Intestinal Dysbiosis and Preventing Barrier Disruption. *J Bone Miner Res* (2019) 34(4):681–98. doi: 10.1002/jbmr.3635

28. Kiesler P, Fuss IJ, Strober W. Experimental Models of Inflammatory Bowel Diseases. *Cell Mol Gastroenterol Hepatol* (2015) 1(2):154–70. doi: 10.1016/j.jcmgh.2015.01.006

29. Kwon SH, Seo EB, Lee SH, Cho CH, Kim SJ, Kim SJ, et al. T Cell-Specific Knockout of STAT3 Ameliorates Dextran Sulfate Sodium-Induced Colitis by Reducing the Inflammatory Response. *Immune Netw* (2018) 18(4):e30. doi: 10.4110/in.2018.18.e30

30. Troy AE, Zaph C, Du Y, Taylor BC, Guild KJ, Hunter CA, et al. IL-27 Regulates Homeostasis of the Intestinal CD4+ Effector T Cell Pool and Limits
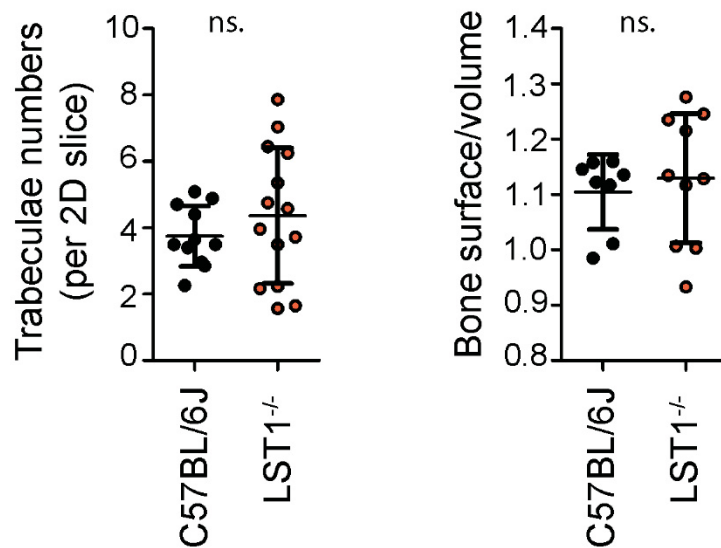
Intestinal Inflammation in a Murine Model of Colitis. *J Immunol* (2009) 183 (3):2037–44. doi: 10.4049/jimmunol.0802918

31. Yanaba K, Yoshizaki A, Asano Y, Kadono T, Tedder TF, Sato S. IL-10-Producing Regulatory B10 Cells Inhibit Intestinal Injury in a Mouse Model. *Am J Pathol* (2011) 178(2):735–43. doi: 10.1016/j.ajpath.2010.10.022

32. Xu X, Wang Y, Zhang B, Lan X, Lu S, Sun P, et al. Treatment of Experimental Colitis by Endometrial Regenerative Cells Through Regulation of B Lymphocytes in Mice. *Stem Cell Res Ther* (2018) 9(1):146. doi: 10.1186/s13287-018-0874-5

33. Yoshihara K, Yajima T, Kubo C, Yoshikai Y. Role of Interleukin 15 in Colitis Induced by Dextran Sulphate Sodium in Mice. *Gut* (2006) 55(3):334–41. doi: 10.1136/gut.2005.076000

34. Wang F, Peng PL, Lin X, Chang Y, Liu J, Zhou R, et al. Regulatory Role of NKG2D+ NK Cells in Intestinal Lamina Propria by Secreting Double-Edged Th1 Cytokines in Ulcerative Colitis. *Oncotarget* (2017) 8(58):98945–52. doi: 10.18632/oncotarget.22132

35. Hall LJ, Murphy CT, Quinlan A, Hurley G, Shanahan F, Nally K, et al. Natural Killer Cells Protect Mice From DSS-induced Colitis by Regulating Neutrophil Function Via the NKG2A Receptor. *Mucosal Immunol* (2013) 6(5):1016–26. doi: 10.1038/mi.2012.140

36. Liu H, Dasgupta S, Fu Y, Bailey B, Roy C, Lightcap E, et al. Subsets of Mononuclear Phagocytes are Enriched in the Inflamed Colons of Patients With IBD. *BMC Immunol* (2019) 20(1):42. doi: 10.1186/s12865-019-0322-z

37. Műzes G, Molnár B, Tulassay Z, Sipos F. Changes of the Cytokine Profile in Inflammatory Bowel Diseases. *World J Gastroenterol* (2012) 18(41):5848–61. doi: 10.3748/wjg.v18.i41.5848

Supplementary Material

Supplementary Figures

Supplementary figure S1. Trabecular bone structure in *Lst1-/-* female mice. Quantification of trabeculae numbers in 2D plane and ratio between trabecular bone surface and bone volume did not show any differences between female WT and *Lst1-/-* (n=8-14) mice. Statistics evaluation was performed by Student´s t-test (two-tailed, unpaired) and two-sided Grubb´s test.
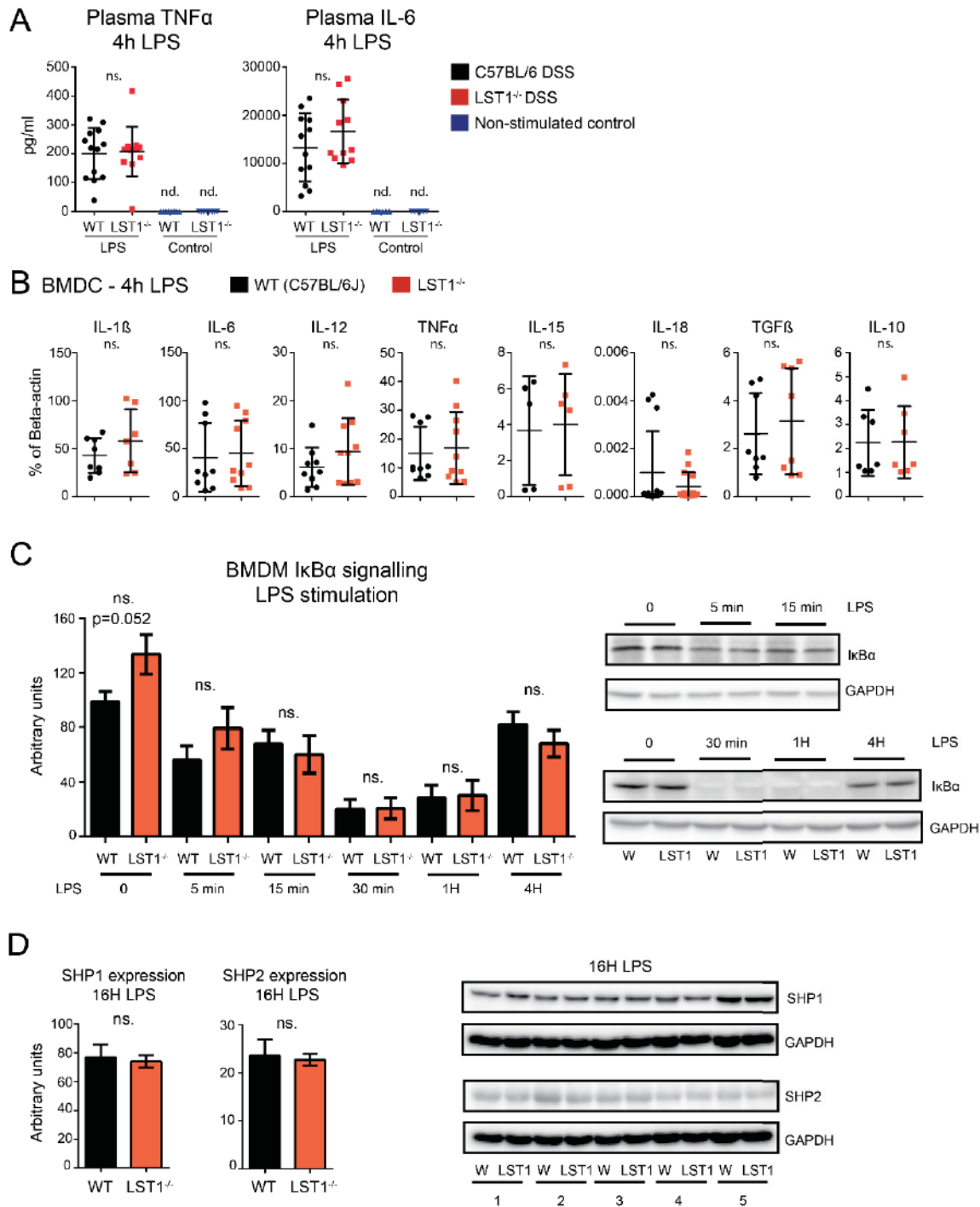
Supplementary figure S2. Inflammatory response in LST1$^{-/-}$ mice. (**A**) TNFα and IL-6 levels in plasma measured by ELISA 4 hours after intraperitoneal LPS injection (n=11-13) (**B**) Cytokine mRNA expression measured by quantitative real-time PCR in BMDC after 4 hours of stimulation with LPS (100 ng/ml), expression was normalized to β-actin. (n=5-13) (**C**) IκBα degradation in BMDM stimulated with LPS (100 ng/ml). Quantification and representative immunoblot (n=4-9) (**D**) Expression of SHP1 and SHP2 phosphatases in BMDM after 16 hour incubation with LPS (100 ng/ml) (n=5). Statistics evaluation was done by Student´s t-test (two-tailed, unpaired), One-way ANOVA with Tukey post test and two-sided Grubb´s test.
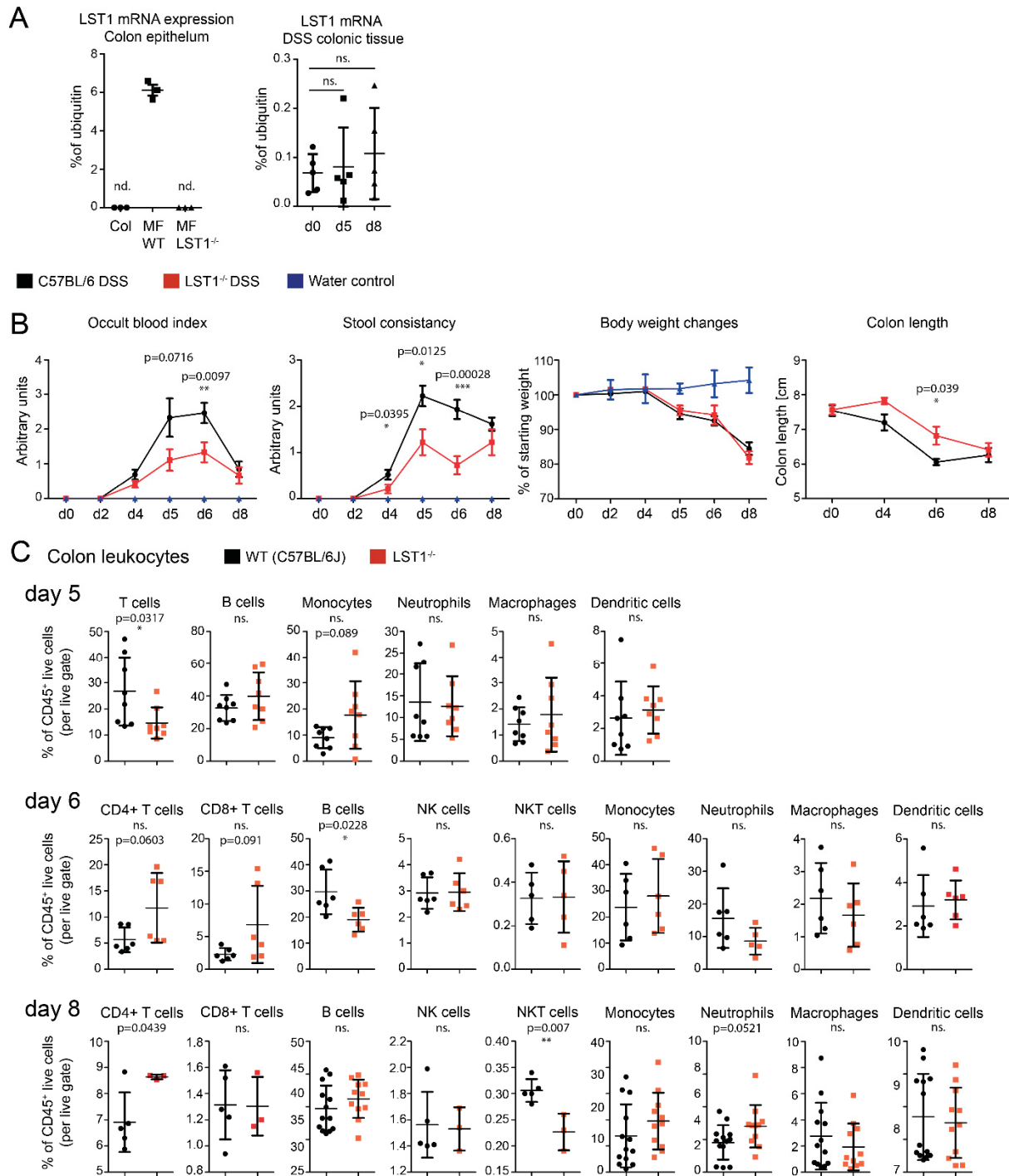
Supplementary figure S3. DSS-induced colitis in LST1$^{-/-}$ mice. (**A**) Expression of LST1 mRNA in colon epithelium cells compared to the WT macrophages and LST1$^{-/-}$ macrophages (n=2, technical triplicates from representative experiment are shown), and of LST1 mRNA in colonic tissue from DSS-treated mice (n=5), expression was normalized to ubiquitin. (**B**) Parameters used for calculation of disease activity index in Figure 5C and changes in colon length, an additional parameter characterizing the disease severity (n=5-20). (**C**) Leukocyte subsets present in the colon at day 5, 6 and day 8 after the initiation of DSS treatment (n=3-13). Statistics evaluation was done by Student´s t-test (two-tailed, unpaired), One-way ANOVA with Tukey post test and two-sided Grubb´s test.

Supplementary tables

Supplementary Table S1. List of flow cytometry antibodies

Marker	Fluorophore – Company - Clone	Fluorophore – Company - Clone
CD8a	PE-CF594 – BD Biosciences – 53-6.7	FITC – ExBio – 53-6.7
NK1.1	APC – BD Biosciences – PK136	PB – Biolegend – PK136
Ly6G	BV421 – BD Biosciences – 1A8	e450 – Biolegend – 1A8
	BV510 – Biolegend – 1A8	
CD19	BV510 – BD Biosciences – 1D3	APC – Biolegend – 605
Ly6C	FITC – BD Biosciences – AL-21	PE-Cy7 – Biolegend – HK1.4
CD11b	PerCP-Cy5.5 – Biolegend – M1/70	PE – Biolegend – M1/70
F4/80	PE-Dazzle594 – Biolegend – BM8	A488 – Biolegend – BM8
CD11c	PE-Cy7 – BD Biosciences – HL3	APC – Biolegend – N418
Fc block	2.4g2 supernatant (produced in lab.)	2G4 – BD Biosciences
CD45	A700 – Biolegend – 30-F11	APC – Biolegend – 104
CD44	PE – Biolegend – IM7	
CD49	BV510 – BD Biosciences – R1-2	
CD5	BV421– BD Biosciences – 53-7.3	
CD4	FITC – BD Biosciences – RM4-5	
Klrg1	PerCP-Cy5.5 – Biolegend – 2F1/KLRG1	
γδTCR	BV605 – BD Biosciences – GL3	
GITR	BV711 – BD Biosciences – DTA-1	
CD25	PE-CY7 – BD Biosciences – PC61	
CD62L	APC-CY7– BD Biosciences – MEL14	
CD21/CD35	PE – BD Biosciences – 7G6	
Bst2	BV605 – Biolegend – 927	
CXCR4	APC – Biolegend – L276F12	
CCR5	PE – Biolegend – HM-CCR5	
CCR6	BV785 – Biolegend – 29-2L17	
CCR7	APC-eFluor 780 – eBioscience – 4B12	
sCD23	BV711 – BD Biosciences – B3B4	
MHCII	APC-Cy7 – Biolegend – M5/114.15.2	
EpCAM	APC – Biolegend - G8.8	
Ghost Dye™	UV450 – Tonbo biosciences –13-0868	

Supplementary Table 2. List of qRT-PCR primers

	Forward	Reverse
IL-1β	TGT-AAT-GAA-AGA-CGG-CAC-ACC	TCT-TCT-TTG-GGT-ATT-GCT-TGG
IL-6	TGA-TGG-ATG-CTA-CCA-AAC-TGG	TTC-ATG-TAC-TCC-AGG-TAG-CTA-TGG
IL-10	CAG-AGC-CAC-ATG-CTC-CTA-GA	TGT-CCA-GCT-GGT-CCT-TTG-TT
IL-12	CCA-GGT-GTC-TTA-GCC-AGT-CC	GCA-GTG-CAG-GAA-TAA-TGT-TTC-A
IL-15	AAC-AGC-TCA-GAG-AGG-TCA-GGA	CCA-TGA-AGA-GGC-AGT-GCT-TT
IL-18	GAC-AAC-ACG-CTT-TAC-TTT-ATA-CGG	CAG-TGA-AGT-CGG-CCA-AAG-TT
TNFα	TCT-TCT-CAT-TCC-TGC-TTG-TGG	GGT-CTG-GGC-CAT-AGA-ACT-GA
TGFβ	TGG-AGC-AAC-ATG-TGG-AAC-TC	CAG-CAG-CCG-GTT-ACC-AAG
Beta-actin	GAT-CTG-GCA-CCA-CAC-CTT-CT	GGG-GTG-TTG-AAG-GTC-TCA-AA
Ubiquitin	ATG-TGA-AGG-CCA-AGA-TCC-AG	TAA-TAG-CCA-CCC-CTC-AGA-CG
LST1	CTG-ATG-ACA-ATG-GGA-TCT-GGT	CAG-GAT-GAT-GAC-AAG-CAG-GA

ORIGINAL ARTICLE

WILEY

Transmembrane adaptor protein WBP1L regulates CXCR4 signalling and murine haematopoiesis

Simon Borna[1,2] | Ales Drobek[1] | Jarmila Kralova[1] | Daniela Glatzova[1,2,3] | Iva Splichalova[4] | Matej Fabisik[1,2] | Jana Pokorna[1] | Tereza Skopcova[1] | Pavla Angelisova[1] | Veronika Kanderova[5] | Julia Starkova[5] | Petr Stanek[6] | Orest V. Matveichuk[7] (ID) | Nataliia Pavliuchenko[1,2] | Katarzyna Kwiatkowska[7] | Majd B. Protty[8] (ID) | Michael G. Tomlinson[9] | Meritxell Alberich-Jorda[10] | Vladimir Korinek[11] | Tomas Brdicka[1] (ID)

[1]Laboratory of Leukocyte Signaling, Institute of Molecular Genetics of the Czech Academy of Sciences, Prague, Czech Republic

[2]Faculty of Science, Charles University, Prague, Czech Republic

[3]Department of Biophysical Chemistry, J. Heyrovsky Institute of Physical Chemistry of the Czech Academy of Sciences, Prague, Czech Republic

[4]Laboratory of Immunobiology, Institute of Molecular Genetics of the Czech Academy of Sciences, Prague, Czech Republic

[5]CLIP - Childhood Leukaemia Investigation Prague and Department of Pediatric Hematology and Oncology, Second Faculty of Medicine, Charles University, Prague, Czech Republic

[6]Second Faculty of Medicine, Charles University, Prague, Czech Republic

[7]Laboratory of Molecular Membrane Biology, Nencki Institute of Experimental Biology, Warsaw, Poland

[8]Institute of Biomedical Research, University of Birmingham, Birmingham, UK

[9]School of Biosciences, University of Birmingham, Birmingham, UK

[10]Laboratory of Hematooncology, Institute of Molecular Genetics of the Czech Academy of Sciences, Prague, Czech Republic

[11]Laboratory of Cell and Developmental Biology, Institute of Molecular Genetics of the Czech Academy of Sciences, Prague, Czech Republic

Correspondence
Tomas Brdicka, Institute of Molecular Genetics of the Czech Academy of Sciences, Videnska 1083, 14220 Prague, Czech Republic.
Email: tomas.brdicka@img.cas.cz

Present address
Majd B. Protty, Sir Geraint Evans Cardiovascular Research Building, Cardiff University, Cardiff, UK

Funding information
European Regional Development Fund, Grant/Award Number: CZ.1.05/1.1.00/02.0109 and OPPK (CZ.2.16/3.1.00/21547); Grantová Agentura České Republiky, Grant/Award Number: 16-07425S and P302-12-G101; H2020 Marie Skłodowska-Curie

Abstract

WW domain binding protein 1-like (WBP1L), also known as outcome predictor of acute leukaemia 1 (OPAL1), is a transmembrane adaptor protein, expression of which correlates with *ETV6-RUNX1* (t(12;21)(p13;q22)) translocation and favourable prognosis in childhood leukaemia. It has a broad expression pattern in haematopoietic and in non-haematopoietic cells. However, its physiological function has been unknown. Here, we show that WBP1L negatively regulates signalling through a critical chemokine receptor CXCR4 in multiple leucocyte subsets and cell lines. We also show that WBP1L interacts with NEDD4-family ubiquitin ligases and regulates CXCR4 ubiquitination and expression. Moreover, analysis of *Wbp1l*-deficient mice revealed alterations in B cell development and enhanced efficiency of bone marrow cell transplantation. Collectively, our data show that WBP1L is a novel regulator of CXCR4 signalling and haematopoiesis.

1 | INTRODUCTION

WW domain binding protein 1-like (WBP1L) also known as outcome predictor of acute leukaemia 1 (OPAL1) has attracted attention because of a report showing that its elevated expression at mRNA level correlates with favourable outcome in childhood acute lymphoblastic leukaemia (ALL).[1] These data suggested that it could potentially serve as a prognostic marker. Later, it was shown that its levels are particularly increased in B cell progenitor ALL (BCP-ALL) with chromosomal translocation t(12;21)(p13;q22), which results in expression of *ETV6-RUNX1* fusion transcription factor.[2,3] In BCP-ALL, this translocation is associated with good prognosis, which likely explains the correlation between WBP1L expression and favourable outcome.[2] However, it is not known whether WBP1L functionally contributes to it.

ETV6, a fusion partner in *ETV6-RUNX1*, is a transcriptional repressor and *WBP1L* is one of its target genes.[4-6] In general, ETV6 targets are of high interest because of critical importance of ETV6 in haematopoiesis and its involvement in leukaemia. Around 30 fusions of *ETV6* to different partner genes and a number of mutations in *ETV6* have been identified so far, many of them implicated in various haematological malignancies of myeloid and lymphoid origin.[7,8] In addition, its critical role in normal haematopoiesis has been revealed in studies of ETV6-deficient mice, which show profound defects in haematopoietic stem and progenitor cell function and inability of these cells to reconstitute haematopoiesis after bone marrow transplantation.[9,10]

Bioinformatic sequence analysis revealed that WBP1L is a transmembrane adaptor protein with a very short extracellular/luminal part followed by a single transmembrane domain and a larger cytoplasmic tail.[11] Although relatively short, the extracellular/luminal part presumably forms a small compact domain held together by disulphide bridges formed among cysteines in the C*C*CC*CC motif.[11] The cytoplasmic part of WBP1L contains several potential interaction motifs corresponding to the consensus sequence of WW domain binding motifs L-P-X-Y or P-P-X-Y.[11]

Except for the limited bioinformatics analysis, WBP1L protein remained completely uncharacterized. Its physiological function has been unknown and whether it has any functional features that may link it to normal haematopoiesis or neoplasia has never been investigated. Here, we show that it binds several members of the NEDD4-family of ubiquitin ligases and that its deficiency results in enhanced surface expression and signalling of critical chemokine receptor CXCR4. WBP1L deficiency also results in alterations in B cell development and altered dynamics of stem and progenitor cells in the bone marrow. Taken together, we establish the role of WBP1L in CXCR4 signalling and in normal haematopoiesis. These findings also form the basis for further research on its potential role in leukaemia.

2 | MATERIALS AND METHODS

2.1 | Protein isolation, detection and quantification assays

Immunoprecipitations (IP) and immunoblotting were performed essentially as reported with adjustments described in online supplement. Western blot quantifications were carried out using Azure c300 imaging system (Azure Biosystems) and Aida Image Analysis software (Elysia-raytest). WBP1L expression in B cell lines was analysed by size exclusion chromatography-microsphere-based affinity proteomics analysis described in detail here,[3] and the data were quantified using Matlab (MathWorks). Tandem purification of WBP1L was based on the following publication[12] with modifications described in online supplement. WBP1L palmitoylation was analysed using metabolic labelling with palmitic acid analogue 17ODYA followed by reaction with biotin-azide and enrichment on streptavidin-coupled beads as described in detail in online supplement.

2.2 | Antibodies

Antibodies are listed in Tables S1 and S2. WBP1L antisera were generated by immunization of rabbits with KLH-conjugated peptide from WBP1L C-terminus while WBP1L monoclonal antibodies were prepared by standard hybridoma technology after immunization of mice with recombinant C-terminal part of murine WBP1L protein as described in online supplement.

2.3 | Cloning, qPCR, DNA transfection, virus preparation and cell infection

cDNA was generated using Quick-RNA kit (Zymo Research), revert aid reverse transcriptase (Thermo-Fisher) and oligo-dT primer. qPCR reactions were run on LightCycler 480 Instrument II using LightCycler 480 SYBR Green I Master mix (Roche). List of qPCR primers is in Table S3. For construct preparation see online supplement and Table S4. Phoenix cell transfection, virus generation and cell transduction were performed as described.[13] For lentivirus production, the procedure was to a minor extent modified as described in online supplement. Infected cells were sorted on Influx (BD) or selected on G418 (Thermo-Fisher).

2.4 | Mouse experiments, homing assays

$Wbp1l^{-/-}$ mice ($Wbp1l^{tm2a(EUCOMM)Hmgu}$) on C57Bl/6J genetic background were obtained from International Mouse Phenotyping Consortium. In these mice, gene trap flanked by FRT sites followed by coding region of exon 5 surrounded by LoxP sites were inserted into $Wbp1l$ locus by homologous recombination ($Wbp1l^{-/-}$). Mice were bred in specific pathogen free conditions. To obtain inducible $Wbp1l^{fl/fl}CreERT$ mice, we crossed animals of the $Wbp1l^{-/-}$ strain to B6.Cg-Tg (ACTFLPe)9205 Dym/J mice to remove the gene trap, and subsequently, to B6.129-Gt(ROSA)26Sor$^{tm1(cre/ERT2)Tyj}$/J animals. Both mouse strains were purchased from the Jackson Laboratory (Bar Harbor). To achieve $Wbp1l$ deletion, mice were injected intraperitoneally with five daily doses of 2 mg of tamoxifen (Merck) in corn oil (Merck). For homing and transplantation assays, congenic Ly5.1 (C57BL/6NCr) or Ly5.1/Ly5.2 (C57Bl/6J) heterozygote recipients were sublethally (three Grey) or lethally (seven Grey) irradiated, followed by injection of transplanted cells into the tail vain. For experiments we used 8- to 12–week-old sex and age matched animals. Housing of mice and in vivo experiments were performed in compliance with local legal requirements and ethical guidelines. The Animal Care and Use Committee of the Institute of Molecular Genetics approved animal care and experimental procedures (Ref. No. 69/2014, 6/2016).

2.5 | Transwell migration

1×10^5 Cells in DMEM with 0.2% BSA were plated in the upper well of 5μm pore Transwell apparatus (Corning). After 4 hours, migrated cells in the bottom well were counted using a flow cytometer (LSRII; BD).
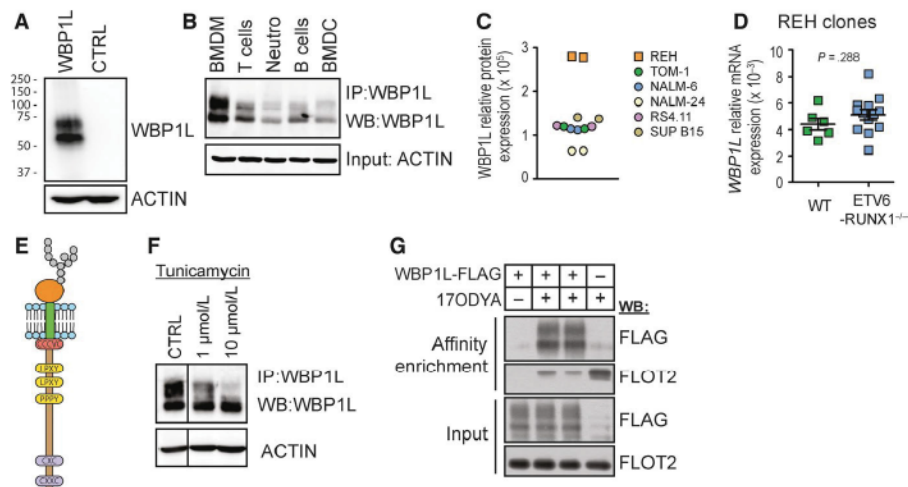

FIGURE 1 WBP1L is a palmitoylated glycoprotein, broadly expressed in haematopoietic cells. (A) Verification of new WBP1L rabbit antisera specificity on the lysates of HEK293 cells transfected or not with WBP1L construct. (B) Western blot analysis of WBP1L expression in murine leucocyte subsets. T cells (CD3$^+$), B cells (CD43$^-$, CD11b$^-$) and neutrophils (Ly6G$^+$) were isolated from the spleen or bone marrow. Bone marrow-derived macrophages (BMDM) and bone marrow-derived dendritic cells (BMDC) were differentiated in vitro from murine bone marrow. N = 3. (C) Expression of WBP1L in BCP-ALL cell lines was probed using size exclusion chromatography-microsphere-based affinity Proteomics method. Expression in $ETV6-RUNX1^+$ B cell line REH and $ETV6-RUNX1^-$ lines TOM-1, NALM-6, NALM-24, RS4.11 and SUP B15 was probed by two antibody clones to WBP1L (OPAL-01, OPAL-02) and quantified as an area under the curve on parts of chromatograms representing fractions corresponding to WBP1L (N = 1 per antibody clone). (D) Expression of $WBP1L$ mRNA in different $ETV6-RUNX1^{-/-}$ REH clones from two independent sources of REH cells. Data are plotted as $2^{-\Delta ct}$ (N = 3). (E) Schematic representation of WBP1L structure and conserved sequence motifs (F) Analysis of WBP1L glycosylation in BMDM. BMDM treated or not with 1 or 10 μmol/L tunicamycin (overnight) were subjected to WBP1L immunoprecipitation followed by immunoblotting with WBP1L antisera. β-actin was stained in the corresponding cell lysates (N = 2). Irrelevant lines from the blot image were removed and replaced with a vertical dividing line. (G) Analysis of palmitoylation of WBP1L. HEK293 cells expressing WBP1L-FLAG-STREP were metabolically labelled with palmitate analogue 17ODYA and lysed. 17ODYA labelled proteins were tagged in a click chemistry reaction with biotin-azide, purified on streptavidin-coupled beads and analysed for the presence of WBP1L with anti-FLAG antibody (upper panel) or FLOTILLIN-2 as a representative of endogenous palmitoylated proteins (middle upper panel). WBP1L expression in cell lysates (middle lower panel) and comparable loading were verified by immunoblotting with antibodies to FLAG-tag (WBP1L) or FLOTILLIN-2, respectively (N = 3)

2.6 | Statistics

Results represent means ± SEM. If not specified otherwise, *P*-values were calculated using two-tailed Student's *t* test, one-way ANOVA or *Q* test. N represents number of animals or values per group or number of independent experiments.

3 | RESULTS

3.1 | WBP1L is a palmitoylated glycoprotein broadly expressed in haematopoietic cells

Analysis of WBP1L protein and mRNA expression in murine and human haematopoietic system with a newly generated polyclonal rabbit antibody (Figure 1A) and with Genevestigator tool, respectively, revealed that WBP1L is broadly expressed across multiple human and murine haematopoietic cell subsets (Figure 1B and S1). In addition and in agreement with previous reports of deregulated WBP1L expression in *ETV6-RUNX1*+ BCP-ALL, we have found elevated levels of WBP1L protein in REH cell line, which is derived from *ETV6-RUNX1*+ BCP-ALL. (Figure 1C and S2A). Interestingly, the genetic deletion of *ETV6-RUNX1* in

REH cells (Figure S2B,C) did not alter WBP1L expression in these cells (Figure 1D).

Imaging of murine bone marrow-derived macrophages transduced with retroviral vector coding for murine WBP1L fused to EGFP revealed relatively broad distribution of WBP1L-EGFP within these cells. We have observed co-localization with plasma membrane, Golgi, endoplasmic reticulum, and to a limited extent with lysosomes and/or other acidic organelles (Figure S3). On the other hand, no co-localization with mitochondria could be detected (Figure S3).

The N-terminal part of WBP1L protein is highly conserved among major vertebrate classes (Figure S4). This region contains several conserved motifs, including potential N-glycosylation (NXS) and palmitoylation sites (Figure 1E and S4). Indeed, we could confirm that WBP1L is both glycosylated and palmitoylated (Figure 1F,G).

3.2 | WBP1L interacts with NEDD4-family E3 ubiquitin ligases

Cytoplasmic part of WBP1L contains three WW domain binding motifs ([L/P]PXY) (Figure 1E and S4). It has been speculated that they may interact with WW domains of NEDD4-family ubiquitin ligases.[11]
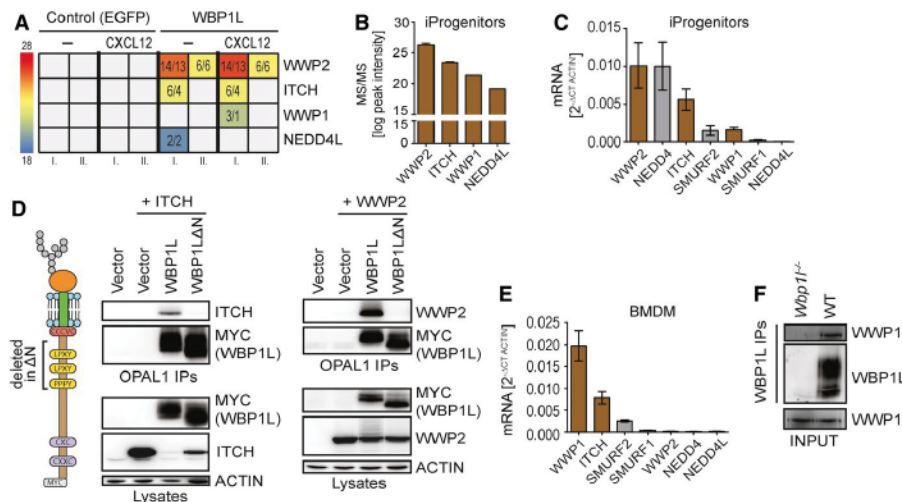

FIGURE 2 WBP1L binds multiple NEDD4-family E3 ubiquitin ligases. (A) Data from two independent mass spectrometry analyses (I. and II.) of WBP1L binding partners. *Wbp1l*−/− monocyte/macrophage progenitors were transduced with the constructs coding for WBP1L-FLAG-STREP or EGFP with the same tag. The cells were stimulated for 2 min with CXCL12 or left untreated. Tagged proteins with their binding partners were isolated by tandem purification and subjected to mass spectrometry analysis. The data are presented as colour-coded intensities obtained by label-free quantification of NEDD4-family E3 ubiquitin ligases. Values represent number of peptides used for intensity calculation/ number of unique peptides. Samples, where no peptides from a particular E3 ligase were detected, are coloured in grey (B) Label-free quantification of interacting E3 ligases from mass spectrometry experiment. Combined average intensities from both CXCR4 stimulated and non-stimulated samples are plotted (experiment I. form (A) only). (C) mRNA expression of NEDD4-family E3 ubiquitin ligases in immortalized monocyte/macrophage progenitors (iProgenitors). Plotted in brown are those ligases that interacted with WBP1L in mass spectrometry experiments (N = 3). (D) WBP1L interaction with NEDD4-family E3 ligases is dependent on WW binding motifs in WBP1L N-terminus. HEK293 cells were transfected with WBP1L-Myc or WBP1LΔN-Myc (with segment containing all WW binding motifs deleted) together with ITCH or WWP2. Following WBP1L immunoprecipitation, the isolated material and the original lysates were immunoblotted with antibody to ITCH or WWP2 and various controls as indicated (N = 3). (E) mRNA expression of NEDD4-family E3 ligases in BMDM. Plotted in brown are those ligases that interacted with WBP1L in mass spectrometry experiment (N = 3). (F) Endogenous interaction of WBP1L with WWP1 in BMDM. WBP1L immunoprecipitates from WT or *Wbp1l*−/− BMDM were immunoblotted with antibody to WWP1 and WBP1L. Input lysates were probed with antibody to WWP1 (N = 3). See also Figure S5
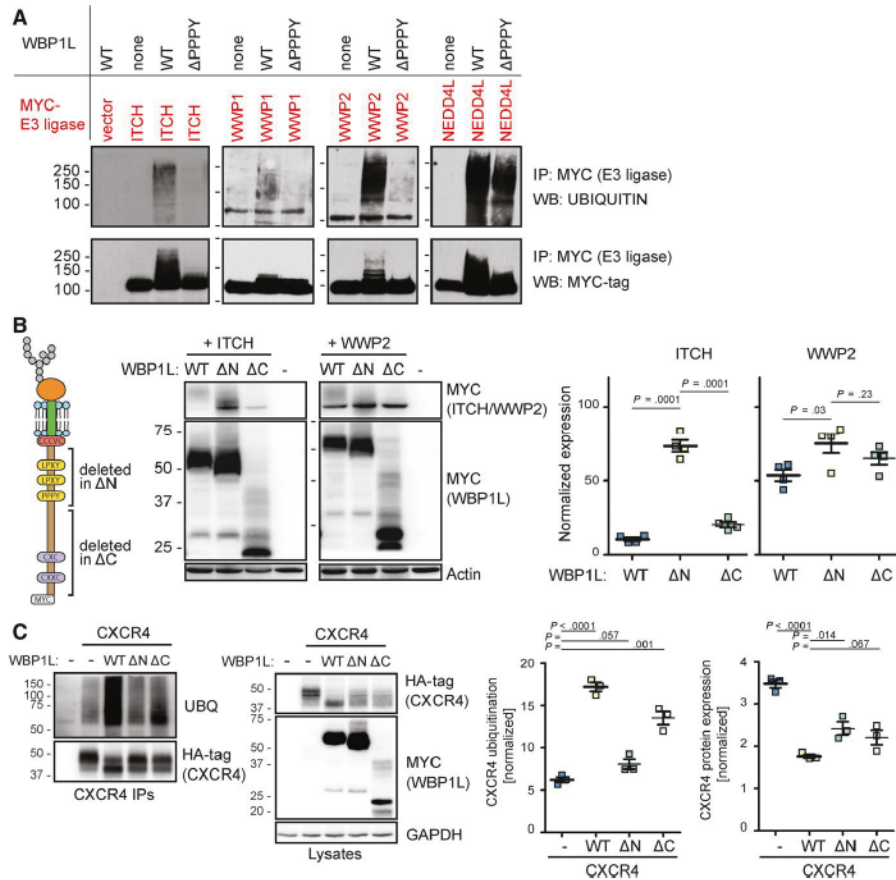
FIGURE 3 WBP1L regulates ubiquitination and expression of NEDD4-family E3 ubiquitin ligases and CXCR4. (A) HEK293 cells were cotransfected with individual Myc-tagged NEDD4-family E3 ubiquitin ligases and non-tagged WBP1L or its mutant lacking PPPY WW domain interacting motif. E3 ligases were immunoprecipitated via the Myc-tag from the lysates of these cells and subjected to immunoblotting with anti-MYC-tag or anti-UBIQUITIN antibody. (B) ITCH and WWP2 stability in HEK293 cells in the presence of WBP1L-MYC, WBP1L ΔC-MYC (deletion of almost entire intracellular part of WBP1L except for WW binding motifs) or WBP1L ΔN-MYC (deletion of WW binding motifs). Lysates from HEK293 cells transfected with ITCH-MYC or WWP2-MYC and WBP1L constructs were immunoblotted with antibody to MYC-tag to visualize ITCH, WWP2 and all forms of WBP1L and with antibody to ACTIN. Quantifications of the data are plotted as values normalized to ACTIN signal and then further normalized to experiment average to allow for comparison among the experiments (N = 3). (C) WBP1L-mediated increase in CXCR4 ubiquitination and down-regulation of CXCR4 protein levels in HEK293 cells. WBP1L-MYC, WBP1LΔC-MYC or WBP1LΔN-MYC were cotransfected with CXCR4-HA followed by CXCR4 imunoprecipitation and immunoblotting with antibodies to ubiquitin or HA-tag. Lysates were probed with antibodies to HA-tag (CXCR4), MYC-tag (WBP1L) or GAPDH (N = 3). For quantification, ubiquitination was normalized to HA-tag (CXCR4) signal (left panel) and CXCR4 expression to GAPDH (right panel). Both were further normalized to experiment average to allow for comparison among the individual experiments

However, this family has nine different members. To investigate whether WBP1L interacts with any of these ligases, we have expressed a FLAG-STREP-tagged WBP1L construct in immortalized monocyte/macrophage progenitors. We have selected this cell type because of a relatively high level of *Wbpl1* mRNA in myeloid progenitors (Figure S1). We isolated the FALG-STREP-tagged construct together with its associated binding partners from the lysates of these cells via a tandem purification on anti-FLAG and Streptactin beads. Mass spectrometry analysis of the isolated material revealed that WBP1L indeed interacts with several members of NEDD4-family. In this particular cell type, WWP2 was the most prominent. However, ITCH, WWP1 and NEDD4L could also be detected in one experiment (Figure 2A). Interestingly, the mass spectrometry signal intensities corresponded to the relative expression levels of these NEDD4-family members in immortalized monocyte/macrophage progenitors (Figure 2B,C). On the

other hand, not all NEDD4-family members expressed in these cells could be co-isolated with WBP1L. These data suggest a certain level of WBP1L selectivity for individual NEDD4-family members.

To find out whether NEDD4-family ligases bind WBP1L via its [L/P]PXY WW domain binding motifs we have co-expressed the two highest scoring NEDD4-family ligases from the mass spectrometry experiment, WWP2 or ITCH, with wild-type WBP1L construct or with mutant WBP1LΔN lacking the membrane-proximal WW domain binding sequences (Figure 2D) in HEK293 cells. These cells allow for relatively high level of overexpression, which was ideal for reliable identification of NEDD4 family binding sites in WBP1L. Both E3 ligases could be readily co-immunoprecipitated with wild-type WBP1L but not with WBP1LΔN (Figure 2D). These data were further confirmed in a similar experiment in J774 macrophage-like cell line, which expresses relatively high level of

ITCH (not shown). The endogenous ITCH could be co-isolated with wild-type WBP1L but not with WBP1LΔN from these cells (Figure S5). To confirm the interaction of WBP1L with a NEDD4-family member at the endogenous protein level, we have selected bone marrow-derived macrophages (BMDM) which express the highest levels of WBP1L among the cell types we have tested so far (Figure 1B). WWP1, which is the most abundant NEDD4-family member in this cell type (Figure 2E), could be co-isolated with WBP1L in this experiment (Figure 2F).

3.3 | WBP1L regulates ubiquitination and expression level of NEDD4-family E3 ubiquitin ligases and of CXCR4

Interaction with WW domain binding motifs is known to result in the activation and autoubiquitination of NEDD4-family ubiquitin ligases.[14,15] To test whether WBP1L can activate NEDD4 family members, we have cotransfected WBP1L-interacting (Figure 2A) NEDD4-family ligases with wild-type WBP1L, or its mutant lacking one of the conserved WW domain binding motifs, into HEK293 cells. This analysis demonstrated that cotransfection with wild-type but not mutant WBP1L resulted in a substantial increase in ubiquitination of all these ligases, which is a sign of their activation (Figure 3A). Published work suggests that in the case of ITCH this ubiquitination results in down-regulation of its protein levels, while WWP2 appears

relatively resistant to this negative feedback regulation. Thus, to further explore the mechanism of how WBP1L regulates these ubiquitin ligases, we co-expressed wild-type WBP1L, WBP1LΔN or WBP1LΔC (lacking C-terminal region of unknown function) with ITCH or WWP2 in HEK293 cells. Co-expression of ITCH with wild-type WBP1L and WBP1LΔC resulted in significantly reduced ITCH protein level when compared to co-expression with WBP1LΔN. As expected, this effect was much more limited in case of WWP2 (Figure 3B).

One of the best-studied targets of NEDD4-family ubiquitin ligases in the haematopoietic system is the chemokine receptor CXCR4. It is involved in the maintenance of haematopoietic stem and progenitor cells and in promoting niche interactions in the bone marrow. It is also thought to support the survival and treatment resistance of leukaemic cells.[16,17] Based on these features, we have selected CXCR4 for a similar set of experiments to test whether WBP1L regulates its protein expression levels and ubiquitination. Indeed, co-expression of WBP1L with CXCR4 in HEK293 cells resulted in increased ubiquitination of CXCR4 (presumably by an endogenous NEDD4-family ligase). This effect was almost completely abolished by mutation of the WW domain binding motifs (WBP1LΔN) while deletion of the C-terminal sequence (WBP1LΔC) had a more limited effect (Figure 3C). CXCR4 ubiquitination was further accompanied by reduction in CXCR4 protein levels (Figure 3C). We also observed that WBP1L co-expression resulted in a striking increase in CXCR4 electrophoretic mobility (Figure 3C). The reason for this mobility shift is at present unknown.
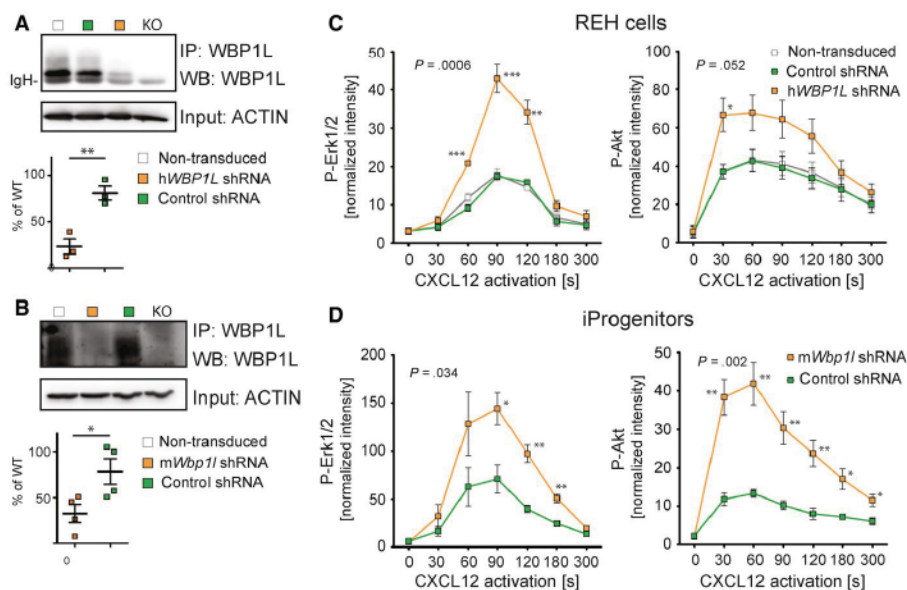

FIGURE 4 ShRNA-mediated down-regulation of WBP1L results in enhanced CXCR4 signalling in human and murine cell lines. (A, B) WBP1L immunoprecipitates from REH cells (A) or immortalized monocyte/macrophage progenitors (B) transduced with *Wbp1l* shRNA were stained with WBP1L antisera to demonstrate WBP1L down-regulation. Equal input of lysates to immunoprecipitation was verified by ACTIN immunoblotting. Quantification of multiple experiments (after normalization to ACTIN signal) was plotted as a percentage of WBP1L expression in non-transduced cells. (C, D) ERK1/2 and AKT phosphorylation downstream of CXCR4 in REH cells (C) and immortalized monocyte/macrophage progenitors (iProgenitors) (D), where WBP1L was down-regulated by shRNA. Cells were stimulated with 100 nmol/L CXCL12, lysed and subjected to Western blot analysis of ERK1/2 and AKT phosphorylation. Data represent mean of fluorescence intensity normalized to GAPDH. The *P*-value was calculated to compare maximum responses of cells transduced with non-silencing control and silencing shRNA. Asterisks denote significant differences in individual time-points. (N = 4)
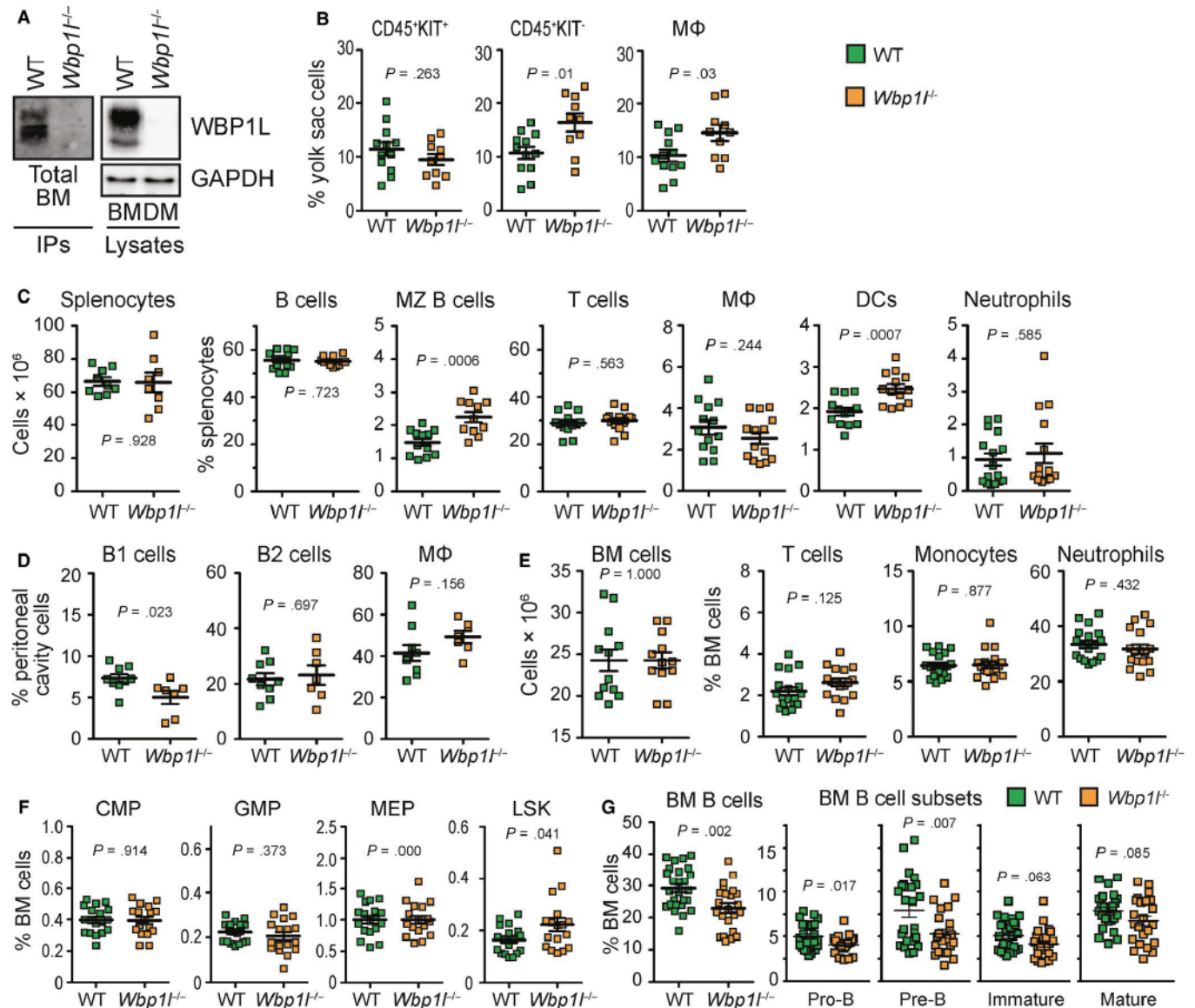
FIGURE 5 Altered leucocyte homeostasis in WBP1L-deficient mice. (A) Western blot analysis of WBP1L immunoprecipitates or whole cell lysates prepared from WT and *Wbp1l*$^{-/-}$ cells. mOPAL-01/03 antibodies were used for immunoprecipitation and WBP1L rabbit antisera for Western blotting. N = 3 (bone marrow), N = 5 (BMDM). (B) Flow cytometry analyses of E10.5 WT and *Wbp1l*$^{-/-}$ yolk sac cell subsets. Primitive macrophages were defined as Ter119$^-$ CD11b$^+$ F4/80$^+$. (C) Absolute numbers of splenocytes obtained from WT and *Wbp1l*$^{-/-}$ mice and flow cytometry analyses of WT and *Wbp1l*$^{-/-}$ splenocytes defined using the following markers: B cells (B220$^+$), MZ B cells (B220$^+$, AA4.1$^-$, CD23$^{-/low}$, CD1d$^+$), T cells (CD3$^+$), macrophages (F4/80$^+$, CD11b^{int}), DC (CD11c$^+$, LY6C$^{-/low}$) and neutrophils (LY6G$^+$, CD11b$^+$, LY6C$^-$). (D) Flow cytometry analyses of WT and *Wbp1l*$^{-/-}$ leucocytes in the peritoneum, defined using the following markers: B1 cells (SSC^{low}, FSC^{low}, B220$^+$, CD23$^{-/low}$), B2 cells (SSC^{low}, FSC^{low}, B220$^+$, CD23$^+$) and macrophages (large peritoneal macrophages, CD11b^{high},F4/80^{high}). (E) Flow cytometry analyses of WT and *Wbp1l*$^{-/-}$ bone marrow cell subsets, defined using the following markers: T cells (CD3$^+$), monocytes (LY6C$^+$, CD11b$^+$, LY6G$^-$, CD19$^-$, TER119$^-$, CD3$^-$, NK1.1$^-$), neutrophils (KIT$^-$, B220$^-$, TER119$^-$, CD3$^-$, LY6G^{high}) (F) Flow cytometry analyses of stem and progenitor cells in the bone marrow. Cell subsets were defined using following markers: common myeloid progenitors—CMP (lin$^-$, c-kit$^+$, CD34$^+$, CD16/32$^{neg-low}$, SCA1$^-$), granulocyte-monocyte progenitors—GMP (lin$^-$, KIT$^+$, CD34$^+$, CD16/32^{High}, SCA1$^-$), megakaryocyte-erythroid progenitors—MEP (lin$^-$, KIT$^+$, CD34$^-$, CD16/32$^-$, SCA1$^-$) and LSK (lin$^-$, KIT$^+$, SCA1$^+$). (G) Flow cytometry analysis of bone marrow B cell subsets. B cells (B220$^+$), pro-B cells (CD43$^+$, B220$^+$, IgM$^-$), pre-B cells (CD43$^-$, B220^{low}, IgM$^-$), immature B cells (CD43$^-$, B220^{low}, IgM$^+$) and mature B cells (CD43$^-$, B220^{high}, IgM$^+$)

3.4 | WBP1L inhibits CXCR4 signalling in murine and human cell lines

To analyse the effects of the endogenous WBP1L on CXCR4, we have selected two cell lines where the expression of WBP1L and/ or CXCR4 is highly relevant. These included human leukaemic cell line REH as a representative of *ETV6-RUNX1*$^+$ leukaemia, where we have down-regulated WBP1L by a single shRNA specific for human *WBP1L* and immortalized murine monocyte/macrophage progenitors as a representative of bone marrow progenitors, where

we used a different shRNA targeting murine *Wbp1l* (Figure 4A,B). After stimulation with CXCR4 ligand CXCL12, these cells showed enhanced activity of downstream signalling pathways, resulting in increased phosphorylation of ERK1/2 and AKT (Figure 4C,D and S6). CXCR7, another known receptor for CXCL12, did not contribute to the signalling output under these conditions (Figure S7). These data demonstrated that WBP1L is involved in the negative regulation of CXCR4 signalling.

3.5 | Altered haematopoiesis in *Wbp1l*-deficient mice

To further analyse the physiological function of WBP1L, we have acquired *Wbp1l*-deficient mouse strain *Wbp1l*[tm2a(EUCOMM)Hmgu] (hereafter referred to as *Wbp1l*^{-/-}) from the International Mouse Phenotyping Consortium. These mice appeared grossly normal and healthy, were born in normal Mendelian ratios and did not express WBP1L protein (Figure 5A).

To characterize the haematopoietic system in *Wbp1l*^{-/-} mice, we have analysed major cell subset frequencies in adult mice and in embryos. The embryonic haematopoietic cell numbers were grossly normal with small increases in the yolk sac CD45^{+} KIT^{-} cells and CD11b^{+} F4/80^{+} yolk sac macrophages (Figure 5B). In the peripheral tissues of the adult mice, there was a significant increase in marginal zone B cell fraction in the spleen (Figure 5C) and a reduction in B1 cell percentages in the peritoneal cavity (Figure 5D). We also observed increased frequencies of splenic dendritic cells in *Wbp1l*^{-/-} mice (Figure 5C). Otherwise, the frequencies of other leucocyte subsets found in peripheral tissues were normal (Figure 5C,D). Bone marrows from *Wbp1l*^{-/-} animals showed the same cell counts as wild-type bone marrows (Figure 5E). Most of bone marrow cell subsets were also found in normal numbers, including T cells, monocytes, neutrophils (Figure 5E) and the majority of progenitor populations (Figure 5F). However, there were two notable exceptions. First, the overall B cell percentages in the bone marrow were significantly reduced (Figure 5G). The reduction was most pronounced in early developmental stages (pro- and pre-B cells). At the later stages, including immature and mature B cells a similar trend was observed, but it was outside the threshold for statistical significance (P-values .06 and .08, respectively) (Figure 5G). The cell cycle of B cell progenitors was not substantially changed with the exception of a very
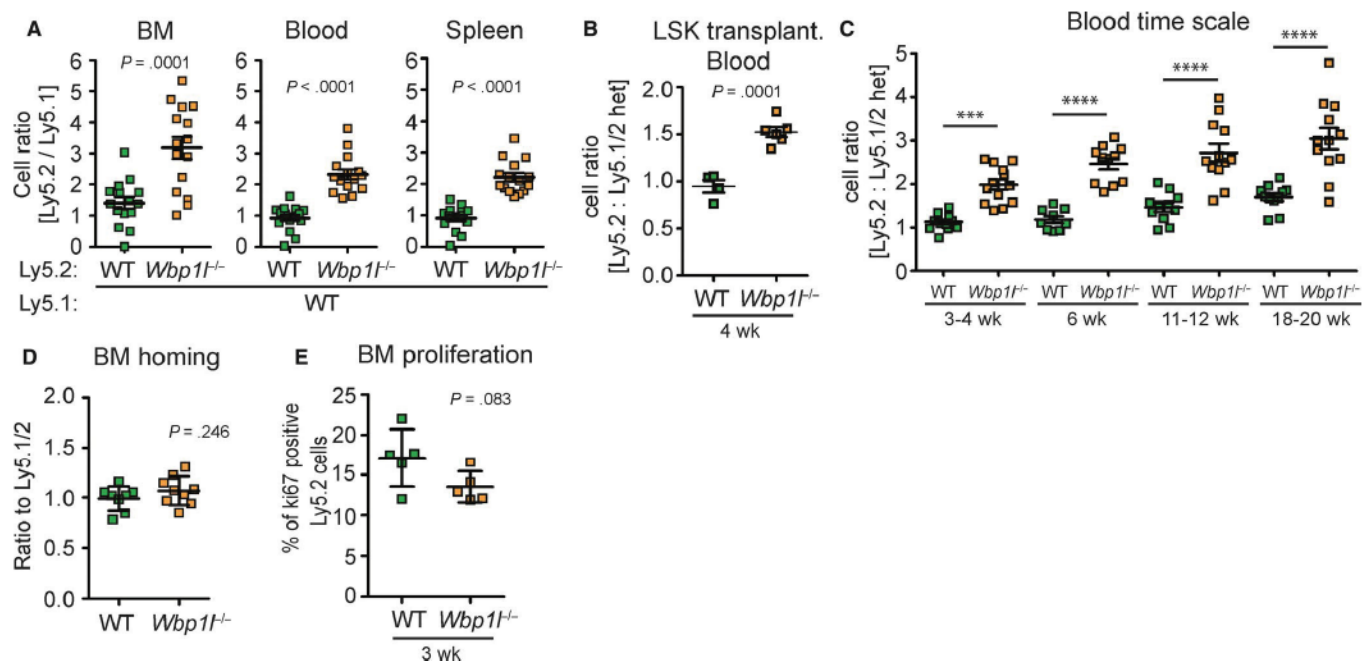

FIGURE 6 Enhanced engraftment of *Wbp1l*^{-/-} bone marrow. (A) Ly5.2[+] bone marrow (WT or *Wbp1l*^{-/-}) was mixed with Ly5.1[+] bone marrow (always WT) in a ratio 1:1 and 2 × 10^{6} cells were transplanted into Ly5.1 lethally irradiated mice. Mice were analysed 2 months post-transplantation. Flow cytometry analyses show the ratio between Ly5.2 and Ly5.1 cells in the bone marrow, blood and spleen. (B) LSK cells sorted from Ly5.2[+] bone marrow (WT or *Wbp1l*^{-/-}) were mixed with LSK from Ly5.1/Ly5.2[+] heterozygous bone marrow (always WT) in a ratio 1:1 and 20 000 cells together with support of 0.5 × 10^{6} Ly5.1 bone marrow cells were injected into tail vain of Ly5.1 lethally irradiated mice. Data represent the ratio between Ly5.2[+] and Ly5.1/Ly5.2^{+} cells detected in the recipient blood 4 wk post injection. One of two independent experiments is shown (N ≥ 8). (C) Ly5.2[+] bone marrow (WT or *Wbp1l*^{-/-}) was mixed with Ly5.1/Ly5.2[+] heterozygous bone marrow (always WT) in a ratio 1:1 and 2 × 10^{6} cells were transplanted into Ly5.1 lethally irradiated mice. At indicated time-points, the ratio between Ly5.2 and Ly5.1/Ly5.2 cells in blood was measured by flow cytometry. (D) Homing of WT and *Wbp1l*^{-/-} bone marrow cells in a competitive set-up. WT or *Wbp1l*^{-/-} bone marrow (Ly5.2[+]) was each combined with WT bone marrow from Ly5.1/Ly5.2[+] heterozygotes in a ratio 1:1 and 2 × 10^{6} cells were injected into the tail vain of sublethally irradiated recipient (Ly5.1[+]). Data represent the ratio between Ly5.2[+] and Ly5.1/Ly5.2^{+} cells detected in the recipient bone marrow 16 h post injection (N ≥ 8). (E) Competitive bone marrow transplantation was performed as in (C) and 3 wk after the transplantation expression of Ki67 proliferation marker was measured in transplanted cells

small but significant increase in G1 phase pre-B cells in *Wbp1l*⁻/⁻ mice (Figure S8). Second, Lin⁻SCA1⁺KIT⁺ (LSK) cells encompassing early progenitors and stem cells (HSPC) showed slightly but significantly increased percentages in these animals (Figure 5F).

To test their functionality in vivo, we performed a competitive bone marrow transplantation assay, whereby we mixed wild-type or *Wbp1l*⁻/⁻ Ly5.2 cells with wild-type Ly5.1 bone marrow cells in a 1:1 ratio and transplanted these mixtures into lethally irradiated recipient mice (Ly5.1). Nine weeks later, we have analysed their engraftment. Strikingly, *Wbp1l*⁻/⁻ bone marrow engrafted significantly better and the ratio between *Wbp1l*⁻/⁻ and wild-type cells increased from 1:1 to ca 3:1 (Figure 6A), whereas wild-type Ly5.2 and Ly5.1 BM engrafted with equal efficiency. The difference could be observed across all bone marrow leucocyte subsets analysed except for LSK cells, where a similar trend in favour of *Wbp1l*⁻/⁻ cells was also present but was not statistically significant (Figure S9). The difference was also maintained in the periphery, where the ratio between *Wbp1l*⁻/⁻ and wild-type cells was roughly 2:1 (Figure 6A). Similar difference in engraftment efficiency was also observed when we transplanted sorted LSK cells in the 1:1 ratio (Figure 6B). Next, we investigated how this ratio changes with time. A significant difference between the engraftment efficiency could be observed as early as 3 weeks after the transplantation and was maintained till at least 18 weeks after the transplantation (Figure 6C). The increased efficiency in the bone marrow engraftment was not the result of increased homing to the bone marrow or increased proliferation, which did not display any alteration (Figure 6D,E). Collectively, these data are showing negative role of WBP1L in HSPC function. Persistence of the engraftment advantage for more than 16 weeks suggests that the haematopoietic system is affected already at the level of haematopoietic stem cells.

3.6 | Compensatory mechanisms restore CXCR4 signalling when WBP1L is lost in the germline, but the effects of WBP1L deficiency on CXCR4 signalling can be observed upon its acute deletion

Part of the data described above are consistent with CXCR4 hyperactivity. However, the same homing capacity of the wild-type and *Wbp1l*⁻/⁻ bone marrow cells (Figure 6D) is incompatible with enhanced CXCR4 function. These results prompted us to test whether bone marrow cells from *Wbp1l*⁻/⁻ mice display similar CXCR4 dysregulation as shRNA-treated cell lines. Surprisingly, we did not observe any alterations in CXCL12-triggered ERK phosphorylation in bone marrow cells from *Wbp1l*⁻/⁻ mice (Figure 7A). This result was in disagreement with our analysis of the effects of shRNA-mediated WBP1L down-regulation in cell lines (Figure 4). To exclude the possibility that enhanced CXCR4 signalling observed there was the result of non-specific off-target effects of *Wbp1l* shRNAs, we expressed shRNA targeting *Wbp1l* in immortalized monocyte/macrophage progenitors from wild-type and *Wbp1l*⁻/⁻ mice. Because of the absence of WBP1L, only non-specific activity of *Wbp1l* shRNA can be detected in *Wbp1l*⁻/⁻ progenitors. As

expected, *Wbp1l* shRNA significantly enhanced CXCL12-triggered ERK activation in wild-type cells. On the other hand, only negligible insignificant changes were detected in *Wbp1l*⁻/⁻ cells (Figure 7B). These results demonstrated that the effects of *Wbp1l* shRNA are dependent on *Wbp1l* and, thus, specific. When we used the same cells in an in vivo homing experiment, we observed that WBP1L down-regulation significantly enhanced bone marrow homing of wild-type cells, when compared to *Wbp1l*⁻/⁻ cells (Figure 7C). This outcome is consistent with the results of our in vitro analyses showing that WBP1L negatively regulates activity of CXCR4.

To definitely prove the validity of our shRNA data, we have generated a mouse strain *Wbp1l*^fl/fl-*CreERT* where the *Wbp1l* gene can be acutely inactivated upon injection of 4OH-tamoxifen. Acute *Wbp1l* deletion in this model resulted in enhanced ERK phosphorylation in response to CXCL12 stimulation in total bone marrow as well as in several major subsets, including T cells, monocytes and neutrophils, whereas in B cells, the difference was small and not statistically significant (Figure 7D and S10). No effects of WBP1L deficiency on total ERK expression were observed (Figure 7E). The enhanced CXCR4 signalling did not translate to any immediate effect on steady-state numbers of major bone marrow and splenic cell subsets (Figure S11A). However, it is likely that only much more substantial increase in CXCR4 signalling would be needed to alter leucocyte bone marrow retention within this timescale.

The data presented above suggested that the effects of WBP1L down-regulation can only be observed after its acute deletion. To further address this possibility, we have established primary culture of isolated KIT⁺ bone marrow cells from *Wbp1l*^fl/fl-*CreERT* mice, where *Wbp1l* could be deleted by 4OH-tamoxifen. Importantly, cells cultured outside the bone marrow are not exposed to continuous CXCL12 stimulation and desensitization and are, thus, having high expression of CXCR4 and stronger signalling capacity. In agreement with our previous observations, after acute *Wbp1l* deletion by CRE recombinase (but not after germline deletion), these progenitors showed increased ERK phosphorylation in response to CXCL12 stimulation (Figure 7F and S11B). *Wbp1l* deletion also resulted in an increase in steady-state CXCR4 surface expression with no other effects on the rate of CXCL12-triggered receptor internalization in these cells (Figure 7G and S11C). The same increase in CXCR4 expression was also observed on KIT⁺ progenitors from peripheral blood of animals after acute *Wbp1l* deletion (Figure 7H). Similar, though not significant, trend was also observed when CXCR4 was measured on fixed and permeabilized cells (Figure S11D). Finally, cells with acute *Wbp1l* deletion showed increased migration towards CXCR4 ligand CXCL12 in a transwell assay in vitro (Figure 7I) and increased bone marrow homing efficiency in vivo (Figure 7J). These data confirm that WBP1L negatively regulates CXCR4 expression and signalling in primary cells.

4 | DISCUSSION

Expression of the *WBP1L* gene is heightened in *ETV6-RUNX1*⁺ paediatric BCP-ALL and was shown to correlate with favourable
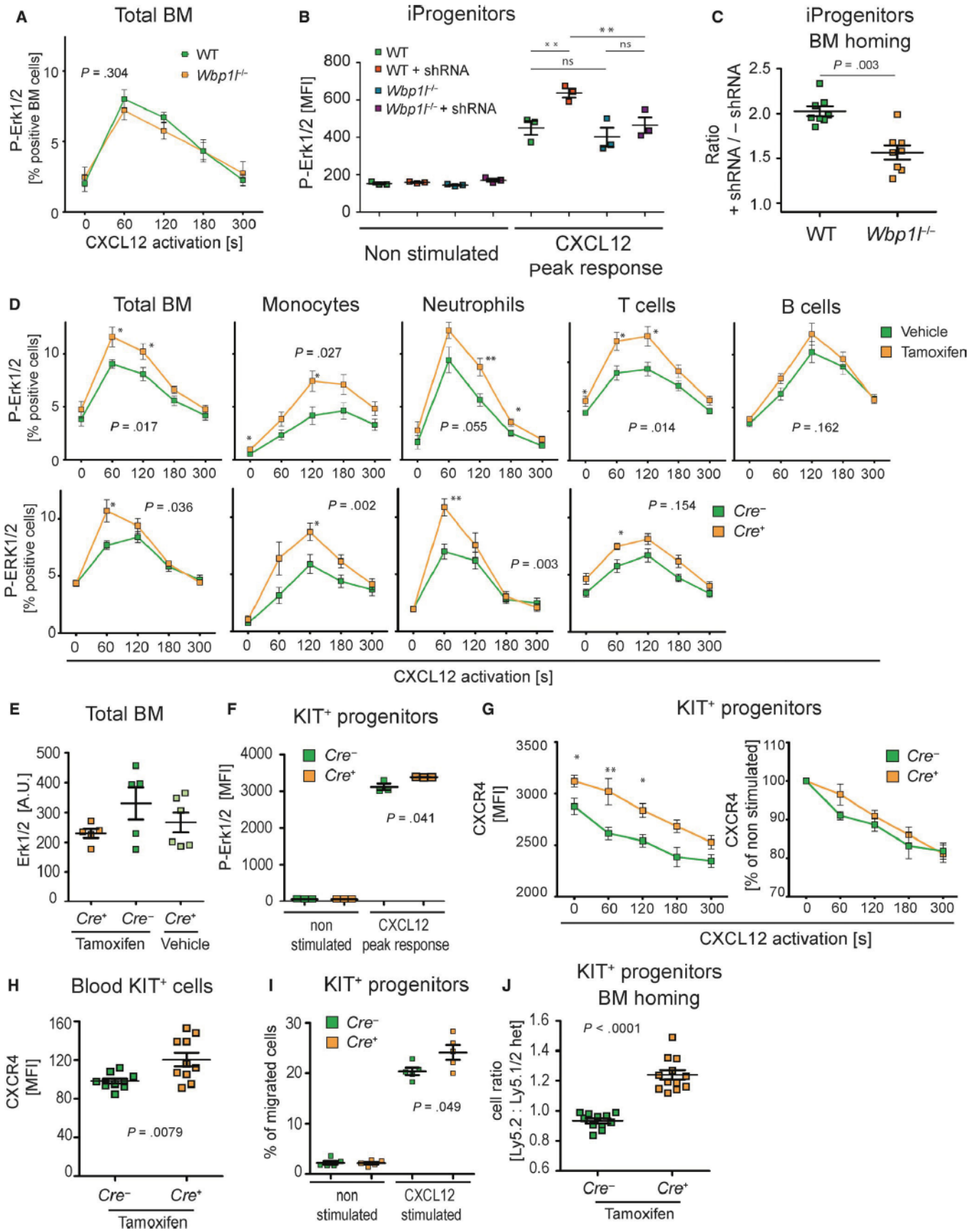
treatment response.[1-3] However, the function of its protein product WBP1L in healthy and leukaemic cells has not been investigated. Here, we attempted to uncover its physiological function. Our initial analysis shows that WBP1L binds several NEDD4-family E3 ubiquitin ligases and its deficiency results in augmented surface expression and signalling of CXCR4, one of their known target proteins.

FIGURE 7 Acute loss of WBP1L results in enhanced CXCR4 signalling but germline deficiency is compensated for. (A) ERK1/2 phosphorylation downstream of CXCR4 in WT and $Wbp1l^{-/-}$ (germline deletion) bone marrow cells. Cells were stimulated with 100 nmol/L CXCL12, fixed, stained for phosphorylated ERK1/2 and analysed by flow cytometry. Data represent percentage of responding cells (N = 6). P-value was calculated for maximum response of WT and $Wbp1l^{-/-}$ cells regardless of the time-point where it was reached. (B) Erk1/2 activation after CXCL12 stimulation (100 nmol/L) of immortalized monocyte/macrophage progenitors (iProgenitors) from WT and $Wbp1l^{-/-}$ mice and of the same cells transduced with $Wbp1l$ shRNA. Erk phosphorylation was measured by flow cytometry of fixed and permeabilized cells stained with fluorescent P-Erk1/2 antibody. Peak response detected during 5 min measurement is shown. Data are represented as medians of fluorescence intensity (N = 3). P-values were calculated using 1way ANOVA with Bonferroni's multiple comparison test. (C) WT cells transduced or not with $Wbp1l$ shRNA were mixed 1:1 and their bone marrow homing ability was analysed as in Figure 6D. As a control $Wbp1l^{-/-}$ cells transduced or not with $Wbp1l$ shRNA and also mixed in a ratio 1:1 were used. Ratios of shRNA transduced and non-transduced cells are plotted for each genotype (n = 8). P-value was calculated for the differences between these two ratios. Significant outliers were discarded based on q test. As not all cells expressed shRNA containing vector after transduction, the true ratio was lower than 1:1 at the time of injection. The final data were normalized to this true ratio. (D) CXCR4 signalling in bone marrow cell subsets after acute deletion of $Wbp1l$. In the top row, $CreERT$ expressing cells treated either with tamoxifen or vehicle (corn oil) are compared. In the bottom row, the comparison is made between tamoxifen-treated $Wbp1l^{fl/fl}$-$CreERT$ and $Wbp1l^{fl/fl}$ (without $CreERT$) bone marrow cells. Cells were stimulated with 100 nmol/L CXCL12, fixed, stained for extracellular markers and intracellular P-ERK and analysed by flow cytometry. Data represent percentage of responding cells from whole bone marrow (N = 7), T cells (CD3$^+$, N = 7/8), monocytes (Ly6C$^+$ Ly6G$^-$, N = 11) and neutrophils (Ly6G$^+$ Ly6C$^-$, N = 7). Significant outliers were discarded based on q test. P-value was calculated for maximum response (regardless of the time-point at which this maximum was reached). In addition, significant differences in individual time-points are labelled with asterisks. (E) Expression of total ERK1/2 in the bone marrow cells where $Wbp1l$ was deleted as in (D). Protein level was measured using Western blot. ERK1 and ERK2 were probed separately and signal was summed and normalized to actin loading control (N ≥ 5) (F). CXCR4 signalling in in vitro 4-hydroxytamoxifen treated KIT$^+$ progenitors isolated from $Wbp1l^{fl/fl}$-$CreERT$ and $Wbp1l^{fl/fl}$ (without $CreERT$) bone marrow. ERK phosphorylation was measured after stimulation with 100 nmol/L CXCL12 by flow cytometry on fixed and permeabilized cells. Peak response detected during 5 min measurement is shown. One of two independent experiments is shown, N = 6. (G) CXCL12-induced changes of CXCR4 surface expression on KIT$^+$ bone marrow progenitors. These cells were isolated from $Wbp1l^{fl/fl}$-$CreERT$ and $Wbp1l^{fl/fl}$ bone marrow, treated with 4-hydroxytamoxifen to induce $Wbp1l$ deletion and stimulated with CXCL12 for indicated time intervals. FACS data are plotted as median fluorescence intensities (left graph) or as percentage of expression level on non-stimulated cells (right graph) (n = 7). (H) CXCR4 expression on KIT$^+$ progenitors detected in the blood of tamoxifen-treated $Wbp1l^{fl/fl}$-$CreERT$ and $Wbp1l^{fl/fl}$ mice. Significant outlier was discarded based on q test (N = 10). (I) Migration of 4-hydroxytamoxifen-treated KIT$^+$ progenitors from $Wbp1l^{fl/fl}$-$CreERT$ and $Wbp1l^{fl/fl}$ mice towards 500 nmol/L CXCR4 in a transwell assay in vitro (N = 5). (J) Ly5.2$^+$ KIT$^+$ progenitors (from $Wbp1l^{fl/fl}$-$CreERT$ or $Wbp1l^{fl/fl}$ mice, treated with 4-hydroxytamoxifen) were mixed 1:1 with Ly5.1/Ly5.2$^+$ heterozygous KIT$^+$ progenitors from WT mice and 10^7 cells were injected into Ly5.1 sublethally irradiated recipients. After 16 h, the ratio between Ly5.2 and Ly5.1/Ly5.2 cells in the bone marrow was measured by flow cytometry (N ≥ 11)

At the organismal level, WBP1L deficiency resulted in perturbations in B cell development and increased ability of bone marrow stem and progenitor cells to reconstitute haematopoietic system after the bone marrow transplantation. In addition, acute $Wbp1l$ deletion resulted in increased progenitor homing to the bone marrow. How much of this phenotype can be attributed to CXCR4 hyperactivity is still an open question. There are at least two other mouse models that show increased CXCR4 activity. One of these strains carries a mutation in CXCR4 that prevents its desensitization and down-regulation ($CXCR4^{WHIM}$). The same mutation in humans causes immunodeficiency known as WHIM syndrome.[18-20] $CXCR4^{WHIM}$ mice display a similar selective dysregulation in the bone marrow B cell compartment as $Wbp1l^{-/-}$ mice with the reduction in B cell percentages that is most profound at the B cell progenitor level.[20] They also show increase in marginal zone B cell percentages. On the other hand, some of their symptoms were not detected in $Wbp1l^{-/-}$ mice, including blood neutropenia and lymphopenia and reduced spleen size.[20] Increased CXCR4 expression and CXCR4-mediated signalling were also observed in mice deficient in the expression of BAR domain containing adaptor protein Missing In Metastasis (MIM). In these animals, leucocyte development and percentages appeared largely normal and no leukopenia has been observed. Rather they showed slightly increased white blood cell counts and splenomegaly.[21,22] Even though MIM deficiency has a number of CXCR4-independent

effects, these data show that enhanced CXCR4 activity does not have to lead to leukopenia in the peripheral tissues, nor to major alterations in leucocyte subset numbers and frequencies in the bone marrow. It is possible that the lack of receptor desensitization rather than alterations in peak signal intensity may be the key factor driving peripheral leukopenia in $CXCR4^{WHIM}$ mice.

Since in mice with germline $Wbp1l$ deletion we have not observed up-regulation in CXCR4 activity, it is difficult to unequivocally answer the question if alterations in $Wbp1l^{-/-}$ B cell development are caused by CXCR4 dysregulation. This phenotype is strikingly similar to the one observed in $CXCR4^{WHIM}$ animals. It is possible that not all haematopoietic cell subsets are able to compensate for the loss of WBP1L. Early B cell progenitors represent a relatively small population, and their WBP1L expression based on the data from ImmGen consortium[23] is similar to other B cell subsets (not shown). The options to analyse their CXCR4 signalling pathways are relatively limited. Those that can be analysed by flow cytometry, including ERK and STAT3 phosphorylation, as well as calcium response appear to be hypo/non-responsive in this particular cell type despite clearly measurable CXCR4 expression (not shown). As a result, B cell progenitors contribute very little to ERK phosphorylation of the entire B cell pool measured in our experiments where the more mature stages dominated the response. The other pathways we were not able to analyse in this relatively rare subpopulation and so it is still

possible that reduction in B cell progenitor numbers in *Wbp1l*$^{-/-}$ mice is caused by some aspect of CXCR4 signalling, which we could not measure.

WBP1L may also have other functions besides regulation of CXCR4. They may be responsible for a part of the phenotype of WBP1L-deficient cells and animals. WBP1L binds multiple NEDD4 family members and very likely other proteins, which can result in pleiotropic effects on leucocyte biology. It has been shown that in competitive transplantation assay HSPC with only one functional CXCR4 allele perform better than wild-type cells, which perform better than *CXCR4*^{WHIM} cells, clearly showing an inverse correlation between CXCR4 activity and transplantation efficiency.[24,25] This observation is rather counterintuitive and opposite to the results we obtained with *Wbp1l*$^{-/-}$ cells. An explanation suggested in these studies was that CXCR4 promotes haematopoietic stem cell quiescence leading to competitive disadvantage when CXCR4 signalling is up-regulated. This leads to the conclusion that though CXCR4 role cannot be completely excluded by our experiments, effects of WBP1L on transplantation efficiency are likely CXCR4-independent. The molecular mechanism of how WBP1L regulates bone marrow engraftment will have to be addressed in future studies. On the other hand, functional effects of acute down-regulation of WBP1L are more clearly connected to CXCR4, leading to increased surface expression of CXCR4, increased CXCR4 signalling and improved homing efficiency, similar to mouse models with increased CXCR4 activity.

It is at present unclear what is the reason for the unequal effects of the acute and constitutive OPAL1 deletion on CXCR4 signalling. We can speculate that WBP1L may be rather general regulator of expression and/or activity of NEDD4 family ligases. However, there are many additional mechanisms regulating these enzymes. In the majority of cases, these might be able to compensate for the loss of WBP1L in the long-term. However, their ability to rapidly react to acute WBP1L loss would likely be more limited, as it may require changes in the gene expression pattern or other time-consuming adaptations.

Another important question is the role that WBP1L potentially plays in leukaemia. The *WBP1L* gene is a target gene of ETV6, which suppresses its expression.[4] In *ETV6-RUNX1*$^+$ BCP-ALL, one allele of *ETV6* is inactivated by fusion with *RUNX1*, while the other is often inactivated as well.[26] This could explain the increase of WBP1L expression in *ETV6-RUNX1*$^+$ BCP-ALL. It is also in agreement with our data showing that in REH cells (which already have both *ETV6* alleles inactivated) *ETV6-RUNX1* genetic deletion did not have any further effect on WBP1L expression. *ETV6* inactivation likely represents part of the mechanism leading to the development of leukaemia and defining its features. In principle, WBP1L in this context can have two different functions. First, negative regulation of CXCR4 by WBP1L could dampen the interactions of leukaemic (stem) cells with protective bone marrow niches, making them more sensitive to treatment. Second, WBP1L may also have negative effect on leukaemic stem cells similar to its negative regulatory effects on HSPCs that were revealed in our competitive transplantation experiment. Our data do not specifically address the role of WBP1L in leukaemia. However, the effects of WBP1L deficiency on normal haematopoiesis that we observed here and the fact that WBP1L is an ETV6 target gene make WBP1L a relevant target of future research in this field.

CONFLICT OF INTEREST

The authors confirm that there are no conflicts of interest.

AUTHOR CONTRIBUTIONS

SB, A.D and JK with contribution from MF, PA, JP, TS, NP and TB conducted majority of experiments and data analysis. DG performed microscopy analysis. IS carried out analysis of *Wbp1l*$^{-/-}$ embryos. OVM and KK analysed palmitoylation of WBP1L. V. Kanderova provided data on WBP1L expression in B cell lines. JS and PS generated ETV6-RUNX1-deficient REH cell line. MBP and MGT generated rabbit antisera to WBP1L. MAJ contributed to design and analysis of homing and competitive transplantation assays. V. Korinek contributed to the generation of *Wbp1l*-CreERT mouse strain. TB with

contribution from SB and AD conceptualized the study, evaluated the data and wrote the paper.

DATA AVAILABILITY STATEMENT

The data that support the findings of this study are available from the corresponding author upon reasonable request.

ORCID

Orest V. Matveichuk ![iD] https://orcid.org/0000-0002-4057-7598

Majd B. Protty ![iD] https://orcid.org/0000-0001-8992-9120

Tomas Brdicka ![iD] https://orcid.org/0000-0002-1560-4398

REFERENCES

1. Mosquera-Caro M, Helman P, Veroff R, et al. Identification, validation and cloning of a novel gene (OPAL1) and associated genes highly predictive of outcome in pediatric acute lymphoblastic leukemia using gene expression profiling [abstract]. *Blood.* 2003;102:4a.

2. Holleman A, den Boer ML, Cheok MH, et al. Expression of the outcome predictor in acute leukemia 1 (OPAL1) gene is not an independent prognostic factor in patients treated according to COALL or St Jude protocols. *Blood.* 2006;108:1984-1990.

3. Kanderova V, Kuzilkova D, Stuchly J, et al. High-resolution antibody array analysis of childhood acute leukemia cells. *Mol Cell Proteomics.* 2016;15:1246-1261.

4. Neveu B, Spinella J-F, Richer C, et al. CLIC5: a novel ETV6 target gene in childhood acute lymphoblastic leukemia. *Haematologica.* 2016;101:1534-1543.

5. Lopez RG, Carron C, Oury C, Gardellin P, Bernard O, Ghysdael J. TEL is a sequence-specific transcriptional repressor. *J Biol Chem.* 1999;274:30132-30138.

6. Chakrabarti SR, Nucifora G. The leukemia-associated gene TEL encodes a transcription repressor which associates with SMRT and mSin3A. *Biochem Biophys Res Commun.* 1999;264:871-877.

7. De Braekeleer E, Douet-Guilbert N, Morel F, Le Bris MJ, Basinko A, De Braekeleer M. ETV6 fusion genes in hematological malignancies: a review. *Leuk Res.* 2012;36:945-961.

8. Rasighaemi P, Ward AC. ETV6 and ETV7: Siblings in hematopoiesis and its disruption in disease. *Crit Rev Oncol Hematol.* 2017;116:106-115.

9. Wang LC, Swat W, Fujiwara Y, et al. The TEL/ETV6 gene is required specifically for hematopoiesis in the bone marrow. *Genes Dev.* 1998;12:2392-2402.

10. Hock H, Meade E, Medeiros S, et al. Tel/Etv6 is an essential and selective regulator of adult hematopoietic stem cell survival. *Genes Dev.* 2004;18:2336-2341.

11. Pei J, Grishin NV. Unexpected diversity in Shisa-like proteins suggests the importance of their roles as transmembrane adaptors. *Cell Signal.* 2012;24:758-769.

12. Draber P, Kupka S, Reichert M, et al. LUBAC-recruited CYLD and A20 regulate gene activation and cell death by exerting opposing effects on linear ubiquitin in signaling complexes. *Cell Rep.* 2015;13:2258-2272.

13. Kralova J, Glatzova D, Borna S, Brdicka T. Expression of fluorescent fusion proteins in murine bone marrow-derived dendritic cells and macrophages. *J Vis Exp.* 2018;140:e58081. https://doi.org/10.3791/58081

14. Lorenz S. Structural mechanisms of HECT-type ubiquitin ligases. *Biol Chem.* 2018;399:127-145.

15. Mund T, Pelham HRB. Control of the activity of WW-HECT domain E3 ubiquitin ligases by NDFIP proteins. *EMBO Rep.* 2009;10:501-507.

16. Ayala F, Dewar R, Kieran M, Kalluri R. Contribution of bone microenvironment to leukemogenesis and leukemia progression. *Leukemia.* 2009;23:2233-2241.

17. de Lourdes PA, Amarante MK, Guembarovski RL, de Oliveira CEC, Watanabe MAE. CXCL12/CXCR4 axis in the pathogenesis of acute lymphoblastic leukemia (ALL): a possible therapeutic target. *Cell Mol Life Sci.* 2015;72:1715-1723.

18. Hernandez PA, Gorlin RJ, Lukens JN, et al. Mutations in the chemokine receptor gene CXCR4 are associated with WHIM syndrome, a combined immunodeficiency disease. *Nat Genet.* 2003;34:70-74.

19. Kawai T, Malech HL. WHIM syndrome: congenital immune deficiency disease. *Curr Opin Hematol.* 2009;16:20-26.

20. Balabanian K, Brotin E, Biajoux V, et al. Proper desensitization of CXCR4 is required for lymphocyte development and peripheral compartmentalization in mice. *Blood.* 2012;119:5722-5730.

21. Zhan T, Cao C, Li L, Gu N, Civin CI, Zhan X. MIM regulates the trafficking of bone marrow cells via modulating surface expression of CXCR4. *Leukemia.* 2016;30:1327-1334.

22. Yu D, Zhan XH, Zhao XF, et al. Mice deficient in MIM expression are predisposed to lymphomagenesis. *Oncogene.* 2012;31:3561-3568.

23. Heng TS, Painter MW. The Immunological Genome Project: networks of gene expression in immune cells. *Nat Immunol.* 2008;9:1091-1094.

24. McDermott DH, Gao JL, Liu Q, et al. Chromothriptic cure of WHIM syndrome. *Cell.* 2015;160:686-699.

25. Gao JL, Yim E, Siwicki M, et al. Cxcr4-haploinsufficient bone marrow transplantation corrects leukopenia in an unconditioned WHIM syndrome model. *J Clin Invest.* 2018;128:3312-3318.

26. Sundaresh A, Williams O. Mechanism of ETV6-RUNX1 Leukemia. In: Groner Y, Ito Y, Liu P, Neil JC, Speck NA, van Wijnen A, eds. *RUNX Proteins in Development and Cancer.* Singapore: Springer Singapore; 2017:201-216.

SUPPORTING INFORMATION

Additional supporting information may be found online in the Supporting Information section.

Supplemental methods

Cell culture

REH cells were cultured in RPMI (Thermo Fisher Scientific, Waltham, MA), 293T and J774 cells and Phoenix cells were cultured in DMEM (Thermo Fisher), other BCP-ALL cell lines were cultivated as described previously [1]. Media were supplemented with 10% fetal bovine serum (Thermo Fisher) and antibiotics. Immortalized monocyte-macrophage progenitors were cultivated and generated using conditional HOXB8 construct as described previously [2,3]. KIT$^+$ cells were cultured in IMDM media supplemented with 0.1% IL-6, 0.2% IL-3, 1% SCF, supplied as supernatants from HEK293 cells transfected with constructs coding for respective cytokines. CRE-mediated *Wbp1l* deletion was induced with 1μM 4-hydroxytamoxifen. BMDM were prepared and cultivated as described [4].

Antibody generation

Preparation of the rabbit anti-WBP1L polyclonal antibody was outsourced to Eurogentec (Seraing, Belgium). The QAREHGHPHLPRPPAC peptide, which is close to the WBP1L C-terminus and is identical in the human and mouse sequences, was conjugated to keyhole limpet hemocyanin (KLH) for use as the antigen. The same peptide was used to affinity purify the antibody. OPAL-01 and OPAL-02 antibodies to human WBP1L were described previously [1]. mOPAL-01 and mOPAL-03 mouse monoclonal antibodies to murine WBP1L were generated by standard hybridoma technology using splenocytes of mice (F1 hybrids of BALB/c × B10) immunized with recombinant intracellular part of murine WBP1L protein and Sp2/0 myeloma cells as a fusion partner.

Flow cytometry

For surface staining, cells were incubated with antibodies and Fc-block (Clone 2.4G2) in PBS with 2% FBS for 30 min. For intracellular staining, cells were fixed with 4% formaldehyde (Thermo Fisher), then stained for surface markers, permeabilized with 90% methanol (Lachner, Neratovice, Czechia), blocked with 5% BSA (Merck, Darmstadt, Germany) 0.3% Triton X-100 (Merck) in PBS and stained for intracellular antigens in 1% BSA 0,3% Triton X-100 in PBS. For cell cycle analyses or Ki67 staining, cells were not permeabilized by methanol and after antibody staining were stained with 2 μg/ml Hoechst 33342 (Merck). Data were collected on LSRII flow cytometer (BD Biosciences, San Jose, CA) and analyzed with FlowJo software (FlowJo LLC, Ashland, OR).

Other reagents and their sources

β-estradiol (Merck), 4-Hydroxytamoxifen (Merck), recombinant murine and human SDF1α (Immunotools, Friesoythe, Germany), Lipofectamine 2000 (Thermo Fisher), Protein A/G (Santa Cruz Biotechnology, Dallas, TX), tunicamycin, Lysotracker Red DND-99, ER-Tracker Red, MitoTracker Red (Thermo Fisher), TC14012 (RanD corporation), AMD3100 (Merck).

Analysis of WBP1L palmitoylation

Palmitoylation of WBP1L was analyzed using click reaction-based approach, essentially as described earlier [5]. Briefly, HEK293 cells (5.5×10^5 in 60-mm dish) were transfected with 6 µg of WBP1L-FLAG-STREP-bearing pBABE using FuGENE (Promega, Madison, WI) according to manufacturer's instruction. After 24 h, cells were labeled with 50 µM 17-octadecynoic acid (17ODYA) or exposed to 0.05% DMSO carrier (1.5 h, 37 °C). Cells were lysed in a buffer containing 4% SDS and lysates subjected to click reaction with biotin-azide (500 µM biotin-PEG3-azide; Merck). Proteins were precipitated with chloroform:methanol [6] and resupended in the presence of 0.5% SDS and 1% Brij97. Biotin-tagged proteins were enriched on streptavidin-coupled beads (Thermo Fisher), eluted in hot H_2O followed by series of buffers and analyzed by immunoblotting using mouse anti-FLAG IgG (Merck) and rabbit anti-FLOTILLIN-2 IgG (Cell Signaling Technology, Danvers, MA).

Microscopy

BMDM were plated overnight on eight well µ-plate (IBIDi). The next day the cells were directly imaged or stained with organelle specific dye (MitoTracker Red 1:500, LysoTracker Red DND-99 1:1000, ER-tracker Red 1:1000, all Thermo Fisher) and directly imaged, or stained with CD11b-APC (Table S1) and subsequently fixed with 4% formaldehyde (Merck) and stained with Hoechst 33342 (Merck). Sequential 2-color imaging was performed using Leica TCS SP8 laser scanning confocal microscope with a 63×1.4 NA oil-immersion objective. Acquired images were manually thresholded to remove signal noise detected outside of the cell using ImageJ software.

Isolation of cell subsets from organs

Mouse blood was collected by cheek bleeding to EDTA tubes (KABE Labortechnik, Numbrecht-Elsenroth, Germany). B cells and T cells were isolated from splenocyte suspensions and neutrophils and KIT+ cells from bone marrow cell suspensions using magnetic microbeads (Miltenyi Biotec, Bergisch Gladbach, Germany, see *Supplementary Table S5*) on an AutoMACS magnetic cell sorter (Miltenyi Biotec). Cells from murine embryo proper and yolk sac were isolated by digestion of respective tissue in dispase (1mg/ml, Thermo Fisher) in HBSS for 10 min followed by erythrocyte lysis with ACK buffer.

Knock-out cell line preparation

ETV6-RUNX1$^{-/-}$ REH cell lines were established using CRISPR/Cas9 technology. pLV-U6g-EPCG plasmid (Merck) was used with guide RNA (GTGCCTCGAGCGCTCAGGATGG) against exon 2 of *ETV6* gene. Since the second allele of *ETV6* is deleted in REH cell line, this targeting sequence is specific for fusion gene only. Knockout of *ETV6-RUNX1* gene was confirmed by Sanger sequencing, on mRNA and protein level (Figure S2 and data not shown). As a control, REH cell line transduced with non-targeting CRISPR/Cas9 vector was used.

Tandem purification of WBP1L for mass spectrometry analysis of WBP1L-binding proteins

Cells were lysed in lysis buffer (30mM TRIS, pH 7.4, 120 mM NaCl, 2 mM KCl, 10% Glycerol, 1% β-D-dodecylmaltoside, 10 mM Chloroacetamide, Phosphatase inhibitor tablets (PhosSTOP, Roche, Basel, Switzerland), Protease Inhibitor Cocktail (Roche)) and tagged proteins were immunoprecipated from postnuclear supernatants on anti-flag M2 affinity gel (Merck), eluted with 3x FLAG peptide (Merck), followed by second round of affinity purification on Strep-Tactin sepharose (IBA Lifesciences, Goettingen, Germany) and elution with 2% sodium deoxycholate (Merck) in 50mM TRIS (pH 8.5). Cysteines in eluted proteins were reduced with 5mM final concentration of TCEP (Tris(2-carboxyethyl)phosphine hydrochloride) and blocked with 10mM final concentration of MMTS (methyl methanethiosulfonate). Samples were cleaved with 1µg of trypsin. After digestion, samples were acidified with TFA (Trifluoroacetic acid) to 1% final concentration. Sodium deoxycholate was removed by extraction to ethylacetate [7]. Peptides were desalted on Michrom C18 column.

nLC-MS 2 Analysis

Nano Reversed phase column (EASY-Spray column, 50 cm x 75 µm ID, PepMap C18, 2 µm particles, 100 Å pore size) was used for LC/MS analysis. Mobile phase buffer A was composed of water and 0.1% formic acid. Mobile phase B was composed of acetonitrile and 0.1% formic acid. Samples were loaded onto the trap column (Acclaim PepMap300, C18, 5 µm, 300 Å Wide Pore, 300 µm x 5 mm, 5 Cartridges) for 4 min at 15 µl/min. Loading buffer was composed of water, 2% acetonitrile and 0.1% trifluoroacetic acid. Peptides were eluted with Mobile phase B gradient from 4% to 35% B in 60 min. Eluting peptide cations were converted to gas-phase ions by electrospray ionization and analyzed on a Thermo Orbitrap Fusion (Q-OT- qIT, Thermo Fisher). Survey scans of peptide precursors from 400 to 1600 m/z were performed at 120K resolution (at 200 m/z) with a 5×10^5 ion count target. Tandem MS was performed by isolation at 1.5 Th with the quadrupole, HCD (Higher-energy collisional dissociation) fragmentation with normalized collision energy of 30, and rapid scan MS analysis in the ion trap. The MS 2 ion count target was set to 10^4 and the max injection time was 35 ms. Only those precursors with charge state 2–6 were sampled for MS 2. The dynamic exclusion duration was set to 45 s with a 10 ppm tolerance around the selected precursor and its isotopes. Monoisotopic precursor selection was turned on. The instrument was run in top speed mode with 2 s cycles [8].

Data analysis of mass spectrometry

All data were analyzed and quantified with the MaxQuant software (version 1.5.3.8) [9]. The false discovery rate (FDR) was set to 1% for both proteins and peptides and we specified a minimum length of seven amino acids. The Andromeda search engine was used for the MS/MS spectra search against the *Mus musculus* database (downloaded from Uniprot on March 2018, containing 25 527 entries). Enzyme specificity was set as C-terminal to Arg and Lys, also allowing cleavage at proline bonds and a maximum of two missed cleavages. Dithiomethylation of cysteine was selected as fixed modification and N- terminal protein acetylation and methionine oxidation as variable modifications. The "match between runs" feature of MaxQuant was used to transfer identifications to other LC-MS/MS runs based on their masses and retention time (maximum deviation 0.7 min) and this was also used in quantification experiments. Quantifications were performed with the label-free algorithms described recently [9]. Data analysis was performed using Perseus 1.5.2.4 software.

Protein immunoprecipitation

Cells were lysed in lysis buffer described in the tandem purification method above. In co-Immunoprecipitation experiments 1% β-D-dodecylmaltoside was replaced with 1% NP-40 substitute (AppliChem GmbH) and in WBP1L immunoprecipitation from multiple B cell lines (Figure S2) RIPA buffer (50 mM TRIS pH7.4, 150 mM NaCl, 1% NP-40 substitute, 1% Deoxycholate (Merck), 0.1% SDS (Merck)) with the same protease and phosphatase inhibitors was used. Lysates were incubated with WBP1L monoclonal antibodies followed by isolation of antibody-bound complexes on protein A/G agarose beads (Santa Cruz Biotechnology) and elution with SDS-PAGE sample buffer.

Construct preparation and lentiviral production

If not otherwise specified, inserts were amplified from cDNA using Q5 polymerase (New England BioLabs, Boston, MA). Myc-tagged *WBP1L WT, ΔN* (with deletion of the following sequence QQRQHEINLIAYREAHNYSALPFYFRFLPNSLLPPYEEVVNRPPTPPPPYSAFQL deleted) *ΔC* (lacking entire C-terminus starting from PPPPQGGPPGGSPPGAD...) were generated by PCR and cloned into pcDNA3 vector. For WBP1L palmitoylation analysis and tandem purification, *WBP1L* or *EGFP* were cloned into tagging vector (pBABE containing C-terminal 3xFlag-2x Srep-tag-UGA –IRES-G418). For microscopy, *WBP1L* was cloned into MSCV vector in front of *MYC-tag-EGFP-UAA*. *Golgi-mApple* was amplified from mApple-Golgi-7 (mApple-Golgi-7 was a gift from Michael Davidson, Addgene plasmid # 54907) and subcloned into MSCV. E3 ligase cloning is summarized in Table S3. *WBP1L* shRNA (silencing/nonsilencing murine TRCN0000297606/085, human TRCN0000282025/275362) was obtained from Merck. Full length *Cre* (a gift from Dušan Hrčkulák) was cloned into pHIV-EGFP vector (pHIV-EGFP was a gift from Bryan Welm & Zena Werb, Addgene plasmid # 21373 [10]).

For lentiviral transductions HEK293T cells were transfected with Lentiviral Packaging vector (Thermo Fisher) and a vector of interest in ratio 1:2.5 using polyethyleneimine (PEI) (Polysciences, Warrington, PA). Virus was concentrated on centrifugal filter (Amicon 100K, Millipore). Cell infection was performed similarly to retroviruses as described here [4]. After infection with shRNA constructs, the infected cells were sorted based on the reporter (EGFP) expression and used in experiments no later than 3 weeks after the infection.

Table S1. List of flow cytometry antibodies

Antigen	Clone	Species tested	Conjugate	Company
P-ERK	197G	Mus musculus	Alexa 647	Cell Signalling Technology
Ly5.1	A20	Mus musculus	APC, FITC	BioLegend
Ly5.2	104	Mus musculus	PE-Cy7, PB,	BioLegend
CD3	17A2, 1452/C11	Mus musculus	PE, PB	BioLegend
Ly6C	HK1.4	Mus musculus	FITC, PE-Cy7	BioLegend
Ly6G	1A8	Mus musculus	PB, FITC, PB, APC	BioLegend
B220	RA3-6B2	Mus musculus	e450	Thermo-Fisher
IgM	EB121-15F9	Mus musculus	FITC	eBioscience
CD43	eBioR2/60	Mus musculus	PE	eBioscience
KIT	2B8	Mus musculus	PE, FITC	BioLegend
SCA-1	E13-161.7	Mus musculus	APC	BioLegend
CD16/32	93	Mus musculus	FITC	BioLegend
CD19	6D5	Mus musculus	FITC	BioLegend
CD11c	N418	Mus musculus	APC	BioLegend
F4/80	BM8	Mus musculus	PE, FITC, PE-Cy7	BioLegend
CD11b	M1/70	Mus musculus	PE, BV785, A700, APC	BioLegend, Sony
TER119	TER-119	Mus musculus	PB, Qdot605	BioLegend,
CD34	RAM34	Mus musculus	FITC	eBioscience
CD93	AA4.1	Mus musculus	PerCP-Cy5.5	BioLegend
CD23	B3B4	Mus musculus	e660, APC	Thermo-Fisher
CD1d	1B1	Mus musculus	FITC	BioLegend
CD5	57-7.3	Mus musculus	PE	Thermo-Fisher
CD45	30-F11	Mus musculus	PerCP-Cy5.5	Biolegend
Ki67	16A8	Mus musculus	APC	Biolegend
anti-mouse Lineage Cocktail	17A2/RB6-8C5/RA3-6B2/Ter-119/M1/70	Mus musculus	PB	BioLegend
KOMBITEST™ CD3 FITC / CD16+ CD56 + PE / CD45 PerCP / CD19 APC	UCHT1/3G8/LT56/MEM-28/LT19	Homo sapiens	FITC, PE, PerCP, APC	Exbio
CD14	MEM-18	Homo sapiens	FITC	Exbio
CXCR4	2B11	Mus musculus and Homo sapiens	APC	Thermo-Fisher

Table S2. List of antibodies for immunoprecipitation and Western blotting.

Antigen	Clone	Company	Comments
WBP1L	Rabbit polyclonal	Custom made, Eurogentec	Human/mouse WBP1L for Western Blotting
WBP1L	OPAL-01	Made in house	Human WBP1L
WBP1L	OPAL-02	Made in house	Human WBP1L
WBP1L	mOPAL-01	Made in house	Mouse WBP1L
WBP1L	mOPAL-03	Made in house	Mouse WBP1L
β-ACTIN	AC15	Merck	
P-ERK	197G2	Cell Signalling Technology	
ERK 1	MK12	BD Bioscience	
ERK 2	Rabbit polyclonal	Santa Cruz Biotechnology	
P-AKT	D9E	Cell Signalling Technology	
GAPDH	Rabbit polyclonal	Merck	
MYC-tag	9B11	Cell Signalling Technology	
UBIQUITIN	Rabbit polyclonal (A100)	Boston Biochem	
UBIQUITIN	P4D1	Cell Signalling Technology	CXCR4 ubiquitination
ITCH	Rabbit polyclonal	LifeSpan BioSciences	Itch staining in Fig. 5C
ITCH	D8Q6D	Cell Signalling Technology	Itch expression in progenitors
WWP1	Rabbit polyclonal	Abcam	
WWP2	Rabbit polyclonal	Abcam	
CXCR4	2B11	BD Bioscience	
HA-tag	C29F4	Cell Signalling Technology	
FLOTILLIN-2	Rabbit monoclonal	Cell Signalling Technology	Western Blotting
FLAG	M2	Merck	
Mouse Anti-Rabbit IgG Antibody conjugated to peroxidase	M205	Genscript	For I.P.
Goat Anti-Mouse, light chain specific, conjugated to peroxidase	Monoclonal, not specified	Jackson Immunoresearch	For I.P.
Mouse Anti-Rabbit, light chain specific, conjugated to peroxidase	Monoclonal, not specified	Jackson Immunoresearch	For I.P.
Goat anti-Mouse IgG (H+L), conjugated to peroxidase	Polyclonal	Bio-Rad	For lysates
Goat anti-Mouse IgG (H+L), conjugated to peroxidase	Polyclonal	Bio-Rad	For lysates

Table S3. List of qPCR primers

Primer	Sequence	Species tested	Company
WBP1L forward	CTCAGCGCTGCCATTTTATT	Homo sapiens	Merck
WBP1L reverse	GCTGGAAGGCACTGTATGGT	Homo sapiens	Merck
GAPDH forward	CCACATCGCTCAGACACCAT	Homo sapiens	Merck
GAPDH reverse	CCAGGCGCCCAATACG	Homo sapiens	Merck
WBP1L forward	CGTTGCCGTTTTACTTCAGG	Mus musculus	Merck
WBP1L reverse	GAGCTGGAAGGCACTGTACG	Mus musculus	Merck
WWP1 forward	GTTGCTGCCAGACCCAAA	Mus musculus	Merck
WWP1 reverse	TAGGACAGATGATGATTCTCCATTA	Mus musculus	Merck
WWP2 forward	GCCGGTTACCAGCTCAAA	Mus musculus	Merck
WWP2 reverse	TCAAAGATACAGGTCTGCAAGC	Mus musculus	Merck
SMURF2 forward	TTACATGAGCAGGACACACTTACA	Mus musculus	Merck
SMURF2 reverse	GCTGCGTTGTCCTTTGTTC	Mus musculus	Merck
SMURF1 forward	GGGTCAGTGGTGGACTGC	Mus musculus	Merck
SMURF1 reverse	CCAGGGCCTGAGTCTTCATA	Mus musculus	Merck
NEDD4L forward	TGAGCAAGCTCACCTTCCA	Mus musculus	Merck
NEDD4L reverse	CCCGTGACAGTTGACGAAC	Mus musculus	Merck
NEDD4 forward	GCCGGTTACCAGCTCAAA	Mus musculus	Merck
NEDD4 reverse	TCAAAGATACAGGTCTGCAAGC	Mus musculus	Merck
ITCH forward	TTGATGCGAAGGAATTAGAGG	Mus musculus	Merck
ITCH reverse	GGTGTAGTGGCGGTAGATGG	Mus musculus	Merck
β-ACTIN forward	GATCTGGCACCACACCTTCT	Mus musculus	Merck
β-ACTIN reverse	GGGGTGTTGAAGGTCTCAAA	Mus musculus	Merck

Table S4. List of Nedd4-family cDNA constructs.

E3 ligase	Species	Plasmid or insert origin	Recloned to pK-MYC-C1 and thus adding Myc-tag
NEDD4L	Homo sapiens	Addgene, Plasmid: 27000 Gift from Joan Massague [11]	+
ITCH	Mus musculus	Addgene, Plasmid 11427 Gift from Allan Weissman [12]	-
WWP1	Homo sapiens	Gift from Paul Bieniasz, ADARC, NY	+
WWP2	Homo sapiens	Gift from Paul Bieniasz, ADARC, NY	+

Table S5 List of magnetic cell sorting reagents.

Antigen	Clone	Species tested	Conjugate	Company
Ly6G	17A2	Mus musculus	Biotin	BioLegend
CD3	145/2C11	Mus musculus	Biotin	BioLegend
CD11b MicroBeads	M1/70	Mus musculus and Homo sapiens	Coated	MiltenyiBiotec
CD43 (Ly48) MicroBeads	not specified by the company	Mus musculus	Coated	MiltenyiBiotec
KIT	Ack2	Mus musculus	Biotin	In house

Supplemental figures
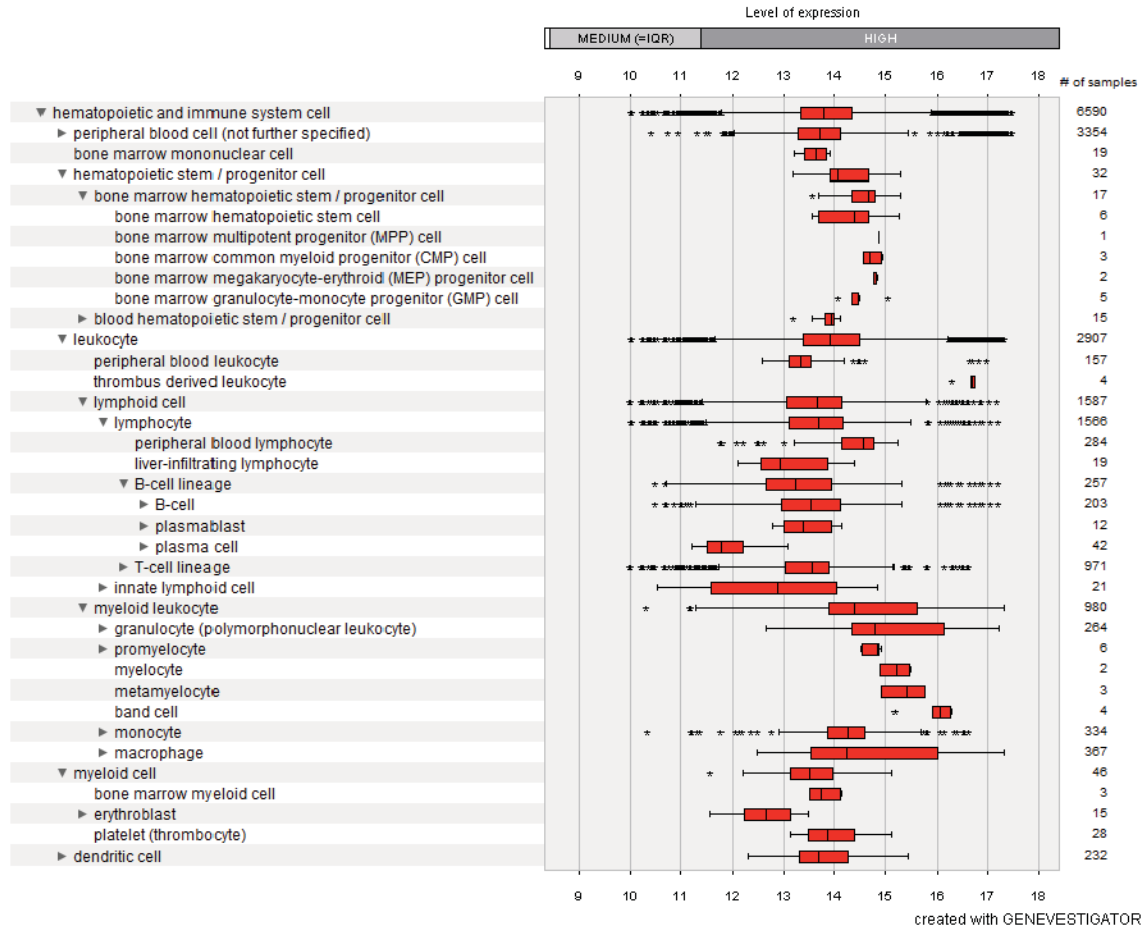
Figure S1. *WBP1L* expression in human leukocytes and leukocyte progenitor subsets. Expression profile of *WBP1L* mRNA generated by Genevestigator gene expression analysis tool, based on manually curated gene expression data from public repositories [13]. The box delimits the area between the upper and lower quartiles. Whiskers represent the lowest or highest data point still within 1.5 times this area in each direction. Stars represent data points outside this range.

A
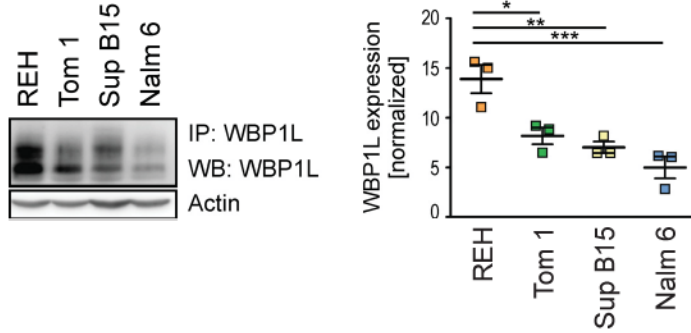
B

```
Original sequence   150 GCCTCGAGCGTCA--------GGATGGAGGAAGACTCG 180
Clone #17              ..................AA-------..............
Clone #23              ..................CG------...............
Clone #190             ..................GG------...............
Clone #192             ..................GGGGC---................
Clone #200             ..................AGATAGAC...............
```

C
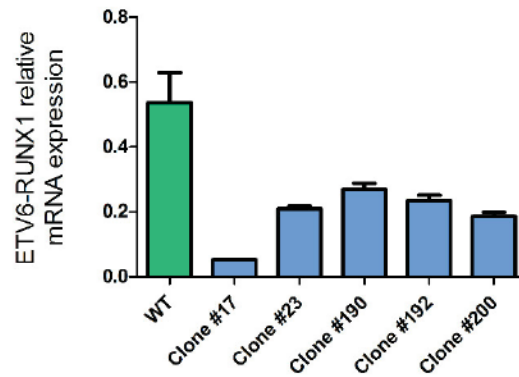
Figure S2. Expression of WBP1L in ETV6-RUNX1⁺ and ETV6-RUNX1⁻ cell lines and deletion of ETV6-RUNX1 in REH cells. (A) WBP1L immunoprecipitates from *ETV6-RUNX1⁺* B cell line REH and *ETV6-RUNX1⁻* lines TOM-1, NALM-6, and SUB B15 were immunoblotted with antibody to WBP1L and actin. For quantification, data were normalized in each experiment to actin and then to experiment average to allow comparison among experiments. Statistical significance was calculated using one way ANOVA with Dunnett's post test. (N=3). **(B)** Results of *ETV6* exon2 CRISPR/CAS9 target site sequencing in individual *ETV6-RUNX1*-deficient REH clones. **(C)** *ETV6-RUNX1* mRNA expression in the clones from (B) determined by qPCR. The data are plotted as $2^{-\Delta CT}$.
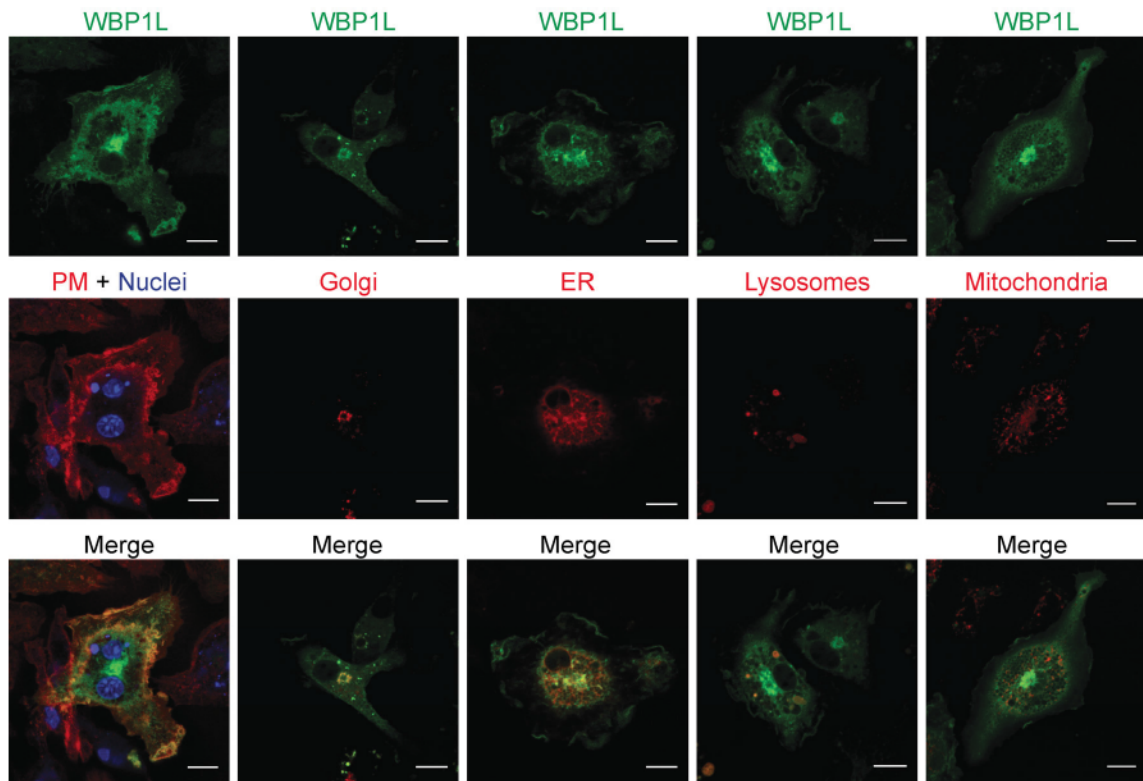
Figure S3. Subcellular localization of WBP1L. Confocal imaging of BMDM from *Wbp1l*$^{-/-}$ mice transduced with WBP1L-EGFP. The following markers were used: Plasma membrane (PM) – CD11b, Nuclei – Hoechst 33342, both on fixed cells; Golgi – Golgi-7-mApple retroviral construct, Endoplasmic reticulum (ER) – ER-Tracker-Red, Lysosomes and other acidic organelles – LysoTracker Red, Mitochondria – MitoTracker Red, all live cell imaging. Bar = 10 μm. N ≥ 3.
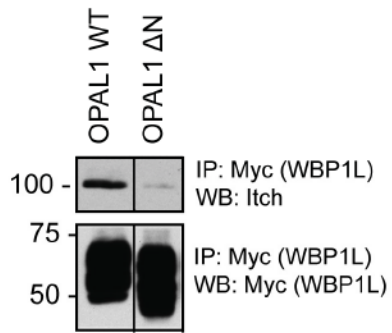
Figure S4. Alignment of WBP1L sequences from representatives of major vertebrate classes. Sequences were aligned with MUSCLE algorithm using MegAlign Pro software from DNASTAR Lasegene suite. Conserved features are highlighted with red boxes.

13

Figure S5. WBP1L interaction with ITCH in J774 macrophage-like cell line. MYC-tag imunoprecipatates from J774 cells stably expressing MYC-tagged WBP1L wild-type form or WBP1LΔN lacking WW domain interacting motifs. Western blots were stained with anti-ITCH antibody and anti MYC-tag antibody. Irrelevant lines from the blot image were removed and replaced with vertical dividing lines. N=2.
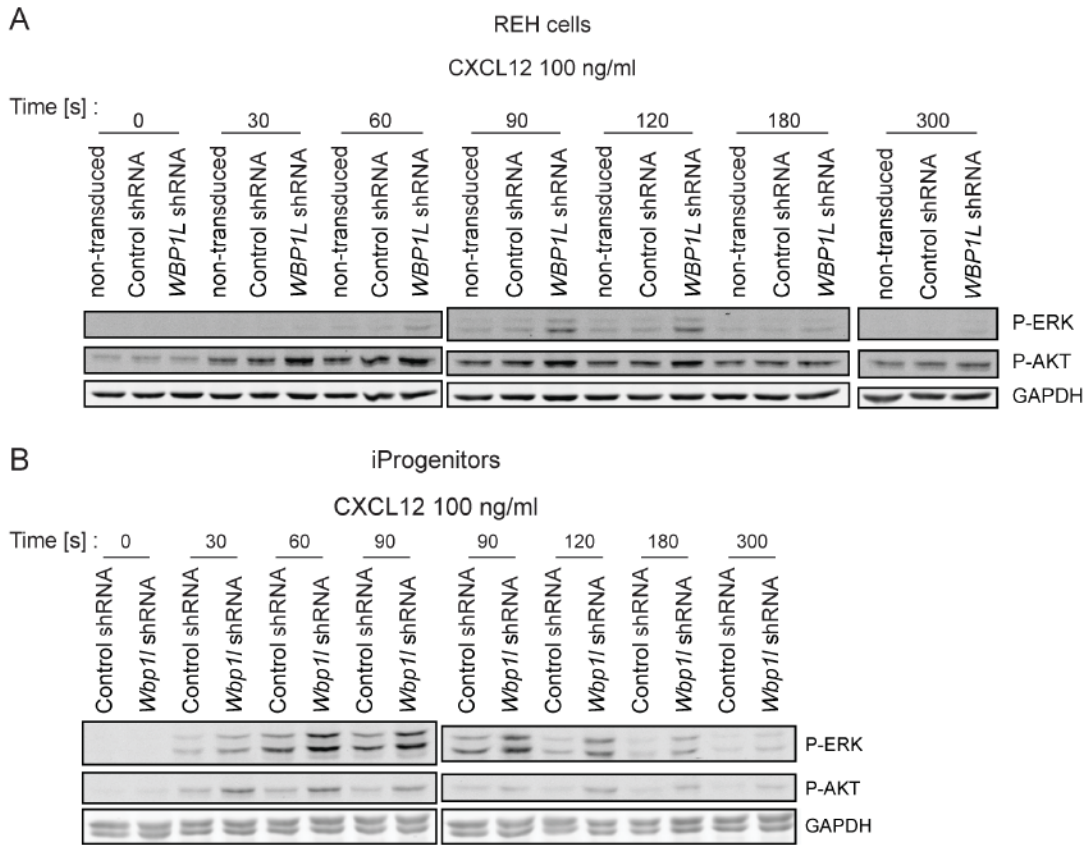
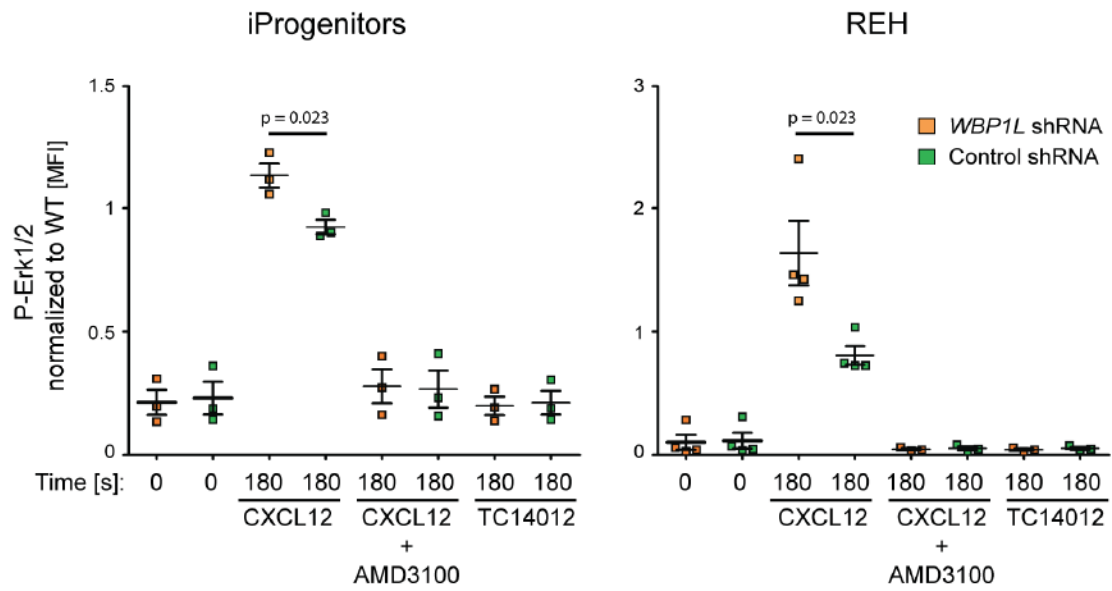**Figure S6. Representative Western blots showing data quantified in Figure 4C (A) and 4D (B).**

Figure S7. ERK1/2 phosphorylation downstream of CXCR4 or CXCR7 in immortalized monocyte/macrophage progenitors and REH cells transduced with *WBP1L* or control shRNA. Cells were treated with 100 nM CXCL12 alone or together with 1 µg/ml of CXCR4 antagonist AMD3100 or treated with 1 µM specific agonist of CXCR7 TC14012. ERK1/2 phosphorylation was analyzed by flow cytometry. Data are normalized to non-transduced cells (left panel N=3, right panel N=4).
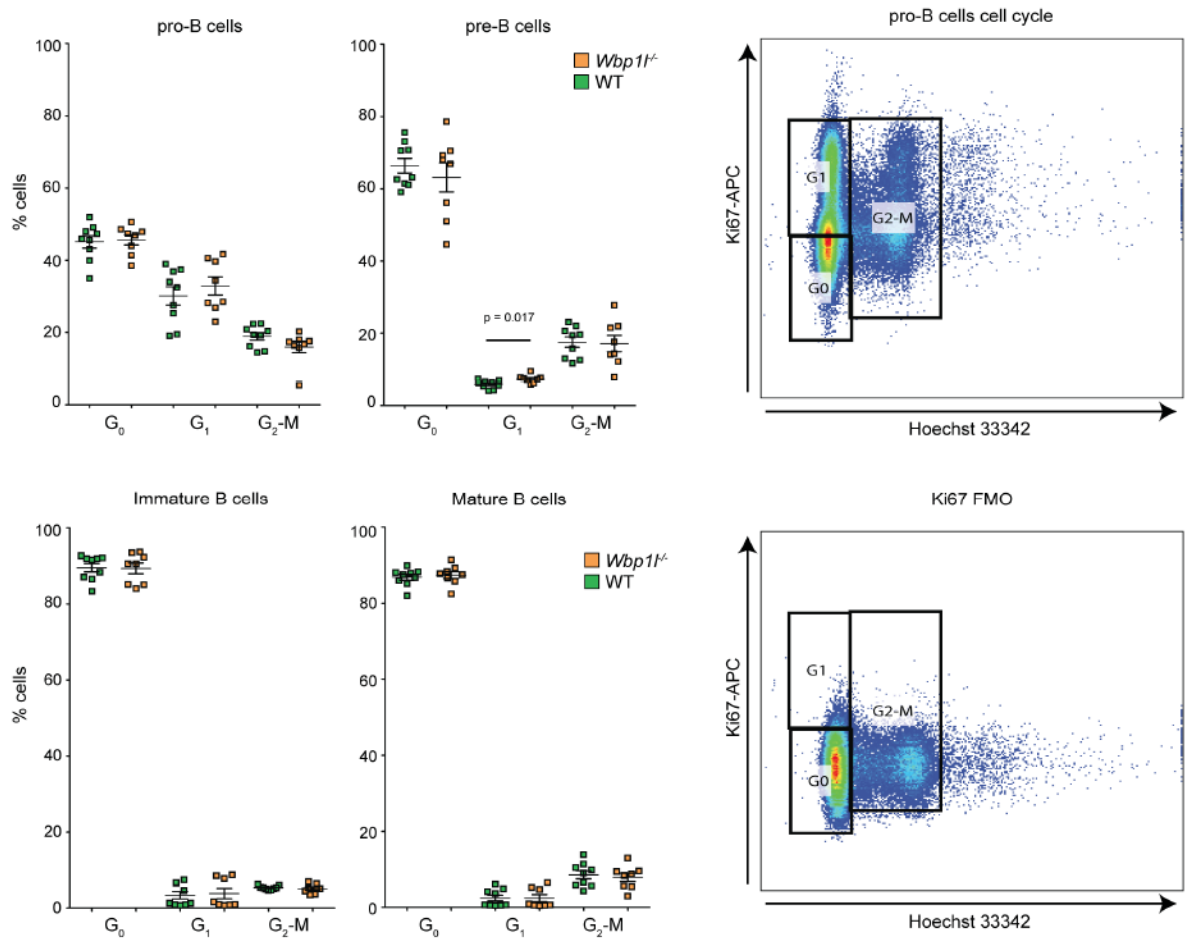
Figure S8. Analysis of cell cycle in bone marrow B cell progenitors from wild-type and *Wbp1l*-deficient mice. Bone marrow cells were fixed, stained for surface markers, permeabilized, and stained with Ki67 and Hoechst 33342. Individual B cell subsets were defined using following markers: Pro-B cells (CD43$^+$, B220$^+$, IgM$^-$), Pre-B cells (CD43$^-$, B220^{low}, IgM$^-$), Immature B cells (CD43$^-$, B220^{low}, IgM$^+$), Mature B cells (CD43$^-$, B220^{high}, IgM$^+$). The right panel of FACS plots shows gating strategy of cell cycle analyses. Representative FACS plots of stained cells with and without (Ki67 FMO) Ki67 staining are shown.
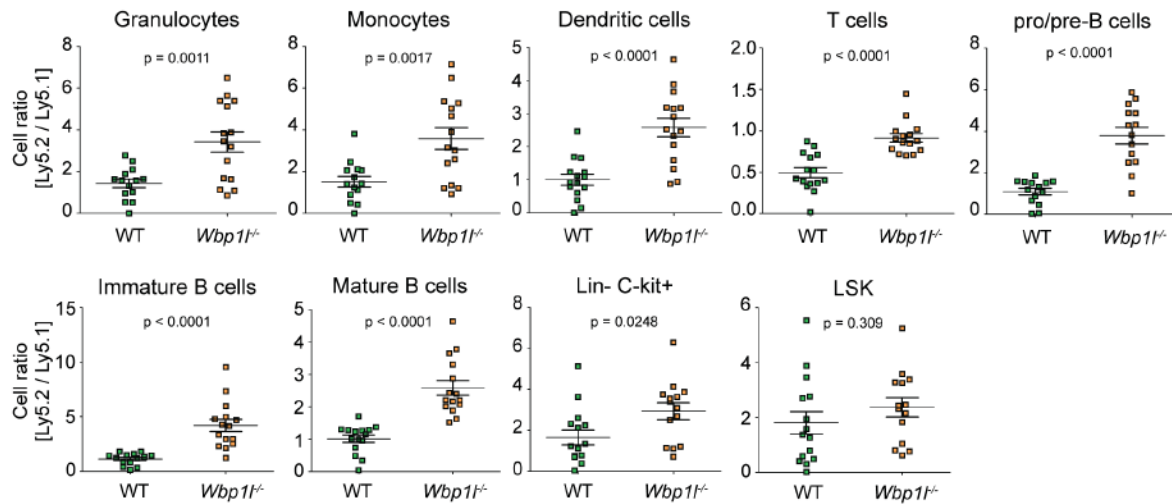
Figure S9. Enhanced engraftment of *Wbp1l*^{-/-} bone marrow. Ly5.2$^+$ bone marrow (WT or *Wbp1l*$^{-/-}$) was mixed with Ly5.1$^+$ bone marrow (always WT) in a ratio 1:1 and 2×10^6 cells were transplanted into Ly5.1 lethally irradiated mice. Mice were analyzed two months post transplantation. Flow cytometry analyses show the ratio between Ly5.2 and Ly5.1 cells determined for individual bone marrow cell subsets. Individual cell subsets were defined using following markers: Granulocytes (LY6C$^-$, CD11b$^+$, LY6G$^+$), Monocytes (LY6C$^+$, CD11b$^+$, LY6G$^-$), Dendritic cells (CD11c$^+$), T cells (CD3$^+$), Pro/Pre B cells (B220^{low}, IgM$^-$), Immature B cells (B220^{low}, IgM$^+$), Mature B cells (B220^{high}, IgM$^+$), Lin$^-$C-kit$^+$ cells (lin$^-$, c-kit$^+$), LSK cells (lin$^-$, c-kit$^+$, SCA1$^+$).
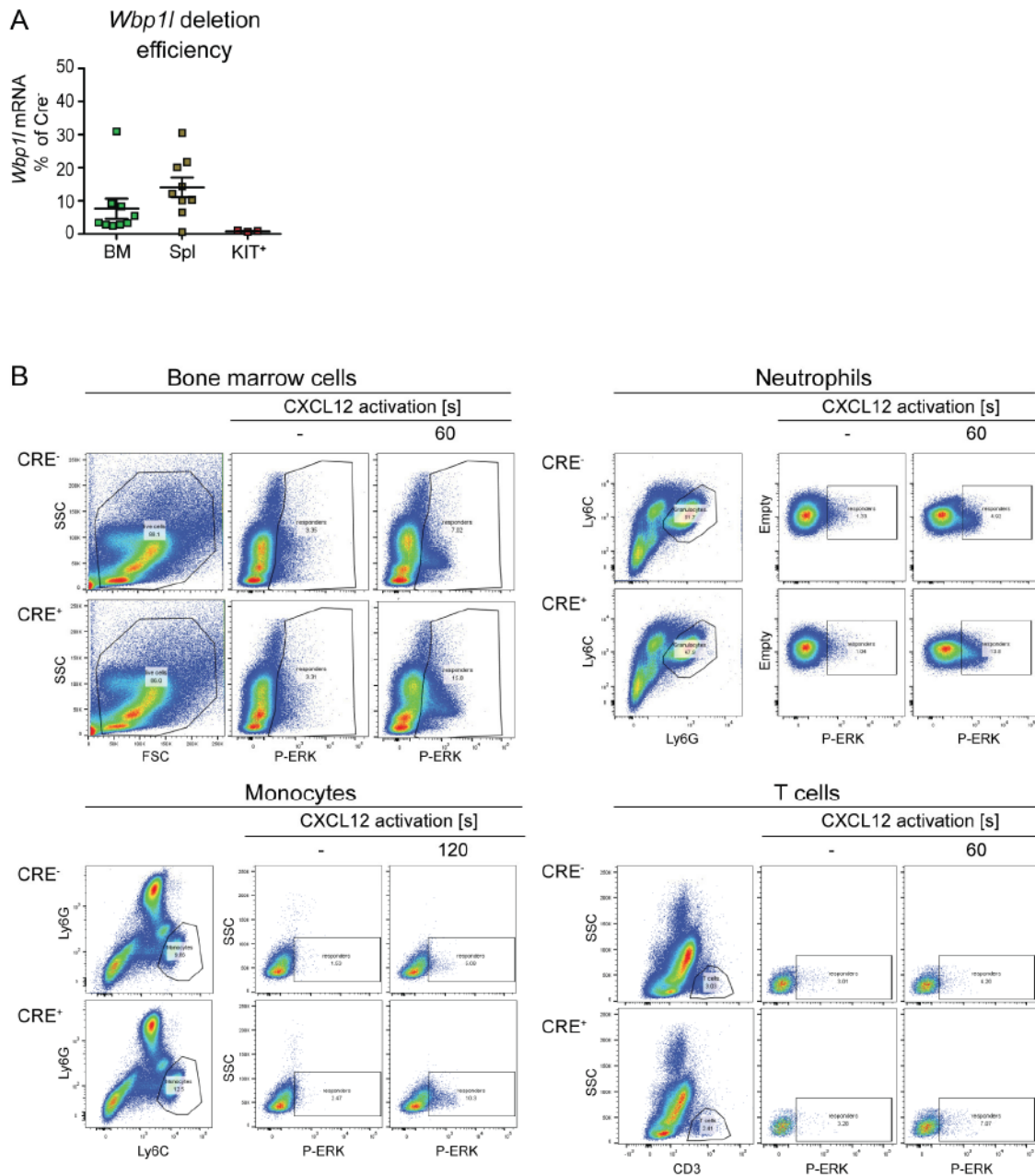
Figure S10. Effects of inducible *Wbp1l* deletion on ERK activation in bone marrow cell subsets. (A) *Wbp1l* mRNA expression after in vitro 4-hydroxytamoxifen induced deletion in samples from Figure 7F compared to 4-hydroxytamoxifen-induced deletion in vivo in the whole bone marrow and spleen from *Wbp1l-CreERT* mice (samples from Figure 7D). (B) Representative FACS plots for data shown in Figure 7D.
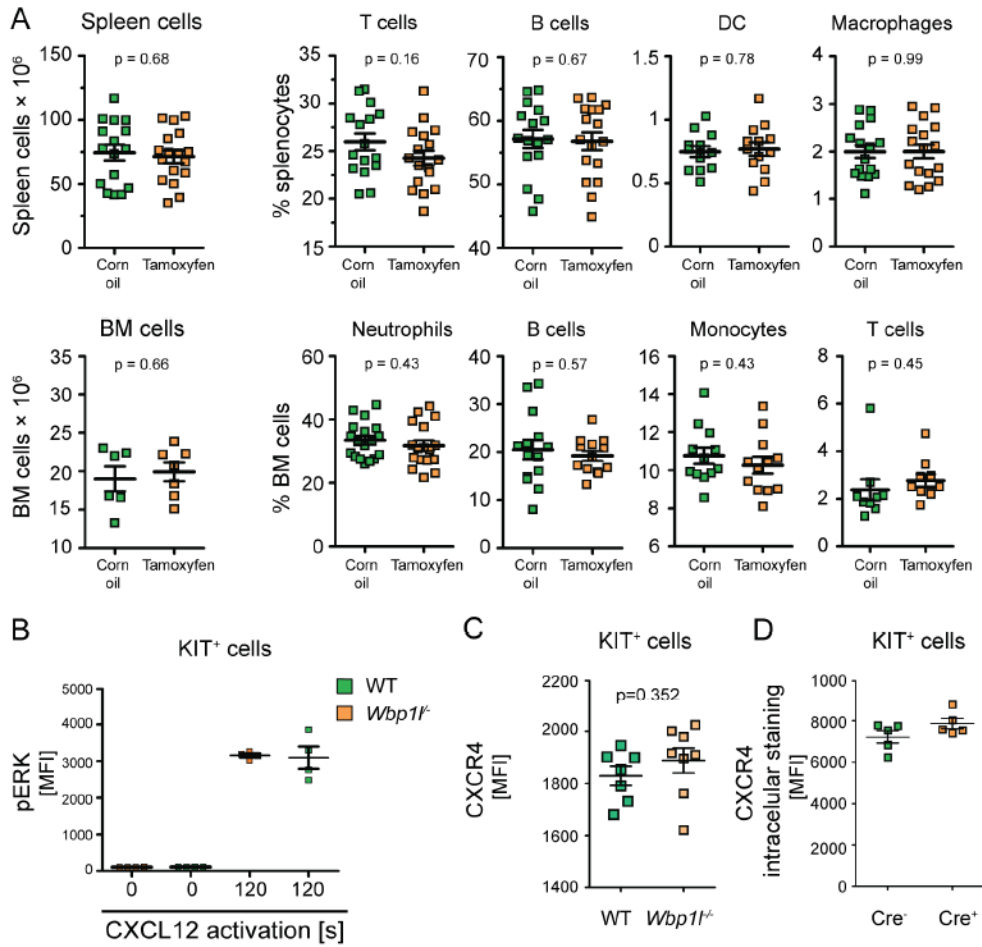
Figure S11. Additional analyses of *Wbp1l^-/-* cells. (A) Total numbers of splenocytes and bone marrow cells and percentages of major leukocyte subsets 5-7 days after Tamoxifen-induced deletion of *Wbp1l*. The splenocyte subsets were defined using the following markers: T cells (CD3⁺), B cells (B220⁺), DC (CD11c⁺, Ly6C^-/low), Macrophages (F4/80⁺, CD11b^int). The bone marrow cell subsets were defined using the following markers: Neutrophils (Ly6C^int, CD11b⁺, Ly6G⁺), B cells (B220⁺), Monocytes (Ly6C^high, CD11b⁺, Ly6G⁻), T cells (CD3⁺). (B) Similar experiment as in Figure 7F. However, here the cells with constitutive *Wbp1l* inactivation were used (N=4). (C) CXCR4 surface expression was measured in cultured KIT⁺ bone marrow progenitors with constitutive *Wbp1l* inactivation by flow cytometry. One significant outlier was removed based on Q test. (D) Total CXCR4 expression was measured in cultured KIT⁺ bone marrow progenitors with constitutive *Wbp1l* inactivation by flow cytometry of fixed and permeabilized cells.

Supplemental References

1. Kanderova V, Kuzilkova D, Stuchly J, Vaskova M, Brdicka T, Fiser K, Hrusak O, Lund-Johansen F, Kalina T. High-resolution Antibody Array Analysis of Childhood Acute Leukemia Cells. *Mol Cell Proteomics*. 2016; 15: 1246-61.

2. Wang GG, Calvo KR, Pasillas MP, Sykes DB, Hacker H, Kamps MP. Quantitative production of macrophages or neutrophils ex vivo using conditional Hoxb8. *Nat Methods*. 2006; 3: 287-93.

3. Drobek A, Kralova J, Skopcova T, Kucova M, Novak P, Angelisova P, Otahal P, Alberich-Jorda M, Brdicka T. PSTPIP2, a Protein Associated with Autoinflammatory Disease, Interacts with Inhibitory Enzymes SHIP1 and Csk. *J Immunol*. 2015; 195: 3416-26.

4. Kralova J, Glatzova D, Borna S, Brdicka T. Expression of Fluorescent Fusion Proteins in Murine Bone Marrow-Derived Dendritic Cells and Macrophages. *J Vis Exp*. 2018; 140: e58081.

5. Sobocinska J, Roszczenko-Jasinska P, Zareba-Koziol M, Hromada-Judycka A, Matveichuk OV, Traczyk G, Lukasiuk K, Kwiatkowska K. Lipopolysaccharide Upregulates Palmitoylated Enzymes of the Phosphatidylinositol Cycle: An Insight from Proteomic Studies. *Mol Cell Proteomics*. 2018; 17: 233-54.

6. Wessel D, Flugge UI. A method for the quantitative recovery of protein in dilute solution in the presence of detergents and lipids. *Anal Biochem*. 1984; 138: 141-3.

7. Masuda T, Tomita M, Ishihama Y. Phase transfer surfactant-aided trypsin digestion for membrane proteome analysis. *J Proteome Res*. 2008; 7: 731-40.

8. Hebert AS, Richards AL, Bailey DJ, Ulbrich A, Coughlin EE, Westphall MS, Coon JJ. The one hour yeast proteome. *Mol Cell Proteomics*. 2014; 13: 339-47.

9. Cox J, Hein MY, Luber CA, Paron I, Nagaraj N, Mann M. Accurate proteome-wide label-free quantification by delayed normalization and maximal peptide ratio extraction, termed MaxLFQ. *Mol Cell Proteomics*. 2014; 13: 2513-26.

10. Welm BE, Dijkgraaf GJ, Bledau AS, Welm AL, Werb Z. Lentiviral transduction of mammary stem cells for analysis of gene function during development and cancer. *Cell Stem Cell*. 2008; 2: 90-102.

11. Gao S, Alarcon C, Sapkota G, Rahman S, Chen PY, Goerner N, Macias MJ, Erdjument-Bromage H, Tempst P, Massague J. Ubiquitin ligase Nedd4L targets activated Smad2/3 to limit TGF-beta signaling. *Mol Cell*. 2009; 36: 457-68.

12. Magnifico A, Ettenberg S, Yang C, Mariano J, Tiwari S, Fang S, Lipkowitz S, Weissman AM. WW domain HECT E3s target Cbl RING finger E3s for proteasomal degradation. *J Biol Chem*. 2003; 278: 43169-77.

13. Hruz T, Laule O, Szabo G, Wessendorp F, Bleuler S, Oertle L, Widmayer P, Gruissem W, Zimmermann P. Genevestigator v3: a reference expression database for the meta-analysis of transcriptomes. *Adv Bioinformatics*. 2008; 2008: 420747.